Characterization of cationic conductance in Red Blood Cells; insights from pharmacological and pathophysiological studies

Aline Hatem

▶ **To cite this version:**

Aline Hatem. Characterization of cationic conductance in Red Blood Cells; insights from pharmacological and pathophysiological studies. Cellular Biology. Sorbonne Université, 2024. English. NNT : 2024SORUS008 . tel-04563223

HAL Id: tel-04563223
https://theses.hal.science/tel-04563223

Submitted on 29 Apr 2024

HAL is a multi-disciplinary open access archive for the deposit and dissemination of scientific research documents, whether they are published or not. The documents may come from teaching and research institutions in France or abroad, or from public or private research centers.

L'archive ouverte pluridisciplinaire **HAL**, est destinée au dépôt et à la diffusion de documents scientifiques de niveau recherche, publiés ou non, émanant des établissements d'enseignement et de recherche français ou étrangers, des laboratoires publics ou privés.

Thèse en vue de l'obtention du diplôme de docteur

Sorbonne Université

Ecole doctorale Complexité du vivant (ED 515)

UMR8227 LBI2M- Équipe Physiology & Cell Fate

Characterization of cationic conductance in Red Blood Cells; insights from pharmacological and pathophysiological studies

Par Aline Hatem

Thèse de doctorat en Biologie cellulaire et développement

-Physiologie cellulaire-

Dirigée par Pr. Stéphane Egée

Présentée et soutenue publiquement le 15 Février 2024

Devant un jury composé de :

Dr. Hélène Guizouarn (CNRS-Université Côte d'Azur) …….Rapportrice

Pr. Marieke von Lindern (Sanquin research, The Netherlands) ……Rapportrice

Pr. Lars Kaestner (Saarland University, Germany) ……..……...Examinateur

Dr. Wassim El Nemer (EFS, Université Aix-Marseille)……..Examinateur

Dr. Olivier Silvie (Inserm-Sorbonne Université)…… Président du jury

Pr. Stéphane Egée (CNRS-Sorbonne Université)…….……...Directeur de thèse

Abstract

English

Over their lifespan, erythrocytes circulate throughout the body to carry respiratory gases and perform their other functions. Therefore, erythrocytes must deform properly to circulate in all vessels, including the smallest of the capillaries. This ability is governed by a complex membrane-cytoskeleton network combined with a finely tuned surface-volume ratio that allows instantaneous shape changes to enable rapid RBC transit. This highlights how important it is to maintain cell volume to ensure a 120-day journey without the possibility of repair. Cell volume or hydration status is directly influenced by the activity of membrane transporters, pumps, and ion channels. The permeability of erythrocytes, which is dominated by anion movement for physiological reasons, implies that cation movement should be kept as low as possible to avoid any change in cell volume. However, in many pathophysiological conditions, cation permeabilities are known to be deregulated, leading to increased intracellular Ca^{2+} and Na^{+} levels. My thesis aimed to better characterize the role of non-selective cation (NSC) channels (PIEZO1, TRPV2), and Gárdos channel in such pathophysiological conditions. Experiments were carried out on healthy erythrocytes as well as on cells from patients suffering from different pathologies like Sickle Cell Disease (SCD), xerocytosis, and stomatocytosis, using electrophysiological methods (MBE and patch-clamp), Ca^{2+} movements semi-quantification (flow cytometry and live-cell imaging) combined with the measurement of morphometric parameters, and the measurements of intracellular cell volume and other ions contents. In two independent studies using blood from sickle cell patients, we were able to demonstrate from one part the central role of PIEZO1 activation in the enhancement of sickling propensity. In the other part, we demonstrated the increased sensitivity of sickle cells to THC stimulation via TRPV2 activation. Along with these published results, we have contributed to the functional characterization of many PIEZO1 and KCNN4 variants, for which we have designed a series of functional experiments to better describe the genetically identified variants. This part with 5 Gárdos and 10 PIEZO1 variants increases the knowledge about the pathogenicity of the identified mutations, often characterized as variants of uncertain significance (VUS). We were also able to demonstrate that Dooku1, a chemical compound described in the literature as an inhibitor of Yoda1's effects, is in fact, a direct activator of PIEZO1 in erythrocytes, contributing to a more accurate pharmacology of PIEZO1. Furthermore, we conducted a series of experiments in patients treated with Alectinib (a lung cancer treatment), for which frequent anemia associated with cell volume dehydration is observed. Taken together, these studies contribute to the understanding of cation permeabilities under physiological and pathophysiological conditions. Finally, all these results highlight the particularity of RBCs regarding cationic permeability and biophysical membrane properties compared to other cell types and, more importantly when mechanosensitive pathways are involved in such ion movements.

Keywords: PIEZO1, TRPV2, Gárdos channel, Sickle Cell Disease, cation conductance, erythrocytes

Français

Au cours de leur vie, les érythrocytes circulent dans tout le corps pour transporter les gaz respiratoires et remplir leurs autres fonctions. Par conséquent, les érythrocytes doivent être capable de se déformer correctement pour circuler dans tous les vaisseaux, y compris les plus petits capillaires. Cette capacité est régie par un réseau complexe associant les protéines de la membrane et du cytosquelette combiné à un rapport surface-volume finement ajusté, permettant ainsi des changements de forme instantanés pour permettre un transit rapide des GR. Cela montre à quel point il est important de maintenir le volume cellulaire pour assurer 120 jours dans la circulation. Le volume cellulaire ou l'état d'hydratation est directement influencé par l'activité des transporteurs membranaires, des pompes et des canaux ioniques. La perméabilité des érythrocytes, dominée par le mouvement des anions pour des raisons physiologiques, implique que le mouvement des cations doit être maintenu aussi bas que possible pour éviter toute modification du volume cellulaire. Cependant, dans de nombreuses conditions physiopathologiques, la perméabilité aux cations est connue pour être dérégulée, conduisant à une augmentation des niveaux intracellulaires de Ca^{2+} et de Na^{+}. L'objectif de ma thèse était de mieux caractériser le rôle des canaux cationiques non sélectifs (PIEZO1, TRPV2) et du canal Gárdos dans ces conditions physiopathologiques. Des expériences ont été réalisées sur des érythrocytes issus de donneurs sains ou de patients souffrant de différentes pathologies telles que la drépanocytose, la xérocytose et la stomatocytose, en utilisant des méthodes électrophysiologiques (MBE et patch-clamp), des mesures semi-quantitatives des mouvements de Ca^{2+} (cytométrie en flux et imagerie cellulaire) combinées à la mesure de paramètres morphométriques, ainsi que des mesures du volume cellulaire et des contenus en ions. Dans deux études indépendantes utilisant du sang de patients drépanocytaires, nous avons pu démontrer d'une part le rôle central de l'activation de PIEZO1 dans l'augmentation de la propension à la falciformation. D'autre part, nous avons démontré une sensibilité augmentée des GR drépanocytaires à la stimulation par le THC *via* l'activation du TRPV2. Parallèlement à ces résultats publiés, nous avons contribué à la caractérisation fonctionnelle de nombreux variants de PIEZO1 et de KCNN4, pour lesquels nous avons conçu une série d'expériences fonctionnelles afin de mieux décrire les variants génétiquement identifiés. Cette partie avec 5 variants Gárdos et 10 variants PIEZO1 apporte des éléments fonctionnels quant à la pathogénicité des mutations identifiées et souvent classées comme des variants de signification incertaine (VUS) par les algorithmes génétiques. Nous avons également pu démontrer que la molécule Dooku1, décrite dans la littérature comme un inhibiteur des effets de Yoda1, est en fait un activateur direct de PIEZO1 dans le globule rouge, contribuant à une pharmacologie plus précise de PIEZO1. En outre, nous avons mené une série d'expériences chez des patients traités à l'Alectinib (un traitement contre le cancer du poumon), pour lesquels on observe une anémie fréquente associée à une déshydratation cellulaire. L'ensemble de ces expériences a contribué à la compréhension des perméabilités aux cations dans des conditions physiologiques et physiopathologiques. Enfin, tous ces résultats remettent en évidence la particularité des GR en ce qui concerne la perméabilité cationique et les propriétés biophysiques des membranes par rapport à d'autres types de cellules et, plus important encore, lorsque des voies mécanosensibles sont impliquées dans de tels mouvements d'ions.

Mots-clés: PIEZO1, TRPV2, canal Gárdos, Drépanocytose, conductance cationique, érythrocytes.

Table of Contents

List of Tables

List of Figures

List of Equations

Foreword

Blood, composition, and function

For more than 300 years, blood has been one of the tissues that have attracted the attention of scientists given its primordial role in the scheme of life in addition to the ease with which blood samples can be withdrawn from humans and animals, facilitating blood-related research and therapies (Bessis and Delpech, 1981).

Blood has three main types of cells: Red Blood Cells (RBCs), White Blood Cells (WBCs), and platelets, in a liquid called plasma. In routine blood tests, complete blood counts (CBC) are required; they include counts of the different types of cells found in the blood, and other specific criteria needed for hematological diseases diagnostics (Table 1). CBC provide an overall look at health and helps diagnosing a variety of conditions, such as anemias, infections, leukemias, and others.

Blood has three major functions that could be summarized in three words: transport, protection, and regulation. It transports oxygen (O_2) and nutrients to the lungs and tissues and carries away carbon dioxide (CO_2) and other waste products, mainly thanks to the presence of RBCs (Hematology Glossary, 2021). It protects the body by fighting against infections through the activity of WBCs, and by forming blood clots to prevent excess blood loss thanks to the activation of the platelets. Finally, it regulates the temperature by distributing heat throughout the body (Functions of blood: regulation, 2021).

Table 1: **Complete blood count. Hb is the total amount of hemoglobin in the blood, HT is the volumetric part of RBCs in the blood, MCV is the measurement of the average volume of RBCs, MCH is the amount of Hb in RBCs, MCHC is the concentration of Hb in RBCs, RDW measures the variability in the RBC's size and shape, and MPV measures the average volume of platelets. Reference rates and the units can vary depending on the laboratory that carried out the test. Table adapted from (Dean, 2005).**

Component	Abbreviation	Values and Ranges
White blood cell	**WBC**	**4.300 and 10.800 cells per microliter of blood**
Red Blood Cells	**RBC**	**4.2 to 5.9 million cells per microliter of blood**
Hemoglobin	**Hb**	**13.8 to 17.2 grams per decilitre (g/dL) for men and 12.1 to 15.1 g/dL for women**
Hematocrit	**HT**	**45% to 52% for men and 37% to 48% for women**
Mean corpuscular volume	**MCV**	**80 to 100 femtoliters (fL)**
Mean corpuscular hemoglobin	**MCH**	**27 to 32 picograms**
Mean corpuscular hemoglobin concentration	**MCHC**	**32 g/dL to 36 g/dL**
Red cell distribution width size and shape	**RDW**	**11% to 15%**
Platelet count	**-**	**150.000 to 400.000 per microliter of blood**
Mean platelet volume	**MPV**	**6 to 12 femtoliters**

My thesis focuses specifically on human Red Blood Cells (RBCs). You will find detailed the properties of these cells, their functions, and pathologies related to RBCs. The interplay between cation channels in the regulation of all the aforementioned characteristics is the main concern in this dissertation.

Introduction

I. Mature Red Blood Cells

RBCs, also known as "erythrocytes", constitute the most numerous type of cell in the body, accounting for approximately 40 to 45 % of the volume of the blood, and are known to be essential for gaseous exchange (Hematology Glossary, 2021). They are enucleated cells, devoid of any translational process during their 120 days of circulation, making any repair mechanism and protein renewal in these cells impossible (Kaestner and Minetti, 2017).

Erythrocytes typically have a diameter of 8 µm, a mean volume of 90 fL, and a surface area of 140 μm^2. Thanks to their biconcave shape and flexible cell membrane, RBCs can expand their volume up to 150 fL, as well as they can fit into capillaries with a much smaller diameter than 8 µm (Figure 1). This special shape presumably originates from differences in densities between the rim and the dimple regions of the plasma membrane (Hoffman, 2016). RBCs thickness varies according to those regions, with 2.5 µm at the thickest parts (rims) and 1µm around the dimple region (Hall, 2015).

Importantly, four globins -two alpha chains (α), two beta chains (β)- make up the oxygen-carrying protein in the erythrocytes, known as hemoglobin (Hb). Each of the globin contains a heme group where is found one iron atom (Fe^{2+}) in its center that binds one oxygen molecule. Hemoglobin molecules confer the redness characteristic of the RBCs (Peter Klinken, 2002). Cell hemoglobin content weights usually 30 pg, representing a huge concentration (about 340 g/L) that implies a cytoplasmic viscosity six times higher than it is of water (Narla and Mohandas, 2017).

Figure 1: Adaptation of RBCs to narrow vascular channels by undergoing deformation leading to their shape change, adapted from (Corrons et al., 2021).

- **RBCs in the flow**

Erythrocytes are highly flexible cells that undergo significant deformation in the microcirculation as a result of the shear stress in addition to geometric constrictions. This deformation is necessary to reduce the blood flow resistance (Noguchi and Gompper, 2005; Tahiri et al., 2013), release ATP, and deliver oxygen (Forsyth et al., 2012). Blood fluidity is strictly dependent on the behaviour of RBCs in the flow, which is crucial for proper tissue perfusion. The flow behavior of RBCs is set by their response to hydrodynamic stress in terms of cell orientation relative to the flow direction and cell deformation; at low shear rates, cells have similar cell orientations which favors the formation of "rouleaux" and increases blood viscosity. At high shear rates, RBCs are more aligned, individualized, and more stretched in the flow, which reduces blood viscosity (Dupire et al., 2012).

RBCs in the flow can assume different shapes, the two most common being the slipper and parachute shapes. The slipper shape is a non-symmetric shape attained by the RBCs in the circulation (Abkarian et al., 2008; Tahiri et al., 2013). On the contrary, parachute shape is a symmetrical shape of the RBC that looks like a semi-spherical cap (Merrikh and Lage, 2008) (Figure 2).

At present, the improvement of microfluidic devices largely favors *in vitro* studies to mimic RBCs in the microcirculation, which, combined with mathematical and physical modeling, lead to a fine comprehension of the *in vivo* behaviors of RBCs in flow (Fedosov et al., 2014).

Figure 2: Main shapes of RBCs. The normal (resting) shape "discocyte" is usually found in static conditions, whether the two other shapes "slipper and parachute" are commonly found in the microcirculation. Figure created using Bio-Render.

A. Gas transport

RBCs play a crucial role in the transport of oxygen from the lungs to tissues and of CO_2 from tissues to the lungs, which constitutes their canonical function (Kuhn et al., 2017).

1. The Jacobs-Stewart Cycle

The CO_2 Jacobs-Stewart cycle was first described in the RBCs in 1942 (Jacobs and Stewart, 1942). Jacobs-Stewart is a system that regulates CO_2 transport and pH; it is essential for efficient gas transport and respiration. This system reverses direction depending on whether the erythrocytes are close to tissues or close to the lungs (Figure 3). The increase in CO_2 levels in peripheral tissues, makes CO_2 diffuse freely throughout the RBC membrane. CO_2 is reversibly hydrated in the RBCs by the action of Carbonic Anhydrase (CA) which induces the formation of $H^+ + HCO_3^-$, resulting in a drop in pH and a reduction in the affinity of Hb for O_2. Protons (H^+) from the reaction are mainly buffered by hemoglobin (HbH^+); hemoglobin has a very high buffering capacity, thanks to numerous histidine residues, which are the sole amino acid to display a wide range of pKa allowing to buffer H^+ at physiological pH (Van Beek and De Bruin, 1980). CO_2 itself, and its impact on pH via the reaction described above ($CO_2 + H_2O \rightarrow H^+ + HCO_3^-$), reduces the oxygen affinity to hemoglobin, thereby promoting O_2 release in the capillaries where the partial pressure of CO_2 is higher (i.e., metabolically active tissues). In the lungs, the reduction of the partial pressure of CO_2 caused due to exhalation has the reverse effect; it increases the affinity of O_2 by hemoglobin.

In this process, the activity of Band 3 (AE1, gene *SLC4A1*) is of particular importance; whilst most biological membranes are permeable to CO_2 (Endeward et al., 2006), HCO_3^- is unable to diffuse

freely through the plasma membrane, and needs a specific transporter to be shuttled. It is the role of Band 3, which is an abundant membrane protein, (≈1.2 x 10^6 copies per cell) (Satchwell and Toye, 2021). Band 3 efficiently exchanges HCO_3^- for Cl^- in and out of the cells at very high rates. Thanks to Band 3, a proper Jacobs-Stewart cycle can take place, leading to a passive distribution of H^+ and HCO_3^- across the membrane, regulating by such CO_2 transport and cellular pH, in other words, gas transport and respiration. Within seconds' worth of capillary transits, the gas exchanges take place. Sharp changes in RBC pH are brought on by each oxygenation-deoxygenation and deoxygenation-reoxygenation transition on hemoglobin, which then cause changes in ion fluxes, and slight changes of membrane potential, and cell volume. Despite being independent, these changes have a cumulative effect within the 120 days of RBCs circulation (Lew, 2023).

In summary, the Jacobs-Stewart cycle is the engine of gas transport. As 80-90% of total CO_2 is transported as HCO_3^- in the blood, a systemic acid/base equilibrium is maintained.

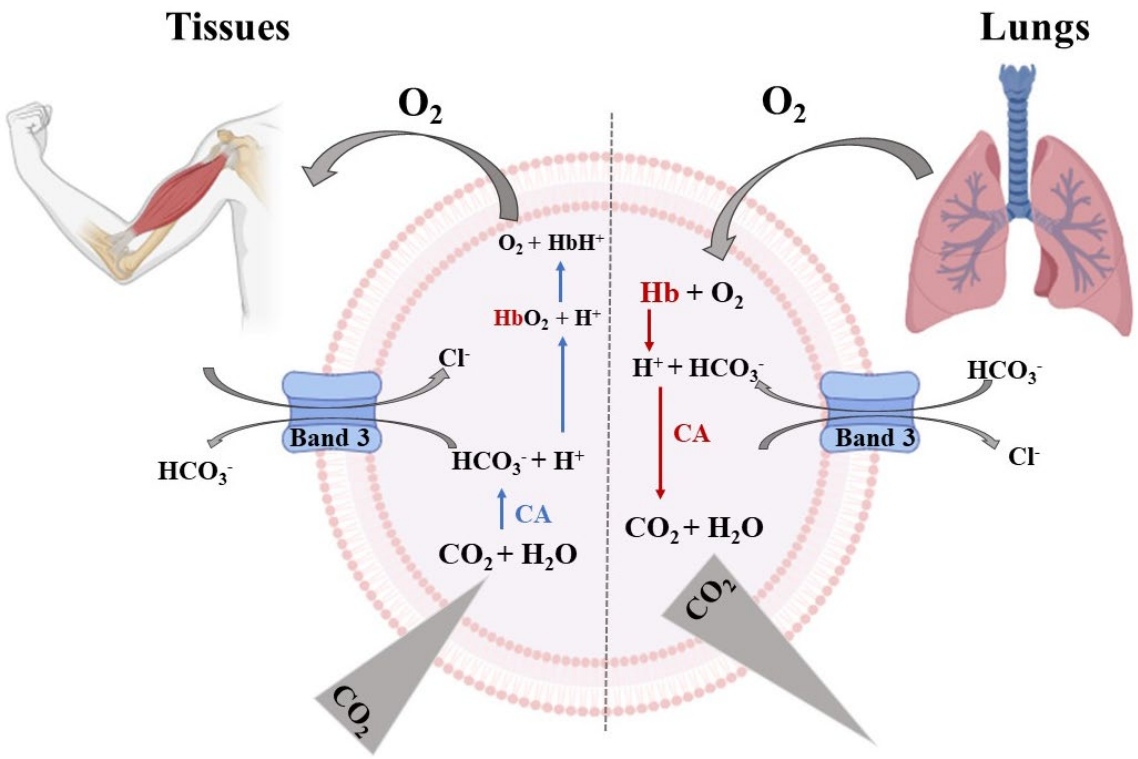

Figure 3: The Jacobs-Stewart cycle in RBCs, in a deoxygenated environment (i.e. tissues), and in an oxygenated one (i.e. lungs). Figure created using Bio-Render.

2. Bohr-Haldane effect

The O_2 binding affinity of hemoglobin is inversely related to both acidity and CO_2 concentration. This is the definition of the Bohr effect. It refers to the shift in the O_2 dissociation curve in response to changes in pH. Thus, Bohr effect underlies the release of oxygen in tissues when CO_2 enters the RBCs and is converted to HCO_3^-, lowering the intracellular pH, and allowing the release of O_2 from Hb. On the other hand, O_2 affects the affinity of Hb for CO_2 and H^+ under the Haldane effect. Bohr and Haldane effects are two strategies that the body uses for increasing the amounts of O_2 and CO_2 delivery going back and forth between the lungs and the tissues. These two mechanisms are key regulators but they are simply linked to the properties of the Hb (Table 2).

Table 2: Bohr *versus* Haldane effect comparison, adapted from (Lakna, 2018)

Bohr effect	**Haldane effect**
Decrease in the oxygen affinity of Hb in response to decreased blood pH resulting from increased CO_2 concentration in the blood	Decrease in the CO_2 affinity of Hb in response to increased blood pH resulting from increased O_2 concentration in the blood
First described by Christian Bohr in 1904 (Bohr, Hasselbalch, & Krogh, 1904).	First described by John Scott Haldane in 1905 (John Scott Haldane | Respiratory Physiology, Gases & Hypoxia | Britannica, 2019)
Occurs at the metabolizing tissue	Occurs in the lungs
Describes the release of O_2	Describes the release of CO_2
Effective under low blood pH	Effective under high blood pH
Caused by the take up of CO_2 at the metabolizing tissue	Caused by the uptake of O_2 in the lungs
Facilitates the release of O_2 at the metabolizing tissue	Facilitates the binding of O_2 to the Hb

Band 3 which mediates the "Chloride shift" phenomenon, together with carbonic anhydrase, and the effects of Hb, play a central role in the recognition of metabolically active tissues, making the RBC the ideal vehicle for oxygen delivery to these tissues, providing them with the required amount of O_2 (Hamasaki, 1999). Nevertheless, in order to successfully exchange gases, erythrocytes must possess other properties, including the ability to control intracellular pH, ATP synthesis, and redox status (Balach et al., 2019), and not forgetting the ability of cells to deform easily and to withstand mechanical and osmotic stress, factors that are directly regulated by Band 3 (Kuo et al., 2021).

3. RBCs Other functions

Next to their canonical role in gas transport and systemic acid/base equilibria, RBCs have other non-canonical functions.

In 1992, it was proposed that erythrocytes are mobile carriers of adenosine triphosphate (ATP), able to sense the need for increased blood flow in metabolizing tissues and provide it by releasing ATP (Bergfeld and Forrester, 1992). ATP release from RBCs is a response to reduced O_2 content, mechanical deformation, endothelial shear stress, adrenergic stimulation, and acidosis (Sprague et al., 2007; Sprague and Ellsworth, 2012; Ellsworth et al., 2016). Some studies have suggested that ATP is not released from the RBCs *per se* in response to hypoxia, but that hemolysis is the main cause (Sikora et al., 2014; Ferguson et al., 2021). Released ATP binds to purinergic P2Y receptors on endothelial cells, initiating by such a signalling cascade mediated by nitric oxide (NO) and prostaglandin, leading to vasodilation in metabolizing tissues (Mortensen et al., 2009).

Talking about NO, it is a free radical that can diffuse at a rate of 50 μm/s in aqueous solutions. RBCs can be a source of NO and can regulate its metabolism which is key to controlling blood rheology (Simmonds et al., 2014).

RBCs can also contribute to cytokine signalling (Karsten and Herbert, 2020) and to the trigger of immune responses (Ren et al., 2023) by modulating the immune cells (Karsten and Herbert, 2020). RBCs use the complement receptor 1 (CR1, CD35) to bind to complement-opsonized bodies in the circulation (Nelson, 1953), and they can transfer them to liver and spleen in order to be removed. This RBC-CR1 binding can increase the membrane deformability (Glodek et al., 2010).

Canonical function of RBCs, consisting in gas transport, is increased by RBC membrane properties, especially the higher surface area to volume that renders the cells more deformable (Jaferzadeh and Moon, 2015).

B. <u>Deformability property</u>

A normal RBC has a total membrane surface area of 140 μm^2 and an approximate volume of 90 fL, as mentioned above. This means that the cells have approximately 1.5 times more membranes surface than the surface of a sphere corresponding to this volume. This ratio, associated with the

special biconcave shape, allows mature erythrocytes to undergo adaptations in their shapes which will permit them to circulate normally to accomplish their roles (Bessis, 1972).

Erythrocytes take advantage of their biophysical properties to keep functioning in physiological conditions (Kuhn et al., 2017). The deformability ability allows the RBCs to squeeze and cross the narrowest capillaries and the splenic sinuses, without being hemolyzed (Huisjes et al., 2018). Erythrocytes must adapt their shape and presumably cell volume as they pass through arteries, capillaries, sinusoids, and veins, and when they adhere to and are released from their interactions with vascular tissues (Cahalan et al., 2015; Lux, 2016; Rogers and Lew, 2021b, 2021a).

Deformability, flexibility, and elasticity are mechanical properties characterizing the RBCs. Shape modifications can exhibit a lot of variation (Nayani et al., 2020). They exist from one side, due to the intracellular ions and water content of the erythrocytes handled by the enormous diversity of membrane channels, pumps, and transporters (Huisjes et al., 2018), and from the other side, thanks to the properties of the cytoskeleton which features distinctive proteinic and structural characteristics; it is composed of a 2D mesh-like spectrin structure that is anchored to the internal leaflet of the lipid bilayer membrane, conferring to the cells their elasticity that interplays with RBC's deformability (Figure 4) (Mohandas and Evans, 1994).

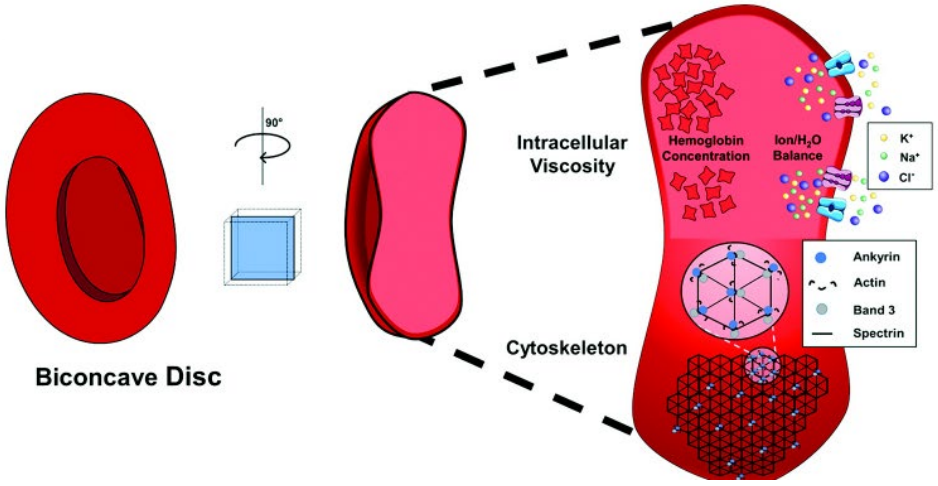

Figure 4: Factors influencing the deformability of RBCs. RBCs are biconcave disks, and their deformability is enabled on the one hand by their intracellular viscosity properties (Hemoglobin concentration, and ion/H_2O balance), and on the other hand by the properties of the cytoskeleton (Kuhn et al., 2017).

The high deformability of RBCs depends on multiple factors. First, it takes place thanks to the biconcave shape of the cells, in other words, the excess of RBC surface area (area/volume ratio), in a second place, due to the cytoplasmic viscosity of the cells and the fine regulation of the intracellular Hb concentration. Third, this property is conferred thanks to the membrane mechanical properties and the robust/flexible spectrin cytoskeleton especially the 4.1R complex and the Ankyrin complex (Byers and Branton, 1985). Furthermore, Ca^{2+} exchange is one of the main keys to the deformability of erythrocytes, as it is present at a low basal concentration (50 nM), and its concentration changes rapidly and transiently in response to stress. In addition, deformability is allowed thanks to the membrane lipid transversal asymmetry. Finally, it is permitted by the membrane lipid lateral asymmetry in submicrometric domains (Tyteca et al., 2010; Leonard et al., 2017; Conrard et al., 2018). Each of these factors will be discussed in detail in the following sections.

RBC stability and structural integrity are conferred by its membrane which main components are the phospholipid bilayer, and the transmembrane proteins (Pivkin and Karniadakis, 2008; Peng et al., 2010).

The main function of the membrane is to confer RBCs the capacity to tolerate the shear stress in the circulation without being distorted, in other words, their deformability (Mohandas and Chasis, 1993; Lee and Discher, 2001).

1. Membrane lipids

a) Composition

Erythrocyte's lipid bilayer membrane is formed of phospholipids and cholesterol with incorporated integral proteins (Discher and Carl, 2001). Phospholipid composition contributes to the blood viscosity (Li et al., 2017b). The human RBC membrane is made up of proteins (52%), lipids (41%), and carbohydrates (7%) (Dodge et al., 1963). Membrane lipids are divided into three classes mainly; phospholipids (62.7%), neutral lipids (25.2%), and glycosphingolipids (~12%). Neutral lipids consist essentially of cholesterol (Bernhardt and Ellory, 2003). Cholesterol is distributed uniformly across the membrane, in addition to four phospholipids that are asymmetrically

arranged. On the outer side of the membrane, sphingomyelin and phosphatidylcholine (PC) are usually found (in addition to glycosphingolipids, such as GM1) whereas on the cytosolic side of the membrane, there are found phosphatidylserine (PS), phosphatidylethanolamine (PE), phosphoinositide (e.g. PI, PIP_2, etc…), and ceramide (Figure 5).

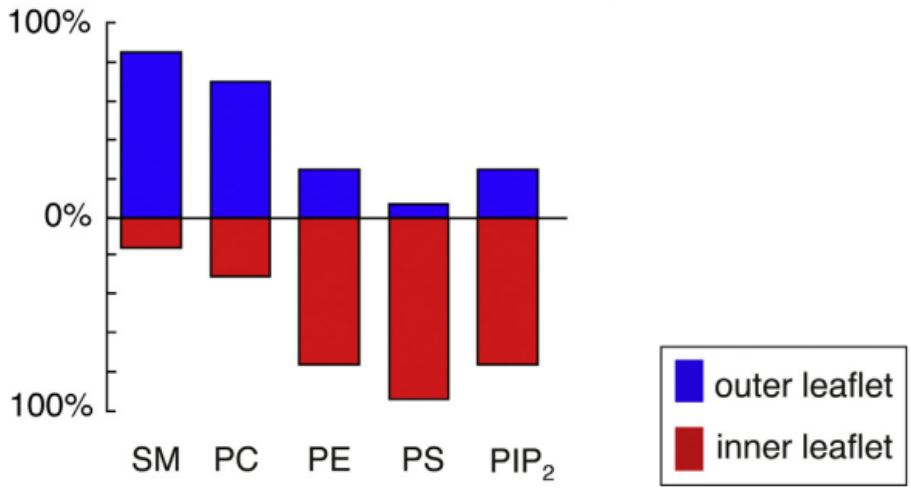

Figure 5: Asymmetrical transbilayer distribution of lipids RBCs membranes. The distribution is given as a percentage of each phospholipid. Figure adapted from (Murate and Kobayashi, 2016).

b) Cholesterol

RBCs are amongst the unique cell types with cholesterol making around 50% of total membrane lipids (Carquin et al., 2016). This forms a high ratio cholesterol/phospholipid (Subczynski et al., 2017). Cholesterol modulates the structure (Lange and Slayton, 1982) and dynamic properties of the lipid part of the membrane; it affects the packing and the rigidity of the membrane (Subczynski et al., 1994). It can also reduce the simple non-electrolyte permeability of the lipid bilayer at physiological temperatures by provoking a decrease in membrane fluidity or a tightening of the hydrogen-belt, rate-limiting barrier for solutes penetrating the membrane (Grunze et al., 1980). In addition, NaK pump activity was showed to be enhanced by cholesterol depletion (Claret et al., 1978).

The activation/inactivation of mechanosensitive non-selective PIEZO1 channel is found to be profoundly affected by the lipid composition of the membrane. Actually, PIEZO1 organizes in the

membrane into nanometric clusters that depend on the integrity of cholesterol domains in order to sense applied force (Ridone et al., 2020). Hence, a disruption of membrane cholesterol amend the organization and activity of PIEZO1 channel (Short, 2020). Moreover, lipids deeply affect the structure and function of other transporter proteins in the RBCs membrane (Stieger et al., 2021).

c) Lipid rafts

The heterogeneity in local membrane lipid composition gives rise to areas that differ in their biophysical properties like lipid order, curvature, and thickness (Conrard and Tyteca, 2019). Hence, lipids in RBCs are found to be clustered in submicrometric domains. Three domains of rapid kinetics have been highlighted in the erythrocytes' outer membrane leaflet (Tyteca et al., 2010; Conrard et al., 2018). The first is found in high-curvature membrane areas. This domain is enriched in cholesterol and is formed upon cellular deformation (Leonard et al., 2017). The two other domains are associated with low-curvature membrane areas; one is found to be enriched in cholesterol, PC, and ganglioside GM1, hence called GM1-enriched domain. The other one is enriched in cholesterol, PC, and sphingomyelin, hence called sphingomyelin-enriched domain. The particularity of these two last domains is that the first (GM1-enriched domain) domain's abundance increases upon PIEZO1 channel activation, whereas the second (sphingomyelin-enriched domain)'s abundance is enhanced with Ca^{2+} efflux (Leonard et al., 2017). In the inner leaflet, only one domain is described and it is found to be enriched in ceramide (Cloos et al., 2020) (Figure 6).

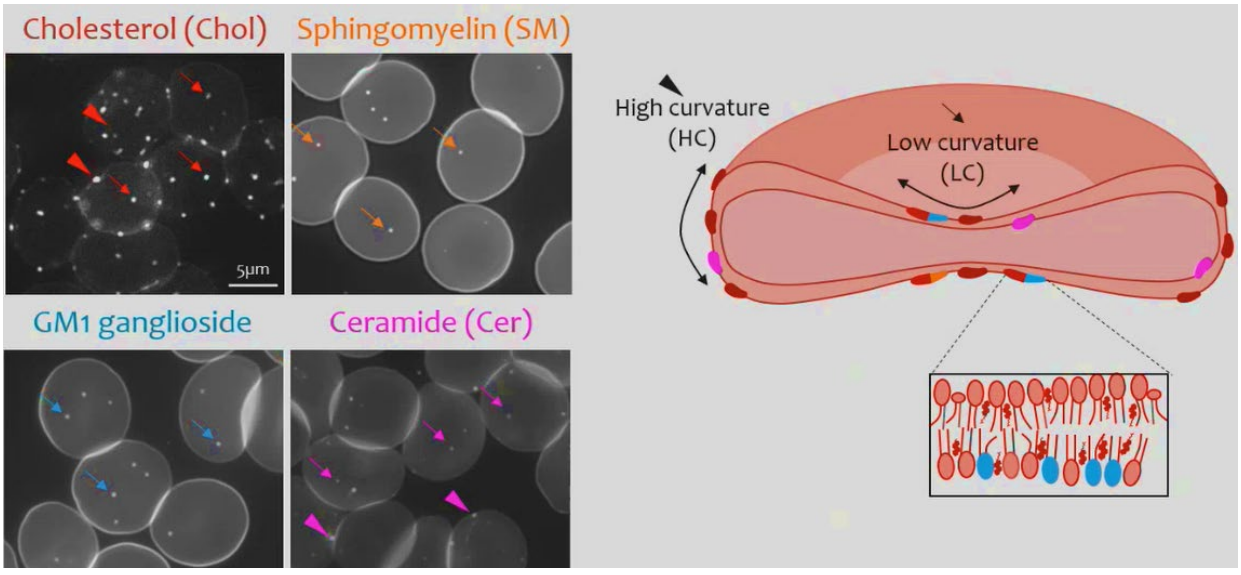

Figure 6: Membrane lipid lateral asymmetry in submicrometric domains or lipid rafts. Figure adapted from Pr. Donatienne Tyteca's presentation in the 11th international meeting on Neuroacanthocytosis syndromes on the 17th of September 2023 in Homburg-Germany. (Tyteca et al., 2010; D'auria et al., 2011; Carquin et al., 2014, 2015; Leonard et al., 2017; Conrard et al., 2018)

2. RBC cytoskeleton

RBC cytoskeleton is a pseudo-hexagonal meshwork of proteins tightly anchored to the plasma membrane by means of two main types of interactions: the vertical interactions known as "ankyrin complex" and the horizontal interactions known as "actin junctional complex" (Marchesi and Steers, 1968; Bennett and Stenbuck, 1979; Li and Lykotrafitis, 2014; Lux, 2016) (Figure 7).

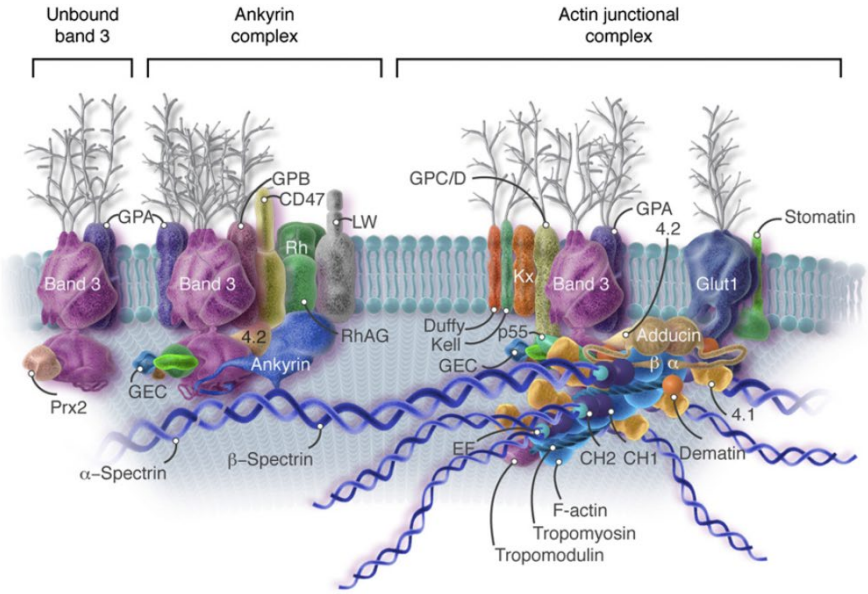

Figure 7: The RBC cytoskeleton's architecture (Lux, 2016).

a) Ankyrin complex

The ankyrin complex is a giant multiprotein complex found in the RBC's cytoskeleton. The cytoskeleton of RBCs is anchored to the membrane by this complex, which is assembled during erythropoiesis. It consists mainly of Ankyrin 1, Band 3, and protein 4.2 (Xia et al., 2022). In RBCs, Ankyrin-1 exists in 120,000 copies per cell (Burton and Bruce, 2011). It helps to maintain the structure of the membrane and coordinates the spatial organization of channels and transporters.

The ankyrin-1 protein has been identified and is known to mediate the linkage between Band 3 protein and underlying spectrin filaments (Bennett and Stenbuck, 1979; Vallese et al., 2022). Spectrin filaments are heterodimeric proteins with α and β subunits that are crucial for maintaining membrane stability, structure, and cell shape (Zhang et al., 2013). Band 3 proteins are present in the membrane in their tetrameric form (Bruce and Gyorffy, 2019), forming large transmembrane segments with attached polylactosaminoglycan molecules from the extracellular side, and a stalk-like cytoplasmic domain that is anchored to ankyrin-1. Ankyrin-1 itself binds to β-spectrin chains and to the adaptor protein 4.2 (Su et al., 2006). Glycophorin A (GPA) and B (GPB) are heterodimers with glycans attached and form part of the Ankyrin complex. The Rh complex is also attached to the Ankyrin complex and is formed of the Rh polypeptides, the RhAG, the CD47, the LW, and the glycophorin B (GPB) dimer. The CD47 enables a contact with the ankyrin-1 group by interacting with the 4.2R protein, and the Rh polypeptides (Mankelow et al., 2012). GLUT1 transporter in its role is linked to the Band 3 protein and form together a protein complex (Jiang et al., 2006a) that can be involved in the Ankyrin-1 complex.

b) Actin junctional complex

Junctional complexes also exist in the cytoskeleton of RBCs. Their main role is to maintain the membrane cytoskeletal connection through interactions of the integral proteins GPC/D with p55 and protein 4.1 (Mankelow et al., 2012). It is centred on the junction of spectrin tetramers which bind to short actin filament (Mankelow et al., 2012). Within this complex, the protein 4.1R interacts with p55 and β-spectrin (Mohandas and Chasis, 1993; Lee and Discher, 2001) in a region containing actin and actin-binding proteins like tropomyosin, tropomodulin, dematin, and β-adducin (An et al., 2007). In addition, Band 3 in its dimeric form (Bruce and Gyorffy, 2019), makes part in this complex together with GPA, GLUT1, GPC/D, Duffy, Kell, Kx and Stomatin, which are all integral membrane components (Mankelow et al., 2012; Li et al., 2023). There are 40,000 junctions per cell (Burton and Bruce, 2011).

3. VPS13

VPS13 is one of the novel RBC protein family with a molecular weight exceeding 340 kDa. It is approximately 16 nm long (Melia and Reinisch, 2022). It has been reported to be associated with β-adducin and β-actin (Shiokawa et al., 2013) and with the Kx protein (Park and Neiman, 2020).

Therefore, VPS13 almost certainly associates with the junctional complex. VPS13 has been reported to be a bulk lipid transporter and to interact with Xk protein (Park and Neiman, 2020; Peikert and Danek, 2023). It was also found to be involved in the vesicle-mediated sorting and is hence required for phagocytosis (Leonzino et al., 2021). The lipoproteins in individuals lacking VPS13 may exchange cholesterol and other lipids with the healthy donor RBCs during transfusion causing acanthocyte formation (Ohkawa et al., 2020; Peikert and Danek, 2023). Mutations in the VPS13 and XK genes cause chorea-acanthocytosis and McLeod syndrome respectively. Those two are syndrome of neuroacanthocytosis (Masana et al., 2021). VPS13 can also have a role in erythropoiesis since numerous cytoskeleton and membrane rearrangements take place during this procedure.

4. RBCs shapes

Given the important role of the cytoskeleton in determining the deformability of RBCs, it is obvious that any change in shape will also modulate deformability. In fact, the normal discocyte shape of RBCs, determined by all the above-mentioned membrane characteristics and others, could be altered by surrounding factors. Moreover, cell shape and surface-volume ratio are often found to be disturbed in diseases (Glogowska and Gallagher, 2015).

Deregulations and defects in any of the membrane lipids and cytoskeleton components lead to the loss of the deformability of RBCs membrane (Chasis et al., 1988). For example, RBCs may be prematurely destroyed if the phospholipid asymmetry is disrupted (Kuypers, 2007).

In the same extent, mutations in the genes related to the cytoskeletal Ankyrin complex (the vertical interactions) produce rapidly within the circulation spherocytic RBCs compromising their lifespan with a fast removal in the spleen (Perrotta et al., 2008). Their size is slightly smaller than an average RBC (Figure 8A) (Zamora and Schaefer, 2023) (see hereditary spherocytosis paragraph: paragraph D-3-a in the introduction).

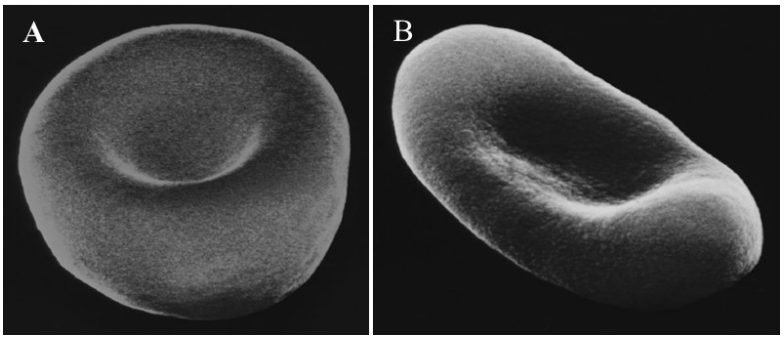

Figure 8: Scanning electron microscopy for a spherocyte (A) and an elliptocyte (B). Adapted from (Bessis, 1974).

Elliptocytes are another form of abnormally shaped RBCs. They appear oval or elongated under the microscope. They have a normal central pallor area with the Hb proteins appearing concentrated at the ends of the elongated cells (Figure 8B). They are commonly associated with hereditary elliptocytosis disease (see hereditary elliptocytosis paragraph: paragraph D-3-b in the introduction). Defects in the horizontal interactions (spectrin-actin interactions) of the cytoskeleton are usually the main reason of elliptocytes formations (Gallagher, 2004).

On the other hand, echinocytes and stomatocytes cell shapes are the result of converging factors like pH variation, the interactions of amphiphilic molecules in the outer layer of the cells, and extracellular ionic strength. These factors provoke reversible shape transformations (to a certain extent) at constant membrane surface area and cell volume (Iglic et al., 1998; Mukhopadhyay et al., 2002; Rudenko, 2010; Chen and Boyle, 2017).

Echinocytes are crenated RBCs, with spiculated membranes (Figure 9C), whereas stomatocytes are cup-like concave shapes (Figure 9A). These two shapes are classified into four subclasses I, II, III, and IV, according to their concavity and crenation stages.

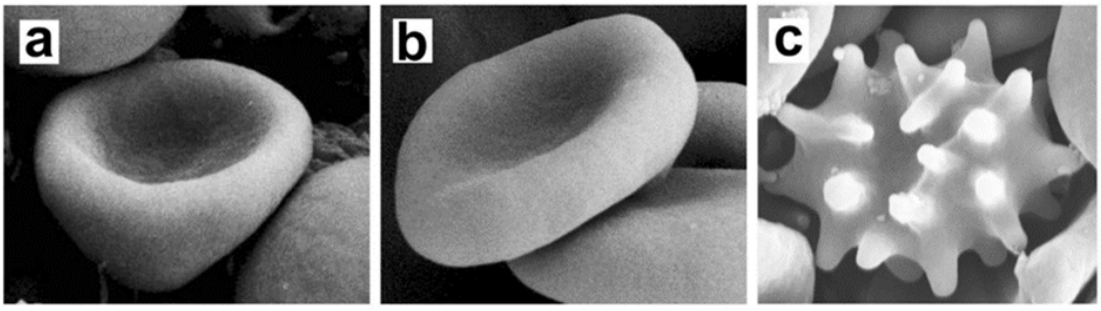

Figure 9: Scanning electron microscopy images of (a) open stomatocyte, (b) discocyte), and (c) echinocyte. Adapted from (Mesarec et al., 2019).

Conditions like anionic amphipaths, high salt, high pH, ATP depletion, cholesterol enrichment, and a proximity to a glass surface can transform a normal discocyte into an echinocyte. On the contrary, cationic amphipaths low salt, low pH, and cholesterol depletion, can transform a discocyte into a stomatocyte (Figure 10) (Gedde and Huestis, 1997; Tachev et al., 2004; Geekiyanage et al., 2019). These form changes are reversible and are known as "SDE transformations", which stands for stomatocyte-discocyte-echinocyte transformation (Rudenko, 2010). These shapes could further be altered into sphero-echinocytes and sphero-stomatocytes when smooth spheres are formed upon small interior buds and vesicles are pinched off from the cell surface leading to irreversible loss of surface area.

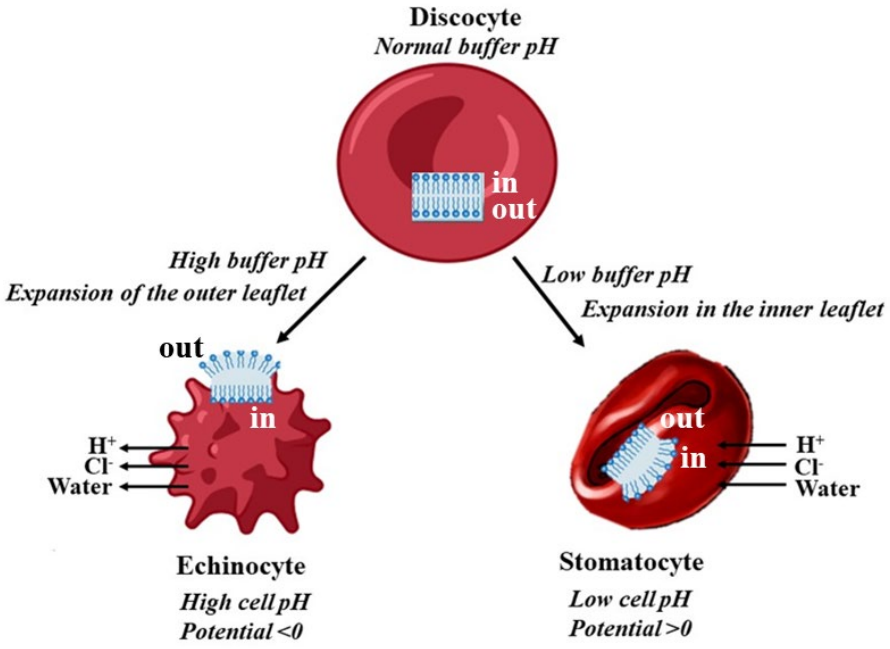

Figure 10: Change of red cells properties with altered external pH. To the left, an echinocyte is represented, and to the right, a stomatocyte. Figure inspired from (Gedde and Huestis, 1997; Lux, 2015) and recreated using Bio-Render.

These shape changes are directly linked to variations in the hydration state of the cells; in the case of stomatocytes formation, an increase in the cellular volume causes the decrease in the surface-area to volume ratio. This ratio is increased in the case of echinocytes formation due to decrease in cell volume (Geekiyanage et al., 2019).

Thus, RBC shape requires a coordinated activity of any membrane transporters that may influence the solute and water content (Brugnara, 2018). Indeed, changes in RBC deformability are thought to be the cause of a variety of diseases (Huisjes et al., 2018) including hereditary anemias with disorders in the hydration state (Gallagher, 2017).

5. Hydration status

Considering the consequences of the above-mentioned parameters that could influence deformability, it is noteworthy that the hydration status of RBCs is fundamental. Indeed, cell volume homeostasis is necessary for the maintenance of an adequate surface area-to-volume ratio, one of the keys for normal cellular deformation and for the maintenance of intracellular hemoglobin concentration at physiological levels (Narla and Mohandas, 2017). Considering a cell with 5 mM of negatively charged protein (Hb) sequestered with no chance to be exchanged at the membrane, this creates a huge oncotic pressure that will tend to attract any permeable cations. Thus, RBCs will encounter the threat of cell swelling up to critical lysis point. This is mostly prevented by an equilibrium of monovalent cations fluxes between the intracellular and extracellular media thanks to the pump-leak equilibrium. At resting state, erythrocytes have a high K^+ and a low Na^+ concentration which is the opposite in the surrounding plasma. A variety of mechanisms controls the intracellular ion concentration and water content of RBCs, which is a dynamic process. First, due to ion channel passive leakage caused by their electrochemical gradients. Second, comes the role of active and passive gradient transport. Finally, the activity of pumps can regulate the hydration status. They need ATP to pump cations against their concentration gradient (Teissie and Yow Tsong, 1981). Water passively adjusts its movement to that of ions, either through free diffusion across the membrane or through aquaporins (Cossins and Gibson, 1997). Water leaks through the erythrocyte membrane when the pump's capacity to stop cation leakage is surpassed, altering the intracellular cation concentration. The ensuing increase in the intracellular water may lead to intracellular diffusion of Na^+ that exceeds the extracellular diffusion of K^+, the cells swell. On the contrary, if the outward K^+ leakage exceeds the inward Na^+ leakage, the cells shrink.

C. Membrane transport

The essential role of any plasma membrane is to separate the cellular contents from the extracellular media, while maintaining controlled exchanges and communications.

1. Homeostasis

What characterizes all mammalian cells including RBCs, is the asymmetrical composition of the membranes and the non-equilibrium distribution of ions across the cell membrane. This difference in distribution is mandatory for cellular processes such as signal transduction, and cellular metabolism. The four main ways through which membrane transport takes place are, simple diffusion, facilitated diffusion, passive transport and active transport. They all work in concert to preserve a physiological volume, necessary for the normal functioning of the erythrocytes (Gallagher, 2017). The volume stability of the highly water-permeable RBCs relies on their low permeability to cations and a high permeability to neutral solutes like glucose or urea; the low cation permeability significantly rate-limits net salt and isosmotic fluid transfer, whereas the high neutral solute permeability allows rapid solute equilibration with minimal osmotic stress and volume displacement (Lew and Tiffert, 2017).

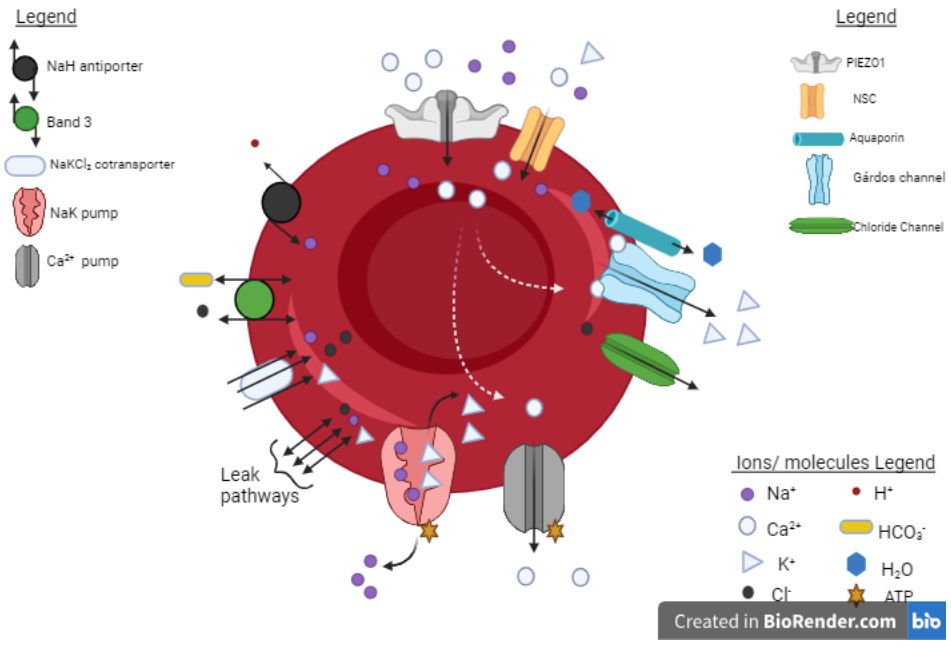

Figure 11: Figure summarizing the major membrane transport systems in the RBCs. Figure created with Bio-Render.

Water and ions homeostasis are regulated by various passive and active transport mechanisms (Figure 11). The balance between passive and active transport phenomenon is the basis of the maintenance of the intracellular cation concentration as well as the cell volume (Bernhardt and Weiss, 2003).

Permeability of all ions present inside and outside of the cell contribute to the determination of its membrane potential according to the Goldman-Hodgkin-Katz equation (Goldman, 1943) (Equation 1):

$$\textbf{Equation 1: } V_M = \frac{RT}{F} ln \frac{P_{K^+}[K^+]_o + P_{Na^+}[Na^+]_o + P_{Cl^-}[Cl^-]_i + 4P_{Ca^{2+}}[Ca^{2+}]_o}{P_{K^+}[K^+]_i + P_{Na^+}[Na^+]_i + P_{Cl^-}[Cl^-]_o + 4P_{Ca^{2+}}[Ca^{2+}]_i}$$

With V_M: the membrane potential (in V),

R: The ideal gas constant (≈8.31 J/(K.mol))

T: The temperature in K

F: The Faraday constant (in C/mol)

P_X: the permeability for ion X (in m/s)

$[X]_o$: The extracellular concentration of ion X

$[X]_i$: The intracellular concentration of ion X

Thus, the movements of ions throughout the cells are determined by their own gradient and permeabilities, and their own equilibrium potential can be calculated using the Nernst equation. Ion transport takes place through specific ion channels, which, although not numerous on the membrane of RBCs (Egée et al., 2002; Kaestner, 2015), are recognized as physiologically important signaling mediators in RBCs (von Lindern et al., 2022). The identification of ion channels on the membrane of RBCs is not a straightforward task, as it is difficult to match functional channel recordings with the channels 'molecular identities' of the channels (Kaestner, 2015).

In fact, human erythrocytes have a higher permeability for anions (especially Cl^- and HCO_3^-) than for cations of the same hydrophilicity and size (such as Na^+ or K^+). Specifically, erythrocytes have a relatively high chloride conductance G_{Cl^-} (anion permeability) of about 25 µS.cm^{-2} (Bennekou, 1999), which dominates the overall membrane permeability of the RBCs. Therefore, the resting

membrane potential of RBCs is near to the Nernst equation for Cl^- (Equation 2), which facilitates CO_2 transport and the "chloride shift" phenomenon that occurs throughout the Band 3 protein (Hoffman and Geibel, 2005).

$$\textbf{Equation 2: } V_M = \frac{RT}{F} ln \frac{[Cl^-]_i}{[Cl^-]_o} = E_{Cl^-} \approx \textbf{-10 mV}$$

2. Pump-leak concept

Investigations about ion transport across RBCs membrane resulted in the formulation of the "pump-leak" concept in the 1960 (Tosteson and Hoffman, 1960).

The pump-leak concept in RBCs refers to the mechanism that helps to maintain the proper balance of ions, in particular Na^+ and K^+, within the cells. A fundamental principle of a non-equilibrium distribution of ions across the membrane lead to the conclusion that RBC membrane is impermeable to cations (Bernhardt and Ellory, 2003). Nevertheless, although negligible in mature healthy cells, cation fluxes exist, they are mainly represented by leaks of Na^+ and K^+ that are efficiently minute compensated by the powerful $3Na^+/2K^+$ ATPase pump (NaK pump) in order to maintain the concentration gradient and a constant cellular volume by preventing any dysregulations leading to cellular lysis (Gallagher, 2017; Caulier et al., 2018). The pump-leak concept is crucial for maintaining the appropriate ion composition within the RBCs which is essential for their normal functioning including O_2 transport and the maintenance of the cell shape (Gatto and Milanick, 2009).

3. Na^+/K^+ pump

Blood serum has a K^+ concentration of 3-5 mM, whereas Na^+ concentration ranges between 136-142 mM. Inversely, inside the RBCs, K^+ concentration ranges between 140-150 mM and Na^+ concentration is around 10-15 mM (Balach et al., 2019). In normal RBCs, the transmembrane distributions of those two ions are preserved far from their electrochemical gradient thanks to the activity of the plasma membrane $3Na^+/2K^+$ ATPase pump that was first discovered in 1957 (Skou, 1957). It is a transmembrane protein with three subunits labelled α,β, and FXYD (Morth et al., 2007). Its main function is the transport of ions against their electrochemical gradient; 3 ions of sodium are pump out and 2 ions of potassium in the cells by using an ATP molecule (Gallagher, 2017). This pump is activated by Na^+ and ATP at the cytoplasmic sites, and by K^+ and ATP at the

extracellular sites (Therien and Blostein, 2000). The pump leak turnover rate of Na^+ and K^+ is about 2-3 mmol/(L_{cells}.h) in middle age RBCs (Lew and Tiffert, 2017).

Hence, the $3Na^+/2K^+$ ATPase pump's main function is to maintain a low Na^+, high K^+ intracellular concentration at normal body temperature. The activity of this pump is essential in the maintenance of the cellular volume and ensures the homeostatic adjustments of RBCs in face of the environmental perturbations; it sets up the major cation gradient across the membrane. There are estimated to be 250 pump sites/cell with 100 ions that pass per second per site (Hamill, 1983). Another source stated that RBCs have only 100 copies of this pump in their membranes (Gatto and Milanick, 2009). Although present at low copy numbers, it is sufficient to maintain the electrochemical gradient of Na^+ and K^+ (Flatt and Bruce, 2018).

This pump participates in maintaining the osmotic equilibrium and the membrane potential in the cells; by regulating the Na^+ and K^+ concentrations, the NaK pump prevents excessive swelling or shrinking of RBCs (Pirahanchi et al., 2023).

NaK pump can be pharmacologically inhibited with ouabain and bumetanide (Flatt and Bruce, 2018).

4. Ca^{2+} pump

If Na^+ and K^+ are the main cations crossing the membrane, calcium leak is also present; RBCs undergo random Ca^{2+} entry, or Ca^{2+} leaks (Baunbaek and Bennekou, 2008).

Ca^{2+} has around four orders of magnitude higher concentration in the plasma than it is inside the RBCs (in the plasma ~ 1.8 mM, inside the cells ~30-60 nM) (Harrison and Long, 1968; Bogdanova et al., 2013). This significant inward Ca^{2+} electrochemical gradient would represent a permanent threat. Fortunately, this situation is monitored by the plasma membrane Ca^{2+} ATPase pump (also known as PMCA: Plasma membrane calcium ATPase) that shifts out Ca^{2+} from the cytosol, against its concentration gradient (Lew et al., 1982), maintaining by such a negligible activity of the Gárdos channel under normal conditions (Lew et al., 2003).

PMCA was first identified in erythrocytes in 1966 (Schatzmann, 1966) and it belongs to the P-type ion pumps (Kubitscheck et al., 1995). It is one of the most efficient calcium pumps found in

eukaryotes (Lew et al., 1982). There exist four different PMCA1-4 expressed by the genes *ATP2B1-4* (Schatzmann, 1983).

PMCA1 is expressed in the membrane of human RBCs and it comprises 1220 amino acids forming ten transmembrane domains, two intracellular loops containing ATP binding and phosphorylation sites and inward-facing *N*- and *C*- terminals. In addition, PMCA4 is found in the membrane of RBCs (Krebs, 2017).

Ca^{2+}-extrusion via PMCA can vary between 4-60 mmol/(L_{cells}.h), three orders of magnitude higher than the turnover rate of Ca^{2+} in physiological conditions which is around 20-50 µmol/(L_{cells}.h) (Lew et al., 1982). Increases in the intracellular free Ca^{2+} concentrations are sensed by the PMCA and occur in response to the interaction of Ca^{2+}-calmodulin complex with C-terminus of the pump (Vincenzi et al., 1980). ATP availability is the limiting factor for PMCA transport capacity (Bogdanova et al., 2013).

Together with the Na/K pump, Ca pump set up the major cation gradients across the membranes.

5. Aquaporin

Erythrocytes have high permeability to water frequently observed via osmosis studies. Lipid bilayer itself, having only a finite permeability to water, cannot be accounted for instantaneous hemolysis occurring when in hypotonic solutions. This is the role of Aquaporin, which is an aqueous channel found across the membrane.

Aquaporins (AQPs) are a family of small channel-forming integral membrane protein of 28-kDa (Agre et al., 1987), found in human erythrocytes. Aquaporin-1 (AQP1) has around 200.000 copies per cell (Sugie et al., 2018). Its selectively permits the transport of H_2O molecules across the membrane (Macey, 1984; Denker et al., 1988; Agre et al., 1993). AQP1 is located at the same interface of Band 3, protein 4.2 (Vallese et al., 2022). It interacts with Stomatin, a widely expressed integral protein that is found to be attached to GLUT1, Band 3, and others (Rungaldier et al., 2013).

AQP1 was also suggested to function as a gas channel, transporting CO_2 (Cooper et al., 2002; Blank and Ehmke, 2003).

6. Band 3

Band 3, also known as the anion exchanger protein (AE1, CD233, or SLC4A1), is the most abundant transmembrane glycoprotein on human RBC membrane. It allows the chloride/bicarbonate exchange throughout the RBCs, as explained in paragraph I-A-1 (The Jacobs-Stewart cycle). It is an anion antiporter with a molecular weight of 95-100000 (Bretscher, 1971; Cabantchik and Rothstein, 1974; Sabban et al., 1981), and a membrane domain with 12 membrane spans (Tanner, 1997). Band 3 can form dimers or tetramers with approximately 120,000 tetramers, and 320,000 "free" dimers (Burton and Bruce, 2011). It plays an important role in maintaining the structure and function of RBCs by controlling gas exchange, pH regulation, and cell membrane stability (Alper, 1991). In addition, Band 3 anchors the sub-membrane protein skeleton to the lipid bilayer, which is essential for maintaining the mechanical properties of RBCs. Band 3-defective RBCs are highly unstable despite containing a normally assembled cytoskeleton. This finding suggests that Band 3 stabilizes the membrane bilayer of normal RBCs by interacting with its lipids. Band 3 mutations (*SLC4A1* gene) are also associated with many hemolytic anemias including hereditary spherocytosis (Tanner, 1997; Perrotta et al., 2008). Next to its function as anion exchanger of Cl^-/HCO_3^-, Band 3 can act as an electrogenic chloride channel; it mediates Cl^- flux and contributes to its electrical conductance (Kaplan et al., 1983).

In addition to Band 3, there are other membrane transporters capable of transporting chloride anions.

7. Chloride channels

Although several studies have attempted to define the exact nature of chloride channels in RBCs, their true identity is still undefined. However, with the discovery of New Permeation Pathways (NPPs) in malaria-infected RBCs (Kirk et al., 1994), research on anionic permeability regained interest as chloride channels were hypothesized to be used in the treatment of malaria (Kirk, 2000; Huber et al., 2002). The use of patch-clamp on human red cells led to the proposal of several candidates for chloride channels (Egée et al., 2002); in addition to the apparent role of Band 3 in Cl^- transport, CFTR (Verloo et al., 2004; Lange et al., 2006), ClC-2 (Huber et al., 2004; Bouyer et al., 2007), and VDAC (Bouyer et al., 2011) have been suggested as candidates.

The next paragraphs succinctly present the different anion channels that have been described in the literature.

a) Voltage-Dependent Anion channel (VDAC)

The VDAC is a multifunctional pore channel with three different isotypes (VDAC1, VDAC2, and VDAC3). It is a protein of the porin family known for its presence in the mitochondrial membrane, and its plasmalemmal form is present in many cell types (Sabirov and Merzlyak, 2012), including RBCs (Bouyer et al., 2011; Marginedas-Freixa et al., 2018). In the membrane of the RBCs, a 32 kDa associated VDAC is found that forms a peripheral benzodiazepine receptor-like complex with a translocator protein (TSPO) and an adenine nucleotide transporter (ANT) (Bouyer et al., 2011; Marginedas-Freixa et al., 2018). The activity of this "channel", whether its conductance or selectivity, is voltage-dependent; it is optimal at a membrane potential close to -10 mV, which is the resting membrane state of a RBC (Cheng et al., 1980). At higher potentials, more negative or positive, the activity of VDAC is altered, resulting in more frequent closing episodes. VDAC is permeable to small ions such as Na^+ and Cl^-, large anions such as ATP (Leal Denis et al., 2016), and large cations such as dopamine. At low conductances, VDAC1 has a remarkable higher permeability to Ca^{2+}, especially when it dimerizes. To date, little is known about the mode of action of VDAC (Kaestner et al., 2020).

b) CFTR

Cystic fibrosis transmembrane conductance regulator (CFTR), the cAMP-regulated Cl^- channel, first described in the epithelia (Riordan et al., 1989), was also found to be expressed in the human RBCs (Abraham et al., 2001). It is a member of the ATP-binding cassette and its activity was described as essential for the deformation-induced release of ATP in RBCs (Sprague et al., 1998), and subsequent activation of the NO synthesis, regulating by such the vessel tone (Sprague et al., 2003; Liang et al., 2005). CFTR is found to be mutated in patients with cystic fibrosis (Sterling et al., 2004). CFTR was also associated to the increased permeability of malaria patients (Verloo et al., 2004). Quantitative studies revealed the presence of about 650 CFTR molecules per normal RBCs, and around 200 CFTR in cystic fibrosis patients (Schillers, 2008). Nevertheless, the presence of CFTR in mature RBCs is still under debate (Hoffman et al., 2004) and was not found

in the recent proteome analysis performed on erythroid progenitors (Gautier et al., 2018; Karayel et al., 2020).

c) ClC-2

ClC-2 is an inwardly rectifying chloride channel (Thiemann et al., 1992) that is activated by membrane hyperpolarization (Pusch et al., 1999) and reversibly activated by hypotonicity-induced cell swelling (Gründer et al., 1992) and decreased extracellular pH (Jentsch et al., 2002). Its activity is also dependent on the intracellular Cl^- concentrations (Pusch et al., 1999). The cell swelling-induced activation, requires oxidative stress stimulation. This suggests that ClC-2 is involved in physiological processes related to oxidative stress and probably in the execution of the suicidal death program. ClC-2 may also contribute to the NPPs pathways in malaria infected RBCs, since part of the currents generated in *Plasmodium* infected RBCs are sensitive to Zn^{2+} (Huber et al., 2004; Bouyer et al., 2007).

Despite the numerous results, the exact nature of the RBC anionic conductance that drives the membrane potential and thus the respiratory function is still elusive. In fact, all the channels described so far, if they really exist, are present in limited number (around 100 copies/cell). Therefore, the hypothesis that Band 3 is the main chloride pathway and generates the chloride conductance is valid (Freedman and Novak, 1997).

8. Cotransporters and antiporters

RBC membrane is privileged with a cotransporter system made of symporters and antiporters (Figure 12).

Symporters like Na^+-K^+-$2Cl^-$, K^+-Cl^-, Na^+-dependent amino acid transport, and Na^+/Mg^{2+} antiporter, Na^+/H^+ antiporter, Na^+/Li^+ antiporter (Semplicini et al., 1989), and $K^+(Na^+)/H^+$ exchanger, are the most studied in RBCs (Bernhardt and Weiss, 2003).

Among these, NKCC and KCC are two Cl^- - dependent transport pathways for K^+ (Ellory and Stewart, 1982).

Figure 12: Summary of the principal transport pathway (cotransporters and symporters), and pumps system in human RBCs. Figure created with Bio-Render.

a) Na-K-2Cl cotransporter

First described in 1989 (Haas, 1989), it makes part of the cation-Cl cotransporters (CCCs) family (Isenring and Forbush, 2001), It is the main cotransporter that is involved in K^+ homeostasis Encoded by the *NKCC1* gene. It moves one Na^+, one K^+, and two Cl^- in the same direction of the cell in an electroneutral manner (Flatman, 2005; Flatt and Bruce, 2018). Therefore, the activity of this cotransporter is not affected by any alterations in the transmembrane potential, neither its activity can affect the membrane potential of the cell. Normally, Cl^- is at electrochemical equilibrium in RBCs, making the cotransporter close to equilibrium and the net direction transport of the ions dependent on the concentration of the extracellular potassium ion. Basically, the cells have recourse to that cotransporter in order to maintain a low cellular volume in mature red cells. NaK2Cl cotransporter is not much effective in human red cells, having a flux of less than 1 mmol. $(1_{cell}. h)^{-1}$. This flux varies among species, and in the same specie it can vary with certain diseases; for instance, women with history of hypertension have lower fluxes through this cotransporter (Tepper et al., 1998; Orlov et al., 2015). Alterations in the phosphorylation of proteins present in the cascade of the activation of NaK2Cl cotransporter (kinases specifically) may alter its activity and its interaction with other regulatory proteins as it was demonstrated in ferret RBCs (Flatman, 2002). These NaCl and KCl fluxes result in rehydration of RBCs (Zheng et al., 2019). Also, in avian erythrocytes there is found an activation of the NaK2Cl by the mediation of cAMP (Palfrey

and Rao, 1983).yet much more is to be made in order to discover that cotransporter functioning in human RBCs (Flatman, 2005). NaK2Cl is inhibited by loop diuretics such as mercury (Isenring and Forbush, 2001) or drugs like bumetanide and furosemide (Flatt and Bruce, 2018).

b) K-Cl cotransporter

It is an electroneutral cation-chloride cotransporter that belongs to the CCCs family (Isenring and Forbush, 2001). It is encoded by the *KCC* gene. Its activation results in an outward flux of K^+, Cl^- and water, leading to a decrease in cell volume and an increase in the cellular hemoglobin concentration. It is considered as a housekeeping membrane protein responsible for normal cell function (Garneau et al., 2019). The activity of this cotransporter is very well remarkable during the reticulocyte maturation, and this activity progressively became negligible in mature, circulating RBCs (Hoffman, 1987). There are three isoforms of KCC in human erythrocyte (KCC1, KCC3 and KCC4) even though the function of each is not determined yet (Gillen et al., 1996). Shear stress can activate the KCl transporter via a cooperation with some components of the cell cytoskeleton (Ellory and Hall, 1988). Dysregulations in KCC lead to various complex cases of Sickle Cell Disease (SCD) (Gibson et al., 1998). Indeed, KCl cotransporter may contribute to fast dehydration since it is also pH sensitive (Lew and Bookchin, 2005), which generally occurs after Gárdos channel activation and the subsequent primary loss of water upon deoxygenation, worsening the sickling up to irreversibility.

9. Cation conductance

Human erythrocytes contain and keep up large levels of intracellular K^+ together with low intracellular Na^+ (Tosteson and Hoffman, 1960). They also have no intracellular Ca^{2+} reserves, although they nonetheless have a cytosolic free Ca^{2+} concentration of roughly 60 nM (David-Dufilho et al., 1988; Soldati et al., 1999). This is made possible by the erythrocyte membrane's extremely low resting Ca^{2+} permeability and strong Ca^{2+} pump (Scharff and Foder, 1982). The homeostasis of RBCs requires stable low cation movements which is necessary for normal RBC shape and for the preservation of rheological properties. Several reports in the literature pointed that cation transport in RBCs could be triggered by raising mechanical stress (i.e.: deformation)

and by abnormal membrane skeleton (Larsen et al., 1981; Johnson, 1994; Joiner et al., 1995; Dyrda et al., 2010).

a) Calcium and RBCs

As the erythrocyte cytosol has a relatively low Ca^{2+} buffering capacity (Tiffert and Lew, 1997), any Ca^{2+} entry can cause a large increase in free intracellular Ca^{2+} concentrations (Lang et al., 2003a). An overabundance of intracellular calcium concentration $[Ca^{2+}]_i$ is a major cause of erythrocyte dysfunction, which can lead to changes in erythrocyte properties (Bogdanova et al., 2013), such as an activation of the protease calpain which digests the cytoskeleton and an increase of PS exposure (Lang et al., 2004, 2005; Zwaal et al., 2005), microvesicles formation (Gonzalez et al., 2009), and membrane scrambling (Woon et al., 1999; Bevers and Williamson, 2010). Elevated intracellular Ca^{2+} concentrations activate the Gárdos channel triggering K^+, Cl^-, and water efflux, and thus cellular shrinkage (see paragraph I-C-9-g in the introduction) (Dyrda et al., 2010; Rapetti-Mauss et al., 2017). This can cause premature RBC clearance in the spleen, according to several shreds of evidences (Kaestner et al., 2020). Changes in RBCs behaviors following Ca^{2+} entry were exhaustively described in the literature (Nguyen et al., 2011; Steffen et al., 2011; Tiffert and Lew, 2011; Muravyov and Tikhomirova, 2012; Hertz et al., 2017).

Ca^{2+} inward has other consequences on RBCs physiology: it induces an ATP release (Cinar et al., 2015) which affects the cells with a wide spectrum of effects including the regulation of the vascular tone (Ellsworth et al., 1995), it induces an increase in the erythrocytes' stiffness with loss of deformability and elasticity (Dreher et al., 1980), and finally it affects the activity of Na^+ pump (Brown and Lew, 1983). Due to the small size of human RBCs, Ca^{2+} diffusion within the cytosol has been recently calculated to be very fast, rising by such the risk of immediate deleterious consequences (Vaisey et al., 2022).

Different cation channels (discussed later) are involved in intracellular Ca^{2+} increase in RBCs, in addition to some pathogenic variants of the electroneutral membrane transporters such as RHAG, SLC2A1/GLUT1, and SLC4A1/AE1 (Flatt and Bruce, 2018).

There are two main families of channels that are directly linked to the activity of calcium ions: on the one hand, there are the Ca^{2+}-activated channels, in particular Gárdos channel, which extrudes K^+ ions out of the cells upon calcium entry, followed by Cl^- , and then water, thus dehydrating the

cells (Fermo et al., 2020). On the other hand, there is (ii) the family of ion channels that make the plasma membrane permeable to Ca^{2+}, such as PIEZO1, NMDA receptor, VDAC, TRPC6, and TRPV2 channels (Figure 13). The Ca^{2+} -permeable cation channels may be activated upon different stress stimuli (Lang et al., 2003a) such as hyperosmotic shock, glucose-depletion, abnormal decreases in extracellular or intracellular Cl^- concentrations (Huber et al., 2001), and oxidative stress (Duranton et al., 2002).

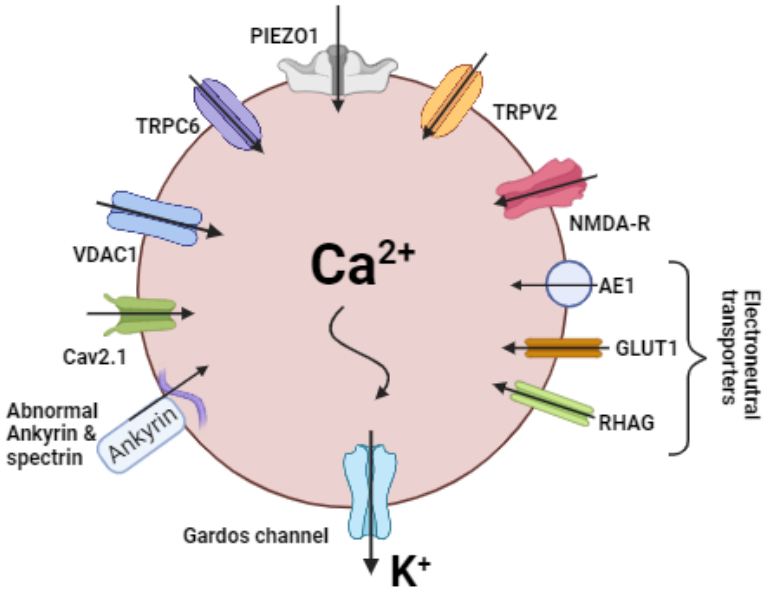

Figure 13: Main transporters leading to Ca^{2+} increase and subsequent Gárdos channel activation. This scheme groups together all the possible causes of an increase in intracellular Ca^{2+} (cytoskeleton abnormalities, ion channels to be discussed, and other electroneutral transporters), and the main effect of this increase, which is the activation of the Gárdos channel. Scheme created with Bio-Render.

b) Non-selective voltage dependent cation channels (NSVDC)

The presence of NSVDC was first suggested in 1989 (Halperin et al., 1989), and then demonstrated by single-channel patch-clamp technique in 1991. Its unitary conductance is around 20 pS, and its activation induces strong depolarizations of the RBC membrane (Christophersen and Bennekou, 1991). Its presence could also be detected following whole-cell and nystatin-perforated patch-clamp recordings (Rodighiero et al., 2004). This channel is permeable to divalent cations such as Ca^{2+}, Mg^{2+}, and Ba^{2+} (Kaestner and Bernhardt, 2002), but also to monovalent cations such as Na^+, K^+ (Kaestner et al., 1999) and its activation produces a hysteretic-like behavior (Kaestner et al.,

2000; Bennekou et al., 2004). NSVDC induces repolarizations under Low Ionic strength (LIS) conditions, in which Na^+ and Cl^- ions of the solution are replaced by sucrose molecules, triggering immediate strong depolarizations of the plasma membrane (Moersdorf et al., 2013). It is sensitive to acetylcholine (Bennekou, 1993) and can be stimulated by PGE_2 receptors (Kaestner et al., 2004; Lang et al., 2005). Clotrimazole and its analogues can directly activate the NSVDCs (Barksmann et al., 2004).

c) PIEZO1

PIEZO1 is a mechanosensitive (Coste et al., 2010, 2012; Wu et al., 2017; Guo et al., 2021), non-selective cation channel (NSC) (Gnanasambandam et al., 2015), present in a few hundred copies per RBC (Gautier et al., 2018), estimated around 80 copies only (Vaisey et al., 2022).

PIEZO1 is a large homotrimer (Ge et al., 2015), each monomer is composed of 2547 amino acids with 4.8 Angstrom of resolution (Ge et al., 2015; Zhao et al., 2018) and 38 transmembrane domains (TM) (Guo and MacKinnon, 2017) (Figure 14).

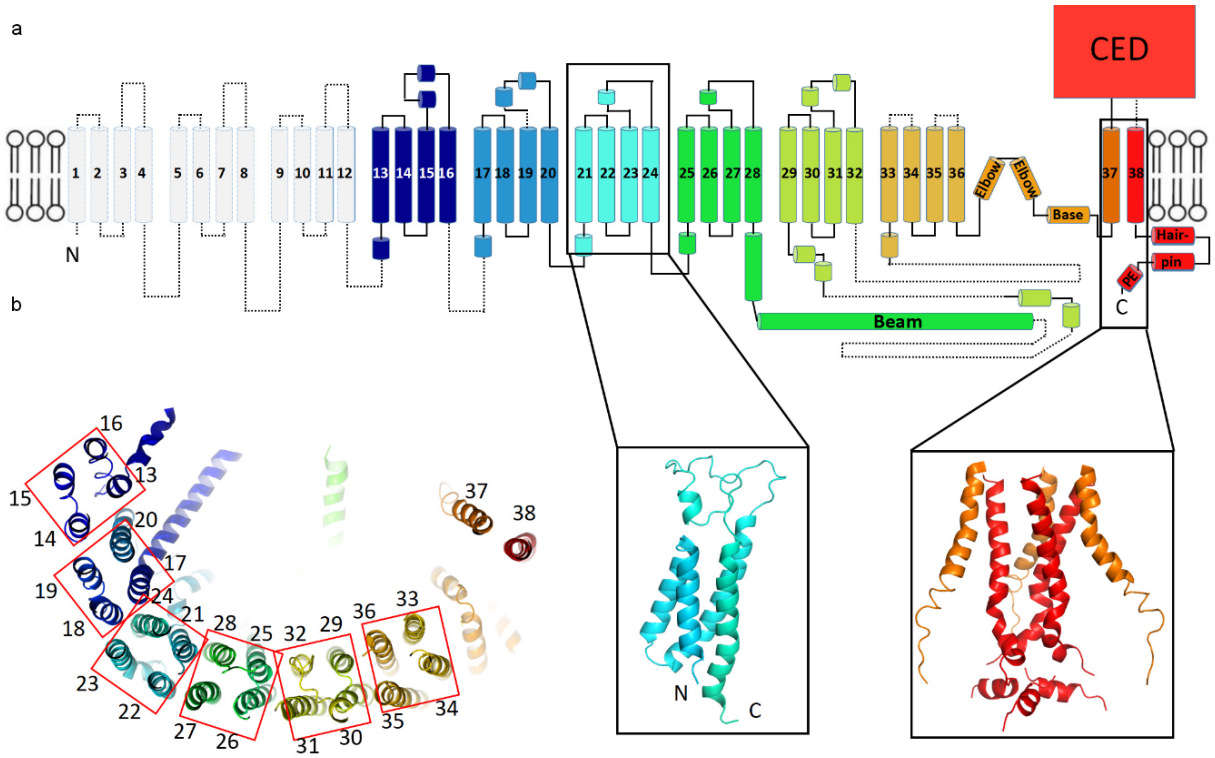

Figure 14: Topology of mPiezo1. (a) Cartoon representation of a monomer, rainbow-colored with C-terminus in red and N-terminus in blue, except for the first 12 TMs that are not visible. Helices within a single 4-TM unit are colored uniquely. Helices are shown as cylinders, loops as solid lines, and unresolved regions as dotted lines. C-terminal extracellular domain (CED) is simplified as a box. A ribbon diagram of 4-TM unit 6, consisting of TM 21 to 24, is shown in the left inset panel with N- and C- termini labelled. The right inset panel shows a ribbon diagram of the pore region, formed by TM37, TM38 and the PE helix from all three subunits. (b) A ribbon diagram of a monomer rainbow-colored as in A, viewed from top. Each 4-TM unit is highlighted in a red box with TM number labelled (Guo and MacKinnon, 2017).

It is encoded by *PIEZO1* or *FAM38A* gene found on chromosome 16q24.3 (Ge et al., 2015), and is a highly polymorphic gene (Lupski, 2012; Andolfo et al., 2019); many mutations can occur on *PIEZO1* gene without being perceptible due to the large structure of this channel (Filser et al., 2021). Its unitary conductance ranges between 35 and 55 pS (Gnanasambandam et al., 2015). PIEZO1 allows the passage of K^+, Na^+, Ca^{2+}, and Mg^{2+} according to their electrochemical gradient, once it is opened and as a result of the mechanotransduction (Coste et al., 2015; Gnanasambandam et al., 2015).

Structure: PIEZO1 channel has a three-dimensional structure (Figure 15), made up of three-bladed homotrimeric transmembrane helix in addition to an external cap. The intra-cytoplasmic domain, which extends from the transmembrane domain, is divided into three parts “the beams”. Each monomer has an extracellular domain (ECD) and an intracellular domain (CTD). This structure guarantees a core transmembrane duct that is hydrophilic and is surrounded by six helices, allowing ions to pass through. Thereby, the flexibility of the three blades makes PIEZO1 a mechanosensitive ion channel (Ge et al., 2015). Mechanical stimulations trigger membrane deformations and subsequent rotation of the PIEZO1’s blades which is transmitted to the ECD and CTD domains which lead to the channel’s opening in a lever-like manner (Figure 15) (Zhao et al., 2018). This structure ensures the ion selectivity of the channel, whether through the cap and its negatively-charged amino acids (Coste et al., 2015; Zhao et al., 2016), through the lateral portals of the CTD domain (Geng et al., 2020; Nosyreva et al., 2021), or via the inner pore at the level of the extracellular opening and the transmembrane domains (Geng et al., 2020; Jiang et al., 2021).

Activation: PIEZO1 channel activation is suggested to be triggered directly through sensing forces in the lipid membrane (Cox et al., 2016; Syeda et al., 2016), in addition to other suggested mechanisms like an activation by $MgCl_2$ (Gottlieb et al., 2012), or by a response to lateral

membrane tension (Lewis and Grandl, 2015), or by being regulated by Stomatin protein (Poole et al., 2014) and others (Peyronnet et al., 2013; Borbiro et al., 2015). PIEZO1 modifies the membrane locally into a dome shape. Hence, PIEZO1 opening is susceptible to alter membrane deformation. This change is proportional to the projected area under the dome (Guo and MacKinnon, 2017). Deformations affecting PIEZO1 are reversible, which shuts-off the channel leading it to return immediately to its original conformation (Guo and MacKinnon, 2017; Liang and Howard, 2018; Lin et al., 2019). The fraction of open PIEZO1 depends on the curvature and the shape of the cell due to the interaction between this channel and the membrane bilayer (Svetina et al., 2019). In other words, physical deformations of the lipid bilayer trigger PIEZO1 channel's activation obeying by such the so-called force-from-lipid paradigm (Cox et al., 2017; Vaisey et al., 2022). Yet, no studies have proven that PIEZO1 deactivation occurs in RBCs (Evans et al., 2020).

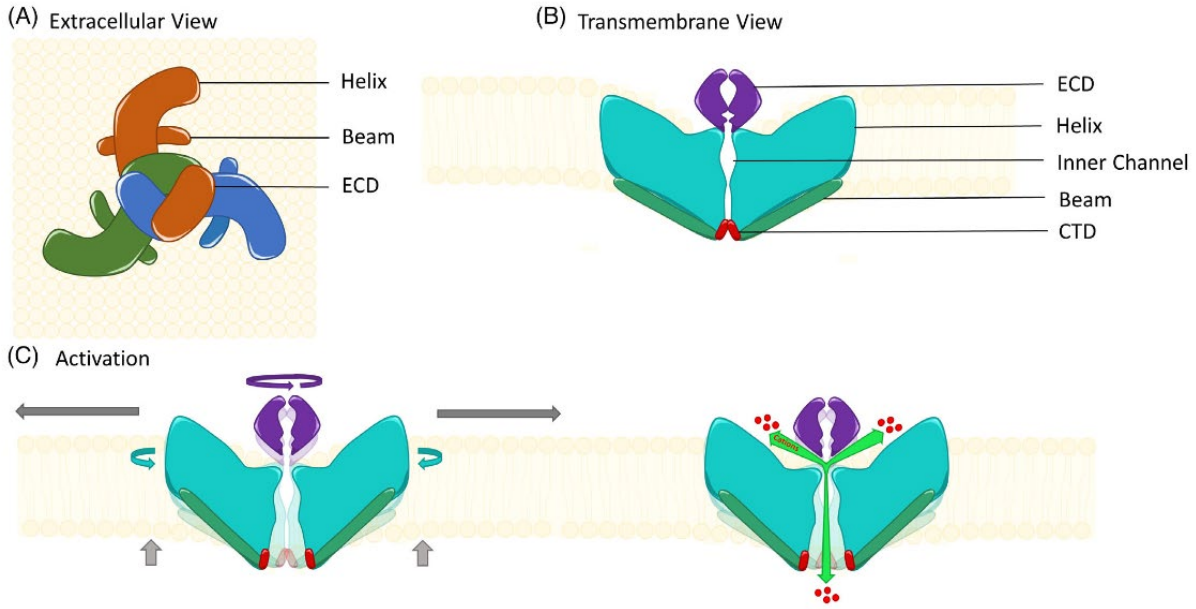

Figure 15: PIEZO1's structure. (A) extracellular view, each monomer is represented in green, blue, or orange. (B) Transmembrane view (C) Schematic activation of PIEZO1. The mechanical forces stretch the outer-dome generating a rotation of the helix followed by a rotation of the ECD. The transmission of the deformation to the beam trigger the channel's opening on the cytoplasmic domain in a lever-like fashion (Jankovsky et al., 2021).

Function in RBCs: At the RBC's level, PIEZO1 plays a role in the volume homeostasis of mature RBCs (Faucherre et al., 2014) and is involved in the erythropoiesis process (Caulier et al., 2020; Narla and Mohandas, 2020). Although it is present at few copies in the cells (Gautier et al., 2018;

Vaisey et al., 2022) PIEZO1 can modulate their hydration state in a considerable way (Risinger and Kalfa, 2020). Mainly it is responsible of the increase in $[Ca^{2+}]_i$ which threatens the cell's homeostasis. Massive calcium entries takes place in the RBCs in response to surrounding mechanical stretches upon PIEZO1 activation (Cahalan et al., 2015; Danielczok et al., 2017). PIEZO1 plays an essential role in erythrocytes because it regulates their hydration state which is mandatory to resist the osmotic pressure (Gallagher, 2017; Caulier et al., 2018).

PIEZO1-Gardos channel interplay: PIEZO1 channels lead to a massive calcium influx in the cells which will activate Gárdos channel (Lai et al., 2022). This will help in the cellular volume adaptation, especially when the cells undergo constrictions in small capillaries (Danielczok et al., 2017; Rogers and Lew, 2021a, 2021b). Thus, PIEZO1 seems to be the primary actor that can detect the curvature of the membrane and adjust the intracellular ionic content and cell volume in response to mechanical deformation (Kuchel and Shishmarev, 2017; Svetina et al., 2019) (Figure 16).

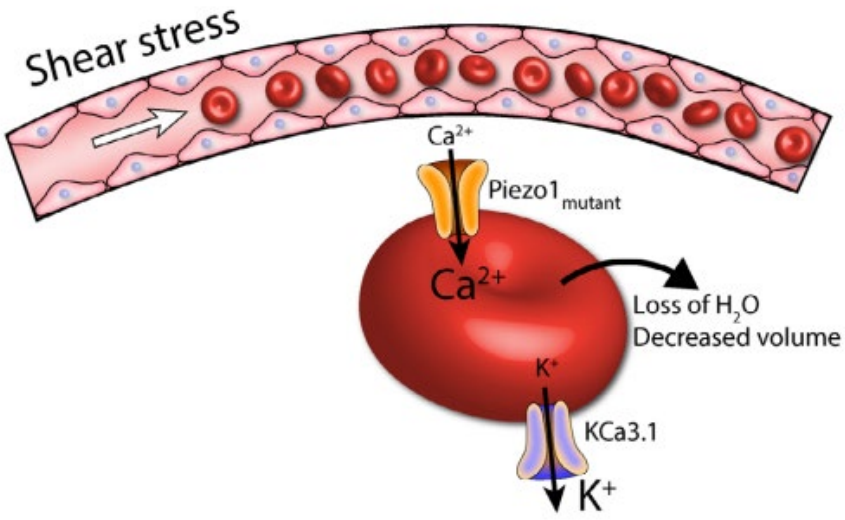

Figure 16: The activation of PIEZO1 by the encountered shear stress and its contribution to the cell volume regulation via the activation of the Gárdos channel (KCa3.1) (Lai et al., 2022).

Diseases and PIEZO1: Mutations in PIEZO1, which are generally gains of functions in RBCs, are commonly encountered in severe hereditary xerocytosis (Zarychanski et al., 2012; Picard et al., 2019; Filser et al., 2021). Also, the increased $[Ca^{2+}]_i$ due to Piezo1 activity has been suggested to be involved in sickle cell disease and the associated membrane transport disorder (Kaestner et al., 2020). Moreover, Filser *et al*. have managed to demonstrate that in several cases of idiopathic

erythrocytosis, there were found different variants of mutated *PIEZO1* resulting in defective hemoglobin and therefore dangerous consequences such as hypoxia, and an increase in 2.3-DPG due to the increase in the glycolysis (Filser et al., 2021). On the contrary, Ma and colleagues suggest that *PIEZO1* gain of function can be protective against malaria. One third of the African population carries a heterozygous PIEZO1 allele, E756del. Their RBCs are dehydrated and exhibit a resistance to the *Plasmodium* parasite reflected by the lowered infection rate of the cells (Ma et al., 2018). The pharmacological activation of human RBCs has recently been shown to prevent *Plasmodium falciparum* invasion by altering the membrane structure resulting in echinocytes formation (Lohia et al., 2023). *PIEZO1* locus was found to affect erythrocytes' MCHC (van der Harst et al., 2012). Mutations in PIEZO1 are associated with HX (Zarychanski et al., 2012; Albuisson et al., 2013; Bae et al., 2013; Glogowska et al., 2017) (paragraph I-D-2-a), and increased cation permeability in erythroid cells (paragraph II- Channels and erythropoiesis) (Andolfo et al., 2013a; Archer et al., 2014).

PIEZO1 can be pharmacologically activated with Yoda1 (Syeda et al., 2015; Lacroix et al., 2018), Jedi-1 and Jedi-2 (Wang et al., 2018), and inhibited using Dooku1 which is Yoda1's antagonist (Evans et al., 2018) or GsMTx-4 toxin (Bae et al., 2011).

The activation of PIEZO1 by Yoda1 is the most efficient with a high binding affinity to purified PIEZO1, and a half maximal effective concentration (EC_{50}) between 10-50 µM (Syeda et al., 2015; Wang et al., 2018). Yoda1 binding site is suggested to take place between two hydrophobic domains of the PIEZO1 monomer (Botello-Smith et al., 2019), and a cross-link between these two domains is suggested to block this Yoda1-mediated activation (Jiang et al., 2023).

d) Transient receptor potential channels (TRP)

Transient receptor potential channels (TRP) share biophysical properties with RBCs cationic electrodiffusive permeability such as Ca^{2+} permeability, cation selectivity, the current-voltage relationship, and the inactivity at resting conditions (Boulay et al., 1997). The two main types of TRP channels (TRPC and TRPV) were found to be present in the membrane of RBCs.

- **Transient receptor potential channels of Canonical type (TRPC)**

TRPCs are non-selective cation channels that are found on the membranes of RBCs. The isoform predominantly expressed on the membrane of circulating human RBCs is the TRPC6; its

expression in circulating RBCs and its role in baseline Ca^{2+} leak and stress-stimulated Ca^{2+} entry was demonstrated (Foller et al., 2008). It was also thought to modulate the calcium influx into RBC in response to progesterone (Fang et al., 2019). TRPC6 was detected in erythroid progenitor cells, and was suggested to participate to the eryptosis process (Foller et al., 2008). Nevertheless, TRPC6 was not found in the most recent proteomic analysis done on cultured progenitors (Gautier et al., 2016; Karayel et al., 2020). This channel thus plays a role in the control of erythrocyte survival. Recently, it has been hypothesized that the TRPC6 channel is transferred during spleen filtration of RBCs (Hertz et al., 2023).

Regarding other members of the TRPC family, an interaction between TRPC2 and TRPC3 was responsible for an erythropoietin-induced increase in Ca^{2+} levels in murine erythroid precursors and splenic erythroblasts (Kaestner et al., 2020). The activation of TRPC3 by erythropoietin leads to Ca^{2+} entry in human erythroid cells (Tong et al., 2008).

- **Transient receptor potential channels of Vanilloid type (TRPV)**

TRPV channels form a subfamily of six members (TRPV1, TRPV2, TRPV3, TRPV4, TRPV5, and TRPV6). They have been suggested to be heat sensors, and channels from TRPV1-4 have non-selective cation conducting pores, whereas the pores of TRPV5 and TRPV6 are only Ca^{2+}-selective (Samanta et al., 2018).

TRPV1 usually found in neurons, is one of the most well characterized and extensively studied TRP channel in mammalian cells usually found in vascular peripheral nerve cells, smooth muscle cells, and vascular endothelial cells (Tóth et al., 2014). It is activated upon temperatures higher than 42°C (Samanta et al., 2018). In human RBCs, TRPV1 was studied in the frame of unveiling the identity of P_{Sickle} conductance, yet it was found not to be implicated (Vandorpe et al., 2021b). Nevertheless, TRPV1 receptor was believed to contribute to primary afferent mechanical sensitization leading to hypersensitivity in mice with sickle cell disease (Hillery et al., 2011).

TRPV2 is a homotetramer (Muller et al., 2018), transmembrane, mechanosensitive (Moore and Liedtke, 2017), thermosensitive (noxious heat sensor of temperatures above 52°C), Ca^{2+}-permeable non-selective cation channel (Perálvarez-Marín et al., 2013; Samanta et al., 2018). It is expressed in most organs of the human body (Uhlén et al., 2015). TRPV2's coding gene is located

on the chromosome 17p11.2 and the result is a glycosylated membrane protein of 764 amino acids with a molecular weight of 86 kDa with six transmembrane regions and a pore-forming loop. N- and C- terminal tails are in the cytoplasmic side. It also contains six ankyrin repeats (Figure 17) (Atlas genetics, 2023).

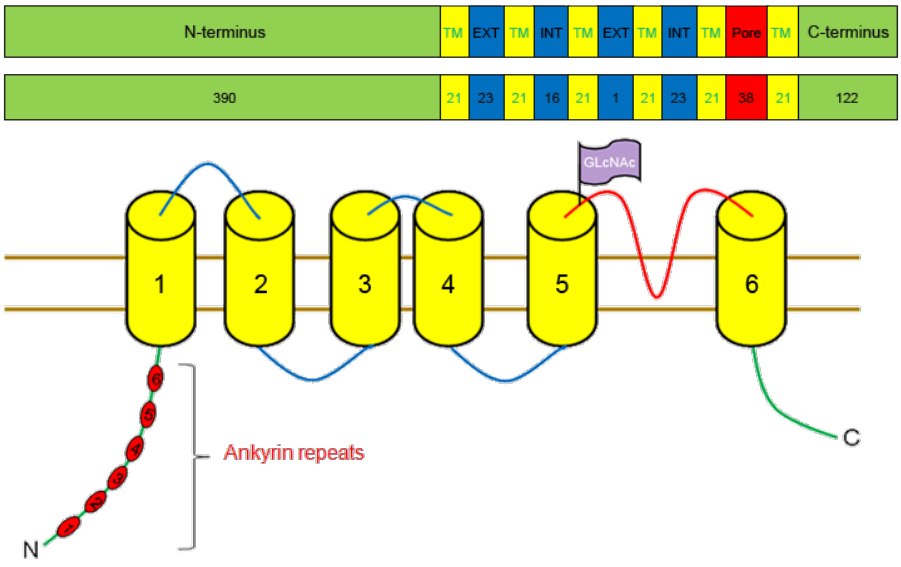

Figure 17: The canonical form of TRPV2 channel by (Atlas genetics, 2023)

Its presence has recently been reported in mouse and human erythrocytes (Belkacemi et al., 2021; Egée and Kaestner, 2021). The unitary conductance of TRPV2 channel ranges between 20-40 pS (Zhang et al., 2016). Its activation leads to Ca^{2+} entry with subsequent Gárdos channel activation (Figure 18). TRPV2 can be activated using *Cannabis sativa* products: CBD and Δ^9THC (Pumroy et al., 2019) making RBCs more resistant to lysis in response to hypotonic solutions (Belkacemi et al., 2021). In addition, 2-aminoethoxydiphenyl borate (2-APB) and probenecid are other exogeneous activators of TRPV2 while, tranilast, piperlongumine, trivalent cations, as well as SKF96365, amiloride, and ruthenium red are the known TRPV2 inhibitors (Moore and Liedtke, 2017). TRPV2 is not activated by vanilloids nor acidic pH (Conde et al., 2021; Pumroy et al., 2022).

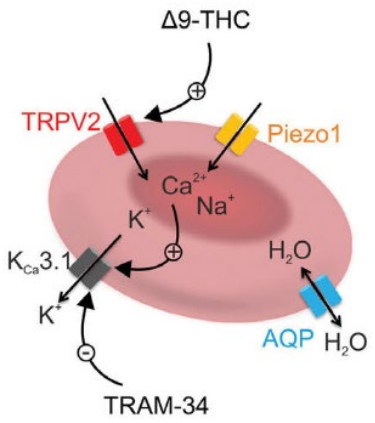

Figure 18: Scheme of TRPV2 activation cascade in RBCs (Belkacemi et al., 2021).

e) N-methyl D-Aspartate Receptor (NMDA-R)

NMDA-R are ionotropic glutamate receptors expressed in human circulating RBCs and they mediate the increase in the Ca^{2+} uptake of RBCs (Makhro et al., 2013) after being stimulated with glutamate or glycine (Makhro et al., 2016a). They act as non-selective cation channels when activated. RBCs progenitors express the Erythroid N-methyl D-Aspartate Receptor (eNMDA-R) (Reinhart et al., 2011), and it is known for its abnormally high activity in sickle cells patients and its high permeability to Ca^{2+} (Kaestner et al., 2020). During the differentiation, a lower number of the eNMDA-Rs are retained, therefore the subunit composition and the number of the expressed receptors vary (Makhro et al., 2013; Kaestner et al., 2020). Actually, there is around five receptors in mature RBCs and the subunit is mainly the GluN2C/2D which has a prolonged inactivation time and some small currents amplitudes (Kaestner et al., 2020).

NMDA-Rs are more abundantly present on the membranes of sickle red cells provoking a massive intracellular Ca^{2+} increase and alterations in the cells' properties and lifespan (Hänggi et al., 2014) eNMDA-R is activated by the homocysteic acid (Reinhart et al., 2011) and inhibited with memantine (Kaestner et al., 2020). Nevertheless, according to Reinhart *et al,* the activation or the inhibition of NMDA-R does not have any effect on the RBCs deformability and aggregability (Reinhart et al., 2011).

f) Voltage-activated calcium channels ($Ca_v2.1$)

$Ca_v2.1$ is the human voltage-gated (P/Q-type) Ca^{2+} channel whose pore-forming α1 subunit is encoded by the *CACNA1A* gene found on chromosome 19p13. It is composed of six transmembrane segments (S1-S6) and a pore connecting S5 and S6 (Pietrobon, 2010). This type of channels is found to be present in the RBCs although it is not detectable using the patch-clamp technique. It was described as a P-type calcium channel that could be specifically blocked by using the ω-Agatoxin-TK toxin (Teramoto et al., 1993). Importantly, it is a voltage-activated Ca^{2+} channel that was demonstrated to be the main isoform expressed in RBCs that necessitates a jump of voltage to be activated despite being non-excitable cells. There is an interaction between $Ca_v2.1$ and Gárdos channel (Figure 19) giving that the inactivation of this latter result in a depolarization in the cell (Kaestner et al., 2020). This channel was thought to be activated by an undetermined isoform of PKC, directly (Andrews et al., 2002) or indirectly via PKCα subunit (Wagner-Britz et al., 2013) provoking Ca^{2+} rise in RBCs (Andrews et al., 2002).

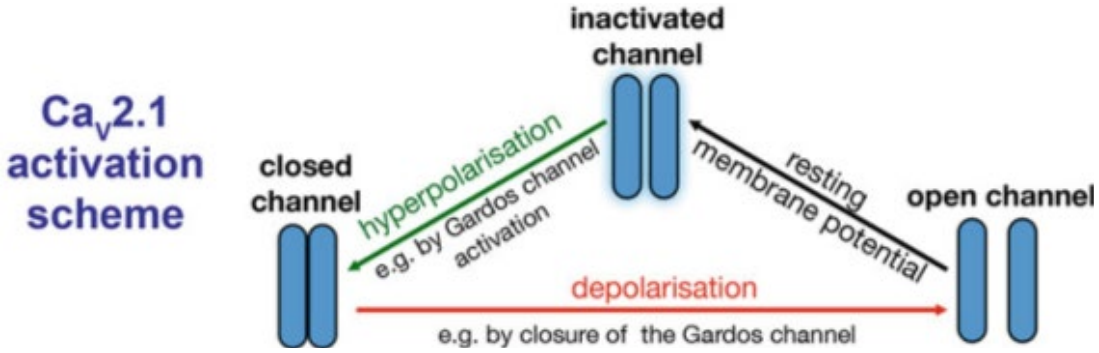

Figure 19: The interplay between $Ca_v2.1$ and Gárdos channel. A closed Gárdos channel is a necessary condition that depolarizes $Ca_v2.1$ (Kaestner et al., 2020)

These were all the channels susceptible to induce Ca^{2+} entry in RBCs. This Ca^{2+} triggers activation of a Gárdos channel.

g) The Ca^{2+}- Activated K^+ channel- The Gárdos channel- $K_{Ca3.1}$-KCNN4- hSK4

The Gárdos channel was originally described by G. Gárdos in 1958 by demonstrating that the K^+ efflux from poisoned human RBCs could be abolished by the use of Ca^{2+}- chelating agents such as EDTA (Gardos, 1958; Hoffman et al., 2003). It is encoded by the *KCNN4* gene found on the 19q13.2 chromosome (Ghanshani et al., 1998). It is a homo-tetramer of six transmembrane

domains (Maher and Kuchel, 2003) (Figure 20). The Gárdos channel is Ca^{2+}-sensitive and its activation leads to membrane hyperpolarization, which drives Cl^- out of the cells for electroneutrality purposes. This results in an obliged water loss, leading to cell shrinkage (Lang et al., 2003b; Myssina et al., 2004). Gárdos channel is voltage-insensitive (Grygorczyk et al., 1984; Christophersen, 1991) and is crucial for volume regulation (Halperin et al., 1989). Patch-Clamp in its excised inside-out configuration, served to characterize the Gárdos channel biophysically and pharmacologically in human RBCs, with a conductance between 15 and 40 pS (Grygorczyk and Schwarz, 1983, 1985).

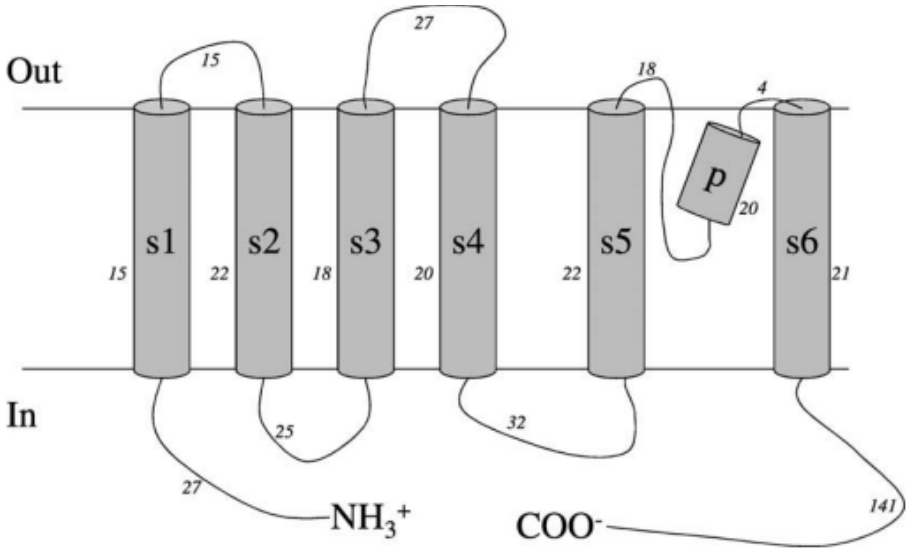

Figure 20: Gárdos channel topology (Maher and Kuchel, 2003)

Gárdos channel is also temperature-dependent, therefore any decrease in the temperature lowers significantly its activity by a reduced open probability (Kaestner et al., 2020).

In normal adult RBCs, Gárdos channel is not active. Once it is fully activated, it induces cellular dehydration (Gallagher, 2017). The activation of Gárdos channel can lead to a decrease of the resting cell membrane from -10 mV to -70 mV (Kaestner et al., 2020). The Gárdos channel is susceptible to be activated by calcium entry through membrane deformations of RBCs membrane (Dyrda et al., 2010) and could be pharmacologically inhibited using charybdotoxin (ChTX) (Brugnara et al., 1993a), nitrendipine, Clotrimazole, Tram34, and Senicapoc (Ellory et al., 1992; Agarwal et al., 2013; Rapetti-Mauss et al., 2016). Ca^{2+} binding to the calmodulin (CaM) subunit mediates the activation of the Gárdos channel (Hamill, 1983). RBCs with a gain of function

mutation in CaM-binding domain showed an increase in the intracellular Ca^{2+} concentrations (Jansen et al., 2021).

Gárdos channel activity (open probability) is proportional to Ca^{2+} entry in a dose-dependent and saturating manner. The saturating component is a "hyperbole" with $K_{0.5}$ near 1µM (Lew et al., 1982; McNamara and Wiley, 1986). Dehydration caused by Gárdos channel activation is considered to be rate-limited by Cl^- effluxes (Bennekou, 1999; Lew and Bookchin, 2005).

Gárdos channel is associated to cell volume regulation in the circulation of RBCs (Cahalan et al., 2015; Danielczok et al., 2017) as well as to cellular death (Kaestner et al., 2020). Mutations in Gárdos channel are demonstrated to cause hereditary xerocytosis (HX) (Glogowska et al., 2015; Rapetti-Mauss et al., 2015) (see paragraph I-D-2-a).

KCNN4 was demonstrated to be linked to DHS caused by mutations affecting this channel (Andolfo et al., 2015, 2018; Fermo et al., 2017, 2020; Picard et al., 2019). Moreover, it is one of the main contributor to the dehydration underwent by sickle cell disease patients (Brugnara et al., 1993b, 1996; Maher and Kuchel, 2003).

Interestingly, the elevated Ca^{2+} levels in RBCs with Gárdos channelopathy patients is suggested to be a result of Gárdos channel interactions with PIEZO1 and $Ca_v2.1$ (Jansen et al., 2021).

D. **Hematological diseases and channels activation**

The activation of specific channels in RBCs can be associated with various diseases and conditions. Anemia is a pathological disease that is characterized by a decreased number of circulating RBCs; below 13 g/dL for males, and 12 g/dL for females (Table 1, (World Health Organization, 2011)). Anemias can be classified according to their morphology, to the Hb concentrations, and to their etiologies (Figure 21). Disorders in the hydration state of RBCs can be the reason of several hereditary anemias (Gallagher, 2017). According to clinical data, anemia is also linked to a number of serious cardiovascular disease (CVD) consequences, including venous thrombosis, thromboembolic events, and stroke. This makes blood transfusion a necessary procedure for patients suffering from anemias (Ducrocq et al., 2015).

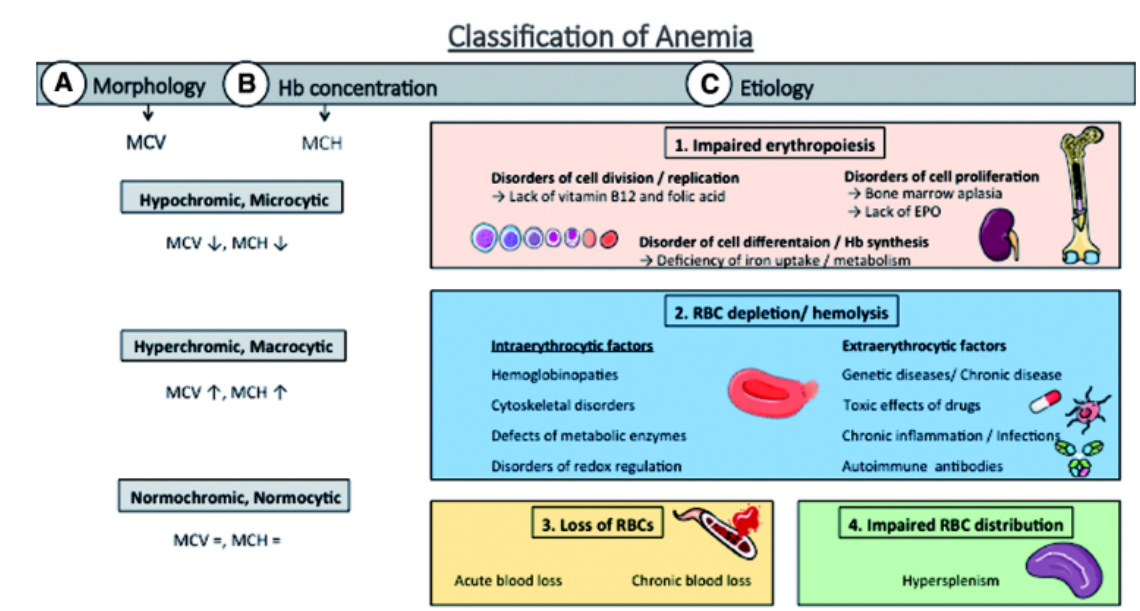

Figure 21: Classification of anemias (Kuhn et al., 2017)

Poikilocytosis is the term used to describe abnormal shapes of RBCs, reaching more than 10% of the total blood population. Their presence signals the presence of an underlying disease. It can be inherited or acquired.

Inherited poikilocytosis include SCD, thalassemia, HS, pyruvate kinase deficiencies, hereditary elliptocytosis, and McLeod syndrome. Acquired poikilocytosis include iron deficiency anemia, megaloblastic anemia, autoimmune hemolytic anemia, liver and kidney disease, lead poisoning, infections (malaria and Babesia) (Bandaru et al., 2023).

In the following sections, we have chosen to describe the most common hematological diseases. They are classified according to their etiologies. The first class of hematological disorders to be described are those associated to hemoglobin defects (Sickle Cell Disease and Thalassemia). Secondly, we will list diseases associated with channels defects, which essentially include stomatocytosis. In addition, we will present diseases that are mainly associated with defects in plasma membrane, in particular hereditary spherocytosis and hereditary elliptocytosis. Finally, we presented other hematological diseases, that may be related either to parasitic infection (such as malaria), or to enzymatic defects in the RBC (such as G6PD deficiency).

1. Hemoglobin-linked diseases

a) Sickle Cell Disease

Sickle Cell Disease (SCD) is the most common inherited blood disorder worldwide (Gibson and Ellory, 2002; Modell and Darlison, 2008; Piel et al., 2013). It is caused by a single mutation in the β-globin chain at the position 6, where a single base pair change from Adenosine to Thymine results in the alteration of glutamic acid to valine (Ingram, 1957), which leads to polymerization of the resulting hemoglobin HbS upon deoxygenation, coupled with a loss of deformability and a significant increase in cell adhesion (Mohandas and Evans, 1985; Kato et al., 2007). There are several reasons why RBCs can sickle, including: a small increase in HbS concentration promotes sickling of RBCs (Eaton and Hofrichter, 1987), the abnormal activation of membrane channels and transporters such as the Gárdos channel (Apovo et al., 1994).

Deoxygenation activates cation channels in sickle RBCs, which fosters dehydration (Mohandas et al., 1986; Joiner et al., 1988, 199, 1993; Joiner, 1993; Browning et al., 2007). This deoxygenation-sensitive cationic activity is termed "P_{Sickle}" and is amplified by membrane distortion (Vandorpe et al., 2010; Ma et al., 2012). Membrane distortion itself is a result of HbS forming long fibers upon deoxygenation, which laterally aggregate and nucleate to form new fibers (Henry et al., 2020). P_{Sicke} is therefore activated by deoxygenation, shear stress, and other stimuli (Bookchin and Lew, 1981), resulting in a 6- to 10- fold increase in the free-intracellular Ca^{2+} levels (Rhoda et al., 1990; Bogdanova et al., 2013).

However, the molecular identity of P_{Sicke} is still ambiguous. So far, PIEZO1 has been proposed as a candidate for P_{Sickle} (Vandorpe et al., 2010; Cahalan et al., 2015; Wadud et al., 2020), since this deoxygenation-induced non-specific cation conductance, could be inhibited by GsMTx4 (Ma et al., 2012). This hypothesis is controversial because, as shown in a 2019 study, a *PIEZO1*-gain-of function mutation, E756del, which is common in African populations because it protects against malaria infection (Ma et al., 2018), did not correlate with P_{Sicke} functional activity (Rooks et al., 2019).

P_{Sickle} increases the intracellular Ca^{2+} concentrations which activates the Gárdos channel, resulting in K^+ loss followed by Cl^- for electroneutrality purposes, and osmotically obliged water (Figure

22) (Ellory et al., 2007). The effects of this phenomenon are exacerbated by the activation of the K-Cl cotransporter, which is stimulated by hypoxia and the acidic environment of the vaso-occlusive episodes (Brugnara, 2018). Such episodes also occur in the renal medulla due to high urea concentrations (Lu et al., 2021).

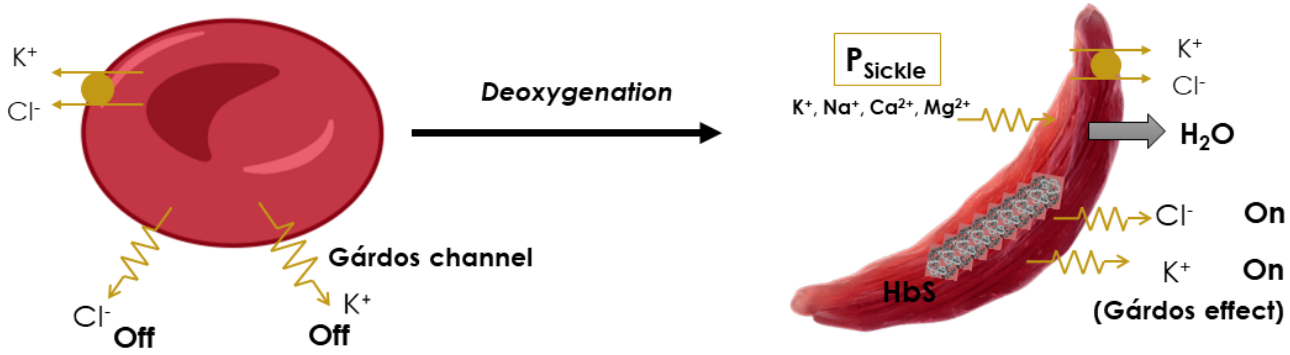

Figure 22: Sickling procedure and P_{Sickle} activation. Created with Bio-Render.

Patients with SCD have a population of hyperdense cells (deregulated cell volume) that makes them more susceptible to sickling and leads to vaso-occlusive crises, promoting the multisystemic morbidity of this disease (Gallagher, 2017; Brugnara, 2018).

Several molecules have been identified as blockers of P_{Sickle} activity; some of them work on the inhibition of the polymerization of HbS (Eaton and Bunn, 2017) (for example, carbon monoxide (Vandorpe et al., 2010) or GBT1118/voxelotor molecule (Al Balushi et al., 2019)). Other molecules work on the inhibition of the stretch-activated cation channels by using GsMTx4 toxin (Vandorpe et al., 2010), in addition to other less specific molecules such as 5HMF (Hannemann et al., 2014b), and o-vanillin (Hannemann et al., 2014a). Gárdos channel inhibitors like Senicapoc have been suggested as treatment of the dehydration occurring in SCD (Brugnara et al., 1993b; Stocker et al., 2003). Furthermore, the inhibition of the Ca^{2+}-dependent cysteine protease calpain-1 is another proposed technique, since it reduces the proteolysis and thus stops the premature clearance of RBCs with HbS (De Franceschi et al., 2013). Finally, a technique consisting in blocking the effects of oxidative stress to stop the formation of superoxide anions has also been proposed for treatment (George et al., 2013).

b) Thalassemia

Thalassemia is a worldwide group of inherited disorders that affect the synthesis of the Hb globin chain. It is characterized by insufficiency or absence of production of α or β globin chains, which are the two main components of adult Hb (Higgs et al., 2012). It evolves in different geographical regions because they are likely to confer resistance to malaria (Kuesap et al., 2015; Malaria and Thalassemia in the Mediterranean Basin, 2021).

In normal individuals, the hemoglobin type is HbA with 2 α-globins and 2 β-globins. The expression of each globin takes place on a different gene, with the heme being synthesized primarily on the mitochondria.

α- Thalassemia presents different clinical phenotypes, ranging from asymptomatic to lethal, depending on the number of nonfunctional copies of the α-globin gene (Piel and Weatherall, 2014). On the other hand, β-Thalassemia, is one of the most frequent causes of inherited anemias with an annual incidence of 1:100.000 worldwide (Galanello and Origa, 2010). It is caused by mutations affecting the β-globin gene or its promoter, resulting in defective β-globin chains (Rivella, 2015).

β-Thalassemia patients undergo ineffective erythropoiesis due to several factors including the increased apoptosis of thalassemic erythroid precursors, the decreased differentiation of erythroid progenitors, oxidative stress, and defective iron metabolism, or iron overload (Oikonomidou and Rivella, 2018).

The total Ca^{2+} content was found to be increased in β-thalassemic RBCs without becoming dense or dehydrated. This phenomenon was explained by an abnormal abundance of residual organelles containing Ca^{2+} ions (Bookchin et al., 1988).

2. Channels-linked diseases-stomatocytosis

It is a group of rare inherited disorders characterized by the presence of stomatocytes in the blood. Stomatocytes are characterized by a central mouth-shaped area. Mutations in various genes, including PIEZO1, RHAG, and SLC4A1 can lead to stomatocytosis. These mutations may affect cation transport and ion channels, leading to altered RBC morphology and function.

a) Hereditary Xerocytosis (HX) or Dehydrated Hereditary Stomatocytosis 1 (DHS1)

HX also known as DHS1 is an autosomal-dominant hemolytic anemia caused by PIEZO1 gain (Zarychanski et al., 2012) of function or RBC dehydration due to secondary Gárdos channel activation (Albuisson et al., 2013; Rapetti-Mauss et al., 2017), in addition to other syndromes (Andolfo et al., 2013a; Picard et al., 2019). Inherited missense mutations in PIEZO1 leading to gain-of-function have been described in the majority of HX patients, located in the COOH terminus (Zarychanski et al., 2012; Albuisson et al., 2013; Andolfo et al., 2013a; Glogowska et al., 2017; Picard et al., 2019) leading to an increased cation permeability in the cells (Na^+ and Ca^{2+}). These gain-of-function mutations slow down the inactivation kinetics of PIEZO1 or lower its stimulating threshold (Albuisson et al., 2013; Glogowska et al., 2017). Erythrocytes of patients with DHS exhibit an alteration of ion transport, and vesicle-mediated transport; an increase in the vesiculation rate was recently proved in these patients (Andolfo et al., 2023).

It is considered as a rare disease although its prevalence could reach up to 1/8000 persons in the American population (Kaufman et al., 2018). Genetic studies proposed an association of this disease with PIEZO1 polymorphisms and to Hb-related parameters (van der Harst et al., 2012; Ulirsch et al., 2019; Vuckovic et al., 2020). Especially, mutations affecting PIEZO1's pore domain are associated with severe phenotypes (Andolfo et al., 2018). Novel studies suggest NGS as an economical and quick tool to understand genetic causes of undiagnosed HX mutants with congenital hemolytic anemia (More et al., 2020)

b) Dehydrated Hereditary Stomatocytosis 2 (DHS2)

Also called "Gárdos channelopathy" or "DHS2", it is caused by the mutation of the *KCNN4* gene. Mutations in this channel result in altered Ca^{2+}-mediated K^+ efflux which leads to dehydration of RBCs and can result in symptoms such as hemolytic anemia (Andolfo et al., 2015; Glogowska et al., 2015; Rapetti-Mauss et al., 2015).

They differ from the DHS1 especially in the severity of the hematological phenotypes, thrombotic risk after splenectomy, the occurrence of perinatal edema, and susceptibly iron overload risk (Fermo et al., 2017; Andolfo et al., 2018; Picard et al., 2019). Patients with DHS2 have normal

ektacytometry profiles, in contrast to DHS1 patients (Andolfo et al., 2015; Rapetti-Mauss et al., 2015).

c) Overhydrated hereditary stomatocytosis (OHS)

It is a rare hereditary anemia with only 20 cases reported worldwide. These cases are due to a 20-40 fold increase in cation loss (Delaunay and Stewart, 2006). Mutations in the *RHAG* gene, which encodes the RhAG glycoprotein, an ammonia-like channel, are the cause of this phenotype (Genetet et al., 2012). Loss of Stomatin has also been reported in OHS patients (Delaunay, 2004).

3. Plasma membrane linked diseases

a) Hereditary Spherocytosis (HS)

It is the most common non-immune hemolytic anemia (Perrotta et al., 2008; Bogardus et al., 2012), with symptoms including jaundice, anemia, and splenomegaly (Perrotta et al., 2008; Gallagher, 2013).

HS is a genetic disorder in which erythrocytes are more spherical and less deformable than normal due to reduced membrane surface area, making them prone to premature destruction in the spleen (Delaunay and Stewart, 2006; Delaunay, 2007; Perrotta et al., 2008).

It can be caused by the disruption of the vertical structure of the cytoskeleton *i.e.*, the loss of the cohesion between the plasma membrane and the membrane skeleton. This reduced membrane cohesion originates from a deficiency of i) membrane proteins that link the lipid bilayer to the membrane skeleton, such as Band 3 and/or RhAG, ii) anchoring proteins, such as Ankyrin and/or Protein 4.2, or iii) the quantitative deficiency (Narla and Mohandas, 2017) and loss of spectrin-actin interactions (Andolfo et al., 2016).

In knock-out mouse models of 4.2 proteins, where loss of membrane surface and membrane instability are observed as in the human disease, an increased activation of, potassium channels, Na^+/H^+ exchanger, and Na-K-2Cl cotransporter is reported (Peters et al., 1999). Increased osmotic fragility has also been described in this disease (Eber et al., 1990). Reduced membrane deformability is a result of defects in membrane cytoskeletal components such as ankyrin (ANK1) (Miya et al., 2012), α- and β- spectrin (SPTA, SPTB), (Whitfield et al., 1991; Gallagher et al.,

1995; Kedar et al., 2003; Lybaek et al., 2008), RhAG (Ballas et al., 1984), Band 3 (SLC4A1) (Ribeiro et al., 2000), and protein 4.2 (EPB42), (Chasis et al., 1988; Eber and Lux, 2004, 200; Perrotta et al., 2008).

b) Hereditary Elliptocytosis (HE)

This disease is characterized by the presence of elliptocytes, with elliptical RBCs shape found on peripheral blood smears (Gallagher, 2004). The global prevalence of HE ranges between 1:2000-4000 subjects although the incidence could be higher in and reaches around 1:100 in some African regions for example (Da Costa et al., 2013).

HE is a hereditary disease caused by the mutation in protein 4.1 or spectrin (*EP41*, *SPTA1*, and *SPTB*) genes which leads to the disruption of the horizontal interactions of the cytoskeleton, in other words, the skeletal attachment to the membrane proteins because of the defect in the association of spectrin dimers and/or tetramers (Iolascon et al., 2003). Spectrin mutation was previously described in HE cases (Marchesi et al., 1987). The key defect in HE RBCs is the membrane skeleton's mechanical fragility as a result of improper horizontal contacts between cytoskeletal proteins, such as spectrin dimer-dimer interactions and spectrin-actin-protein 4.1 at the junctional complex (Andolfo et al., 2016).

An increase in the inward Na^+ leak takes place in patients subjected to HE, inducing an increase in the ATP needed for the NaK pump functioning. In the majority of the cases, HE is imperceptible, and asymptomatic with patients not undergoing anemias and other complications. (Da Costa et al., 2013)

Hereditary pyropoikilocytosis (HPP) is a severe subtype of HE that is thermosensitive (Zarkowsky et al., 1975), caused by homozygous or heterozygous mutations in the α-spectrin gene and consequent severe disruption of spectrin self-association (Narla and Mohandas, 2017).

Table 3 summarizes the red cell membrane disorders associated with the genes whose mutations cause the disorder in each case (Table 3).

Table 3: Inherited red cell membrane disorders and gene mutations. AD stands for autosomal dominant, and AR for autosomal recessive inheritance. OMIM: Online mendelian inheritance in man (Narla and Mohandas, 2017)

Disorder	OMIM	Inheritance	Gene	Gene name
Spherocytosis, type 1	182900	AD	ANK1	Ankyrin
Spherocytosis, type 2	616649	AD	SPTB	Spectrin β
Spherocytosis, type 3	270970	AR	SPTA1	Spectrin α
Spherocytosis, type 4	612653	AD	SLC4A1	Band 3
Spherocytosis, type 5	612690		EPB42	Protein 4.2
Dehydrated hereditary stomatocytosis	194380	AD	PIEZO1	Piezo 1
Overhydrated hereditary stomatocytosis	185000	AD	RHAG	RhAG
Cryohydrocytosis	185020	AD	SLC4A1	Band 3
Dehydrated hereditary stomatocytosis 2	616689	AD	KCNN4	Gardos Channel
Elliptocytosis-1	611804		EPB41	Protein 4.1
Elliptocytosis-2	130600	AD	SPTA1	Spectrin α
Ovalocytosis, SA type	166900	AD	SLC4A1	Band 3
Pyropoikilocytosis	266140	AR	SPTA1	Spectrin α

4. Other hematological diseases

a) Malaria

Malaria disease, caused by the parasite, *Plasmodium falciparum*, is an infection that affects RBCs. RBCs are thus invaded by the *P. falciparum* parasite which then reproduces there. Changes in ion channels activity and membrane permeability occur during this phase, contributing to the pathophysiology of the disease (Kirk, 2015).

RBCs infected by *P. falciparum* exhibit an increase in intracellular Na^+ concentration in parallel with a decrease in K^+(Figure 23) (Overman, 1948; Lee et al., 1988). This is accompanied by the induction of new permeability pathways (NPP) in the RBC membrane. NPP permeability includes organic solutes such as nucleosides, polyols, and amino-acids. In addition, NPP induces permeability to monovalent cations such as Cs^+, Rb^+, K^+, Na^+, and Li^+ (Kirk, 2015). NPP permeates Cl^- orders of magnitude faster than Na^+ or K^+(Kirk et al., 1994; Egée et al., 2002). Malaria infection is also characterized by an increase in intracellular Ca^{2+} concentrations (Kramer and Ginsburg, 1991; Desai et al., 1996).

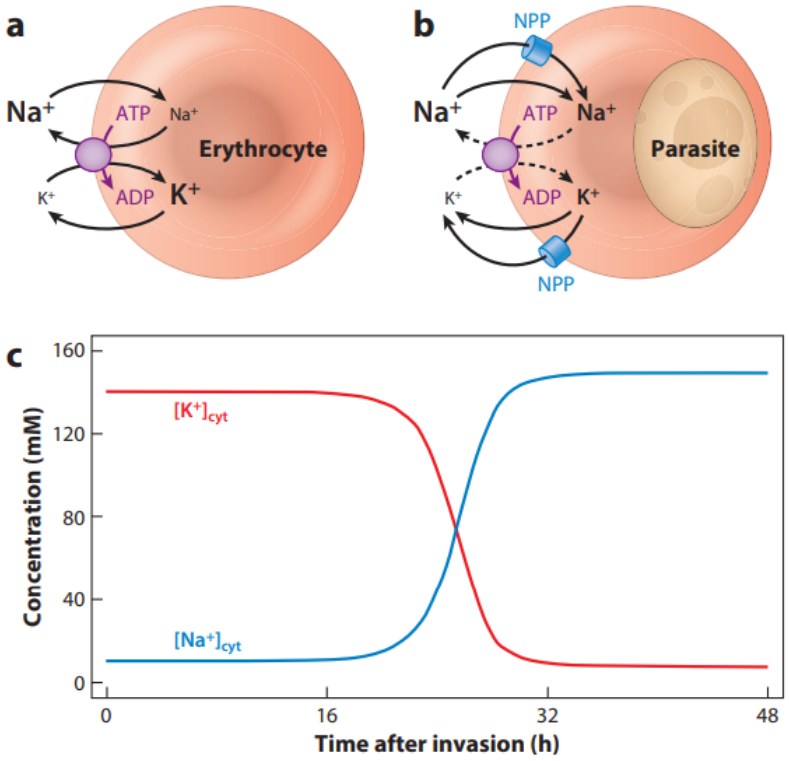

Figure 23: The perturbation of Na^+ and K^+ homeostasis in human RBCs. (a) schematic representation of the pump-leak balance in normal human erythrocytes. In purple is represented the Na^+, K^+, ATPase pump. (b) perturbation of the pump-leak balance following malaria parasite infection. The NPP (in blue) is the conductance induced by the parasite. The dashed arrows of the NaK pump, points to its impairment throughout cell's aging. (c) simulation showing the prediction of cytosolic concentrations of Na^+ and K^+ after 48 hours of infection by malaria parasite. This stimulation was generated using the integrated mathematical modeling of Lew and colleagues (Kirk, 2015)

Sickle Cell Anemia (SCA) is the most famous condition granting resistance to malaria infection (Allison, 1954). Moreover, variations in the hydration status of the RBCs modify their susceptibility to be invaded by *P. falciparum*; invasion was systematically reduced in dense/dehydrated cells (Tiffert et al., 2005).

A common mutation in the PIEZO1 channel (E756del) is associated with resistance to the infection by malaria parasites in mice and in human RBCs *in-vitro*, suggesting that PIEZO1 is an important innate factor determining malaria susceptibility in humans, and that the mechanism of protection may be related to impaired export of P. falciparum virulence protein (Nguetse et al., 2020). In a recent study, Lohia and colleagues demonstrated that the pharmacological activation of PIEZO1 by Yoda1 or Jedi2 contributes to effective protection against malaria infection (Lohia et al., 2023).

b) G6PD Deficiency

Glucose-6-phosphate dehydrogenase (G6PD) is a housekeeping enzyme, ubiquitously expressed in all the cells with the function of catalyzing Glucose 6 Phosphate (G6P) to 6-phosphoglucono-δ-lactone in the pentose phosphate cycle, in order to regulate the glycolytic flux. Its importance includes the production of NADPH, the essential cofactor for GSH generation to sustain multiple biosynthetic pathways in the cell, and to maintain its redox equilibrium (Tian et al., 1998; Salvemini et al., 1999) and to protect against oxidative stress (Pandolfi et al., 1995). G6PD is particularly important in the RBCs because it is the only source by which they can produce NADPH (Luzzatto, 1967; Scott et al., 1991).

G6PD deficiency is an inherited genetic hemolytic disorder (Luzzatto et al., 2020). Its prevalence ranges from 300 to 400 million people worldwide (Jiang et al., 2006b; Jamerson et al., 2020). G6PD deficiency has been associated with Covid-19 complications (Chaney et al., 2020; Jamerson et al., 2020; Yang et al., 2021).

G6PD deficiency is an inherited enzyme disorder that can lead to hemolysis when RBCs are exposed to certain triggers, such as oxidative stress.

Patients with G6PD deficiency have been shown to have severely disturbed Ca^{2+} homeostasis, with significantly impaired CaATPase activity (De Flora et al., 1985). Increased intracellular Ca^{2+} concentrations as well as the altered distribution of Band 3 are particularly pronounced in hemolytic G6PD-deficient patients (Fang et al., 2016).

II. Erythropoiesis

Albeit erythropoiesis was not explored during my thesis, it is noteworthy that all channels present in mature RBCs originate from the late differentiation of erythroblastic progenitors. Thus, it is important to consider this fundamental step in the lifespan of “RBCs” when looking for the role of ion channels in health and disease.

Erythropoiesis is defined as a series of steps required for the formation of a mature erythrocyte, starting from a pluripotent hematopoietic stem cell and progenitor cells (HSPC) mainly located in the bone marrow (Dzierzak and Philipsen, 2013; Koulnis et al., 2014).

New erythrocytes are continuously produced in the bone marrow (around 2.4 x 10^6 cells per second in adults), which provides a niche composed of osteoblasts, stromal cells, endothelial cells, hematopoietic cells, and the extracellular matrix (Dzierzak and Philipsen, 2013). The first wave of hematopoiesis is characterized by the formation of nucleated megaloblastic erythroblasts known as primitive erythroblasts (PE), in addition to macrophages and diploid platelet progenitors (Potts et al., 2014).

There exist two different erythroid progenitors; the first is the early stage burst-forming unit-erythroid (BFU-E), whose growth is dependent on the presence of factors such as stem cell factor (SCF), interleukin 3 and 1 (IL-3, IL-1), FLT3 ligand, and thrombopoietin (TPO). Cells at this stage are found in the bone marrow and can also circulate in the peripheral blood (Migliaccio et al., 2001). The second is the later stage colony-forming unit-erythroid (CFU-E) progenitors, which are five to eight times more abundant than the BFU-E and are found only in the bone marrow (Dzierzak and Philipsen, 2013).

Progenitors respond to growth factors and cytokines, including those mentioned above, especially SCF. The developing erythroid progenitors expand and proliferate thanks to the synergistic effect of SCF with EPO. After proliferation steps, proerythroblasts are formed. These are the first morphologically recognizable erythroblasts. These proerythroblasts undergo three to four mitotic divisions to produce reticulocytes. After each successive mitosis, a distinct population of erythroblasts is produced. The proerythroblasts are followed successively by basophilic, polychromatic, and orthochromatic erythroblasts. Orthochromatic erythroblasts shed their nucleus, endoplasmic reticulum and mitochondria, and become reticulocytes (Figure 24) (Dzierzak and Philipsen, 2013).

Reticulocytes no longer synthesize proteins, including hemoglobin. On the contrary, they undergo two phases of maturation; the first takes place in the bone marrow through autophagy, proteolysis, ubiquitylation, and formation of Multi-vesicular bodies (MVB), which are then released, contributing to the removal of several membrane proteins, and to the reduction of surface area, given the fact that reticulocytes have a large volume and large surface area (Fader and Colombo, 2006). Recently, it has been suggested that during this late phase of maturation, ion channels such as the Gárdos channel, and others, are involved to reduce the cell volume (Minetti et al., 2023). Reticulocytes are recognized in the circulation as CD71 (transferrin receptor) positive. The second

phase of maturation takes place in the vasculature through lipid remodeling by lipid exchange with the plasma (Minetti et al., 2023).

Erythropoiesis is promoted by deoxygenation; the kidneys detect the decreased O_2 concentration in the circulation and secrete erythropoietin hormone, which triggers the erythropoiesis process (Tsiftsoglou, 2021). In response, erythroid precursors proliferate, differentiate, and enucleate in specialized niches called "erythroblastic islands" in the bone marrow. They contribute to normal erythroid development and in case of defective erythropoiesis as seen in several diseases such as anemia, inflammation, thalassemia, etc… (Chasis and Mohandas, 2008). In addition, erythropoiesis can be stimulated by increased levels of physical activity (Handelsman, 2000).

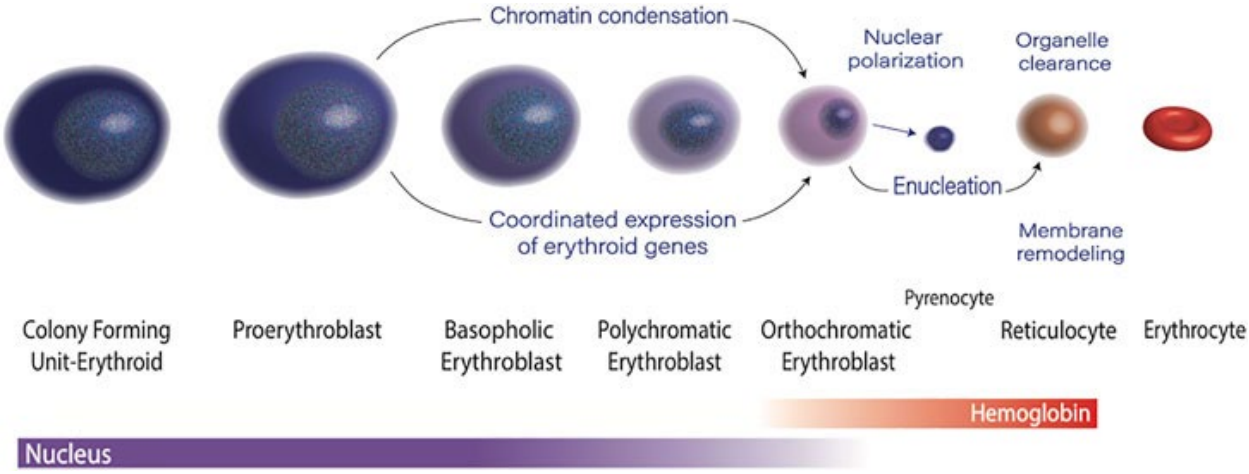

Figure 24: Overview of erythropoiesis (Wells and Steiner, 2022).

- **Channels and Erythropoiesis**

Ca^{2+} is involved in erythropoiesis either by acting synergistically with EPO to initiate the clonogenicity of progenitors in the bone marrow (Misiti and Spivak, 1979) or by participating in the enucleation process (Wölwer et al., 2016). Erythroblasts are also endowed with several PIEZO1-dependent transduction pathways, whether in nuclear translocation (Aglialoro et al., 2021), integrins (VLA-4, VLA-5) activation following protein kinase C (PKC) and calpain activation (De Maria et al., 1999; Aglialoro et al., 2020), and ERK/STAT5 phosphorylation, thus modulating EPO-dependent signaling (Caulier et al., 2020).

PIEZO1 is expressed during the earliest stages of erythropoiesis and gradually decreases during the terminal maturation phase (Karayel et al., 2020). Case report studies have described an association between PIEZO gain-of-function mutations and dyserythropoiesis (Paessler and Hartung, 2015; Park et al., 2018). Activation of PIEZO1 during *in-vitro* differentiation was able to keep the cells in an immature stage, slowing down the differentiation process (Caulier et al., 2020) as well as disturbing the reticulocyte maturation (Moura et al., 2020). Mutations in Band 3 have also been associated with dyserythropoiesis (Iolascon et al., 2009). In addition, the expression of ABCB6, a homologous protein belonging to the family of the ABC transporter family, is increased during erythroid differentiation of the CD34+ cells (Andolfo et al., 2013b).

III. RBC ageing

RBCs remain stable and functional in the circulation for nearly 120 days in perfect shape due to the strong reducing and repair redox stress in the cells (Bernhardt and Ellory, 2003).

RBC senescence is characterized by a loss of membrane deformability due to occurring vesiculation, resulting in a significant loss of surface area. This phenomenon is accompanied by an increase in the intracellular Ca^{2+} concentrations culminating in PS exposure (Thiagarajan et al., 2021), dehydration, ATP depletion (McMahon et al., 2021), and increased cellular adhesion (Klei et al., 2020).

Senescent RBCs have lower concentrations of ATP, which makes ATP- dependent pumps less active (Klei et al., 2020; Seki et al., 2020), leading to increased intracellular calcium concentrations (Lew and Tiffert, 2017).

The majority of senescent RBCs are subsequently destroyed by erythrophagocytosis by macrophages in the spleen. In addition, a small percentage of senescent RBCs are hemolyzed in the vessels of the circulation (Alaarg et al., 2013; Huisjes et al., 2018).

RBC densities increase with age, as demonstrated by gradient separations techniques (Maurer et al., 2022). RBCs lose surface and volume and remain functional (Waugh et al., 1992). The increased density of aged RBCs is mainly due to the loss of K^+ and Cl^- causing dehydration (Lew et al., 1995; Bernhardt and Ellory, 2003). Interestingly, a subpopulation of old cells with elevated

Na^+ concentrations, and therefore a rehydrated and less dense fraction has also been found (Bookchin et al., 2000).

In very old erythrocytes, the concentration of ATP stays relatively constant (Kirkpatrick et al., 1979), as does the concentration of glutathione (Piccinini et al., 1995). Young erythrocytes contain more K^+ than Hb because younger erythrocytes are larger, and the cation concentration remains stable over time, demonstrating the efficacy of pump activity with aging (Minetti et al., 2001). Aged RBCs are smaller (Kim et al., 2020) and less deformable (Barshtein et al., 2021) due to increased cytoplasmic viscosity (Simmonds et al., 2013). PS and PE are exposed during RBC storage and senescence, allowing recognition by splenic macrophages and removal of the less deformable RBCs from the circulation.

The structure and mechanical characteristics of the membrane are the main determinants of the "apoptotic" behavior of the RBCs (Mohandas and Gallagher, 2008).

It is interesting to note that erythrocytes lacking a nucleus, mitochondria, and other vital organelles are nonetheless able to experience some morphological signs of "apoptosis", including PS exposure, cell shrinkage, and membrane blebbing (Lang et al., 2003a, 2012).

Objectives

In the course of the introduction, ion channels were shown to be pillars in the maintenance of normal RBCs function and characteristics. Importantly, cation permeabilities were proven to be regulated and implicated in different stages of erythrocytes life: whether during erythropoiesis, circulation or aging, cation channels are present and changes in their activity can be involved in all these processes. Moreover, deregulation of cation channel activity has been shown to have a major impact on the development and severity of various hematological disorders, in particular, sickle cell disease and other rare hereditary anemias (HX, HS, HE, etc…). In general, there are three main cation channels that have been shown to be present in the erythrocyte membrane thanks to transcriptomics / proteomics at the stage of erythropoiesis and proteomics in mature erythrocytes: Gárdos channel, PIEZO1, and TRPV2. The activity of these channels is regulated under physiological and pathophysiological conditions.

Given the importance of this topic, I focused during my Ph.D. on deciphering the activity of cation channels in healthy erythrocytes as well as in the erythrocytes from patients suffering from sickle cell disease, or carrying mutations in PIEZO1 or Gárdos channel; knowing that in physiological conditions these channels are not active, we were interested in studying them in pathological conditions. Therefore, we studied mutations in KCNN4 and PIEZO1 channels, or blood samples from SCD patients.

Thus, the main objectives of my thesis were:

First, the understanding of PIEZO1 channel activation from a pharmacological perspective

All the experiments performed in the laboratory to understand of the role of PIEZO1 have used agonists or inhibitors (GsMTX-4, Jedi-1, Jedi-2, Yoda1). The introduction of Dooku1 as a new molecule with the potential to modify the activating effects of Yoda1 led us to characterize the effects of Dooku1 on red blood cells and add it to our repertoire of pharmacological tools.

Second, the understanding of cation deregulations in sickle RBCs

As a step towards understanding the mechanisms of cation deregulation in SCD, the question arises whether PIEZO1 (Vandorpe et al., 2010; Wadud et al., 2020) and thus other cation channels such as TRPV2 are involved in the manifestation associated with the so-called P_{Sickle}. To this end, we independently investigated the influence of the pharmacological activation of PIEZO1 in oxygenated and deoxygenated conditions on SCD patient cells. Similarly, the discovery of TRPV2 during my thesis (Belkacemi et al., 2021) led us to test the influence of TRPV2 activation by its natural agonist (Δ^9-THC) in sickle red cells.

Third, the analysis of blood samples of patients with channels mutations

Knowing that different variants of KCNN4 and PIEZO1 channels lead to pathologies, our laboratory is involved in a large European network of clinicians and academics to decipher the relationship between genotypes and pathophysiological phenotypes. Therefore, one of the goals of my thesis was to functionally assess the link between the genetic detection of variants and defects in channel activity using multiple approaches.

Fourth, the study of Alectinib effects on RBCs

The last objective arose from a recent observation that patients treated with Alectinib for lung cancer have dehydrated RBCs with echinocytosis, raising the question of whether this state results from a deregulation of cation channels.

Materials and Methods

A. **Ethics approval**

Healthy donors, PIEZO1, and Gárdos channel patients

Blood from healthy volunteers was withdrawn upon written informed consent (EFS, Etablissement Français du Sang), in accordance with the guidelines of the Helsinki Declaration of 1975, as revised in 2008. This work has been approved by the institutional (CNRS) Ethical Committee and by the French Ministry of Research (declaration DC-2019-3842). All patients were followed by their medical doctors, all being our collaborators. We have been authorized by the Ministry to carry out studies for clinicians who request studies in which we are specialized.

Sickle Cell Disease patients

All patients were followed up in the Hospitals of Lyon (France). The study was conducted in accordance with the guidelines set by the Declaration of Helsinki and approved by the Regional Ethics Committees (L14-127, Université de Lyon) with informed consent. All subjects were in clinical-steady-state at the time of the study; without experiencing any vaso-occlusive crisis or other acute medical complication within the past two months and without any blood transfusions for at least 3 months before inclusion.

B. **Blood samples**

Blood from healthy donors was drawn into lithium-heparin vacutainer (BD Switzerland Sarl, Vaud. Switzerland) on-site.

SCA patients 'blood was drawn into EDTA vacutainer (BD Switzerland Sarl, Vaud. Switzerland) and shipped from Lyon to collaborating laboratories at room temperature.

Blood from patients suffering from *PIEZO1* or *KCNN4* mutations was withdrawn either in lithium-heparin tubes or in EDTA tubes.

Lithium-heparin and EDTA are two of the most commonly used anticoagulants for blood storage (Guzman et al., 2008). Heparin's main function is to bind and soar the activity of antithrombin III which intercepts the action of thrombin and other proteases involved in the coagulation process while EDTA acts by chelating Ca^{2+} which is the most important ion in the coagulation cascade and for cellular interactions (Ali, 2020). Several studies were conducted to understand the effects of these anticoagulants on blood parameters (Guzman et al., 2008; Akorsu et al., 2023). Studies have revealed a preference for EDTA because it preserves blood components for longer and is highly effective in preventing blood clots (Walencik and Witeska, 2007; Weber and Nakashima, 2021). On the contrary, EDTA was reported to be inadequate for the assessment of the RBC's osmotic fragility. Other studies showed that Heparin should not be used for blood smear preparations (Walencik and Witeska, 2007; Akorsu et al., 2023).

Widely known, lithium-heparin tubes are used for the collection of heparinized plasma for routine chemistry tests such as, cholesterol, ions, hormones, etc… (Research gate, 2015) whereas EDTA tubes are used for hematological testing (FL Medical, 2023). In our experiments, we usually get healthy blood withdrawn in Heparin tubes. However, we received patients' blood samples mostly in EDTA tubes. To assume that the anticoagulant type did not interfere with our experiments, MBE experiments were performed on blood from the same donors withdrawn at the same time in both Heparin and EDTA tubes. Maximum hyperpolarizations were compared in both oxygenated and deoxygenated conditions. (Figure 25).

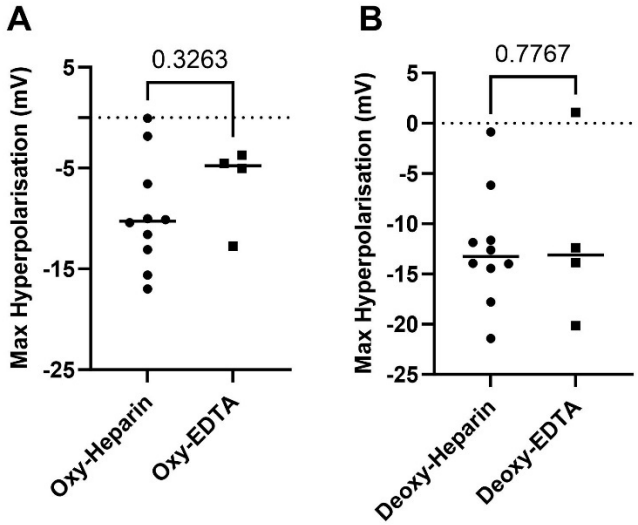

Figure 25: Comparison of the maximal hyperpolarizations of control cells stored in heparin or in EDTA tubes in oxygenated (panel A), and in deoxygenated conditions (panel B). An unpaired t-test

was used to assess the statistical differences. n=10 for Heparin condition, and n=4 for EDTA conditions. Statistical comparison using unpaired t-test.

Our results showed no difference between Heparin and EDTA tubes both in oxygenated and deoxygenated conditions. Therefore, comparisons between control and patients should not consider differences of tubes' anticoagulants types.

C. Salts and reagents

All salts were purchased from Sigma-Aldrich unless stated otherwise. They were of analytical grade or better. Details about the chemicals used in this thesis are listed in Table 4 (Table 4).

Table 4: List of chemicals

Chemical-current name	Chemical-detailed named	Function	Purchasing company
CCCP	carbonyl cyanide 3-chlorophenylhydrazone	H^+ ionophore. Used to increase the permeability of H^+ across the membrane in order to reach equilibrium state of H^+	Sigma-Aldrich, France
Yoda1	2-[5-[[(2,6-Dichlorophenyl)methyl]thio]-1,3,4-thiadiazol-2-yl]pyrazine	Modulates PIEZO1's mechanosensitivity (activates PIEZO1)	Tocris, France
Dooku1	2-[(2,6-Dichlorobenzyl)thio)-5-(1H-pyrrol-2-yl)-1,3,4-oxadiazole	Inhibits the effects of Yoda1	Sigma-Aldrich, France
GsMTx4	*Grammastola spatulata* mechanotoxin #4	Inhibits cation permeable mechanosensitive channels like PIEZO1	Alomone labs, Israel
Charybdotoxin	Charybdotoxin, venom from scorpion *Leiurus quinquestriatus hebraeus*	KCNN4 blocker	Alomone labs, Israel
Tram34	1-[(2-Chlorophenyl)diphenylmethyl]-1H-pyrazole	KCNN4 blocker	Alomone labs, Israel
Δ^9- THC	Δ9-Tetrahydrocannabinol	TRPV2 agonist	Sigma Aldrich, Saint Louis, MO, USA
NS309	(6,7-Dichloro-1H-indole-2,3-dione 3-oxime)	Increases the sensitivity of the Gárdos channel to Ca^{2+}	Tocris, France

A23187	(calcymicin;5-(methylamino)2-[[(2S,3R,5R,6S,8R,9R)-3,5,9-trimethyl-2-[(2S)-1-oxo-1-(1H-pyrrol-2-yl) propan-2-yl] -1,7-dioxaspiro [5.5] undecan-8-yl] methyl -1,3-benzoxazole-4-carboxylic acid)	Ca^{2+} ionophore: induces rapid Ca^{2+} uptake	Tocris, France
NS3623	N-(4-bromo-2- (1H-tetrazol-5-yl) phenyl)-N' -(3 trifluoromethyl-phenyl) urea)	Inhibits the Cl^- conductance	Tocris, France
Fluo-4, AM	*N*-[4-[6-[(Acetyloxy)methoxy]-2,7-difluoro-3-oxo-3H-xanthen-9-yl]-2-[2-[2-[bis[2-[(acetyloxy)methoxy]-2-oxoethyl]amino]-5-methylphenoxy]ethoxy]phenyl]-*N*-[2-[(acetyloxy)methoxy]-2-oxoethyl]glycine (acetyloxy)methyl ester	Fluorescent Ca^{2+} indicator	Invitrogen, France
Triton™ X-100 Detergent	Polyethylene glycol p-(1,1,3,3-tetramethylbutyl)-phenyl ether Octyl phenol ethoxylate Polyoxyethylene octyl phenyl ether 4-Octylphenol polyethoxylate Mono 30 TX-100 t-Octylphenoxypolyethoxyethanol Octoxynol-9	Used to lyse the cells in the MBE method at the end of the experiment	Sigma Aldrich, St Louis, MO, USA
Alectinib	Alectinib	ALK inhibitor for ALK-positive cancers	MedChemExpress-USA
Crizotinib	Crizotinib	ALK inhibitor for ALK-positive cancers	MedChemExpress-USA
Brigatinib	Brigatinib	ALK inhibitor for ALK-positive cancers	MedChemExpress-USA
MBCD	Methyl-β-cyclodextrin	Used for cholesterol depletion from the cell membranes	Sigma-Aldrich-St Louis, MO, USA
Anti-human TRPV2	Anti-human TRPV2 (VRL1) antibodys	Used in Western-Blot to identify the presence of TRPV2 in the membranes	Alomone labs-Israel
DMSO	Dimethyl sulfoxide	Vehicle solution	Sigma-Aldrich, France
Oxy-PVP	Oxy-Iso polyvinylpyrrolidone	Solution used in the oxygenscan measurements (ektacytometry) with a mean viscosity of 28-34 mPa.s, and an	Mechatronics- The Netherlands.

		osmolality of 282-286 mOsm/kg.	
EIon-ISO PVP	Polyvinylpyrrolidone	Solution used in the deformability measurements (ektacytometry) with a mean viscosity of 28-30 mPa.s and osmolality of 282-286 mOsm/kg	Mechatronics- The Netherlands.

All drugs are used at 1000X stock solution in DMSO, except Charybdotoxin, GsMTx4, and MBCD in water, and Δ^9- THC in ethanol.

D. **MBE method**

***Solution for MBE Method**:* Unbuffered Calcium Ringer: 154 mM NaCl, 2 mM KCl, 2 mM or 0 mM (4 µM) of $CaCl_2$.

Red Blood Cells: Blood from healthy donors are withdrawn into heparinized vacuum tubes, washed thrice with unbuffered saline by centrifugation for 5 minutes at 2500 rcf, the buffy coat and plasma removed, then packed with a final step of 1-minute centrifugation at 12000 rcf, and the packed cells stored at 4°C until used.

Principle: The MBE method (Macey et al., 1978; Bennekou and Christophersen, 1986; Jansen et al., 2021; Pérès et al., 2021) is used to monitor membrane potential evolution. Briefly, when RBCs are suspended in a nominally buffer-free solution in the presence of the CCCP protonophore (20 µM), changes in extracellular pH reflect membrane potential changes since protons are kept at equilibrium across the membrane. The membrane potential (V_M) can, thus, be estimated from the equation:

Equation 3: $V_M = 61.51. (pH_i - pH_o)$, in mV

Due to the high red cell buffer capacity, the intracellular pH (pH_i) remains constant (at about 7.2) throughout an experiment and can be estimated as the pH of the solution after lysis with Triton™ X-100 at the end of the experiment.

Procedure: Regarding the experimental procedure, 2900 µL of the experimental solution containing 20 µM of CCCP are heated at 37°C under constant magnetic stirring. For each experiment, 100 µL of packed RBCs (99% hct) are added, to reach a final cytocrit of 3.3%. All inorganic compounds are added at stock solution 1000X in DMSO, unless stated otherwise. The final DMSO concentration never exceeds 0.3%, a concentration that has no effect on either fluxes or membrane potential. Extracellular pH is measured using a G200 pH electrode (Radiometer, Copenhagen, Danemark) coupled to a red Rod 200 reference electrode (Radiometer) and a PHM210 pHmeter (Radiometer). Sampling and acquisition are done with an electrode amplifier (EA-BTA, Vernier, USA) at a rate of 1 Hz connected to an AD LABQUEST Mini interface (Vernier, USA) with a resolution of 0.01 pH unit. The data are visualized and stored with the Logger Lite software (Vernier, France). At the end of each experiment, Triton X-100 detergent (1% in 3M NaCl) is added, causing total cell lysis and a resulting solution that attains the intracellular pH.

Analysis: Results are represented using GraphPad Prism 10. Generated curves usually contain 4 points of interest while we analyze the curves (Figure 26):

- the resting membrane potential (E_m) which is usually equal to the equilibrium potential of Cl^- since Cl^- conductance is predominant at the resting state of the RBC.
- Second, there is the hyperpolarization phase, induced by a hyperpolarizing molecule that generates an increase in the K^+ efflux due to Ca^{2+} entry and the subsequent activation of the Gárdos channel, making K^+ currents take over the predominant Cl^- currents.
- Afterwards, usually we reach a point where all ion movements are equal; the K^+ efflux starts to decrease and reaches again levels that are equal to other ions like Cl^- or Na^+. This point is called “maximum hyperpolarization”.
- Finally, there is the repolarization phase, where currents generated by the activation of Non-Selective cation (NSC) channels, or Cl^- channels become stronger than the currents generated by the efflux of K^+.

Of note, the experimental solution used in this method varies depending on the experiment itself and the hyperpolarizing molecule; when A23187 is used as a hyperpolarizing molecule, the media contains 0 mM of Ca^{2+} which represents in fact 4 µM of nominal free Ca^{2+} due to salts contamination. When Yoda1, Dooku1, or TRPV2 are used, the media contains 2 mM of Ca^{2+}.

When NS309 is used, the media contained 2 mM or 0 mM (4 µM) of Ca^{2+}. This information is precised in the legend of each picture when NS309 is used.

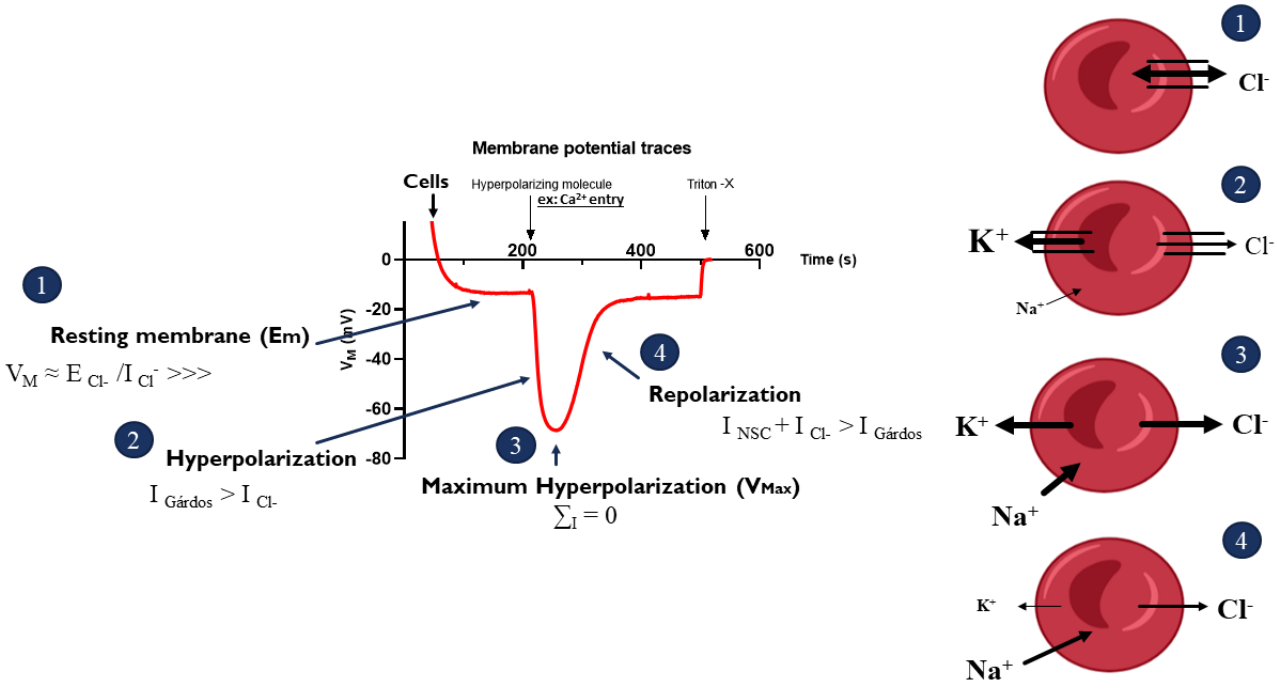

Figure 26: Scheme describing the analysis of the MBE method. A typical membrane potential trace in the middle surrounded with the important points that are studied on the curve. Important points are labeled consecutively from 1 to 4. On the right of the Figure, red blood cells that correspond to the studied points on the curves. 1 represents the resting membrane state; 2 represents hyperpolarization of the red cells; 3 represents the maximal hyperpolarization, and 4 represents the repolarization state. Arrows represent inward or outward currents depending on their direction. The figure was created using Bio-Render.

E. Intracellular Water, Na^+, and K^+ measurements

Washing solution (For Dooku1 study only) consisted of a Buffered Ringer for water and ion content measurements: 150 mM NaCl, 2 mM KCl, 2 mM CaCl2, 1 mM MgCl2, 10 mM HEPES, 5 mM Glucose with pH 7.4 adjusted with NaOH.

***RBCs preparations (For Dooku1 study)*:** Fresh blood collected into heparinized tubes from healthy donors were washed thrice at 2500 rcf for 5 minutes using the described solution. A final solution at 20% hematocrit was prepared. Cells were placed in a warmed stirring incubator at 37°C with 400 rpm shaking. Drugs were added at their designed concentration. 0.5 mL aliquots of the cell suspension were taken at each timepoint, using 2.5 mL syringe (Terumo, Leuven-Belgium)

and 21G (0.8x50 mm) Agani needles (Terumo, Leuven-Belgium), distributed in Beckman polyethylene micro test tubes (Dutscher, France) and centrifuged at 19600 rcf for 7 minutes at 10°C. After centrifugation, the packed cell mass was separated from the supernatant by slicing the tube with a razor blade below the top of the red cell column prior weighting (see intracellular ionic and water section measurements).

RBCs preparation (For other studies): 0.5 mL aliquots of the total blood were handled using 2.5 mL syringe (Terumo, Leuven-Belgium) and 21G (0.8x50 mm) Agani needles (Terumo, Leuven-Belgium), and distributed in Beckman polyethylene micro test tubes (Dutscher, France) and centrifuged at 19600 rcf for 7 minutes at 10°C. After centrifugation, the packed cell mass was separated from the supernatant by slicing the tube with a razor blade below the top of the red cell column prior weighting.

Water content

After weighting, the packed cells were dried to constant weight for at least 48 hours at 90°C and re-weighted. RBC volume depends on the intracellular water content, which is estimated to be about 90 fL for a healthy discocyte.

Na^+ and K^+ content

The packed cells within the sliced tubes were lysed in 1 mL MilliQ water. Proteins were denatured to ease separation by addition of 232 µM of perchloric acid. The tubes were spun at 12000 rcf for 7.5 minutes at 4°C and the supernatant was passed onto sample tubes and diluted 10 times. The ionic content was measured using a flame photometer (PFP7 Jenway, France). The amounts of Na^+ or K^+ measured are reported as mmol/liter of cell water (mmol/lcw) or micrograms/mol of intracellular contents (µmol/g dcs). A technical error occurred in flame photometer during my Ph.D., leading to abnormally lower range of K^+ concentrations. We couldn't know until now the reason of this error but we consider the comparison between patients and control valid since the error is applied to all samples in the same manner.

F. **Flow Cytometry for Ca^{2+} monitoring**

Live flow cytometry and imaging solution: 137 mM NaCl, 3.5 mM KCl, 2 mM CaCl2, 1 mM MgCl2, 10 mM HEPES, 10 mM Glucose, 0.05% BSA with pH 7.4 adjusted with NaOH.

RBCs preparation: 25 µL of blood from healthy donors were washed thrice with the described solution for 5 minutes at 2500 rcf. RBCs were loaded with Fluo-4, AM at a concentration of 5 µM for 1 hour at 37°C with 400 rpm shaking. Cells were rinsed thrice with this solution for 5 minutes at 2500 rcf.

Protocol (for Dooku1 study): At t=0 s, 2.5 µL of Fluo-4 loaded RBCs were added to 500µl of solution containing drugs at desired concentration and immediately observed on the cytometer. Flow cytometry measurements were performed on a BD FACSCanto^{TM} II (RECYF platform, Station Biologique, Roscoff, France). Dooku1 dose-response curve (1 µM, 10 µM, 100µM), Yoda1 (625 nM), and Yoda1+ Dooku1 (10 µM) testing was realized on 3 independent healthy donors. For each sample, data were recorded during 5 minutes after starting drugs incubation. The results were assessed and analyzed using Kaluza (Beckman Coulter- USA).

Protocol (for TRPV2 study): Flow cytometry was used to assess the intracellular Ca^{2+} levels after the incubation of RBCs with Δ^9THC. 25 µL of blood were washed three times in the Tyrode buffer. RBCs were loaded with Fluo-4 AM (Molecular Probes, Eugene, OR, USA) at a concentration of 5 µM for 1 h at 37°C with 400 rpm shaking. After washing three times in the Tyrode buffer, 2.5 µL of Fluo-4 loaded RBCs were added to a 500 µL designed Tyrode buffer in 5 mL round bottom polystyrene test tubes (Corning Inc., Corning, NY, USA). Flow cytometry measurements were performed on a BD FACSCanto^{TM} II (BD Biosciences, Erembodegem, Belgium) or LSRFortessa (Becton Dickinson, San Jose, CA, USA). For the Δ^9THC treated group, data were recorded for 10 minutes directly after Δ^9THC application. For control conditions in the Tyrode solution, 30000 cells were measured.The results were assessed using Kaluza (Beckman Coulter, USA) and Flow Jo (Becton Dickinson, USA) softwares.

G. **<u>Flow cytometry for PS exposure, and others</u>**

PS exposure on the outer membrane leaflet of the RBCs was evaluated using Annexin V-FITC binding. RBC suspensions (in 0.4% Hct in PBS containing 2.5 mM Ca^{2+}) were protected from light and incubated for 30 min at room temperature (RT) with Annexin V-FITC (1:200 dilution, Beckman Coulter). As a PS-negative control, cells were incubated in the presence of 5 mM EDTA. Immediately after incubation, samples were diluted and analysed by FACS (BD Accuri C6 or BD Calibur). The RBC surface expressions of CD47, CD49 and BCAM were also evaluated by flow

cytometry (incubations, as above) using the anti-CD47-PE (1:33 dilution, Miltenyi Biotec), or anti-CD49-PE (clone ALC1/1; Abcam) and/or anti-CD239(BCAM)-APC (clone REA276, 1:11 dilution Miltenyi Biotec) antibodies. For each sample, 50 000 events were acquired and gated for the appropriate forward scatter (FSC)/ side scatter (SSC).

H. Confocal imaging for Ca^{2+} imaging

2.5 µL of Fluo-4- loaded RBCs were diluted in 300 µL of the described solution and deposited on Polylysine-coated coverslips. At t=0, 300 µl of 2X drug containing solution was added, to reach desired final concentration, and imaged on a SP8 confocal microscope (Leica-Germany) linked to a LAS-X software (Merimage platform, Station Biologique, Roscoff, France). Fluorescence analysis was done using Fiji software (Schindelin et al., 2012).

I. Patch-Clamp

Solution: Patch-clamp experiments were performed using the following solutions: pipette solution (in mM): 140 KCl, 2 $MgCl_2$, 10 Hepes; pH adjusted to 7.20 with KOH. Bath solution (in mM): 140 NaCl, 2 $MgCl_2$, 2 $CaCl_2$, 10 Glucose, 10 Hepes; pH adjusted to 7.40 with NaOH.

Protocol: For the patch-clamp technique, 2 µL of whole blood were diluted in 500 µL of bath solution. Characterization of currents was performed in the whole-cell patch configuration. 3-5 GΩ seals were obtained by suctions applied for less than 20 s. Patch pipettes (tip resistance ranging between 10 and 14 MΩ) were prepared from borosilicate glass capillaries (Clark Electromedical Instruments, England GC150F-10), pulled and polished on a horizontal programmable puller (DMZ, Werner Zeitz Augsburg, Germany). Currents were elicited at room temperature by a 500 ms ramp voltage protocol from -100 to 100 mV, at a holding potential of 0 mV. After recording a stable baseline current in external solution (ES), cells were exposed to drugs. Current amplitudes (pA) and slope values (conductance, pS) were measured between 80 mV and 100 mV of the voltage ramp before and after compound addition for both patients and controls. If the current amplitude elicited upon Δ^9THC addition (I Δ^9THC) exceeded 3σ of the current amplitude at baseline conditions a cell was considered as Δ^9THC responder: $I\ \Delta^9\text{THC} > IES + 3\sigma IES$. Traces were analyzed by Clampfit 10.7 (Molecular Devices LLC).

J. Ektacytometry

1. Deformability analysis (for TRPV2-SCD study)

Deformability of RBCs from patients and controls, with and without Δ^9THC, was evaluated using the Deformability LoRRca protocol by using LORRCA MaxSis analyzer (Laser-assisted optical rational cell analyzer) (RR Mechatronics, Zwaag, The Netherlands). The ektacytometry measurement is performed at 37°C in a Couette system, which consists of two separate concentric cylinders with a narrow gap between each other. The blood sample is placed in the gap between the two cylinders to be analyzed. During the measurement, the inner cylinder (called bob) remains static, while the external one (cup) moves in rotation creating a shear stress in a range of 0.3 to 30 Pa, which allows the deformation of RBCs. For the deformability measurement, 10 µL of RBCs were resuspended in 1 mL of PVP with 30 µM or 80 µM final concentration of Δ^9THC for 5 minutes. The PVP has a greater viscosity than the intracellular viscosity of RBCs, for this reason the RBCs can deform in the direction of the flow with an elliptical shape. A 670 nm red laser passes through the suspension and projects the resulting diffraction pattern onto a screen, and it is analyzed using LoRRca software provided by the manufacturer. From the diffraction spectrum of each blood sample, the software calculates the Elongation Index (EI) at each shear stress, corresponding to the long and short axis of the ellipse: EI = (length − width) / (length + width). Data obtained at 30 Pa are reported.

2. Oxygenscan (for PIEZO1-SCD study)

RBC deformability was measured under an oxygen gradient by oxygenscan ektacytometry, as previously described (Boisson et al., 2021). A volume of 50 µL of blood, standardized to a fixed total RBC count of 200 × 106, was mixed with 5 mL of Oxy-Iso polyvinylpyrrolidone (PVP) suspension with a mean viscosity of 28–30 cP (Mechatronics, The Netherlands) and osmolality of 282–286 mOsm/kg. The suspension was sheared at 30 Pa and 37°C while the oxygen partial pressure (pO_2) was gradually decreased from 160 to 20 mm Hg (deoxygenation) and then returned to normoxic values. The diffraction pattern was analysed by computer to determine the maximum RBC deformability in normoxia (EImax), the minimum RBC deformability reached during deoxygenation (EImin), and the oxygen partial pressure at which RBC start to sickle (i.e. the Point

of Sickling, PoS). PoS is defined as a decrease of at least 5% of EI_{max} during deoxygenation (Figure 27).

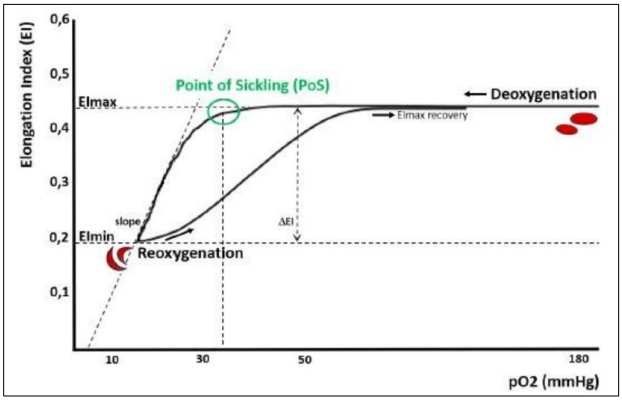

Figure 27: Principle and representative oxygenscan result (Oxygenscan – Lorrca – Functional RBC Analysis, 2020).

K. Cell morphology analysis

Patient and control blood smears were prepared on glass slides, fixed with methanol, and stained with freshly prepared Giemsa (10%, 15 min) (Sigma-Aldrich). Pictures were taken under a microscope with a 100x objective and morphological analysis was performed using Fiji (Schindelin et al., 2012) to determine four parameters: projected area, circularity, roundness, and aspect ratio.

Roundness, circularity, and aspect ratio were obtained using ImageJ according to their respective formulas:

Equation 4: Roundness = $4 \times \frac{[Area]}{\pi \times [Major\ Axis]2}$

Equation 5: Circularity = $4\,\pi \frac{[Area]}{[Perimeter]2}$

Equation 6: Aspect ratio = $\frac{Major\ axis}{Minor\ axis}$

L. MBCD- Cholesterol depletion

Cells were washed (same as cell preparation for MBE method) and adjusted to 10% hematocrit value using normal Ringer solution. Cells were incubated with MBCD solution for 30 minutes at 37°C.

MBCD (Sigma Aldrich) was tested at 1, 5, 10, and 30 mM. Stock solutions were prepared with respect to dilution factor 1/1000 in H_2O. After incubation, the cells were centrifuged to remove the extracellular media and used directly in the MBE experiments. For this type of experiment, cells were challenged with Yoda1 at 100 nM or 500 nM, and with Dooku1 at 10 µM.

M. **Statistics**

GraphPad Prism version 9 and 10 (GraphPad Software, San Diego, California USA) was used for the statistical analysis and presentation of the data. When data followed a Gaussian distribution (Shapiro-Wilk test), paired t-test or ordinary one-way ANOVA with multiple comparisons was used to test for statistical significance. Data are presented as mean ± standard deviation (SD) or mean ± standard error of mean (SEM). When data did not follow a Gaussian distribution, the Wilcoxon test was used for comparisons between two data sets, and the Kruskal-Wallis test was used for multiple comparisons within the same data set. $p < 0.05$ was deemed as significant.

N. **Funding**

This thesis received funding from the European Union Horizon 2020 Research and Innovation Program under the Marie Skłodowska-Curie grant agreement No 860436 – EVIDENCE (Aline Hatem).

Chapter I- Dual action of Dooku1 on PIEZO1 channel in human RBCs

I. Introduction

As explained in the introductory section of this manuscript, the discovery of PIEZO1 and of the important role it plays in the life of the RBCs, from differentiation in the bone marrow (Caulier et al., 2020; Aglialoro et al., 2021) to the rheological properties required for the 120 days of circulation (Cahalan et al., 2015; Danielczok et al., 2017), senescence and withdrawal from circulation (Lew and Tiffert, 2017), and its importance in pathologies such as xerocytosis (Zarychanski et al., 2012; Glogowska et al., 2017), has led many laboratories to focus their research on this particular channel. However, as with any study of ion channel activity in a physiological process, a well-defined pharmacology is required. The screening of chemical compound libraries quickly identified Yoda1 as the most effective agonist in HEK293 cells transfected with PIEZO1, potentiating the channel's intrinsic mechanosensitivity (Syeda et al., 2015). Nevertheless, the numerous experiments performed on red blood cells with this agonist have shown that Yoda1 at very low concentrations is capable of directly activating the channel, leading to sufficient calcium entry (at physiological extracellular calcium concentrations) to activate the Gárdos channel, at least transiently (Rapetti-Mauss et al., 2017). More recently, a new compound, named Dooku1 for its ability to antagonize the activating effects of Yoda1, has been proposed as a new tool in the pharmacopeia that can be used to study PIEZO1 functions (Evans et al., 2018).

In this chapter (article published in Frontiers in Physiology), we used Dooku1 to modulate the activating effects of Yoda1, and surprisingly demonstrated that Dooku1, at the concentrations previously recommended to antagonize the effects of Yoda1, was able to have an activating effect on PIEZO1, and was ultimately only marginally inhibitory of the activating potency of Yoda1-induced calcium entry. These results underline the need for caution when using PIEZO1 modulators in RBCs, which are extremely deformable compared to other cell types.

II. Published article

frontiers | Frontiers in Physiology

TYPE Original Research
PUBLISHED 10 July 2023
DOI 10.3389/fphys.2023.1222983

Check for updates

OPEN ACCESS

EDITED BY
Richard Van Wijk,
Utrecht University, Netherlands

REVIEWED BY
Asya Makhro,
University of Zurich, Switzerland
John Stanley Gibson,
University of Cambridge, United Kingdom
Immacolata Andolfo,
University of Naples Federico II, Italy

*CORRESPONDENCE
Stéphane Egée,
egee@sb-roscoff.fr

RECEIVED 15 May 2023
ACCEPTED 27 June 2023
PUBLISHED 10 July 2023

CITATION
Hatem A, Poussereau G, Gachenot M, Pérès L, Bouyer G and Egée S (2023), Dual action of Dooku1 on PIEZO1 channel in human red blood cells.
Front. Physiol. 14:1222983.
doi: 10.3389/fphys.2023.1222983

COPYRIGHT
© 2023 Hatem, Poussereau, Gachenot, Pérès, Bouyer and Egée. This is an open-access article distributed under the terms of the Creative Commons Attribution License (CC BY). The use, distribution or reproduction in other forums is permitted, provided the original author(s) and the copyright owner(s) are credited and that the original publication in this journal is cited, in accordance with accepted academic practice. No use, distribution or reproduction is permitted which does not comply with these terms.

Dual action of Dooku1 on PIEZO1 channel in human red blood cells

Aline Hatem[1,2], Gwendal Poussereau[1], Martin Gachenot[3], Laurent Pérès[1,2], Guillaume Bouyer[1,2] and Stéphane Egée[1,2]*

[1]Sorbonne Université, CNRS, UMR8227 LBI2M, Station Biologique de Roscoff, Roscoff, France, [2]Laboratory of Excellence GR-Ex, Paris, France, [3]Sorbonne Université, CNRS, FR2424, Station Biologique de Roscoff, Roscoff, France

PIEZO1 is a mechanosensitive non-selective cation channel, present in many cell types including Red Blood Cells (RBCs). Together with the Gárdos channel, PIEZO1 forms in RBCs a tandem that participates in the rapid adjustment of the cell volume. The pharmacology allowing functional studies of the roles of PIEZO1 has only recently been developed, with Yoda1 as a widely used PIEZO1 agonist. In 2018, Yoda1 analogues were developed, as a step towards an improved understanding of PIEZO1 roles and functions. Among these, Dooku1 was the most promising antagonist of Yoda1-induced effects, without having any ability to activate PIEZO1 channels. Since then, Dooku1 has been used in various cell types to antagonize Yoda1 effects. In the present study using RBCs, Dooku1 shows an apparent IC_{50} on Yoda1 effects of 90.7 µM, one order of magnitude above the previously reported data on other cell types. Unexpectedly, it was able, *by itself*, to produce entry of calcium sufficient to trigger Gárdos channel activation. Moreover, Dooku1 evoked a rise in intracellular sodium concentrations, suggesting that it targets a non-selective cation channel. Dooku1 effects were abolished upon using GsMTx4, a known mechanosensitive channel blocker, indicating that Dooku1 likely targets PIEZO1. Our observations lead to the conclusion that Dooku1 behaves as a PIEZO1 agonist in the RBC membrane, similarly to Yoda1 but with a lower potency. Taken together, these results show that the pharmacology of PIEZO1 in RBCs must be interpreted with care especially due to the unique characteristics of RBC membrane and associated cytoskeleton.

KEYWORDS

Dooku1, Piezo1, Yoda1, $[Ca^{2+}]_i$, non-selective cation channels, erythrocyte

1 Introduction

PIEZO1 is a mechanosensitive ion channel, present in most eukaryotic species (Coste et al., 2010), it has been shown to be the effector of transduction of mechanical force sensing in multiple cell types and tissues (Syeda, 2021). PIEZO1 allows the passage of mono- and divalent cations (Gnanasambandam et al., 2015) in response to mechanical signals, with two putative mechanisms for signal transduction: either via contact with the actin cytoskeleton (Wang et al., 2022) or via sensing of membrane curvature and tension (Cox et al., 2016) as recently demonstrated in mouse RBCs (Vaisey et al., 2022).

The presence of the PIEZO1 channel in human RBC membranes was first established from the link between gain-of-function mutations of PIEZO1 and a RBC pathology, termed Dehydrated Hereditary Stomatocytosis (DHS) or Xerocytosis (Zarychanski et al., 2012;

Andolfo et al., 2013; Bae et al., 2013). RBCs possess a repertoire of membrane ion transporters, which maintain cell homeostasis and volume. Cation transporters represent an efficient tool for cell volume regulation. Among them, cation channels are the most efficient, given their rapid kinetics and permeability rates. Most notably, the tandem constituted by the Gárdos channel (KCNN4, KCa3.1), a Ca^{2+}-activated K^+ channel, and PIEZO1 is often cited as a key regulator of RBC volume (Lew and Tiffert, 2017; Caulier et al., 2018; Jankovsky et al., 2021); PIEZO1 appearing as a sensor and the Gárdos channel as an effector of the volume decrease accompanying deformability. Given the very small number of copies of PIEZO1 (30-80) in the RBC membrane (Gautier et al., 2018; Vaisey et al., 2022), a convenient way to observe PIEZO1 effect is through the activity of the Gárdos channel.

The unravelling of the molecular identity of PIEZO1 has allowed the development of PIEZO1-specific pharmacology; this has allowed the characterization of its role in various situations. Like most mechanosensitive channels, it is inhibited by the spider toxin GsMTx4 (Bowman et al., 2007; Bae et al., 2011). In 2015, a small synthetic molecule termed Yoda1 was described as an agonist for human and mouse PIEZO1, prominently affecting the sensitivity and the mean time of the open state of the channel (Syeda et al., 2015). Later it was proposed that Yoda1 acts by lowering the mechanical threshold for channel activation (Botello-Smith et al., 2019) or by voltage-activating PIEZO1 (Wijerathne et al., 2022). Since then, the molecule has proven to be a useful tool in studies targeting PIEZO1. In 2018, a series of Yoda1 analogues were designed and tested on the PIEZO1 channel in an attempt to expand its pharmacology (Evans et al., 2018). By modifying the pyrazine ring of Yoda1, or substituting its thiadiazole group with oxadiazole, several analogues that can reversibly antagonize Yoda1, were obtained. Among them, a compound judiciously named Dooku1 gave the most promising initial results. Based on tests either on HEK293 cells expressing human PIEZO1 or on HUVECs,

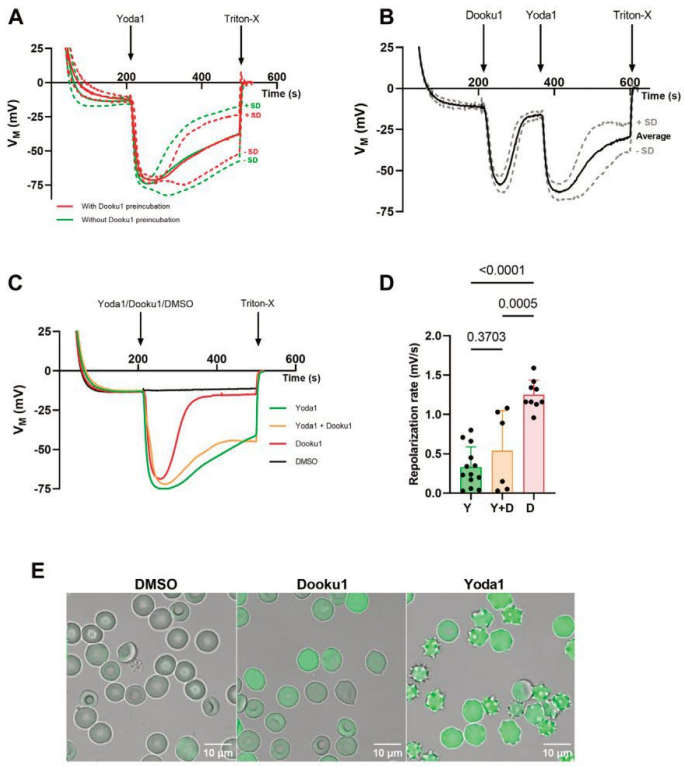

FIGURE 1
Dooku1 alone can trigger a Gárdos effect. **(A)** Evolution of RBC membrane potential after injection of Yoda1 (625 nM, green, $n = 13$) without any pre-incubation, and Yoda1 (625 nM, red, $n = 5$) after a pre-incubation for 15 min at 37°C with Dooku1 (10 µM). Mean traces are plotted with their SD envelopes **(B)** Evolution of membrane potential after challenging the cells successively with Dooku1 (10 µM) and then with Yoda1 (625 nM). Traces represent average ± SD, $n = 6$. The mean trace was plot with its SD envelope **(C)** Changes in RBC membrane potential after injection of Yoda1 (625 nM, green, n = 13), Dooku1 (10 µM, red, $n = 9$), and simultaneously Yoda1 (625 nM) and Dooku1(10 µM, orange, $n = 6$). The black line represents control done with vehicle alone (DMSO, $n = 4$). Traces represent average (SD envelope is not drawn for sake of clarity). **(D)** Repolarization rate in different conditions measured right after maximum hyperpolarization. The repolarization values were obtained by calculating the derivative values between two-time points during which the repolarization takes place. Histograms represent means ± SD for each condition. **(E)** Confocal microscopy images of Fluo-4-loaded RBC 1 min after perfusion of DMSO 0.1% (left), Dooku1 (10 µM; middle) or Yoda1 (625 nM; right).

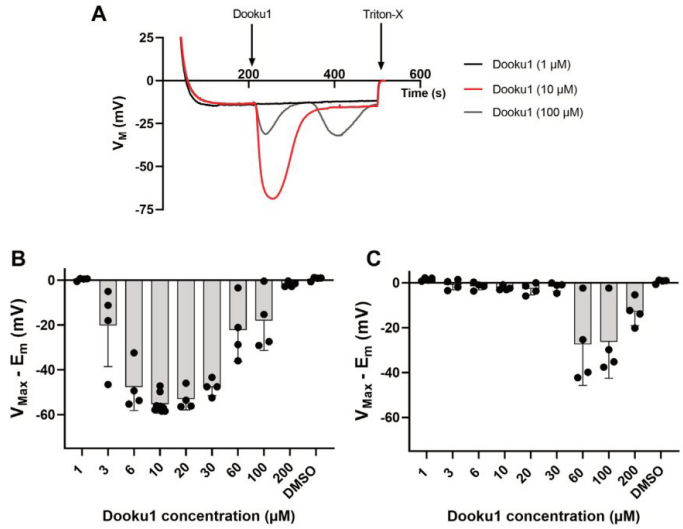

FIGURE 2
Dooku1 dose-response curve. **(A)** Variations in membrane potential after addition of Dooku1 at different concentrations: 1 µM (black trace), 10 µM (red trace), and 100 µM (grey trace). Traces represent means of n = 4 independent replicates for each condition. SD envelopes were not added for clarity reasons **(B,C)** Maximal hyperpolarizations induced by increasing concentrations of Dooku1. Histograms represent the maximal hyperpolarizations (V_{Max}) that were reached, from which were deduced the nominal resting membrane potential (E_m). In **(B)** values of the first hyperpolarization occurring immediately after Dooku1 injection; and in **(C)** values of the second hyperpolarization, when occurred, which was delayed in time. Histograms represent means ± SD of n = 4 experiments.

Dooku1 showed no effect by itself on PIEZO1. Nevertheless, it was able to inhibit a 2 µM Yoda1-induced Ca^{2+} entry with an IC_{50} of 1.3–1.5 µM. Thus, a competitive effect on the same or similar binding site by Yoda1 was proposed (Evans et al., 2018). Since then, Yoda1 and Dooku1 have been used in combination in several cell types to decipher PIEZO1 activity and functions (Deivasikamani et al., 2019; Matsunaga et al., 2021; Barnett et al., 2022; Szabó et al., 2022), including RBCs (Wadud et al., 2020).

In the present work, we have investigated the consequences of Dooku1 addition on Yoda1-induced effects on human RBCs. To our surprise, we observed that Dooku1 itself has effects on RBC membrane potential and triggers a rise in intracellular Ca^{2+}; this in turn leads to the activation of the Gárdos channel, similarly to Yoda1 but with a lower potency. We also unravel a moderate inhibitory capacity for Dooku1 on Yoda1 effects in RBCs. Finally, we show that Dooku1 is able to activate PIEZO1 within the RBC membrane.

2 Materials and methods

2.1 Reagents and drugs

All salts were acquired from Sigma and were of analytical grade or better. Dooku1: 2-[(2,6-Dichlorobenzyl)thio)-5-(1H-pyrrol-2-yl)-1,3,4-oxadiazole (Sigma-Aldrich, France). Yoda1: 2- [5-[[(2,6-Dichlorophenyl)methyl]thio]-1,3,4-thiadiazol-2-yl]pyrazine (Tocris, France). Charybdotoxin (Alomone labs, Israel). CCCP: carbonyl cyanide 3-chlorophenylhydrazone (Sigma-Aldrich, France). GsMTx4 (Alomone labs, Israel). Fluo-4, AM (Invitrogen, France). All drugs are used at 1000X stock solution in DMSO, except Charybdotoxin and GsMTx4 in water.

2.2 Solutions

Solution A: Buffered Ringer for water and ion content measurements: 150 mM NaCl, 2 mM KCl, 2 mM $CaCl_2$, 1 mM $MgCl_2$, 10 mM HEPES, 5 mM Glucose with pH 7.4 adjusted with NaOH.

Solution B: Unbuffered Calcium Ringer for membrane potential measurements using MBE method: 154 mM NaCl, 2 mM KCl, 2 mM $CaCl_2$.

Solution C: Live flow cytometry and imaging solution: 137 mM NaCl, 3.5 mM KCl, 2 mM $CaCl_2$, 1 mM $MgCl_2$, 10 mM HEPES, 10 mM Glucose, 0.05% BSA with pH 7.4 adjusted with NaOH.

2.3 Ethical statement

Blood from healthy volunteers was withdrawn upon written informed consent (EFS, Etablissement Français du Sang), in

10.3389/fphys.2023.1222983

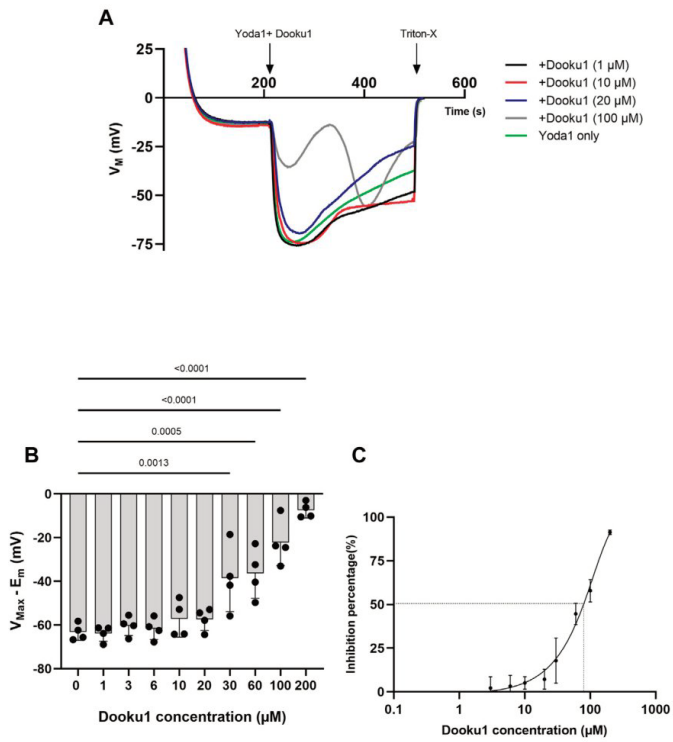

FIGURE 3
Dooku1 inhibitory effects on Yoda1-induced hyperpolarizations **(A)**Variations in membrane potentials in response to Dooku1 at different concentrations 1 µM (black trace), 10 µM (red trace), 20 µM (blue trace), and 100 µM (grey trace), added simultaneously with Yoda1 (625 nM). Yoda1 alone (green trace). Traces represent means of 4 independent experiments for each condition. SD envelopes were not added for clarity reasons **(B)** First maximal hyperpolarization observed with increasing Dooku1 concentrations, added simultaneously with Yoda1 (625 nM). Histograms represent means ± SD (n = 4), **(C)** Dose-response curve of Yoda1-induced hyperpolarizations inhibition by Dooku1 (n = 3) according to the first hyperpolarization only.

accordance with the guidelines of the Helsinki declaration of 1975, as revised in 2008. This work has been approved by the institutional (CNRS) Ethical committee and by the French Ministry of Research (declaration DC-2019-3842).

2.4 Red blood cells

2.4.1 For membrane potential measurements

Blood from healthy donors was withdrawn into heparinized vacuum tubes, washed thrice with unbuffered saline by centrifugation for 5 min at 2,500 rcf, the buffy coat and plasma removed, then packed with a final step of 1-min centrifugation at 12,000 rcf, and the packed cells stored at 4°C until used.

2.4.2 For microscopy acquisition and flow cytometry

25 µL of blood from healthy donors were washed thrice with *Solution C* for 5 min at 2,500 rcf. RBCs were loaded with Fluo-4, AM at a concentration of 5 µM for 1 h at 37°C with 400 rpm shaking. Cells were rinsed thrice with the *Solution C* for 5 min at 2,500 rcf.

2.4.3 For intracellular sodium, potassium, and water content

Fresh blood collected into heparinized tubes from healthy donors were washed thrice at 2,500 rcf for 5 min using the *Solution A*. A final solution at 20% haematocrit was prepared. Cells were placed in a warmed stirring incubator at 37°C with 400 rpm shaking. Drugs were added at their designed concentration. 0.5 mL aliquots of the cell suspension were taken at each timepoint, distributed in Beckman polyethylene micro test tubes (Dutscher, France) and centrifuged at 19,600 rcf for 7 min at 10°C. After centrifugation, the packed cell mass was separated from the supernatant by slicing the tube with a razor blade below the top of the red cell column prior weighting (see intracellular ionic and water section measurements).

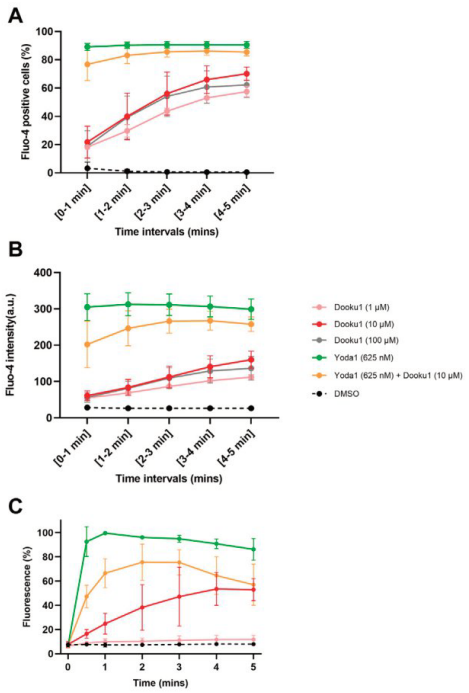

FIGURE 4
Dooku1 can generate an increase in intracellular calcium. **(A,B)** Flow cytometry follow-up of Fluo-4-loaded RBCs, measuring the percentage of Fluo-4 positive cells **(A)** and the mean fluorescence intensity (MFI) **(B)** during 5 min of Dooku1, Yoda1 or both molecules perfusion. Traces are means ± SD of n = 3 independent experiments. **(C)** Mean fluorescence of Fluo-4-loaded RBCs in confocal imaging, after perfusion with Dooku1, Yoda1 or both. Mean fluorescence of RBCs was calculated and are expressed as percentages of Yoda1-induced maximum fluorescence. Data are averages ±SD of n = 3 independent experiments.

2.5 Membrane potential measurement

The CCCP method or MBE method (method of Macey, Bennekou, and Egee) as it was recently named by Jansen et al., 2021(Macey et al., 1978; Bennekou and Christophersen, 1986; Jansen et al., 2021; Pérès et al., 2021) was used to monitor membrane potential evolution. Briefly, when RBCs are suspended in a nominally buffer-free solution in the presence of the CCCP protonophore (20 µM), changes in extracellular pH reflect membrane potential changes since protons are kept at equilibrium across the membrane. The membrane potential (V_M) can, thus, be estimated from the equation:

$$V_M = 61.51.\ (pH_i - pH_o), \text{in mV}$$

Due to the high red cell buffer capacity, the intracellular pH (pH_i) remains constant (at about 7.2) throughout an experiment and can be estimated as the pH of the solution after lysis with Triton™ X-100 at the end of the experiment. Regarding the experimental procedure, 2,900 µL of the experimental solution containing 20 µM of CCCP was heated at 37°C under constant magnetic stirring. For each experiment, 100 µL of packed RBCs (99% hct) were added, to reach a final cytocrit of 3.3%. All inorganic compounds were added at stock solution 1000X in DMSO, unless stated otherwise. The final DMSO concentration never exceeded 0.3%, a concentration that has no effect on either fluxes or membrane potential. Extracellular pH was measured using a G200 pH electrode (Radiometer, Copenhagen, Denmark) coupled to a red Rod 200 reference electrode (Radiometer) and a PHM210 pHmeter (Radiometer). Sampling and acquisition were done with an electrode amplifier (EA-BTA, Vernier, United States) at a rate of 1 Hz connected to an AD LABQUEST Mini interface (Vernier, United States) with a resolution of 0.01 pH unit. The data were visualized and analyzed with the Logger Lite software (Vernier, France). At the end of each experiment, Triton X-100 detergent (1% in 3M NaCl) was added, causing total cell lysis and a resulting solution that attains the intracellular pH.

2.6 Flow cytometry

At t = 0, 2.5 µL of Fluo-4 loaded RBCs were added to 500 µL of *solution C* containing drugs at desired concentration and immediately observed on the cytometer. Flow cytometry measurements were performed on a BD FACSCanto™ II (BD Bioscences, Erembodegem, Belgium, RECYF platform, Station Biologique, Roscoff, France). Dooku1 dose-response curve (1 µM, 10 µM, 100 µM), Yoda1 (625 nM), and Yoda1+ Dooku1 (10 µM) testing was realized on 3 independent healthy donors. For each sample, data were recorded during 5 min after starting drugs incubation. The results were assessed and analyzed using Kaluza (Beckman Coulter, Life Sciences, France).

2.7 Confocal microscopy

2.5 µL of Fluo-4- loaded RBCs were diluted in 300 µL of *solution C* and deposited on Polylysine-coated coverslips. At t = 0, 300 µL of 2X drug containing solution was added, to reach desired final concentration, and imaged on a SP8 confocal microscope (Leica-Germany) linked to a LAS-X software (Merimage platform, Station Biologique, Roscoff, France). Fluorescence analysis was done using Fiji software, n = 40 to 170 cells quantified for each time point (Schindelin et al., 2012).

2.8 Intracellular water, Na^+, and K^+ measurements

2.8.1 Water content

After weighting, the packed cells were dried to constant weight for at least 48 h at 90°C and re-weighted. RBC volume depends on the intracellular water content, which is estimated to be about 90 fL for a healthy discocyte. Shape change can be misleading in the estimation of cellular water content due to the great plasticity of the

10.3389/fphys.2023.1222983

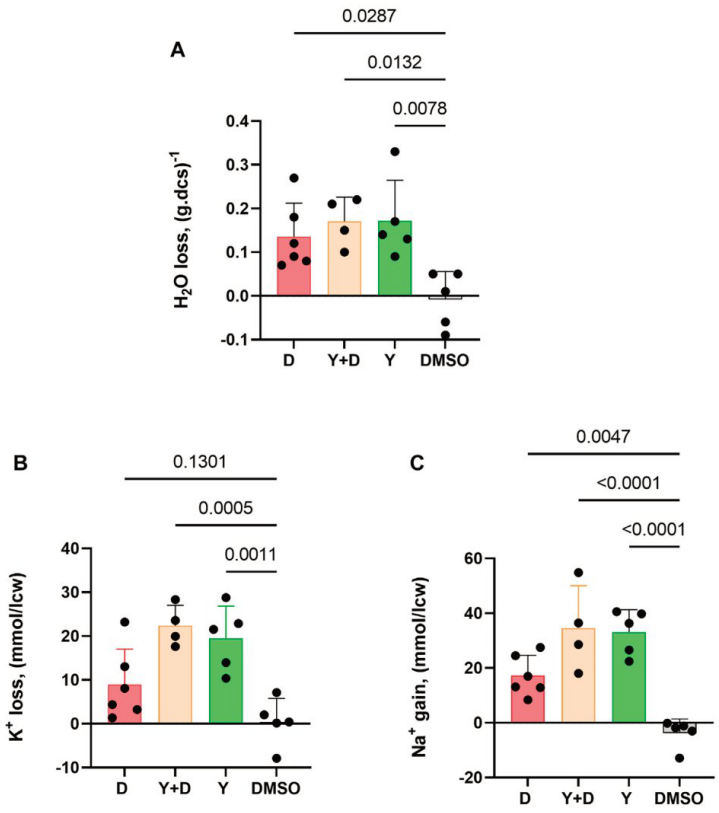

FIGURE 5
Dooku1 can alter the intracellular water, K^+, and Na^+ contents of the RBC. Measurements of **(A)** Water content loss **(B)** K^+ loss and **(C)** Na^+ gain after 30 min of incubation with Dooku1 (10 μM), Yoda1 (625 nM) or both. Histograms represent means ± SD of n = 6 for Dooku1 (D, in red), n = 4 for Yoda1+Dooku1 (Y + D, in orange), n = 5 for Yoda1 only (Y, in green), and n = 5 DMSO (black).

red cell membrane. These measurements are independent of cell shape.

2.8.2 Na^+ and K^+ content

The packed cells within the sliced tubes were lysed in 1 mL MilliQ water. Proteins were denatured to ease separation by addition of 232 μM of perchloric acid. The tubes were spun at 12,000 rcf for 7.5 min at 4°C and the supernatant was passed onto sample tubes and diluted 10 times. The ionic content was measured using a flame photometer (PFP7 Jenway, France). The amounts of Na^+ or K^+ measured are reported as mmol/L of cell water.

2.9 Statistics and data analysis

GraphPad Prism version 9 (GraphPad Software, San Diego, California United States) was used for the statistical analysis and presentation of the data. One-way ANOVA with multiple comparisons was used to test for statistical significance. Data are represented as mean ± standard deviation (SD). $p < 0.05$ was deemed as significant.

3 Results

3.1 Dooku1 can trigger a Gárdos effect

Yoda1 is the most efficient chemical agonist of the PIEZO1 channel identified thus far, leading to calcium entry and eventually Gárdos channel opening once its threshold of activation is reached. Gárdos channel current strength is strictly dependent on intracellular calcium concentration (channel opening probability). This results in noteworthy K^+ efflux and hyperpolarization (Figure 1A; Supplementary Figure S1A). Dooku1 has been described recently as an antagonist of this effect (Evans et al., 2018; Wadud et al., 2020). In our

10.3389/fphys.2023.1222983

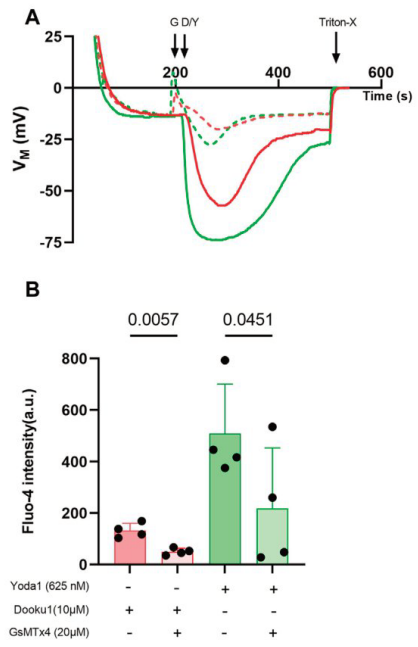

FIGURE 6
GsMTx4 can inhibit Dooku1 effects. **(A)** A representative trace showing the partial inhibition of membrane potential variations after using GsMTx4 (G). Cells were preincubated with GsMTx4 (20 μM) for 20 min at 37°C, then GsMTx4 (20 μM) was added to the medium at 190 s. Cells were challenged with Dooku1 (10 μM, in red; plain line without GsMTx4, dotted line with GsMTx4) or Yoda1 (625 nM, in green; plain line without GsMTx4, dotted line with GsMTx4) at 210 s. **(B)** Comparison of Fluo-4 intensity observed by flow cytometry. Histograms represent means ± SD (n = 4). Statistical differences were assessed using paired one-way ANOVA.

observations, contrary to what was described by others, preincubation of RBCs with Dooku1 (10 μM) did not affect neither Yoda1-triggered hyperpolarization (Figure 1A) nor repolarization rate (Figures 1B–D). Even more surprisingly, Dooku1 alone induces hyperpolarization, to the same extent as observed with Yoda1 (Figures 1B, C; Supplementary Figure S1B). This result indicates that Dooku1 can provoke a sufficient entry of Ca^{2+} within RBCs to activate the Gárdos channel. In the case of Dooku1, however, the repolarization rate is faster than with Yoda1 (Figures 1C, D), suggesting that the amount of calcium entry triggered by Dooku1 is lower than with Yoda1. This was verified by microscopy on Fluo-4 loaded RBCs, where Ca^{2+} entry after Dooku1 perfusion can clearly be seen; the magnitude is demonstrably lower than with Yoda1 (Figure 1E). To ensure that the observed hyperpolarizations were indeed due to Gárdos channel activation, Gárdos was inhibited with 100 nM of Charybdotoxin (ChTX) prior to addition of Dooku1 and Yoda1 addition. In the presence of ChTX, all hyperpolarization was abolished (Supplementary Figure S1C).

3.2 Dooku1, an activator as well as an antagonist of Yoda1

Next, a dose-response study of the effects of Dooku1 on erythrocyte membrane potential was performed. Between 1 and 10 μM, there was a direct dose-dependent effect (Figures 2A, B), with an increased maximal hyperpolarization observed immediately after Dooku1 injection. With a Dooku1 level of 3 μM, Dooku1-induced hyperpolarization was significant (p = 0.014 for 3 μM, p < 0.0001 for 6 μM–30 μM, p = 0.0057 for 60 μM, p = 0.0326 for 100 μM, $n \geq 4$) compared to the vehicle control (DMSO). However, at 200 μM of Dooku1, the value of hyperpolarization attained was not significant; it was close to that obtained with 1 μM (p = 0.999). Since maximum hyperpolarization is related to Gárdos channel activity which is only dependent on $[Ca^{2+}]i$, this suggests that Dooku1 allows a dose-dependent calcium entry.

Furthermore, at concentrations greater than 30 μM, the response to Dooku1 became more complex: i) a progressive decrease in the hyperpolarization amplitude appeared and ii) a delayed second hyperpolarization which occurred 55 ± 17 s (n = 11) after the end of the first hyperpolarization, irrespective of the concentration used (Figures 2A, C). However, the magnitude of this second hyperpolarization decreased at Dooku1 concentrations between 60 and 200 μM (Figure 2C). We hypothesize that the poorly observed solubility of the Dooku1 molecule at high concentrations, as reported by Evans et al., 2018, explains this unexpected but reproducible phenomenon (See Section 4).

We also tested the dose-response of Dooku1 inhibition on Yoda1 effects on RBC membrane potential by adding the two drugs simultaneously. Below 20μM, Dooku1 was unable to block Yoda1-induced hyperpolarization (Figures 3A, B). At 20 μM, a slight, but not statistically significant inhibition was observed. It became significant at 30 μM (17.9% ± 12.9%, n = 4, p = 0.0013), reaching 91.3% ± 1.26% (n = 4), p < 0.001, and at 200 μM with an IC_{50} of 90.7 ± 10.7 μM (n = 3, Figures 3B, C).

3.3 Dooku1 induces an increase in intracellular calcium

Given that hyperpolarization can be fully inhibited by ChTX (100 nM, Supplementary Figure S1C), it can be assumed that this phenomenon is driven by Gárdos channel activation. Thus, this result suggests that prior to Gárdos activation, $[Ca^{2+}]_i$ reaches the threshold for increasing the open probability of the latter channel. To assess that Dooku1 is able to induce a calcium entry by itself, both imaging and flow cytometry were performed. Cells were loaded with 5 μM of Fluo-4 to detect cells with increased intracellular calcium concentration. Cells were perfused with Dooku1 and/or Yoda1, and fluorescence was measured during a 5-min interval. Yoda1 (625 nM) evoked an instantaneous increase in intracellular calcium in 89.1% of the cells, showing that Yoda1 has induced an immediate intracellular entry of calcium. On the contrary, Dooku1 at 10 μM induced a progressive calcium entry, with only 21% of the cells showing increased intracellular calcium after 1 min, to reach 70.1% after 5 min. Interestingly, at this concentration, simultaneous perfusion of both Dooku1 and Yoda1 delayed the entry of

calcium (only 76.79% of Fluo-4 positive cells after 1min and 85.5% of Fluo-4 positive cells at 5 min) (Figure 4A).

In addition, the mean fluorescence intensity recorded upon Dooku1 stimulation either by flow cytometry or microscopy imaging indicates that the mean fluorescence reached only 20% of the one obtained with Yoda1 after 1 min (Figures 4B, C). As for the number of Fluo-4 positive cells, progressively mean fluorescence intensity extends to reach around 53% (53.5% for flow cytometry and 52.9% with confocal microscopy) of the one obtained with Yoda1 after 5 min. When Dooku1 was added simultaneously with Yoda1, it was able to delay the load of Ca^{2+} (Figures 4B, C). Essentially, Dooku1 can induce a significant calcium entry by itself even at 1 μM, as seen with flow cytometry (Figures 4A, B) and confocal microscopy (Supplementary Figure S2).

Taken together, these results show that Dooku1 can trigger a calcium entry, by itself, albeit more slowly and with a lower extent than Yoda1 but sufficient to induce a Gárdos channel activation.

3.4 Dooku1 activates a non-selective cation channel

It has been widely reported that the activation of PIEZO1 by Yoda1 induces a cell dehydration accompanied by a reversal of sodium and potassium gradients due to its nature of being a non-selective cation channel (Monedero Alonso et al., 2021; Pérès et al., 2021).

The impact of Dooku1 and Yoda1 molecules on the hydration status and ion contents of the cells has been evaluated. Dooku1, Yoda1, or both molecules added simultaneously, all induced water loss reiterating the results that these molecules trigger a Gárdos effect that leads to dehydration (Figure 5A).

Gárdos channel activation is accompanied by K^+ loss. Compellingly, K^+ effluxes generated using Dooku1 were smaller than in the presence of Yoda1. This result is in accordance with previous results presented here, in which we demonstrated that Dooku1 leads to $[Ca^{2+}]_i$ rise, but with an intensity lower than that observed with Yoda1. As a result, Gárdos channel is logically less activated with Dooku1, resulting in lower K^+ loss (Figure 5B).

Finally, Dooku1, Yoda1, and both molecules added together, all induced significant $[Na^+]_i$ increase (Figure 5C). This result suggests that both molecules activate a non-selective cation channel, and both have the same target, presumably PIEZO1. The effects of Dooku1, as for Yoda1, were inhibited by GsMTx4, supporting the latter hypothesis (Figure 6).

4 Discussion and conclusion

Deciphering non-selective cation permeability in erythrocytes, and PIEZO1 behavior in particular, is essential to understand the hydration state of the cells in physiological and pathophysiological conditions (Gallagher, 2017; Caulier et al., 2018; Evans et al., 2020; Yamaguchi et al., 2021). Pharmacological tools are a pre-requisite for these studies. Yet, PIEZO1 pharmacology is still at its infancy as stated by Evans *et al* (Evans et al., 2018). To address this deficit, Evans and coworkers designed Dooku1, a Yoda1 analogue that lacks any agonist effect on PIEZO1.

The present study shows unambiguously the capacity of Dooku1, by itself, to activate a Ca^{2+} permeability in human RBC membrane that is able to turn on the Gárdos channel. MBE measurement on a RBC population, flow cytometry or confocal imaging of individual RBCs all gave proof that in the human RBC PIEZO1 is sensitive to Dooku1.

The human RBC has unique characteristics, that allow a tremendous capacity to undergo the required deformations to flow and bend into the narrowest of the capillaries. The first relates to the cell's surface area to volume ratio and the second to the membrane deformability. This membrane deformability relies on a submembranous cytoskeleton composed of a network of spectrin filaments bounds to nodes connected to transmembrane proteins (Fowler, 2013), and a unique lipid composition with one of the highest cholesterol/phospholipid ratio (Subczynski et al., 2017). Moreover, mechanosensitivity of the PIEZO1 channel is strictly dependent on lateral tension and curvature that act as the mechanosensory stimulus to trigger channel openings and deactivation. These two parameters are themselves determined by lipid composition (Božič and Svetina, 2022; Vaisey et al., 2022). PIEZO1 can also be activated with voltage changes (Kaestner and Egee, 2018; Moroni et al., 2018). Altogether, these characteristics make a very special environment for PIEZO1, such that its gating in RBCs is probably specific. Indeed, a report on mouse RBCs has already shown that this specific environment impairs the rapid inactivation mechanism of PIEZO1 that was observed in other cell types, shedding light on a slower deactivation mechanism in RBCs that could be modified upon PIEZO1 mutations (Evans et al., 2020). Similarly, it has been demonstrated that gain-of-function mutations of PIEZO1, reported as deleterious in RBCs, lose their phenotypes once heterologously expressed in HEK293 cells (Yamaguchi et al., 2021).

Even the pharmacology of PIEZO1 can be affected by surrounding composition, since the effects of Yoda1 in RBCs activates the channel without mechanical stimulation, whereas in other cell types, Yoda1 acts by increasing the sensitivity to membrane stretch (Lacroix et al., 2018; Botello-Smith et al., 2019). The elegant study of Wijerathne et al., 2022, has biophysically characterized the effects of Yoda1 on the activation of PIEZO1 in HEK293 cells, revealing that Yoda1 activates the channel by energetically stabilizing and destabilizing its conducting and non-conducting parameters (Wijerathne et al., 2022).

In the current study, we have shown that a drug, Dooku1, that has no effects on PIEZO1 in other cell types is able to activate the channel in human RBCs at rest (1–3 μM). Further, Dooku1 shows only mild antagonizing effects in RBC (IC_{50} 90.7 μM) compared to those described in other cell types such as HEK293 (IC_{50} 1.3 μM) or HUVEC (IC_{50} 1.5 μM) (Evans et al., 2018). Consistent with these results, Dooku1 would be expected to have a competitive antagonism effect on the Yoda-1 binding site rather than directly blocking the channel (Evans et al., 2018). Our present results sustain this hypothesis. The study of Wijerathne *et al*, despite being having been performed in HEK cells, corroborates this hypothesis since they clarified that Dooku1 has an effect on the kinetics of the channel, an effect too small to affect the open probability and the macroscopic behavior of the channel, therefore Dooku1, at 30 μM, acts as a silent binder on PIEZO1 (Wijerathne et al., 2022).

The MBE method is rapid and accurate for studying ion channel regulation and pharmacology (Monedero Alonso et al., 2021). Membrane potential variations towards electronegative values indicate a K^+ efflux, which translates into Gárdos channel activation. Via the MBE method, hyperpolarizations speeds and magnitudes recorded with Dooku1 or Yoda1 were comparable. This implies that in both cases, the Ca^{2+} threshold required for full Gárdos activation was reached rapidly. However, the pace of repolarization was faster upon Dooku1 stimulation, indicating by such that Ca^{2+} entry is probably lower in magnitude, facilitating Ca^{2+} removal by the calcium pump, and thus more quickly reducing the open probability of the Gárdos channel. Another mechanism behind the faster repolarization could be the special PIEZO1 potential-dependent conformational rearrangement in response to Dooku1, as was described by Wijerathne and colleagues, resulting in a higher probability of repetitive Dooku1 binding and in a faster repolarization (Wijerathne et al., 2022). This assumption is strengthened by flow cytometry and confocal microscopy measurements of calcium content.

The dose-response curves established in this present study (flow cytometry and imaging) show that Dooku1, even at 1 µM, evokes significant Ca^{2+} entry (Figure 4; Supplementary Figure S2). Nevertheless, hyperpolarizations could only be detected from 3 to 6 µM. This apparent discrepancy is due to a particularity of MBE method. Albeit fast and accurate, MBE method is an indirect measurement of membrane potential through the measurement of extracellular pH in an unbuffered extracellular medium. Thus, in that case the extent of extracellular pH change depends on the simultaneity of all cells to respond to the stimulation at the same pace. In the present case, at low Dooku1 concentrations (below 3 µM), a limitation of the method occurs. Moreover, both MBE method and flow cytometry, induce shear stress that are not fully comparable. So, it is possible that the difference lies also in this slight but not negligible difference considering the mechanosensitivity of Piezo1.

Unlike our results, Wadud *et al* showed in Sickle RBCs that Dooku1 at 10 µM neither increases Ca^{2+} content nor favors phosphatidylserine PS exposure. On the contrary, they demonstrated a significant but partial inhibition of the consequences of calcium increase triggered by Yoda1 (Wadud et al., 2020). These differences in results could originate within the well-known more pronounced rigidity and lack of deformability of Sickle RBCs (Gutierrez et al., 2021). Our preliminary data about Dooku1 on sickle RBCs showed lower hyperpolarization amplitude and Ca^{2+} increase (unpublished data).

Interestingly, in a series of experiments using the efficacious concentration of 10 µM of Dooku1, cells underwent significant Na^+ increase, K^+ loss, and dehydration (Figure 5). Whereas K^+ loss can be related to Gárdos channel activity, Na^+ entry indicates that Dooku1 activates a non-selective cation channel. This last result, associated with the strong inhibition of Ca^{2+} entry by GsMTx4, points out towards a direct effect of Dooku1 on PIEZO1.

Surprisingly, above 60 µM, Dooku1 induced two successive and reproducible hyperpolarizations. Our suggestion is that Dooku1 molecules precipitate at high concentrations. These precipitates could solubilize progressively over time. Due to its lipophilic nature, the insertion of Dooku1 in the lipid bilayer is likely progressive and as a consequence permits the diffusion of the compound in the solution as crystals.

In this study we highlighted the activator capacity of Dooku1. It is a realistic hypothesis that this agonist effect might be observed in RBCs only, given the particularities of PIEZO1 environment in RBC membrane. Still, the need to develop new pharmacological tools to study the non-selective cation channels (PIEZO1 indeed) is urgent: the inhibitors available so far - GsMTx4 toxin from *Grammastola Spatulata* venom, Ruthenium Red (Syeda et al., 2015) or gadolinium Gd^{3+} (Matsunaga et al., 2021)—are not specific for PIEZO1 (Bowman et al., 2007).

From our studies reported here, we can conclude that Dooku1, a molecule that is considered as an antagonist of Yoda1 without any agonist effects of PIEZO1, is sufficient to activate PIEZO1 in the RBC membrane, whilst simultaneously maintaining, at least partially, its antagonist capacities towards Yoda1. Knowing the potency of both drugs allows the opportunity to investigate PIEZO1-linked channelopathies with subtle tools (Dooku1 and Yoda1).

Data availability statement

The raw data supporting the conclusion of this article will be made available by the authors, without undue reservation.

Author contributions

Conceptualization: SE. Methodology: SE, AH, MG, and GB. Realisation of experiments: AH, GP, LP, MG, GB, and SE. Formal analysis: SE, GB, AH, and GP. Review and editing: AH, GB, and SE. All authors contributed to the article and approved the submitted version.

Funding

This work received funding from the European Union Horizon 2020 Research and Innovation Program under the Marie Skłodowska-Curie grant agreement No. 860436—EVIDENCE (AH). This study was supported by grants from Laboratory of Excellence GR-Ex, reference ANR-11-LABX-0051. The labex GR-Ex is funded by the program "Investissements d'avenir" of the French National Research Agency, reference ANR-11-IDEX-0005-02.

Acknowledgments

The authors want to thank Mrs Jeanette Chloë Bulinski for kindly reading and improving English throughout the manuscript. We also want to thank Mrs. Sophie Le Panse at MerImage's optical platform at the Biological station of Roscoff for their support with the confocal microscopy part.

Conflict of interest

The authors declare that the research was conducted in the absence of any commercial or financial relationships that could be construed as a potential conflict of interest.

Publisher's note

All claims expressed in this article are solely those of the authors and do not necessarily represent those of their affiliated organizations, or those of the publisher, the editors and the reviewers. Any product that may be evaluated in this article, or claim that may be made by its manufacturer, is not guaranteed or endorsed by the publisher.

Supplementary material

The Supplementary Material for this article can be found online at: https://www.frontiersin.org/articles/10.3389/fphys.2023.1222983/full#supplementary-material

References

Andolfo, I., Alper, S. L., De Franceschi, L., Auriemma, C., Russo, R., De Falco, L., et al. (2013). Multiple clinical forms of dehydrated hereditary stomatocytosis arise from mutations in PIEZO1. *Blood* 121 (3925–3935), 3925–3935, S1-S12. doi:10.1182/blood-2013-02-482489

Bae, C., Gnanasambandam, R., Nicolai, C., Sachs, F., and Gottlieb, P. A. (2013). Xerocytosis is caused by mutations that alter the kinetics of the mechanosensitive channel PIEZO1. *Proc. Natl. Acad. Sci. U. S. A.* 110, E1162–E1168. doi:10.1073/pnas.1219777110

Bae, C., Sachs, F., and Gottlieb, P. A. (2011). The mechanosensitive ion channel Piezo1 is inhibited by the peptide GsMTx4. *Biochemistry* 50, 6295–6300. doi:10.1021/bi200770q

Barnett, S. D., Asif, H., and Buxton, I. L. O. (2022). Novel identification and modulation of the mechanosensitive Piezo1 channel in human myometrium. *J. Physiol.* 601, 1675–1690. doi:10.1113/JP283299

Bennekou, P., and Christophersen, P. (1986). Flux ratio of valinomycin-mediated K+ fluxes across the human red cell membrane in the presence of the protonophore CCCP. *J. Membr. Biol.* 93, 221–227. doi:10.1007/BF01871176

Botello-Smith, W. M., Jiang, W., Zhang, H., Ozkan, A. D., Lin, Y.-C., Pham, C. N., et al. (2019). A mechanism for the activation of the mechanosensitive Piezo1 channel by the small molecule Yoda1. *Nat. Commun.* 10, 4503. doi:10.1038/s41467-019-12501-1

Bowman, C. L., Gottlieb, P. A., Suchyna, T. M., Murphy, Y. K., and Sachs, F. (2007). Mechanosensitive ion channels and the peptide inhibitor GsMTx-4: History, properties, mechanisms and pharmacology. *Toxicon* 49, 249–270. doi:10.1016/j.toxicon.2006.09.030

Božič, B., and Svetina, S. (2022). Membrane localization of Piezo1 in the context of its role in the regulation of red blood cell volume. *Front. Physiol.* 13, 879038. doi:10.3389/fphys.2022.879038

Caulier, A., Rapetti-Mauss, R., Guizouarn, H., Picard, V., Garçon, L., and Badens, C. (2018). Primary red cell hydration disorders: Pathogenesis and diagnosis. *Int. J. Lab. Hematol.* 40, 68–73. doi:10.1111/ijlh.12820

Coste, B., Mathur, J., Schmidt, M., Earley, T. J., Ranade, S., Petrus, M. J., et al. (2010). Piezo1 and Piezo2 are essential components of distinct mechanically activated cation channels. *Science* 330, 55–60. doi:10.1126/science.1193270

Cox, C. D., Bae, C., Ziegler, L., Hartley, S., Nikolova-Krstevski, V., Rohde, P. R., et al. (2016). Removal of the mechanoprotective influence of the cytoskeleton reveals PIEZO1 is gated by bilayer tension. *Nat. Commun.* 7, 10366. doi:10.1038/ncomms10366

Deivasikamani, V., Dhayalan, S., Abudushalamu, Y., Mughal, R., Visnagri, A., Cuthbertson, K., et al. (2019). Piezo1 channel activation mimics high glucose as a stimulator of insulin release. *Sci. Rep.* 9, 16876. doi:10.1038/s41598-019-51518-w

Evans, E. L., Cuthbertson, K., Endesh, N., Rode, B., Blythe, N. M., Hyman, A. J., et al. (2018). Yoda1 analogue (Dooku1) which antagonizes Yoda1-evoked activation of Piezo1 and aortic relaxation: Yoda1 antagonist. *Br. J. Pharmacol.* 175, 1744–1759. doi:10.1111/bph.14188

Evans, E. L., Povstyan, O. V., De Vecchis, D., Macrae, F., Lichtenstein, L., Futers, T. S., et al. (2020). RBCs prevent rapid PIEZO1 inactivation and expose slow deactivation as a mechanism of dehydrated hereditary stomatocytosis. *Blood* 136, 140–144. doi:10.1182/blood.2019004174

Fowler, V. M. (2013). "Chapter two - the human erythrocyte plasma membrane: A rosetta stone for decoding membrane–cytoskeleton structure," in *Current topics in membranes functional organization of vertebrate plasma membrane*. Editor V. Bennett (Academic Press), 39–88. doi:10.1016/B978-0-12-417027-8.00002-7

Gallagher, P. G. (2017). Disorders of erythrocyte hydration. *Blood* 130, 2699–2708. doi:10.1182/blood-2017-04-590810

Gautier, E.-F., Leduc, M., Cochet, S., Bailly, K., Lacombe, C., Mohandas, N., et al. (2018). Absolute proteome quantification of highly purified populations of circulating reticulocytes and mature erythrocytes. *Blood Adv.* 2, 2646–2657. doi:10.1182/bloodadvances.2018023515

Gnanasambandam, R., Bae, C., Gottlieb, P. A., and Sachs, F. (2015). Ionic selectivity and permeation properties of human PIEZO1 channels. *PLOS ONE* 10, e0125503. doi:10.1371/journal.pone.0125503

Gutierrez, M., Shamoun, M., Seu, K. G., Tanski, T., Kalfa, T. A., and Eniola-Adefeso, O. (2021). Characterizing bulk rigidity of rigid red blood cell populations in sickle-cell disease patients. *Sci. Rep.* 11, 7909. doi:10.1038/s41598-021-86582-8

Jankovsky, N., Caulier, A., Demagny, J., Guitton, C., Djordjevic, S., Lebon, D., et al. (2021). Recent advances in the pathophysiology of PIEZO1-related hereditary xerocytosis. *Am. J. Hematol.* 96, 1017–1026. doi:10.1002/ajh.26192

Jansen, J., Qiao, M., Hertz, L., Wang, X., Fermo, E., Zaninoni, A., et al. (2021). Mechanistic ion channel interactions in red cells of patients with Gárdos channelopathy. *Blood Adv.* 5, 3303–3308. doi:10.1182/bloodadvances.2020003823

Kaestner, L., and Egee, S. (2018). Commentary: Voltage gating of mechanosensitive PIEZO channels. *Front. Physiol.* 9, 1565. doi:10.3389/fphys.2018.01565

Lacroix, J. J., Botello-Smith, W. M., and Luo, Y. (2018). Probing the gating mechanism of the mechanosensitive channel Piezo1 with the small molecule Yoda1. *Nat. Commun.* 9, 2029. doi:10.1038/s41467-018-04405-3

Lew, V. L., and Tiffert, T. (2017). On the mechanism of human red blood cell longevity: Roles of calcium, the sodium pump, PIEZO1, and gardos channels. *Front. Physiol.* 8, 977. doi:10.3389/fphys.2017.00977

Macey, R. I., Adorante, J. S., and Orme, F. W. (1978). Erythrocyte membrane potentials determined by hydrogen ion distribution. *Biochim. Biophys. Acta BBA - Biomembr.* 512, 284–295. doi:10.1016/0005-2736(78)90253-5

Matsunaga, M., Kimura, M., Ouchi, T., Nakamura, T., Ohyama, S., Ando, M., et al. (2021). Mechanical stimulation-induced calcium signaling by Piezo1 channel activation in human odontoblast reduces dentin mineralization. *Front. Physiol.* 12, 704518. doi:10.3389/fphys.2021.704518

Monedero Alonso, D., Pérès, L., Hatem, A., Bouyer, G., and Egée, S. (2021). The chloride conductance inhibitor NS3623 enhances the activity of a non-selective cation channel in hyperpolarizing conditions. *Front. Physiol.* 12, 743094. doi:10.3389/fphys.2021.743094

Moroni, M., Servin-Vences, M. R., Fleischer, R., Sánchez-Carranza, O., and Lewin, G. R. (2018). Voltage gating of mechanosensitive PIEZO channels. *Nat. Commun.* 9, 1096. doi:10.1038/s41467-018-03502-7

Pérès, L., Monedero Alonso, D., Nudel, M., Figeac, M., Bruge, J., Sebda, S., et al. (2021). Characterisation of Asp669Tyr Piezo1 cation channel activity in red blood cells: An unexpected phenotype. *Br. J. Haematol.* 194, e51–e55. doi:10.1111/bjh.17467

Schindelin, J., Arganda-Carreras, I., Frise, E., Kaynig, V., Longair, M., Pietzsch, T., et al. (2012). Fiji: An open-source platform for biological-image analysis. *Nat. Methods* 9, 676–682. doi:10.1038/nmeth.2019

Subczynski, W. K., Pasenkiewicz-Gierula, M., Widomska, J., Mainali, L., and Raguz, M. (2017). High cholesterol/low cholesterol: Effects in biological membranes: A review. *Cell biochem. Biophys.* 75, 369–385. doi:10.1007/s12013-017-0792-7

Syeda, R. (2021). Physiology and pathophysiology of mechanically activated PIEZO channels. *Annu. Rev. Neurosci.* 44, 383–402. doi:10.1146/annurev-neuro-093020-120939

Syeda, R., Xu, J., Dubin, A. E., Coste, B., Mathur, J., Huynh, T., et al. (2015). Chemical activation of the mechanotransduction channel Piezo1. *eLife* 4, e07369. doi:10.7554/eLife.07369

Szabó, L., Balogh, N., Tóth, A., Angyal, Á., Gönczi, M., Csiki, D. M., et al. (2022). The mechanosensitive Piezo1 channels contribute to the arterial medial calcification. *Front. Physiol.* 13, 1037230. doi:10.3389/fphys.2022.1037230

Vaisey, G., Banerjee, P., North, A. J., Haselwandter, C. A., and MacKinnon, R. (2022). Piezo1 as a force-through-membrane sensor in red blood cells. *eLife* 11, e82621. doi:10.7554/eLife.82621

Wadud, R., Hannemann, A., Rees, D. C., Brewin, J. N., and Gibson, J. S. (2020). Yoda1 and phosphatidylserine exposure in red cells from patients with sickle cell anaemia. *Sci. Rep.* 10, 20110. doi:10.1038/s41598-020-76979-2

Wang, J., Jiang, J., Yang, X., Zhou, G., Wang, L., and Xiao, B. (2022). Tethering Piezo channels to the actin cytoskeleton for mechanogating via the cadherin-β-catenin mechanotransduction complex. *Cell Rep.* 38, 110342. doi:10.1016/j.celrep.2022.110342

Wijerathne, T. D., Ozkan, A. D., and Lacroix, J. J. (2022). Yoda1's energetic footprint on Piezo1 channels and its modulation by voltage and temperature. *Proc. Natl. Acad. Sci. U. S. A.* 119, e2202269119. doi:10.1073/pnas.2202269119

Yamaguchi, Y., Allegrini, B., Rapetti-Mauss, R., Picard, V., Garçon, L., Kohl, P., et al. (2021). Hereditary xerocytosis: Differential behavior of PIEZO1 mutations in the N-terminal extracellular domain between red blood cells and HEK cells. *Front. Physiol.* 12, 736585. doi:10.3389/fphys.2021.736585

Zarychanski, R., Schulz, V. P., Houston, B. L., Maksimova, Y., Houston, D. S., Smith, B., et al. (2012). Mutations in the mechanotransduction protein PIEZO1 are associated with hereditary xerocytosis. *Blood* 120, 1908–1915. doi:10.1182/blood-2012-04-422253

Supplementary Material (Published)

Dual action of Dooku1 on PIEZO1 channel in human red blood cells

Aline Hatem[1,2], Gwendal Poussereau[1], Martin Gachenot[3], Laurent Pérès[1,2], Guillaume Bouyer[1,2], Stéphane Egée[1,2]*

*** Correspondence :** Pr. Stéphane EGEE, egee@sb-roscoff.fr

Supplementary Figures and Tables

Supplementary Figures

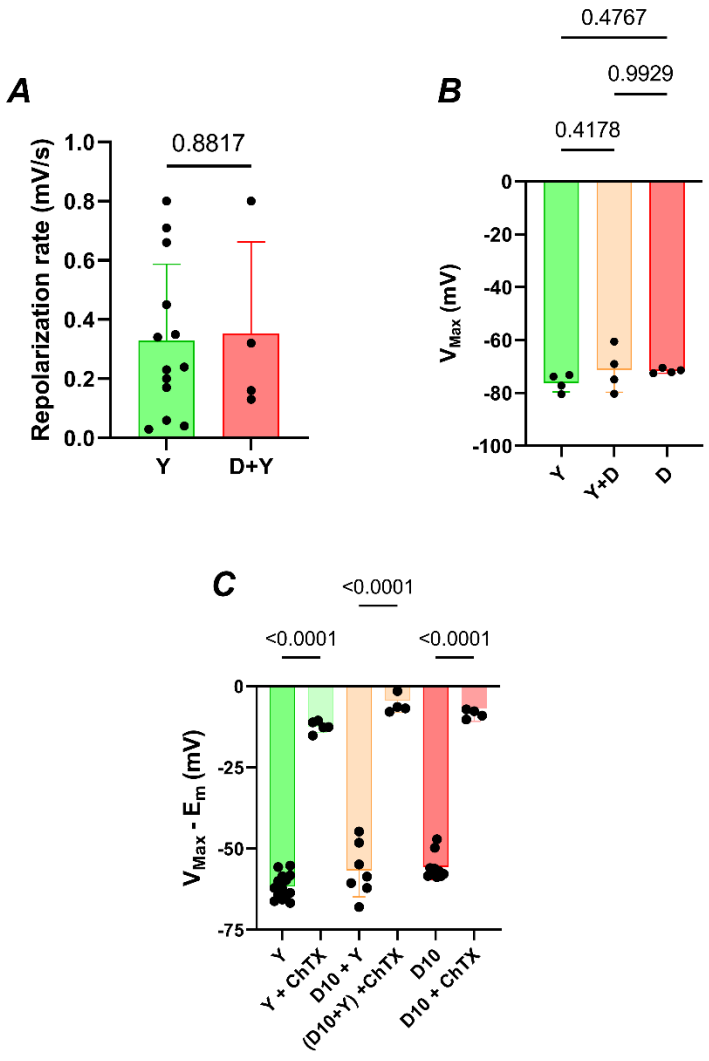

Supplementary Figure 1

Supplementary Figure 1. (A) Repolarization rate comparison between Yoda1 only condition (green) and Yoda1 after preincubation with Dooku1 (10 µM, red) at 37°C for 15 minutes. (B) Maximum hyperpolarization comparison (corresponding to Fig 1C, same n) (C) Membrane potential variation comparison with and without inhibition with charybdotoxin (ChTX, 100 nM, n=5) Charybdotoxin was added to the cell 10s seconds before hyperpolarizing drugs addition. Each point represents the mean ±SD (same n for each condition as previously mentioned).

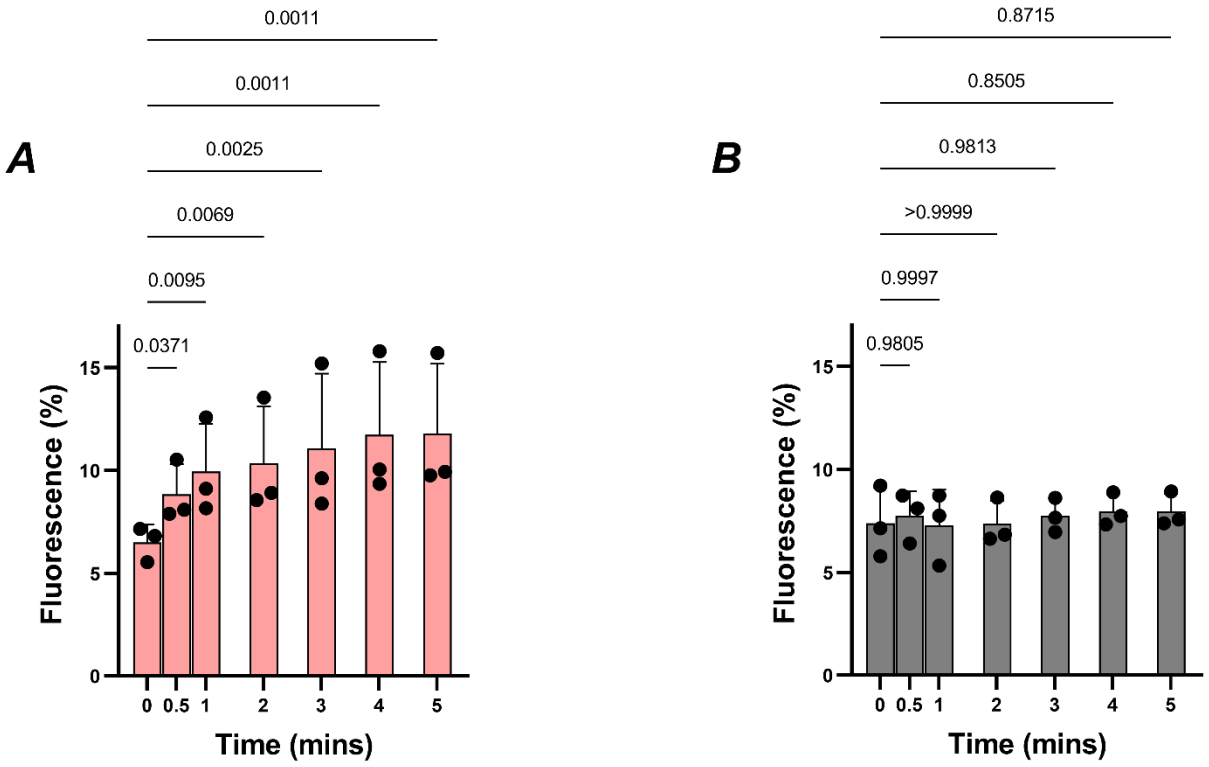

Supplementary Figure 2

Supplementary Figure 2. Confocal imaging of Fluo4-loaded RBCs perfused with 1µM Dooku1 (a) or DMSO (b). Fluorescence is expressed as a percentage of Yoda1-induced maximal intensity. Histograms are means ±SD of 3 independent experiments.

III. Unpublished results- Effects of the inhibition of chloride permeability on PIEZO1 activation

The previous article clearly shows that we need to be relatively cautious about the effects observed with chemical compounds that are supposed to activate or inhibit a transporter or even a cell signaling pathway. Certainly, the concentrations used are important, but it is also clear that the cell type or the physiological conditions the cell is exposed to are also important. In David Monedero Alonso's thesis, it was shown that NS3623, an inhibitor described as a potassium channel activator and then described as a potent inhibitor of red blood cell chloride conductances, including band 3 (Bennekou et al., 2001, 2003), at high concentrations could activate a non-selective cation conductance pathway in the red blood cell (Monedero Alonso et al., 2021).

In order to better characterize the transient aspect of Yoda1- or Dooku1-induced activation of Gárdos channels, we performed experiments to determine whether this transient activity is related i) to a reduction in Gárdos channel activity, which in turn is related to a decrease in intracellular calcium concentration *via* the work of the PMCA pump; or, ii) to an increase in the intensity of anionic currents that compensate for potassium currents. In fact, when the Gárdos channel is activated, the driving force (V_M-E_K) is in favor of the Gárdos channel, while that corresponding to the chloride conductance or the non-selective cationic conductance is low, these two ionic entities being at equilibrium with the membrane potential (-12mV), except for calcium, which benefits from a strong chemical gradient.

Therefore, we used NS3623 at a concentration of 10 µM, which inhibits 98% of the chloride conductance without activating the non-selective cationic conductance (Monedero Alonso et al., 2021). Surprisingly, NS3623 significantly inhibited the hyperpolarizations that were due to PIEZO1 activation (Figure 28 A, C) without disturbing the resting membrane potential (Figure 28 B). This might be attributed to an overall disruption of the physiology of RBCs after blocking the Cl^- conductance because, as it was mentioned in the general introduction, the Cl^- conductance is directly linked to the canonical functions of an erythrocyte, in particular through the activity of Band 3 in the gas transport cycle.

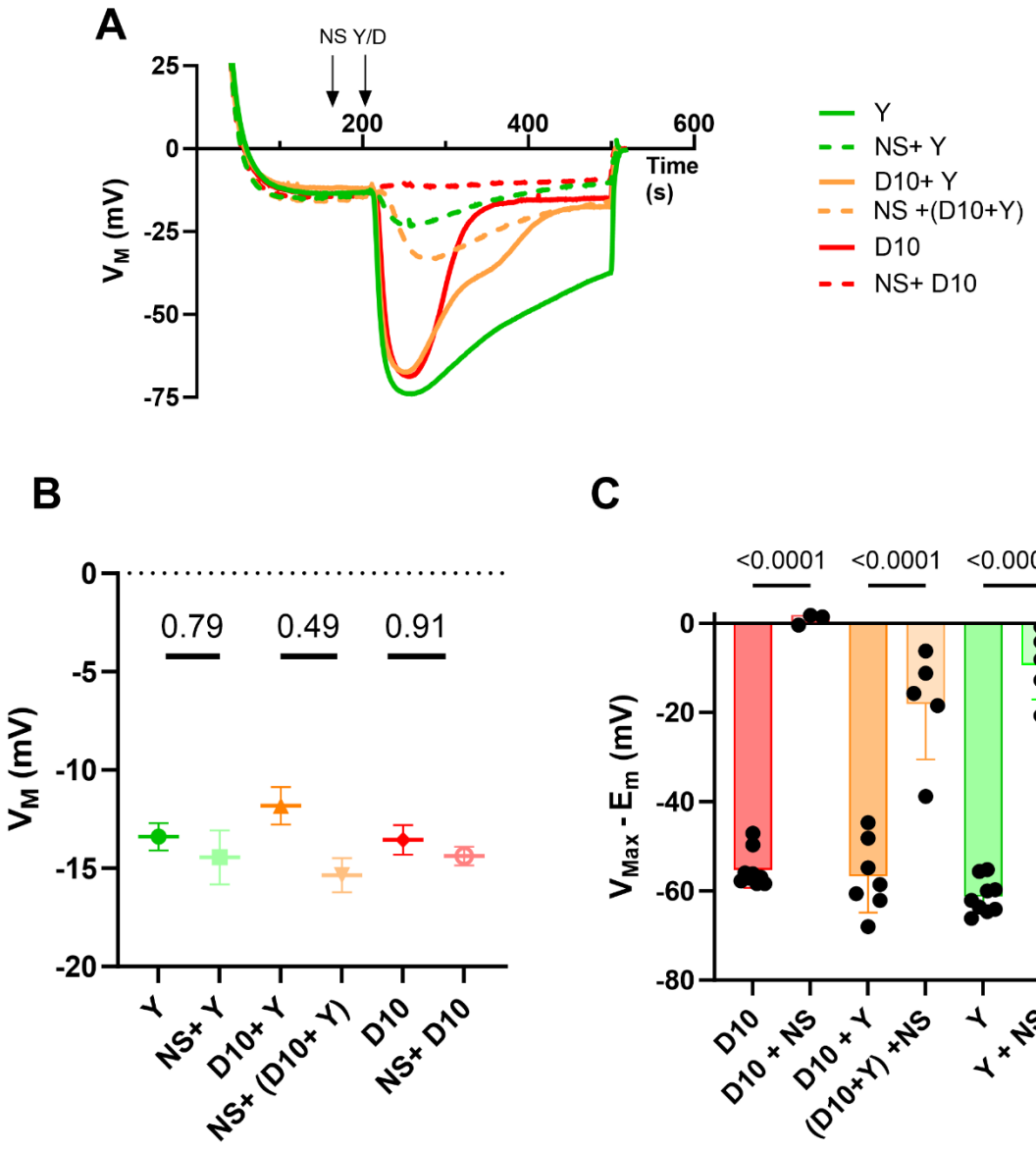

Figure 28: The inhibition of Dooku1 and Yoda1 effects by NS3623 (NS; 10 µM) using the MBE method. (A) Mean MBE traces showing variations in membrane potential in response to Dooku1 (10 µM; D10; red trace), Yoda1 (625 nM; Y; green trace), Yoda1 (625 nM), and Dooku1 (10 µM) added simultaneously. Dashed traces represented the same conditions but with the presence of NS3623 in the media (added at 180 seconds) (B) Comparison of the resting membrane potential of different conditions in the presence and absence of NS3623. (C) Comparison of the hyperpolarization magnitude of the same conditions. One-way ANOVA was the statistical test. n= 9 for D10, n=7 for D10+Y, n=9 for Y, n=5 for all conditions with NS3623.

IV. Discussion and Conclusion

We demonstrated through this article that Dooku1 activates by itself the PIEZO1 channel, which triggers the subsequent activation of the Gárdos channel. This is an important pharmacological finding about PIEZO1 in the RBCs. We proposed a scenario in which Dooku1 binds to the same binding site as Yoda1 on the PIEZO1 protein: it activates the channel in a milder way, and when Yoda1 and Dooku1 are present simultaneously in the media, Dooku1 partially inhibits the effects of Yoda1 (Figure 29). In this study, we reminded our community about the specificity of the characteristics of RBCs: the first is related to the cell's surface area to volume ratio, and the second to the membrane deformability; RBCs are endowed with a submembranous cytoskeleton composed of a network of spectrin filaments bounds to nodes connected to transmembrane proteins (Fowler, 2013), and a unique lipid composition with one of the highest cholesterol/phospholipid ratios (Subczynski et al., 2017). Moreover, the mechanosensitivity of PIEZO1 is tightly dependent on lateral tension and curvature, which are determined by the lipid composition (Božič and Svetina, 2022; Vaisey et al., 2022). All these characteristics create a special environment for PIEZO1 in RBCs, which has an impact on its gating and deactivation.

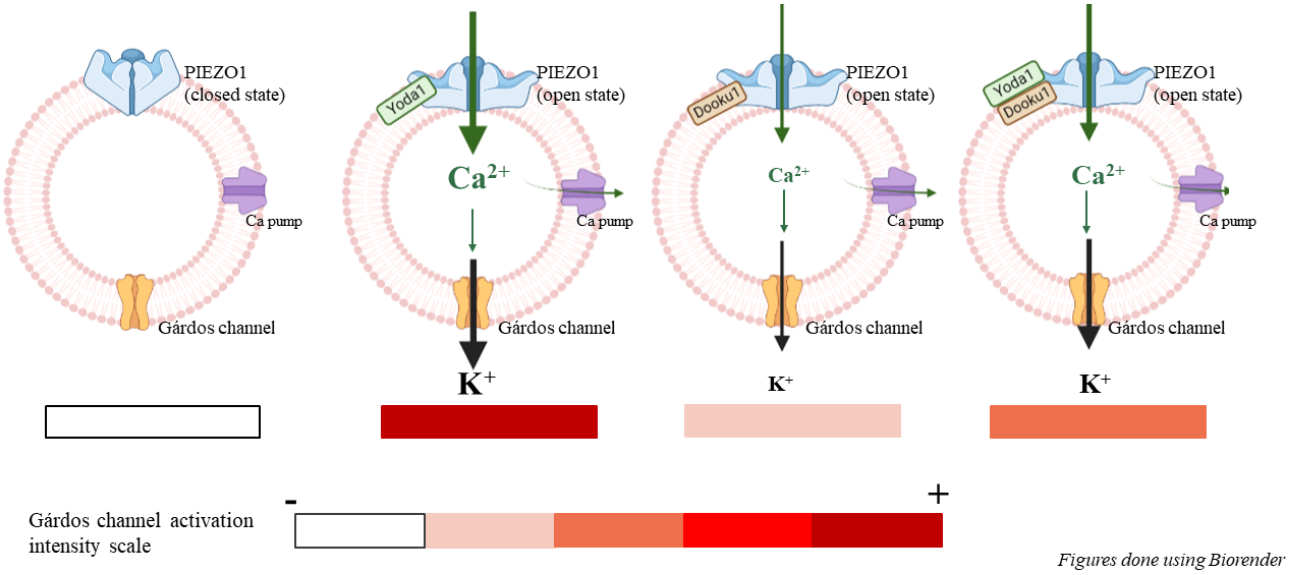

Figure 29: The proposed scenario of Dooku1 activity in RBCs. Cells from the left to the right are exposed to different conditions. From the left to the right: inactivated PIEZO1, PIEZO1 activated with Yoda1, PIEZO1 activated with Dooku1, and PIEZO1 simultaneously challenged with Yoda1 and Dooku1. The thickness of the arrows indicates the magnitude of the ion fluxes. The font sizes of "Ca^{2+}"and "K^{+}", are proportional to the suggested concentrations of these ions. In addition, the Gárdos channel activation intensity scale is indicated in shades of red under each condition. The figure was created using Bio-Render.

Chapter II- PIEZO1 and KCNN4 variants

I. Introduction

A. PIEZO1-KCNN4 interplay in RBCs

The functional link between PIEZO1 and the Gárdos channel (KCNN4) seems evident in RBCs physiological studies (Cahalan et al., 2015). The Gárdos channel has been demonstrated to be transiently activated by membrane deformation, leading to the conclusion that fast local mechanosensitive Ca^{2+} entry was generated by slight deformation upon seal formation (Dyrda et al., 2010). PIEZO1 is activated in the microcirculation in response to mechanical and hydrostatic stress leading to Ca^{2+} entry (Cahalan et al., 2015; Danielczok et al., 2017). This induces subsequent activation of the Gárdos channel which dissipates K^+, creating a cation imbalance and fast transient hyperpolarization (Dyrda et al., 2010; Rogers and Lew, 2021b). This in turn causes osmotically obliged water to escape, dehydrating the cells. This loss of water culminates in the local adaptation of the volume to facilitate the passage of RBCs in the microcapillaries (Danielczok et al., 2017). PIEZO1-KCNN4 tandem activation is of particular interest in the physiological studies of RBCs, especially in pathological conditions (Rapetti-Mauss et al., 2016, 2017). Several pathologies of the RBCs are linked to gain-of-function mutations in PIEZO1 and Gárdos channels (Zarychanski et al., 2012; Beneteau et al., 2014; Rapetti-Mauss et al., 2017; Andolfo et al., 2023).

Being devoid of a nucleus, the study of the channels' variants is ideally feasible using cells from patients carrying these mutations.

B. Tools to study variants

Large-scale clinical and biological descriptions at diagnosis constitute important steps to understand mutations and link the genotype to phenotypes (Picard et al., 2019). Phenotypic diagnostic tools are usually based on the establishment of a complete blood count (CBC) with measurement of the reticulocytes count, accompanied by a careful reading of the blood smear to look for abnormal RBCs shapes (Simionato et al., 2021), in addition to auto-immune, biochemical, hemoglobin, and enzymatic tests to try to know the origin of occurring hemolytic anemias. Several

tests are also used to determine if the origin of the disease is caused by red cells membrane pathologies. For instance, Eosine-5-maleimide test (EMA) test is highly specific and sensitive for proving hereditary spherocytosis (Girodon et al., 2008). Also, ektacytometry measures RBCs deformability in variable osmotic conditions (Da Costa et al., 2016). Finally, the high-throughput next generation sequencing (NGS) is considered a particularly specialized test that only comes in the last line of diagnosis (Bianchi et al., 2020); it can targets gene panels, exomes, and even whole-genome panels (Russo et al., 2020). Nevertheless, NGS leads to the diagnosis only in 65% of all cases of hemolytic anemia (Mansour-Hendili et al., 2020). Standard terminology and graduated criteria were recommended for the classification of variants in genetics laboratories. The five classes of variants are "pathogenic", "likely pathogenic", "uncertain significance", "likely benign", and "benign" variants. A variant is classified as pathogenic or benign based on the frequency of the variant in the general population, *in-silico* predictions, family detections, and functional studies (Richards et al., 2015; Nykamp et al., 2017). Among these, a novel category of variants has been introduced called variant of uncertain significance (VUS). NGS has contributed to the exponential growth of VUS (Figure 30). Hence, the reclassification of these variants is essential for successful diagnosis. NGS made in parallel with phenotypic tests can reveal the association between the presence of variants and pathologies (Russo et al., 2020).

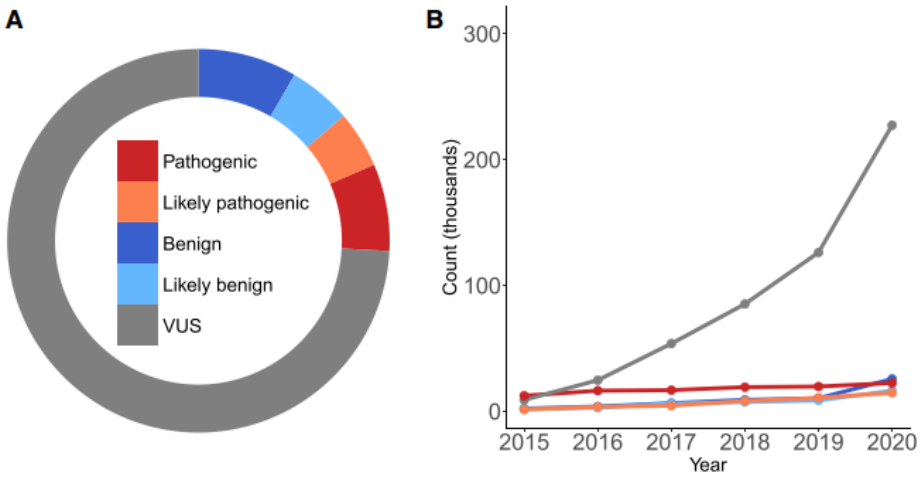

Figure 30: Single-nucleotide missense variants of uncertain significance are a large and growing problem by ClinVar. Adaped from (Fayer et al., 2021).

C. **PIEZO1 channel**

PIEZO1 (FAM38A) (Coste et al., 2010) is a mechanosensitive non-specific cation channel (Albuisson et al., 2013; Andolfo et al., 2013a). As described in the introduction, the PIEZO1 protein is a homotrimer made up of 2521 amino acids (~900 kDa). Typically, loss-of-function mutations in the human *PIEZO1* gene cause autosomal recessive congenital lymphatic dysplasia whereas gain-of-function mutations cause the autosomal dominant hemolytic anemia hereditary xerocytosis (HX, MIM #194380), also known as DHS1 (Zarychanski et al., 2012; Alper, 2017). HX is characterized by a decrease in the total cation and K^+ content that is not accompanied by a proportional net gain of Na^+ and water. HX patients undergo mild to moderate, compensated hemolytic anemia. MCHC is increased and erythrocyte osmotic fragility is decreased, reflecting cellular dehydration in these patients. Mutations in *PIEZO1* (M2225R and R2456H) are the first mutations in mechanosensitive channels associated with human disease (Zarychanski et al., 2012). A list of mutations in *PIEZO1* have been proposed as the major cause of DHS1 or HX (Table 5). Most gain-of-function *PIEZO1* mutations are due to facilitation of its opening by changing the threshold of mechanosensitivity or by slowing down its fast neutral inactivation kinetics (Albuisson et al., 2013; Glogowska et al., 2017). Knowing the high permeability for Ca^{2+}, RBC dehydration due to gain-of-function mutations in *PIEZO1* is explained by an excessive *KCNN4* stimulation (Rapetti-Mauss et al., 2017).

In fact, mutations in *PIEZO1* are linked to HX or DHS1, whereas mutations in *KCNN4* are associated with DHS2 (Picard et al., 2019). Approximately 90% of HX cases are called DHS1 and are associated with heterozygous *PIEZO1* gain-of-function mutations with autosomal dominant transmission. The remaining cases are due to the Gárdos channel-activating mutations, called DHS2. Thus, RBC dehydration in DHS2 is mainly a result of an inappropriate activation of the Gárdos channel. DHS1 and DHS2 differ not only in their etiology, but also in the severity of the hematologic phenotype, perinatal edema, thrombotic risk after splenectomy, and also iron overload; perinatal edema and post-splenectomy thrombosis have been mostly reported in DHS1, whereas severe anemia appears to be frequent in DHS2, with iron overload observed in both entities (Fermo et al., 2017; Andolfo et al., 2018; Picard et al., 2019; Mansour-Hendili et al., 2021).

Table 5: *Piezo1* variants leading to DHS1 or HX, adapted from UniProt.

Position	Change	Description
203	L>P	(Andolfo et al., 2021)
334	A>V	(Andolfo et al., 2021)
338	S>Y	(Picard et al., 2019)
457	R>C	(Russo et al., 2018)
483	V>M	(Andolfo et al., 2021)
598	V>L	(Picard et al., 2019)
598	V>M	(Rapetti-Mauss et al., 2017; Yamaguchi et al., 2021)
599	V>L	(More et al., 2020)
605	M>I	(Picard et al., 2019)
605	M>V	(Andolfo et al., 2021)
669	D>Y	(Pérès et al., 2021)
681	F>S	(Rapetti-Mauss et al., 2017; Yamaguchi et al., 2021)
718	G>S	(Andolfo et al., 2013a)
737	L>M	(Glogowska et al., 2017)
756	E756del	(Ma et al., 2018)
782	G>S	(Andolfo et al., 2013a; Yamaguchi et al., 2021)
808	R>Q	(Andolfo et al., 2013a; Beneteau et al., 2014; Yamaguchi et al., 2021)
972	R>H	(More et al., 2020)
1064	C>F	ClinVar
1066	D>G	ClinVar
1117	S>L	(Andolfo et al., 2013a)
1223	V>I	(Filser et al., 2021)
1312	A>V	(Andolfo et al., 2021)
1357	I>M	(Picard et al., 2019)
1357	I>V	(Picard et al., 2019)
1358	R>P	(Albuisson et al., 2013)
1398	P>L	ClinVar
1494	E>A	(Andolfo et al., 2021)
1519	Q>P	(Picard et al., 2019)
1617	T>M	ClinVar
1708	L>Q	SIFT, HVAR, UniProt, Mutation tester
1797	R>C	(Russo et al., 2018)
1851	T>M	ClinVar
1857	P>S	ClinVar
1878	K del	ClinVar
1898	E>D	(Russo et al., 2018)
1910	E>L	(Picard et al., 2019)
1925	R>W	(Picard et al., 2019)
1926	R>Q	ClinVar
1943	R>Q	(Glogowska et al., 2017)
1930	F>L	(Richards et al., 2015)
1945	F>L	(Filser et al., 2021)
1994	S>F S>C	(Picard et al., 2019) (Andolfo et al., 2021)
2003	A>D	(Andolfo et al., 2013a)

	A>T	(Picard et al., 2019)
2006	V>I	(Picard et al., 2019)
2020	1. A>T 2. A>V	1. (Albuisson et al., 2013; Filser et al., 2021) 2. (Andolfo et al., 2013a)
2069	V>M	(Andolfo et al., 2021)
2088	R>G	(Glogowska et al., 2017)
2094	L>F	ClinVar
2110	R>Q	(Picard et al., 2019)
2110	R>W	(Russo et al., 2018)
2127	T>M	Gives rise to mechanically activated currents that inactivate more slowly than wild-type currents, dbSNP (Albuisson et al., 2013; Andolfo et al., 2013a; Filser et al., 2021)
2151	C>R	(Picard et al., 2019)
2160	P>I	(Picard et al., 2019)
2166-2169	Missing	(Andolfo et al., 2013a)
2192	L>I	(Picard et al., 2019)
2201	V>F	(Picard et al., 2019)
2225	M>R	Gives rise to mechanically activated currents that inactivate more slowly than wild-type currents, dbSNP (Zarychanski et al., 2012)
2227	A>T	ClinVar
2266	V>I	(Russo et al., 2018)
2277	I>M	(Picard et al., 2019)
2302	R>H	(Glogowska et al., 2017)
2308	Q>E	(Picard et al., 2019)
2394	G>S	(Andolfo et al., 2021)
2407	E>Q	(Andolfo et al., 2021)
2433	G>R	(Picard et al., 2019)
2456	R>H R>C	Gives rise to mechanically activated currents that inactivate more slowly than wild-type currents (Zarychanski et al., 2012; Andolfo et al., 2013a; Bae et al., 2013; Beneteau et al., 2014; Shmukler et al., 2014)
2458	F>L	(More et al., 2020)
2462	I>M	(Filser et al., 2021)
2464	H>P	(Picard et al., 2019)
2474	V>M	(Picard et al., 2019)
2488	R>Q	Increased cation transport in erythroid cells; dbSNP (Andolfo et al., 2013a)
2491	R>W	(Picard et al., 2019)
2496	E>ELE	Gives rise to mechanically activated currents that inactivate more slowly than wild-type currents (Albuisson et al., 2013)
2520	K>E	(Andolfo et al., 2021)

D. **Gárdos channel**

The Gárdos channel (KCNN4) consists of a total of 427 amino acids with a molecular mass of 47.8 kDa (Vandorpe et al., 1998). Its quaternary structure is an association of four monomers, forming a homotetramer (Figure 31). Each monomer is composed of six transmembrane segments with a pore forming between segments S5 and S6. The N- and C-terminal domains are cytosolic. The C-terminal domain consists of three parts; HA, HB, and HC, where HA and HB are the calmodulin-binding sites. CaM is constitutively bound to the Gárdos channel and regulates its activity in a Ca^{2+}-dependent manner (Lee and MacKinnon, 2018). The Gárdos channel also requires phosphorylation of histidine 358 residue for activation (Srivastava et al., 2006).

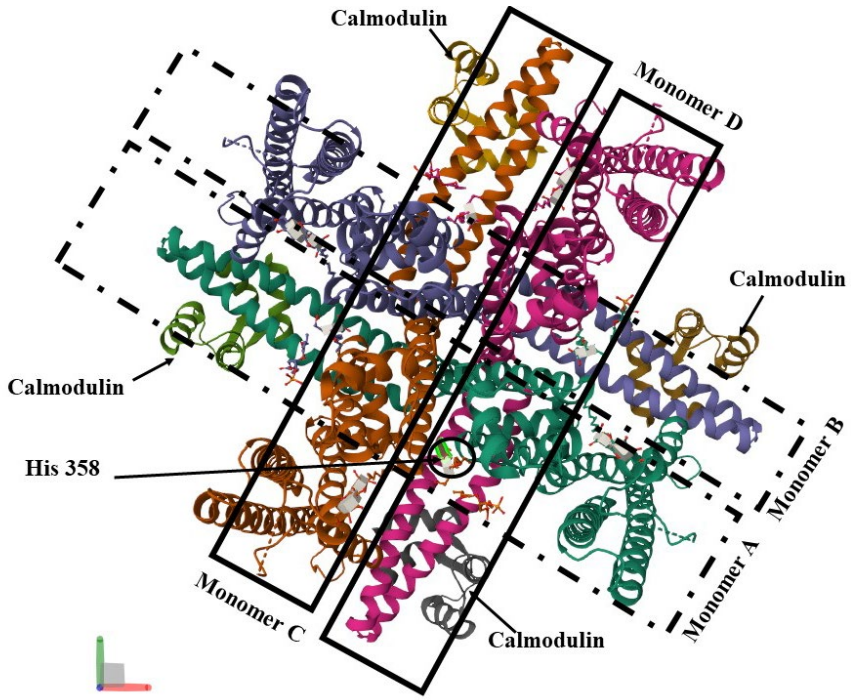

Figure 31: 3D structure of Gárdos channel. The four monomers are represented each in a different color in addition to the bonded calmodulin. Source of the figure PDB. 6CNM 5Z10 structure from PDB.

KCNN4 has two highly conserved regions: the region between the 231 and the 289th amino acids, which forms a two-pore K^+ channel domain, and the region between the 304 and 377th amino acids, which forms the calmodulin-binding domain (Rivera et al., 2022; Nakahara et al., 2023).

Mutations in *KCNN4* induce an increase in the channel's activity which may be associated with an increase in the sensitivity of the channel to Ca^{2+}. Until nowadays, only ten *KCNN4* variants were reported to cause DHS2 (Table 6).

V282M and V282E are two gain-of-function mutations affecting the same residue (V282) in the K^+ pore domain (Andolfo et al., 2015; Rapetti-Mauss et al., 2015, 2016, 2017). This residue has a leading role in Gárdos channel gating, and mutations affecting this site may lead to a constitutive channel activity even in the absence of Ca^{2+} (Garneau et al., 2009) depending on the substituting residue. For instance, the V282M mutant leads into a constitutive channel activity at resting Ca^{2+} concentrations whereas V282E mutant activation is still Ca^{2+}-sensitive and its activation threshold is unchanged like the R352H mutation (Rapetti-Mauss et al., 2016; Rivera et al., 2017). Both V282M and V282E mutations lead to net dehydration with a left-shifted ektacytometry curves (Andolfo et al., 2015; Rivera et al., 2019). V282M leads to compensated anemia with a normal level of haemoglobin associated with hyperreticulocytosis (Allegrini et al., 2022).

R352H is another gain-of-function mutation which leads to higher Ca^{2+} sensitivity in the calmodulin-binding domain by modifying the Ca^{2+} threshold for activation, increasing current density, and delaying channel deactivation. This *KCNN4* mutation was discovered to be associated with chronic hemolysis and constituted the first report of a human disease caused by defects in Gárdos channel (Rapetti-Mauss et al., 2015). In a four-generation French family with chronic congenital hemolytic anemia, whole-exome sequencing was performed in 2015 (Rapetti-Mauss et al., 2015), and identified a heterozygous missense mutation in the *KCNN4* gene that segregated with disease, which is R352H. In parallel, sequencing of *KCNN4* in affected individuals from 3-generation Polish family revealed heterozygosity for the same R352H mutation. In this paper, Rapetti-Mauss *et al*. revealed a variability in disease severity between the two families; while French family members had severe levels of anemia, Polish family members revealed normal or subnormal hemoglobin levels. Functional analysis pointed out that the mutant channel had a 10-fold increase in activation by Ca^{2+} compared to wildtype, in addition to a delayed channel inactivation. This missense mutation leads to DHS2; DHS2 is an autosomal dominant hemolytic anemia characterized by primary erythrocyte dehydration. Erythrocytes exhibit decreased total cation and potassium content that are not accompanied by a proportional net gain of sodium and water. Affected individuals typically manifest mild to moderate compensated hemolytic anemia

with an increased erythrocyte mean corpuscular haemoglobin concentration and a decreased osmotic fragility, both of which reflect cellular dehydration. Their red cells exhibit a panel of various shape abnormalities such as elliptocytes, with the most characteristic shape being stomatocytes, with a straight or crescent-shaped central pallor (Rapetti-Mauss et al., 2015). Complications such as splenomegaly and cholelithiasis may occur, resulting from increased red cell trapping in the spleen and elevated bilirubin levels (Andolfo et al., 2015; Glogowska et al., 2015; Rapetti-Mauss et al., 2015; Fermo et al., 2020).

Thanks to these preliminary studies of cases with deleterious mutations in the Gárdos channel, a systematic search was started for cases in which the usual targets of the gene panels searched were not affected by any mutation.

Most of the described mutations are located within or close to the calmodulin binding site and show a more or less pronounced tendency towards increased sensitivity to Ca^{2+}. Among them, the S314P (Fermo et al., 2020), H340N (Allegrini et al., 2022) and A322V (Mansour-Hendili et al., 2021) cause a hypersensitivity of KCNN4 to Ca^{2+} and allow more frequent transient activation of the Gárdos channel, which may lead to dehydration. Nevertheless, some other mutations from the calmodulin binding site region have been described, such as V222L, characterized by an increase in Ca^{2+} sensitivity once expressed in HEK293 (Allegrini et al., 2022), and A279T, which has been associated with the disease state of the patient but without any functional test (Nakahara et al., 2023).

Table 6: List of the Gárdos channel variants. The representation of the Gárdos channel and the associated mutation are adapted from UniProt. KCNN4 variants known to cause DHS2 until nowadays, are written in red. Point mutations are represented by red dots.

Position	**Change**	**Description**	**Literature**	**3D representation** (mutations in red)-Figure from UniProt
204	P>R	DHS1	(Utsugisawa et al., 2017)	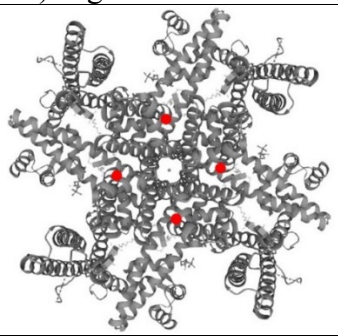

222	1.V>L 2.V>G 3.V>A	1.DHS2 2-3: Probably damaging	(Rivera et al., 2017; Allegrini et al., 2022)	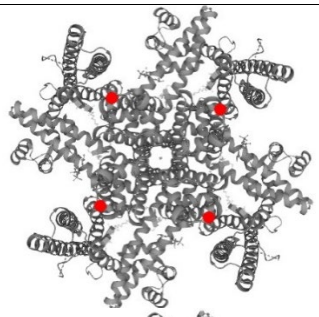
279	1.A>V 2.A>T 3. A>D	1. Benign mutation 2-3 : Pathogenic <u>P.S:</u> K^+ pore channel domain	1.UniProt 2.(Nakahara et al., 2023) 3. In the present study	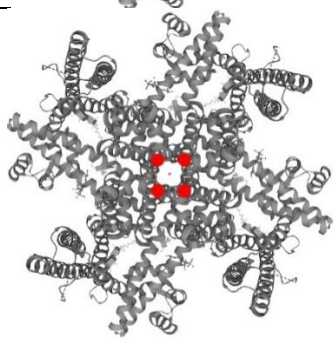
282	V>E V>M	DHS2 P.S: K^+ pore channel domain	(Glogowska et al., 2015; Rivera et al., 2017)	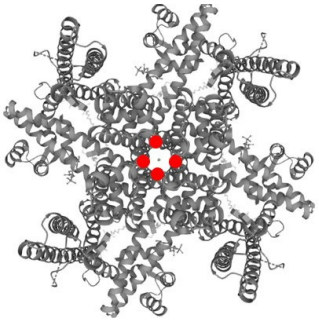
314	S>P	DHS2 with or without pseudohyperkalemia and/or perinatal edema	(Fermo et al., 2020)	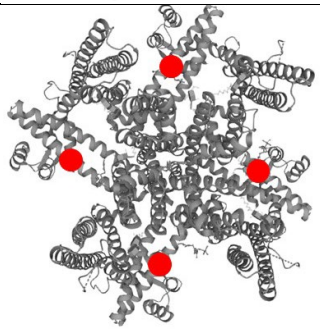
322	A>V	DHS2 Pathogenic	(Mansour-Hendili et al., 2021)	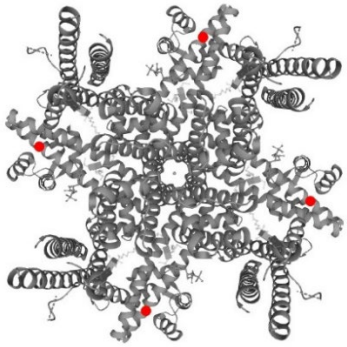

328	H>R	DHS2 Pathogenic P.S: Region 304-377 is calmodulin-binding region.	(Andolfo et al., 2021)	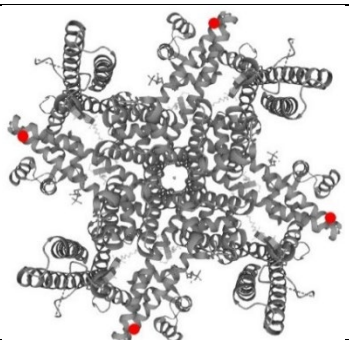
340	1.H>N 2.H>R	1 & 2. DHS2 Likely pathogenic or pathogenic variant P.S: Region 304-377 is calmodulin-binding region.	(Andolfo et al., 2021; Allegrini et al., 2022)	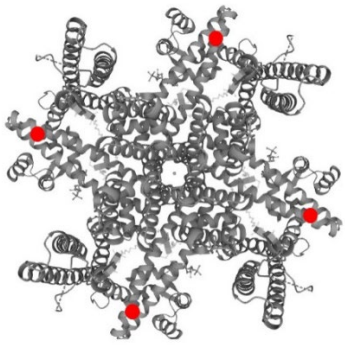
352	R>H	DHS2 In binding chain D P.S: Region 304-377 is calmodulin-binding region.	(Andolfo et al., 2015; Glogowska et al., 2015; Rapetti-Mauss et al., 2015; Monedero Alonso, 2019)	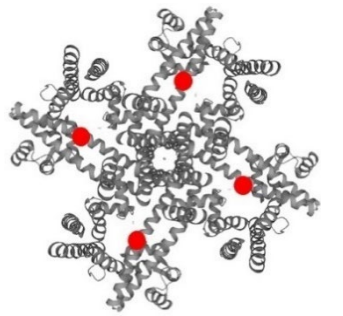
369-377	Del p.V369_Lys373del	DHS2 Pathogenic P.S: Region 304-377 is calmodulin-binding region.	(Picard et al., 2019)	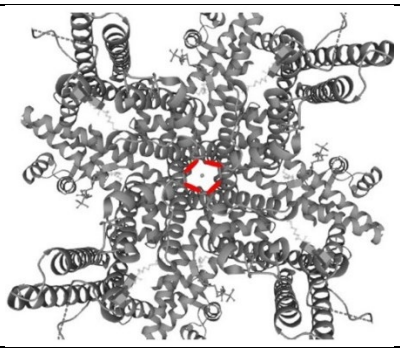

387	S>R	Benign mutation P.S: 368-386 is a partially modelled/unmodeled region.	UniProt	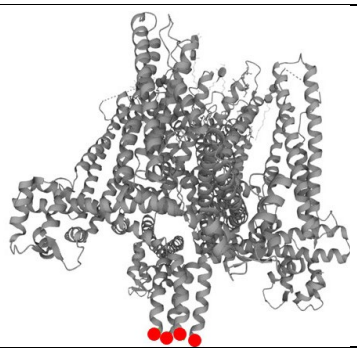

II. Objectives

Knowing that different variants of KCNN4 and PIEZO1 channels lead to pathologies, our laboratory is involved in a large European network (Utrecht, Paris, Dijon, Nancy, Milan, Marseille, Lyon, Toulouse) of clinicians and academics to decipher the relation between genotypes and pathophysiological phenotypes. Therefore, the goal is to functionally assess the link between the genetic detection of variants during diagnostic process and defects of channel activity using several approaches.

To this end, our task was to establish a functional characterization upon receipt of the samples. Channel activity was directly assessed using MBE method with specific protocols dedicated either for Gárdos channels or PIEZO1 channels. To strengthen the electrophysiological data, we also determine hydration status of RBCs, and cation content (K^+ and Na^+), associated to morphological analysis on fixed stained blood smears.

A23187 is the Ca^{2+} ionophore used to test the maximal activity of Gárdos channel. However, it is important to note that under these experimental conditions, the amplitude of the hyperpolarization obtained depends on several parameters. The hyperpolarization obtained depends *in fine* on the membrane currents resulting from the activity of all the channels (Gárdos, anionic and NSC channels). When the Gárdos channel is activated, K^+ ions leave the cell, but anionic currents (of opposite charge) will counteract the development of hyperpolarization; more importantly, when the non-selective cationic activity is increased, sodium enters *via* the NSC channels (since the cations are no longer in electrochemical equilibrium) and either slows down the development of hyperpolarization or reduces its amplitude. Finally, once equilibrium is reached, the currents resulting from Gárdos channel activity will be at their minimum and therefore membrane repolarization can occur, which will be more or less rapid depending on the activity of the non-

selective cation channels. For simplicity, we will assume that the anion conductance is similar between cells. We are well aware that this is an *a priori* assumption, but given the importance of this conductance, it will generally be true. The observed variations may also be due to the number of Gárdos channels present at the membrane, but they may also be modified by the intracellular K^+ concentration, since the currents are directly related to the concentration gradient. Finally, since activation of the Gárdos channel induces dehydration, hyperpolarization may also depend on the initial hydration state of the cells, since this state cannot go beyond a certain point.

NS309 has the unique ability to shift the sensitivity of the Gárdos channel to calcium (by approximately one order of magnitude). Thus, this compound allows the activation of Gárdos-dependent hyperpolarization without altering the initial intracellular Ca^{2+} content. Thanks to this property, we can indirectly estimate (by comparison) the initial Ca^{2+} content of cells (for PIEZO1 variants) or to test the calcium sensitivity of the Gárdos channel. By using different concentrations associated with variable extracellular Ca^{2+} concentrations and by comparison these experiments provide elements to determine the differences between patients and controls.

Finally, Yoda1 is used at a concentration of 625 nM, which is the EC_{50} determined to activate the PIEZO1 channel in the red blood cell.

The morphometric analysis of blood samples is based on four parameters: the projected surface area, which reports the size of RBCs on the examined smear, the circularity, which is related to the granularity status of RBCs, the roundness which indicates the presence of elliptocytes on the smear, and the aspect ratio which gives an idea of the total number of abnormal shapes of RBCs present on the smear.

All samples received were treated with the same set of experiments: a morphometric analysis of the samples (surface area, circularity, roundness, and aspect ratio), investigation of their hydration status and intracellular Na^+ and K^+ contents, in addition to challenging the activity of the channels using the MBE method (Yoda1-NS309-A23187).

For the sake of clarity, we have chosen to present only experiments performed using Yoda1 (625 nM), NS309 (100 µM- 0 mM Ca^{2+}), or NS309 (10 µM- 2 mM Ca^{2+}), and A23187 (10 µM). In the morphometric part, we chose to present only the result of the projected area, and the circularity (or the aspect ratio in the *KCNN4* variant part).

In addition, we have only detailed the results obtained with known mutations, as we couldn't obtain much detail about the mutations in the unknown mutation cases, nor about the clinical satus of the patients.

Pictures of blood smears samples are visible in the Appendix 1.

III. Results

A. PIEZO1 variants

During my Ph.D., we received a total of 10 PIEZO1 variants, four of which we still do not have the position of the mutation. Table 7 lists the known biological and clinical data for each case, the duration of transportation, and the hematocrit on arrival. In this part, we present the results we obtained after analyzing 6 PIEZO1 variants (Figure 32, Table 8).

Table 7: Biological and clinical information of blood samples received with PIEZO1 channel mutations

Date	Designation in Figures	Mutation description	Received samples	Clinical observations of proband	Time laps (withdrawal-experiment)	Hematocrit
18/03/2021	R2019H	Heterozygous *Piezo1* mutation : R2109H (VUS mutation) + heterozygous β-spectrin mutation (P920L) + Homozygous HBB	-Proband PIEZO1 (+ β-Thalassemia+ β-spectrin) -Control	Major β-thalassemia, recurrent thrombosis since splenectomy in 1981. Blood Transfusion every 4 weeks	1 day- 4 °C	N/A
31/03/2021	L1697F + A344V	- 2 heterozygous mutations on *Piezo1*: L1697F (deletreious) + A344V (benign) -heterozygous mutation in α-spectrin gene *SPTA1*(D1021 V). -Homozygous HbSS	-Proband SS+ PIEZO1 -Control SS - Healthy control	Severe SCD syndrome (HbSS) + Li Fraumeni syndrome; 30% of dense cells.	2 days- 4 °C	Proband SS: 19% Proband SS+ PIEZO1: 10.8% Control: 43%
25/01/2022	L1708Q	L1708Q heterozygous mutation	-Proband (Child-daughter) -Father -Mother -Control	-Proband: Hemolytic anemia and hereditary spherocytosis -Father: No *Piezo1* mutations. He needed blood transfusion with his sister in their childhood. Their uncle had β-Thalassemia -Mother: L1708Q	2 days- 4 °C	Proband: 41% Father: 48.8% Mother: 42.1% Control: 42%

				Piezo1 heterozygous mutation. Normal profile.		
27/01/2022	P2282A	P2282A - Heterozygous mutation	-Proband (DB) -Control (BY)	Hemolytic anemia	2 days- 4 °C	Proband: 47.9% Control: 44.1%
23/02/2022	Unknown 4	PIEZO1+β-Thalassaemic patient	-Proband (Daughter) -Mother -Control -Control β-Thalassaemic	N/A	1 day- 4 °C	Proband:29% Mother:43.1% Control:40.85% Control β-Thalassaemic : 35.5%
06/10/2022	Unknown 1	Unknown	-Proband -Control	N/A	3 days	Proband: 35.3% Control: 39.9%
15/02/2023	Unknown 2	Unknown (Paris)	-Proband -Control	N/A	2 days- 4 °C	Proband: 48% Control: -
15/03/2023	S1726T	S1726T- (Mutation at the Yoda1-binding site)	Patient (S1726T) Relative 1 Relative 2 Control 1 Control 2	The patient suffers from polycythemia vera	2 days- 4 °C	Patient1 (S1726T) :46.5% Patient2 (RK) : 35% Patient3 (GK) : 49.5% Control1 (MZ) : 46.6% Control2 (CR): 37.3%
16/06/2023	Unknown 3	Unknown	-Proband -Control	- High CCMH - Dehydrated stomatocytosis -Non-recurrent PIEZO1 abnormality -Undefined mutations of PIEZO1,	3 days- 4 °C	Proband: 58.7% Control: 46.8%

				HFE, AND NT5C3A		
29/09/2023	Y2143C	Y2143C	-Proband (Neonate) -Father -Mother - Control	Hemolytic anemia Decreased PK activity No mutations in PKLR gene	2 days- 4 °C	N/A

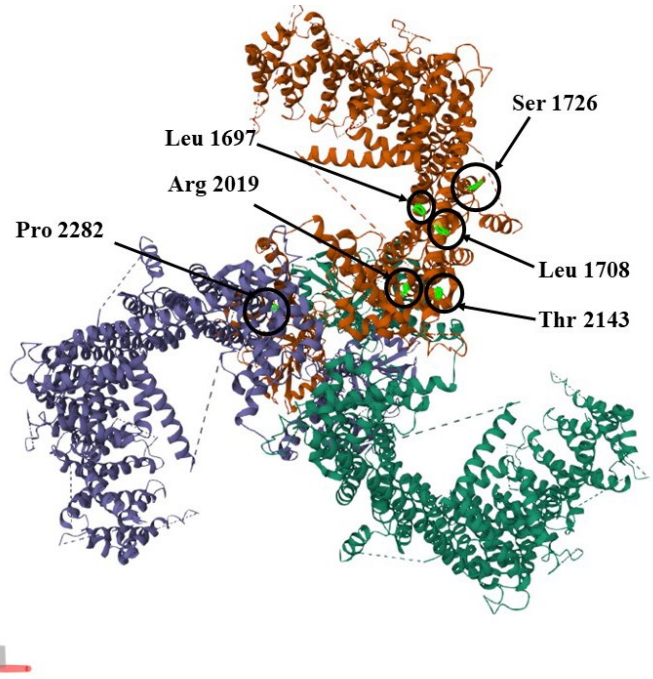

Figure 32: Summary of studied mutations on PIEZO1 channel. 3D structure (PDB; 5Z10 structure). Pro 2282 is in a disulfide binding bridge; Thr 2143 is a buried residue.

Table 8: Information known about the studied PIEZO1 mutations

Position	Change	Description	Source
344	A>V	Benign	UniProt
1697	L>F	Deletrious	UniProt
1708	L>Q	Probably pathogenic -Probably causes DHS1	Mutation tester SIFT HVAR UniProt
1726	1.S>R 2.S>T	1.Deleterious 2.Benign mutation	UniProt
2019	R>H	Deleterious	PolyPhen SIFT
2143	Y>C Y>H	Probably damaging	UniProt
2282	P>S P>T P>L P>A	Possibly damaging	UniProt

1. **L1697F + A344V**

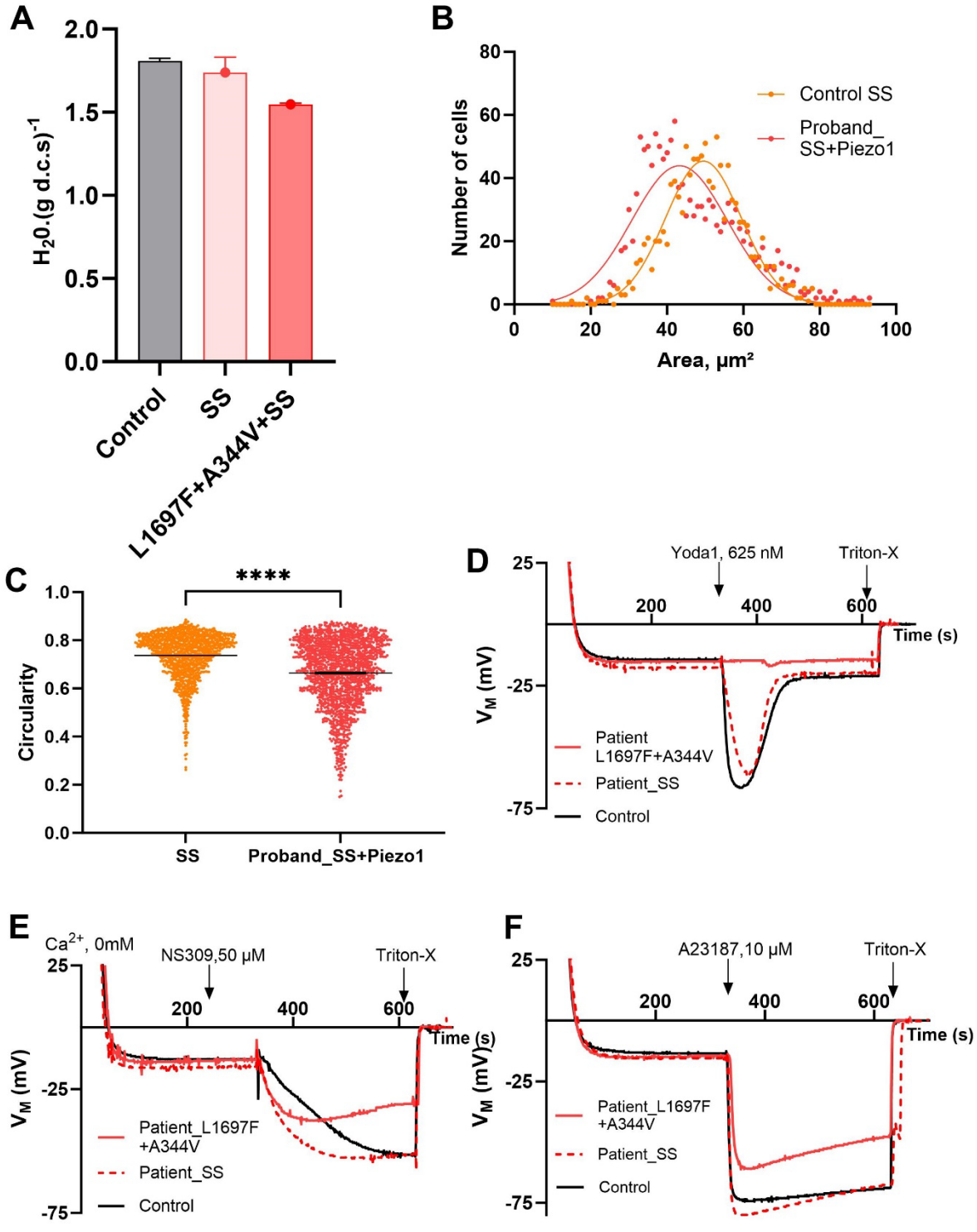

Figure 33: L1697F and A344V *Piezo1* variant. (A) Intracellular water content of healthy control, SS control, and patient. Histograms represent means ± SD of experimental duplicates with n=2, (B)

projected surface area, and (C) circularity. Number of analyzed cells for sickle cell patient: 1137, for patient having SCD and PIEZO1 mutation: 1403. Statistical difference was assessed using the one-way ANOVA ****p<0.0001. (D-F) Membrane potential measurements of *Piezo1* patient (in red, plain lines), SS control (in red, dashed lines), and healthy control RBCs (in black) in response to (D) Yoda1, 625 nM, (E) NS309, 50 µM without calcium in the extracellular media, and (F) A23187, 10 µM.

In this case study, we have a proband who has two heterozygous mutations of *Piezo1*: L1697F (a predicted deleterious mutation) and A344V (a predicted benign mutation). In addition, the proband is homozygous for sickle cell disease (HbSS) and has a heterozygous mutation for α-spectrin. The spectrum of symptoms includes a high population of dense cells, which is probably worsened by the VUS *Piezo1* mutation. Therefore, this proband is compared to two controls; a healthy control, and an HbSS control. In this case, the patient shows a drastic reduction in the cell water (Figure 33A) associated with a significant reduction in the projected surface area (Figure 33B). In addition, morphological analysis shows highly dispersed shapes with very heterogeneous circularity (Figure 33C). It should be noted that the sample received showed very strong hemolysis on arrival (hematocrit around 10%), admittedly linked to transportation but probably exacerbated by the various mutations present in this patient. The activation of the proband RBCs with Yoda1, did not induce any hyperpolarization, which is a completely unexpected result. This phenomenon could be explained by the fact that the majority of cells are hyperdense and thus already irreversibly sickled (see blood smears in Appendix 1). In this case, the membrane is already extremely rigid and could therefore become refractory to any stimulation by Yoda1 (Figure 33D). This hypothesis is somehow confirmed by experiments performed with 100 µM of NS309, where the hyperpolarization develops more slowly and is more limited (Figure 33E). Moreover, it is noteworthy that the hyperpolarization obtained with the HbSS patient cells develops slightly faster than in the control cell (Figure 33E), which is a common feature of the HbSS patient cells we have tested so far (see Chapter III). In response to A23187, the hyperpolarization was less important compared to the other SS patients tested, which may be due to the fact that the proband cells have less Gárdos channel, or less intracellular K^+ content, or are so dehydrated that water efflux becomes rate limiting for Gárdos activity. Unfortunately, sample sizes do not allow to determine intracellular K^+ and Na^+ concentrations. Nevertheless, both the HbSS control and the proband have a greater repolarization slope, which may indicate an overactivation of the NSC channel (Figure 33F).

In such patients, it is difficult to definitively conclude what the consequences of the two mutations found in the PIEZO1 gene are. Nonetheless, the association of PIEZO1 mutations with homozygous HbSS, and α-spectrin mutation is undoubtedly what amplifies the severity of this disease, rendering the profiles atypical and extreme. The L1697F mutation is probably a gain-of-function mutation and is indeed deleterious.

2. L1708Q

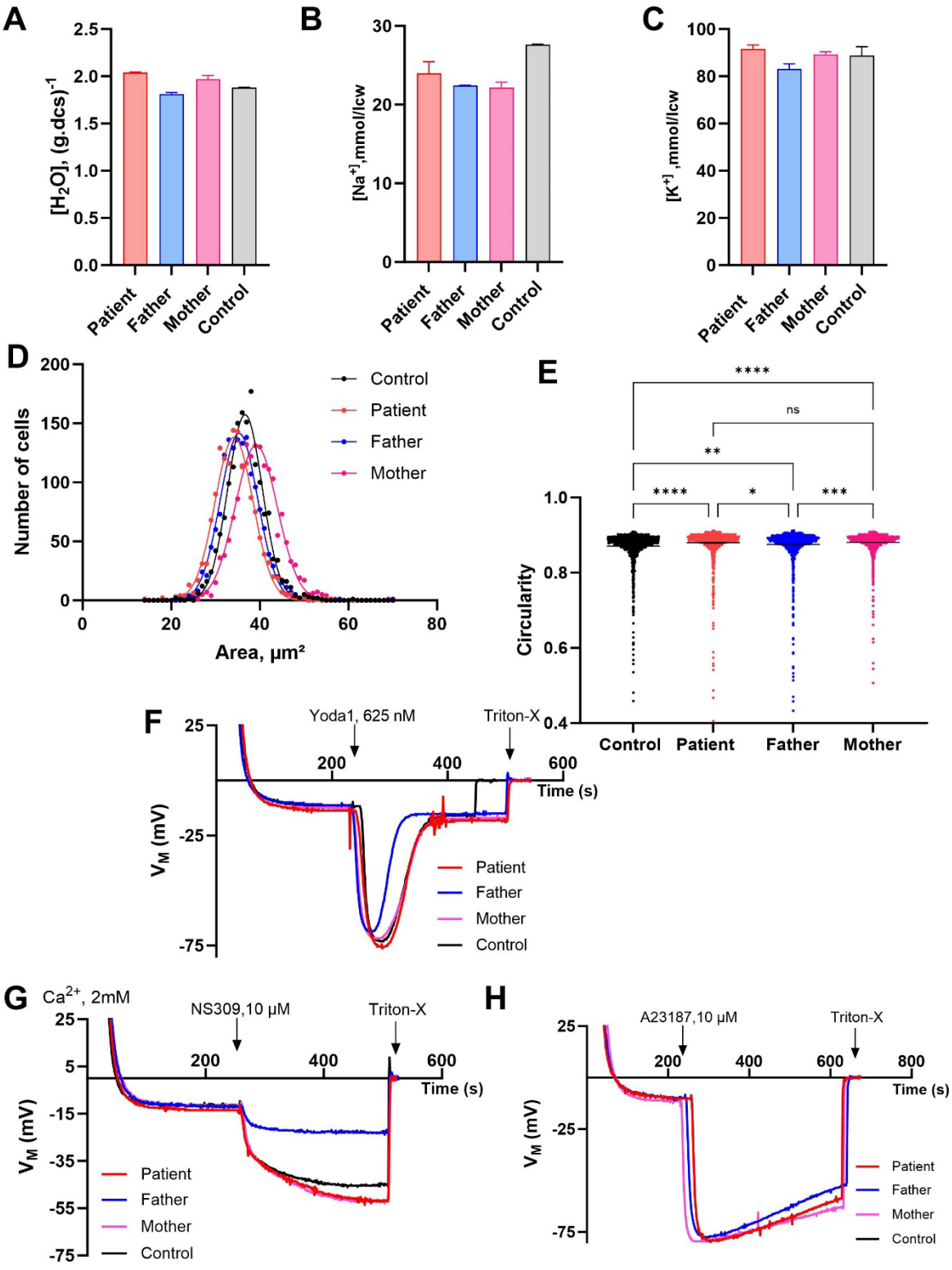
A
[H2O], (g.dcs)-1
Patient
Father
Mother
Control
B
[Na+],mmol/lcw
C
[K+] ,mmol/lcw
D
Number of cells
Area, µm²
E
Circularity
****
ns
**
*
***
F
Yoda1, 625 nM
Triton-X
Time (s)
VM (mV)
G
Ca2+, 2mM
NS309,10 µM
H
A23187,10 µM

Figure 34: *Piezo1* variant L1708Q. (A) Intracellular water content of healthy control, patient (the daughter), her father, and her mother. (B) Intracellular Na^+ content, and (C) K^+ content of the samples. Histograms represent means ± SD of experimental replicates, with n=2. (D) projected surface area, (E) circularity. Number of analyzed cells for control: 1575, patient: 1501, father: 1513, and mother: 1580. Statistical difference was assessed using the unpaired t-test, *p<0.05, **p<0.01, ***p<0.001, ****p<0.0001. (F-H) Membrane potential measurements of *Piezo1* patient, control, father, and mother in response to (F) Yoda1, 625 nM, (G) NS309, 10 µM with Ca^{2+} (2 mM) in the extracellular media, and (H) A23187, 10 µM.

In this case study, the proband is a 2-year-old baby who was found to be anemic at birth, with an abnormally low hematocrit value (18.9%). Enzymatic tests showed normal results. Genetic red blood cell membrane enzymopathy reported the heterozygous mutation L1708Q in the *Piezo1* gene. It is an undescribed mutation in different databases, with *in-silico* prediction that this mutation is pathogenic, eventually leading to DHS1. The father's medical history showed that he needed blood transfusion as a child, the same for the father's sister. The father's uncle had mild thalassemia. At the time of the study, the father had a normal blood test with very few Howell-Jolly bodies on the blood smear, and a normal ektacytometry profile except for a discrete dehydration. No *Piezo1* mutations were found in the father's gene. Regarding the mother, she had no personal or family history of transfusion with normal enzymatic results and no hemoglobinopathies. Nevertheless, the mother had a discrete hyperhydration ektacytometry profile and the heterozygous L1708Q mutation. This mutation (PIEZO1: c.5123T>A) is classified as heterozygous class 3 and predicted as pathogenic *in silico* by almost all software (Mutation Taster, SIFT, Polyphen2 HDIV) and is also found in the proband. The mother and the proband show a slightly hyperhydrated profile compared to the control, while the father shows a slightly dehydrated profile (Figure 34A). The Na^+ content was slightly lower for the family as a whole (Figure 34B), while the K^+ content was similar to the control (Figure 34C). The projected surface area of the proband and parents also differs slightly from the control, with a mean surface area shifted to the right for the mother, while it is shifted to the left for the proband and the father. Nevertheless, the range of dispersion of samples is more important in father and mother with 39.4 μm^2 for the control, 41.5 μm^2 for the proband, 44.7 μm^2 for the mother and 55.7 μm^2 for the father, which may indicate benign conditions in the parents (Figure 34D). Circularity also shows that the samples are homogeneous, although slightly dispersed for the proband (0.51 vs. 0.45, 0.48 and 0.40 for proband, control, father and mother, respectively) (Figure 34E). Interestingly, the circularity between the mother, who also carried the mutation, is similar to that obtained for the proband, indicating by such a certain similarity between the mother and the proband with cell more

spherical (see smears in Appendix 1). The MBE experiments clearly show that the father's sample behaves differently from the three other samples. In the three experiments presented, the responsiveness of the sample to the different experimental conditions was significantly reduced (Figure 34F, G & H). This result could be associated with the state of dehydration observed in the father. On the other hand, while the response to stimulation by Yoda1 was similar for the other three samples (Figure 34F), activation of Gárdos channels by NS309 showed that hyperpolarization developed more rapidly in the mother and the proband (Figure 34G). Accelerated hyperpolarization may indicate a slightly higher Ca^{2+} content than in the control. This observation is also associated with the fact that the amplitude of hyperpolarization is greater in these two patients compared to the control (mother -53.5 mV, proband -52.8 mV, control -46.0 mV). This last observation is also related to the rate and amplitude of hyperpolarization observed when the cells are stimulated with A23187, with a maximum hyperpolarization potential of -86.8 mV for the proband vs -79.6 mV for the control and the mother. All of these results tend to indicate that the proband (at least, but may be also for the mother) has a nominal level of intracellular Ca^{2+} that could, under certain circumstances, become detrimental to cell survival in the circulation. Interestingly, both parents had hemolytic episodes in their youth, which required transfusions, but which do not require any intervention today. In addition, a few months after this analysis, the proband's hematocrit returned to normal, with almost normal smears and a complete absence of hemolysis. It is therefore likely that this patient has a mutation that would be pathogenic in the early years for an unknown reason.

3. S1726T

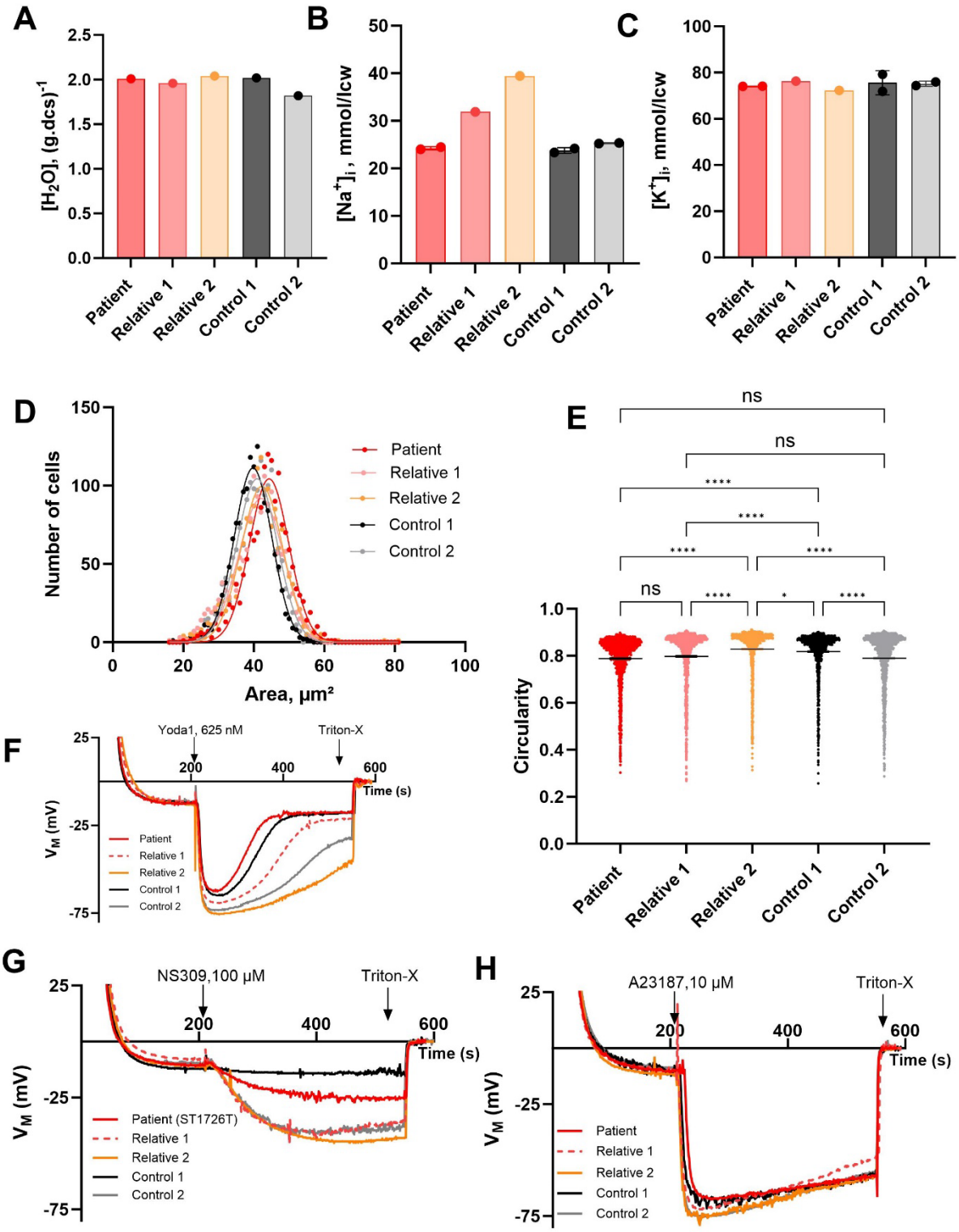

Figure 35: *Piezo1* S1726T variant (A) Intracellular water content of healthy controls, *Piezo1* variant, and her two relatives (B) Intracellular Na^+ content, and (C) K^+ content of the samples. Histograms represent means ± SD of experimental replicates, with n=2 or 1. (D) projected surface area, and (E) circularity. Number of analyzed cells for control 1: 1500, control 2: 1524, patient: 1521, relative 1:

1524 and for relative 2: 1531.Statistical difference was assessed using one-way ANOVA, *p<0.05, ****p<0.0001. (F-H) Membrane potential measurements of the samples in response to (F) Yoda1, 625 nM, (G) NS309, 10 µM with Ca^{2+} (2 mM) in the extracellular media, and (H) A23187, 10 µM.

These samples were analyzed in the context of a patient with symptoms of polycythemia, who had been followed for many years, but was negative for the commonly suspected mutations (HIF and JAK2). A mutation search on PIEZO1 identified a heterozygous mutation S1726T. The patient's sample was sent along with two samples from the same family (Relative 1 and Relative 2), and two control samples. The water content of the cells showed no significant variation compared to the control, nor did the K^+ content vary significantly (Figure 35A, B & C). Analysis of the projected surface area of the proband cells showed a significantly higher average than that of the controls: 44.3 ± 6.4 µm² (proband) vs 39.4 ± 5.6 µm² (control 1) and 40.2 ± 6.0 µm² (control 2) (Figure 35D). Similarly, although less pronounced, the projected surface area of the proband is larger than that of the two relatives: 40.8 ± 7.0 µm² (relative 1) and 41.6 ± 6.8 µm² (relative 2) (Figure 35D). On the other hand, the circularities of all the samples, although significantly different, are very close and within the range of values representing normal red cell shapes (Figure 35E). Stimulation of PIEZO1 channels by Yoda1 shows a relatively complex response pattern. The proband behaves similarly to control 1, while the other two behave like control 2 with a very pronounced response from relative 2, *i.e.* greater hyperpolarization and a much slower rate of repolarization (Figure 35E). It should be noted that not only is control 2 slightly dehydrated compared to the other samples, but relative 2 has a higher Na^+ content than any of the other samples (Figure 35B). Similarly, the stimulation response to NS309 (100µM) is quite identical, with the control 1 showing no hyperpolarization, the proband showing a very limited hyperpolarization, and the other three samples (control 2 and relatives 1 and 2) showing the same rate and extent of hyperpolarization (Figure 35F). Finally, the results obtained by activation of Gárdos channels by A23187 (10µM), although less pronounced, showed the same trend, with control 1, proband, and relative 1 identical, whereas control 2 and relative 2 showed a slightly more pronounced hyperpolarization but a much faster repolarization (Figure 35G). The mutation S1726T is located at the Yoda1 binding site, which might lead to the conclusion that this mutation is a loss-of-function mutation. Unfortunately, the genetic study was not continued in the relatives, making it impossible to determine whether one or the other carried the same mutation. However, the behavior of relative 2 suggests that she has an overactivation of the PIEZO1 channel. Finally, it is

difficult to say what the effect of the mutation is, given the large difference observed between the two shipment controls (control 1 and control 2).

4. **R2019H**

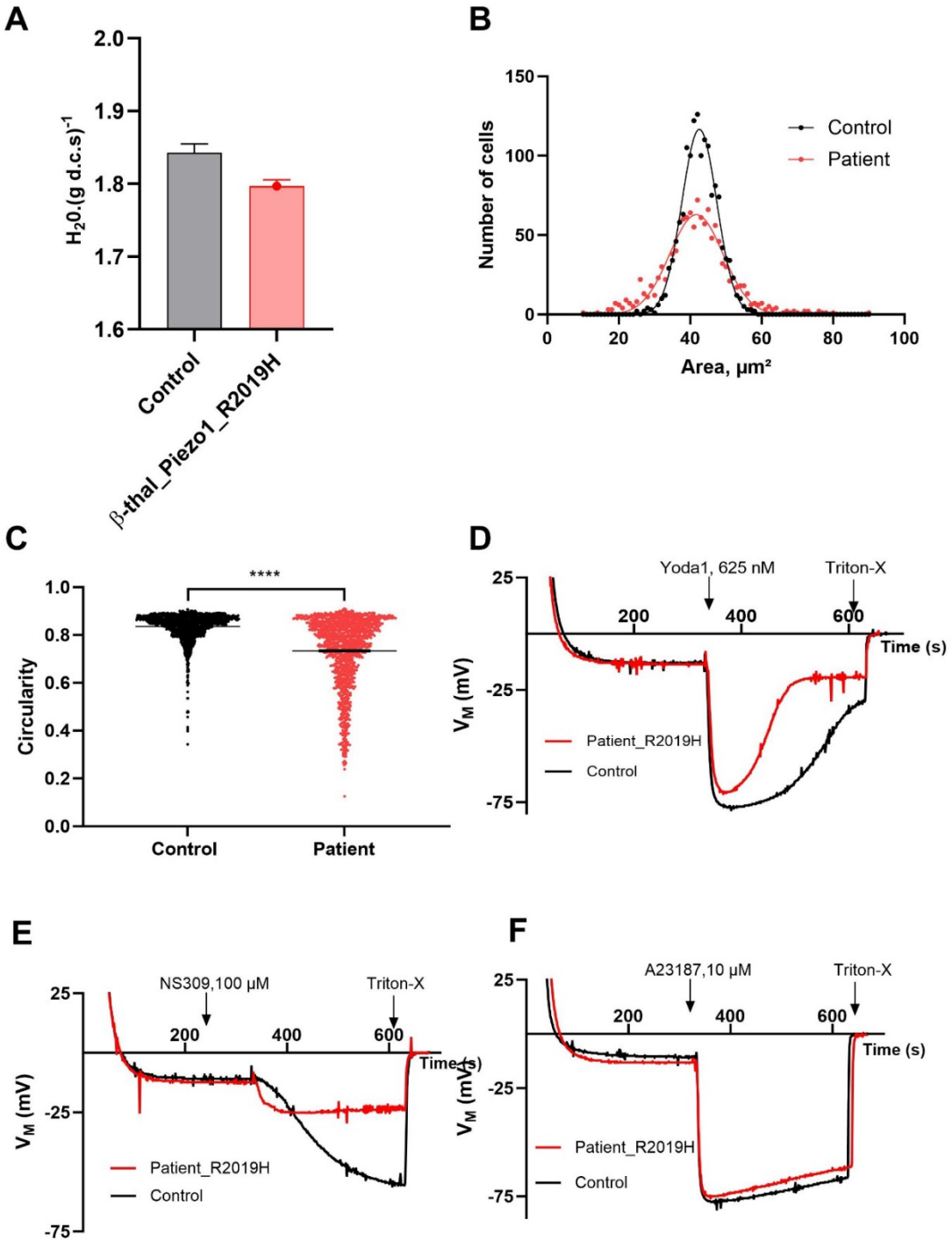

Figure 36: R2019H *Piezo1* mutation. (A) Intracellular water content of control and patient. Histograms represent means ± SD of experimental replicates, with n=2. (B) surface area, and (C)

circularity. Number of analyzed cells for control: 1438, for patient: 1246. Statistical difference was assessed using the unpaired t-test, ****p<0.0001. (D-F) Membrane potential measurements of *Piezo1* R2019H patient (in red) and control blood (in black) in response to (D) Yoda1, 625 nM, (E) NS309, 100 µM without Calcium in the extracellular media, and (F) A23187, 10 µM.

This patient, who was β-thalassemic and had undergone splenectomy, presented with recurrent thrombosis and further genetic investigation showed that he was heterozygous for a mutation in β-spectrin (P920L) and also for a mutation in the gene encoding the PIEZO1 channel (R2109H) in the heterozygous state and was declared as a VUS mutation.

The cells showed a slightly dehydrated state (1.84 *vs.* 1.79 $(gH_20.\ (g\ d.c.s))^{-1}$, Figure 36A), accompanied by a slight reduction in projected surface area (Figure 36B). The size distribution in the projected area is much larger in the patient than in the control (control area 33 µm² *vs.* patient area 80 µm²), which is confirmed by the significantly lower circularity index 0.83 ± 0.06 vs. 0.73 ± 0.14, showing the heterogeneity of shape in this patient (Figure 36C).

Investigations using the MBE method showed little explanatory power. Indeed, the response to stimulation with Yoda1 produced less hyperpolarization accompanied by a more rapid repolarization, suggesting that calcium entry was certainly less important in this patient. This result echoes the results obtained in the presence of NS309, where the hyperpolarization is much less pronounced and, more surprisingly, develops immediately to reach a minimum value that remains stable. This behavior, combined with the previous observation in the presence of Yoda1, could indicate that the cells are in a very heterogeneous state (Figure 36D). The MBE method has the resolving disadvantage of measuring only the average behavior of the cells. Thus, if the activation kinetics are not simultaneous for all the cells, the result is scrambled and does not represent the reality of ion movement. In addition, this patient is regularly transfused and it is likely that the splenectomy leaves a large number of aged cells in the circulation that do not fully respond to stimulation by the pharmacological agents used here. Unfortunately, the volume of samples sent did not allow the determination of Na^+ and K^+ contents, which would have provided additional information on the ionic state of the patient' s cells.

5. Y2143C

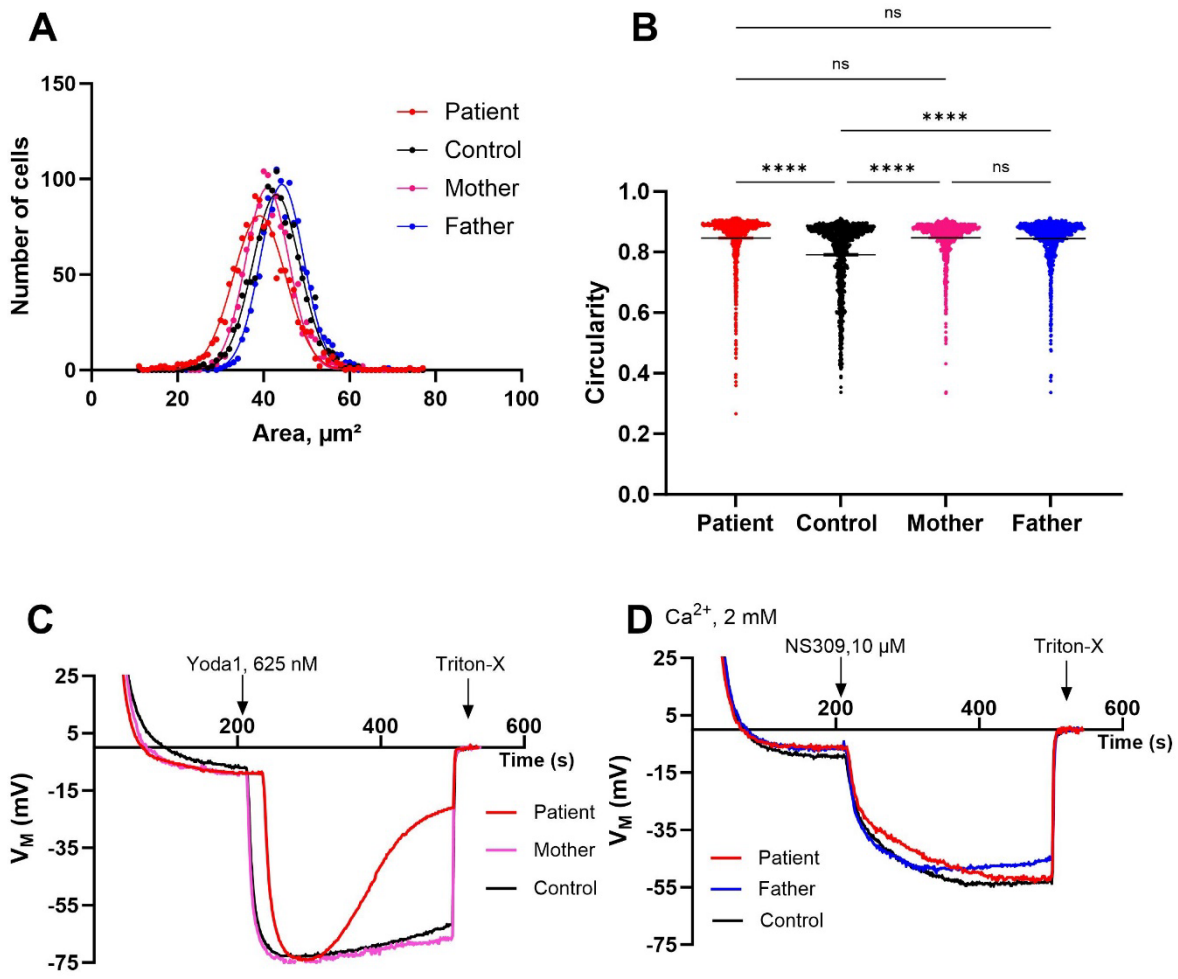

Figure 37: *Piezo1* variant Y2143C mutation. (A, B) Morphometric study of healthy control, patient, his father, and his mother. (A) projected surface area, and (B) circularity. Number of analyzed cells for control: 1280, for patient: 1265, father: 1240, and mother: 1220. Statistical difference was assessed using the one-way ANOVA ****p<0.0001. (C-D) Membrane potential measurements of *Piezo1* patient, control, father, and mother in response to (C) Yoda1, 625 nM, and (D) NS309, 10 µM with Ca^{2+} (2 mM) in the extracellular media.

The proband in this study is a neonate of 2-month-old neonate with hemolytic anemia at birth. Physicians found a decreased PK activity. NGS showed no PKLR gene mutation, but a new variant in PIEZO1, p. Y2143C, with ektacytometry at birth not suggestive of dehydration. Without the evidence of Lorrca, physicians couldn't assign a pathogenic profile to this variant. Molecular studies provided by our collaborators, showed that the mutation of the proband was found to be transmitted by the father. For this case study, we received only 400 µL of blood for each sample, the reason why we couldn't study the effects of more than two hyperpolarizing molecules, with no intracellular water and ions investigations. Patient cells have a transient repolarization compared

to mother and control samples (Figure 37C), and the same profiles of hyperpolarizations in response to NS309, 10 µM with the presence of Ca^{2+} in the intracellular media (Figure 37D). Yoda1 results show that this could be a loss-of-function mutation. Morphological studies showed that patient cells have a profile that is shifted to the left, indicating that patient cells might be smaller (patient: 38.17 μm^2- father: 44.86 μm^2- mother: 40.96 μm^2- control: 42.7 μm^2) (Figure 37A). On the other hand, the circularity indices of the patient, mother, and father were significantly different from the circularity of the control ($p<0.001$) and similar to each other ($p>0.05$). Knowing that the mutation is carried by the father, but that the mother also has a large number of cells with abnormal shapes, it would be appropriate to explore this further. In fact, it is possible that the mother carries a benign mutation in another gene that aggravates the mutation inherited from the father. In view of these results, it is difficult to say whether the Y2143C mutation is pathogenic or not.

6. P2282A

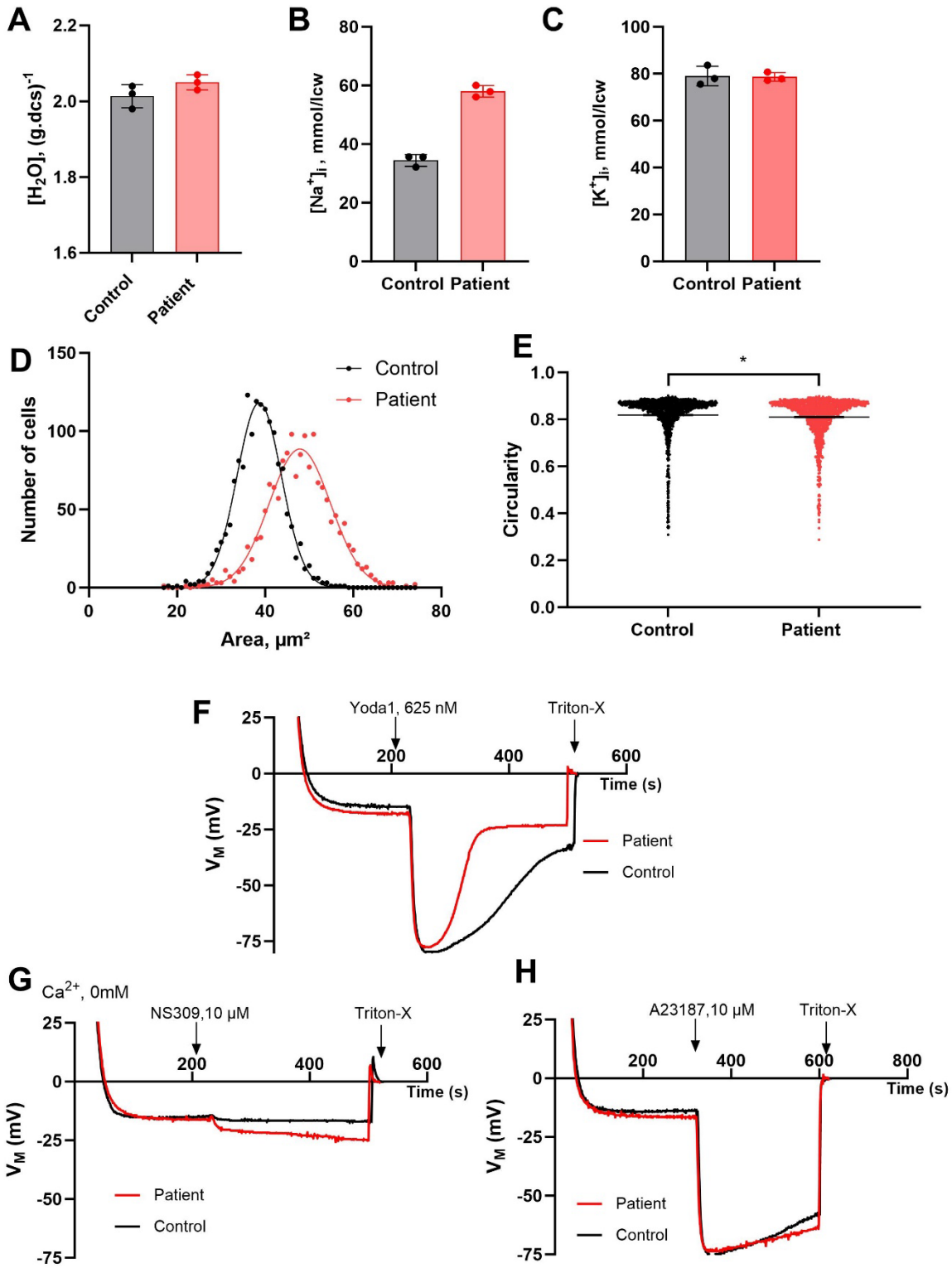

Figure 38: *Piezo1* mutation P2282A. (A) Intracellular water content of healthy control and patient. (B) Intracellular Na^+ content, and (C) K^+ content of the samples. Histograms represent means ± SD

of experimental replicates, with n=3. (D) projected surface area, (E) circularity. Number of analyzed cells for control: 1507, for patients: 1507. Statistical difference was assessed using the unpaired t-test, *p<0.05. (F-H) Membrane potential measurements of *Piezo1* patient, control, father, and mother in response to (F) Yoda1, 625 nM, (G) NS309, 10 µM without Ca^{2+} (2 mM) in the extracellular media, and (H) A23187, 10 µM.

The proband is an elderly man (71 years old) with hemolytic anemia. He was found to be heterozygous for *Piezo1* with the P2282A variant. The patient showed slightly hyperhydrated red blood cells (Figure 38A) associated with an almost doubled of Na^+ content (34.4 ± 2.0 *vs.* 58.0 ± 2.0 mmol/lcw, Figure 38B), without any change in K^+ content (Figure 38C), a significantly larger projected surface area in the patient compared to the control: 47.9 ± 7.3 µm² *vs.* 38.6 ± 5.3 µm² (n=1500 cells, p<0.0001, Figure 38D), and a lower circularity in the patient compared to the control 0.818 ± 0.09 *vs.* 0.810 ± 0.09 (n=1500 cells, p<0.05, Figure 38E), indicating the presence of numerous cells with altered shapes, easily visible on smears.

Injection of Yoda1 (625 nM, Figure 38F) produces a similar hyperpolarization in both samples, although slightly more pronounced in the patient. Stimulation with NS309 clearly shows that the calcium content is likely to be higher in the patient than in the control (Figure 38G), as the extent and speed of hyperpolarization is much more pronounced in the patient cells than in the control cells. This observation reinforces the observation of a much higher Na^+ content in the patient. The mutation undoubtedly causes a greater cation leak than is normally observed in control cells. However, the effect of Yoda1 is more transient (Figure 38F), indicating that calcium entry, which is sufficient to activate the Gárdos channel to the same extent as in control cells, is counterbalanced either by an increase in Cl^- efflux, a greater Na^+ entry or an increased efficiency of the calcium pump. These hypotheses are possibly concomitant and cannot be attributed to a defect in Gárdos channel reactivity (Figure 38H).

These results indicate that this mutation may be a gain-of-function mutation but with very mild symptoms.

B. **Gárdos channel variants**

We have also received 5 KCNN4 variants, for one of them the point mutation was still not communicated. Table 9 presents the biological and clinical data available regarding each patient, as well as the duration of the shipment and the hematocrit upon arrival. In this section, we present the results we obtained after analyzing the 4 identified KCNN4 variants (Figure 39, Table 9).

Table 9: Blood samples received during my PhD with Gárdos channel mutations

Date	**Mutation**	**Received samples**	**Clinical observations**	**Time laps (withdraw-experiment)**	**Hematocrit upon arrival**
07/05/2021	S386N	Proband Control	N/A	1 day	Control:46.15% Patient: 50%
06/10/2022	R352H	Father Son Control	Father: Hereditary stomatocytosis with Gárdos syndrome. P.S: NGS showed a heterozygous mutation of *Piezo1* (A1210V) Son: Gárdos syndrome; no *Piezo1* mutation	1 day	Father: 32.8% Son: 33.1%
09/11/2022	Unknown	Proband Control	N/A	2 days	Control:52.4% Patient: 53.7%
22/06/2023	A279D	Proband Control	Compensated chronic hemolysis -Atypical ektacytometry profile -no iron overload	1 day	Control: 44.3% Patient: 38.1%
29/09/2023	H340N	Proband (son) Father Mother Control	Very mild anemia Splenomegaly	2 days	Control: 31.25% Patient: 41% Father: 52.2% Mother: 41.1%

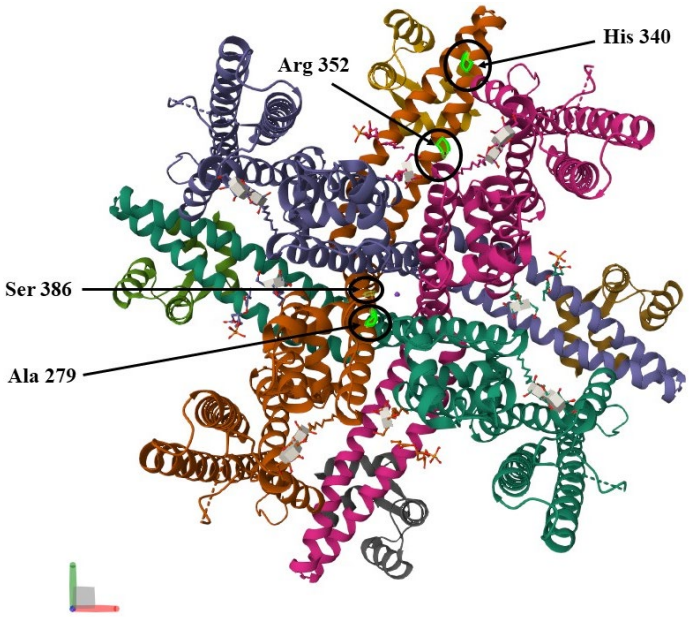

Figure 39: Summary of studied mutations on a KCNN4 3D structure (PDB; 6CNM structure).

1. A279D

Amino acid 279 is located in the K^+ pore domain. More than one mutation has been reported to take place on this position. The substitution of Alanine by Threonine is the most recent mutation described on this channel, which is pathogenic without further precisions (Nakahara et al., 2023). In our laboratory, we received a variant in which alanine was substituted by aspartic acid at the position 279. The patient presents a compensated chronic hemolysis.

The patient has dehydrated cells (1.96 ± 0.05 g H_2O. (g. dcs)$^{-1}$ *vs.* 1.77 ± 0.04 g H_2O. (g. dcs)$^{-1}$) associated with identical ionic contents: Na^+ 14.8 ± 0.9 mmol/lcw *vs* 9.4 ± 0.8 mmol/lcw, K^+ 77.8 ± 2.0 *vs* 84.5 ± 3.4 mmol/lcw for controls and patients respectively (Figure 40A). Nevertheless, the projected surfaces showed a significant decrease in the latter, in agreement with the volume measurement (proband: 40.3 ± 6.2 µm²- control: 42.3 ± 4.8 µm²) (Figure 40C), associated with a circularity that, although significant, was fairly similar (0.84 ± 0.05 *vs.* 0.82 ± 0.06 for control and patient, respectively).

Irrespective of the condition used for NS309 stimulation, the development of hyperpolarization was systematically faster and more pronounced in the patient than in the control. For example,

while hyperpolarization reached a value of -40 mV in the control (10 µM with 2mM $[Ca^{2+}]_o$), a hyperpolarization of -64 mV was reached in the patient cells under the same conditions (Figure 40F). Similarly, the experiment carried out with NS309, 10µM but without calcium in the extracellular medium, did not induce any manifestation of Gárdos channel activity in control cells, whereas it induced a hyperpolarization reaching -20 mV in the patient cells (Figure 40E). These results clearly indicate that, in this patient, either the Gárdos channels are intrinsically more active in A279D variants, or this mutation induces a greater sensitivity to calcium. We can rule out the hypothesis that the patient cells are initially more loaded with calcium because fluorescence measurements (Fluo-4) show that the calcium levels are similar between the two samples (7.1 ± 1.2 a.u. vs 7.0 ± 1.6 a.u., p=0.56, unpaired t-test, n=188 cells for control samples and n= 186 for patient cells). However, the experiment with A23187 (10 µM), which allows to obtain the maximum activity of the Gárdos channels to be obtained, again showed a slightly greater hyperpolarization in the patient than in the control (Figure 40H). Such a result would tend to support the hypothesis that this channel (once activated) would be more permeable. In electrophysiological terms, this would mean that the unitary conductance of this variant would be higher than that of wild-type channels. Patch-clamp experiments could therefore be used to determine and draw definitive conclusions about this mutation.

All these results, together with clinical observations such as the compensated chronic hemolysis, the atypical ektacytometric profile, and the absence of iron overload, lead us to believe that this mutation can cause DHS2.

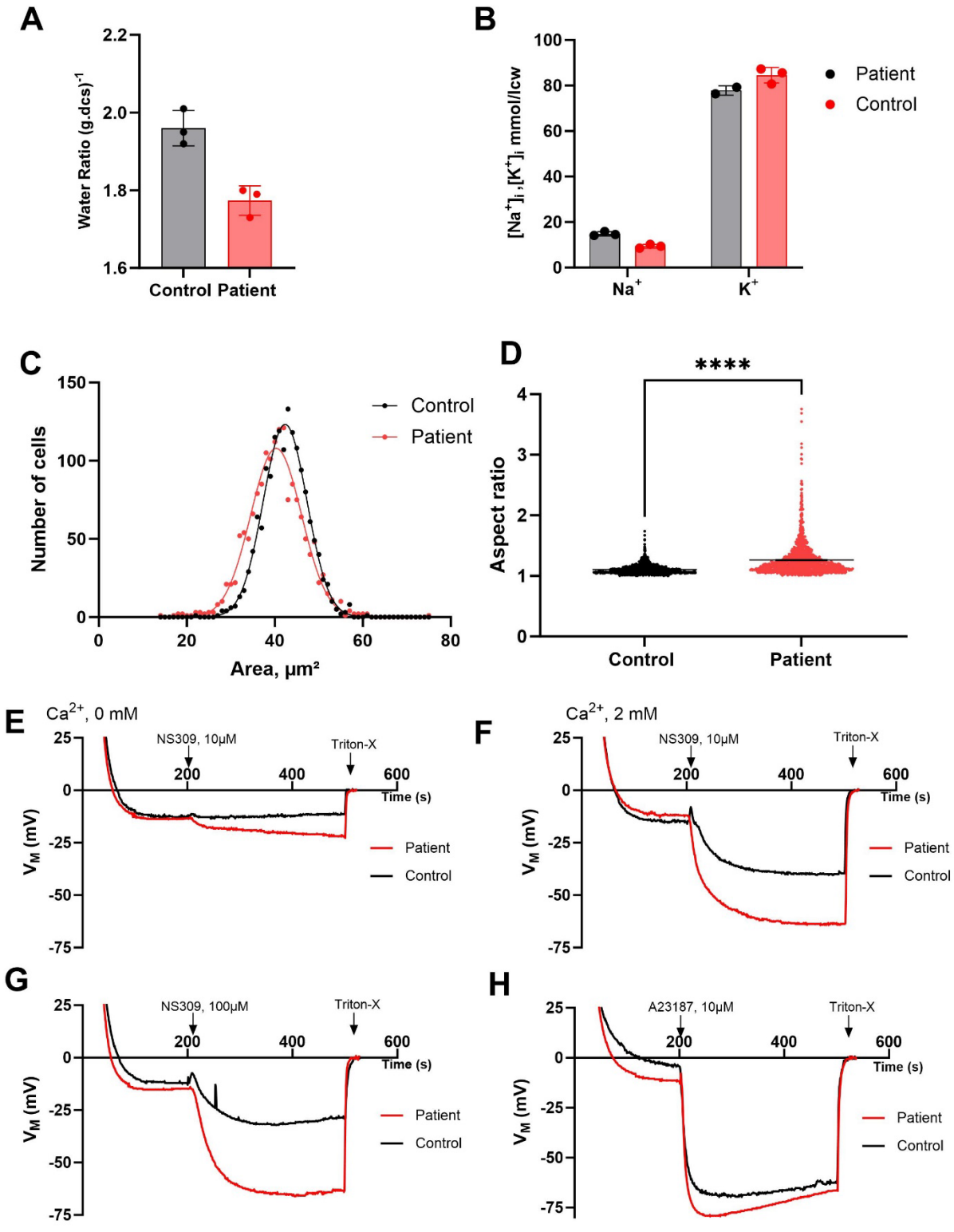
A
Water Ratio (g.dcs)-1
2.2
2.0
1.8
1.6
Control Patient
B
[Na+]i, [K+]i mmol/lcw
100
80
60
40
20
0
Na+
K+
Patient
Control
C
Number of cells
150
100
50
0
0
20
40
60
80
Area, µm²
Control
Patient
D
****
Aspect ratio
4
3
2
1
0
Control
Patient
E
Ca2+, 0 mM
NS309, 10µM
Triton-X
200
400
600
Time (s)
VM (mV)
25
0
-25
-50
-75
Patient
Control
F
Ca2+, 2 mM
NS309, 10µM
Triton-X
200
400
600
Time (s)
VM (mV)
25
0
-25
-50
-75
Patient
Control
G
NS309, 100µM
Triton-X
200
400
600
Time (s)
VM (mV)
25
0
-25
-50
-75
Patient
Control
H
A23187, 10µM
Triton-X
200
400
600
Time (s)
VM (mV)
25
0
-25
-50
-75
Patient
Control

Figure 40: *KCNN4* A279D variant. (A) Intracellular water content of control and patient. (B) Intracellular Na^+ and K^+ contents (in mmol/lcw). Histograms represent means ± SD of experimental replicates with n=3. (C) surface area characterization, and (D) aspect ratio. Number of analyzed cells for control: 1528, for patients: 1590. Statistical difference was assessed using the unpaired t-test, ****p<0.0001. (E-H) Membrane potential measurements of *KCNN4* A279D patient (in red) and control blood (in black) in response to (E) NS309, 10 µM without Ca^{2+} in the extracellular media, (F) NS309, 10 µM with Ca^{2+} in the extracellular media NS309, (G) NS309, 100 µM without Ca^{2+} in the extracellular media, and (H) A23187, 10 µM.

2. H340N

Amino acid 340 is located in the calmodulin binding domain. A missense mutation at this site, substituting histidine by arginine has been described as a *de novo* mutation that results in KCNN4 opening to lower Ca^{2+} concentrations (Allegrini et al., 2022). The anemia of this treated patient was sporadic, as was that of the patient treated in the Allegrini *et al*. paper (Allegrini et al., 2022). The shipment included a control sample, a patient sample, and samples from the father and mother, the latter also carrying the H340N mutation. The patient's cells had a slightly higher water content than the control (1.9 *vs* 2.0) (Figure 41A), while the father's cells were very dehydrated (1.76). Na^+ values were identical between samples, while K^+ content measurements showed a decrease in potassium in the patient compared to the control and the parents (Figure 41B). The volume of samples sent did not allow for multiple replicates and these results should be treated with caution.

Morphometric analysis showed very similar profiles. However, it should be noted that the mean projected areas of the patient and parents are significantly lower than those of the control and are not statistically different from each other (one-way ANOVA multiple comparisons) (Figure 41C). Analysis of the circularity index shows a much lower index for the patient and mother (0.75 ± 0.1 and 0.72 ± 0.12) compared to the control and father (0.80 ± 0.06 and 0.82 ± 0.05), with greater inter-cell variability, indicating that the mother and patient samples have a large number of cells with abnormal shapes (Figure 41D).

The experiments carried out show that this mutation probably induces a hypersensitivity of the Gárdos channel to Ca^{2+} (Figure 41F). Indeed, while stimulation at 10µM in a calcium-free environment showed no difference between the samples (Figure 41E), the experiment performed with the same concentration of NS309 (10µM) but with 2mM $[Ca^{2+}]_o$ induced a faster and more pronounced hyperpolarization in the son and the mother, while the father behaved like the control

(Figure 41F). In addition, the hyperpolarizations obtained with A23187 (Figure 41H), although similar for all samples, showed a slightly greater hyperpolarization for the mother (a few mV) than that obtained in the other three samples. Finally, it should be noted that the profile obtained with A23187 for the father shows a rapid repolarization, generally a sign of an overactivated non-selective cationic conductance. This last result should be considered in the context of the experiment carried out with 100µM NS309, where the hyperpolarization obtained for the father was faster and greater than in all the other samples (Figure 41G). Such behavior could indicate that the father has a Ca^{2+} entry pathway (a non-selective cationic conductance) that is slightly higher than normal. Such a phenomenon could also explain the dehydrated state of the father's cells. The behavior of the father's cells shows abnormalities, or at least behavior that deviates from control. The patient's cells are very similar to those of the mother's cells in many respects. It is therefore likely that the H340N mutation is, as described above, relatively benign, but in this patient, the case is probably accentuated by a mutation or as yet unidentified pathology in the father. Nevertheless, these results are in accordance with Allegrini's article in 2022 (Allegrini et al., 2022) with mild anemia.

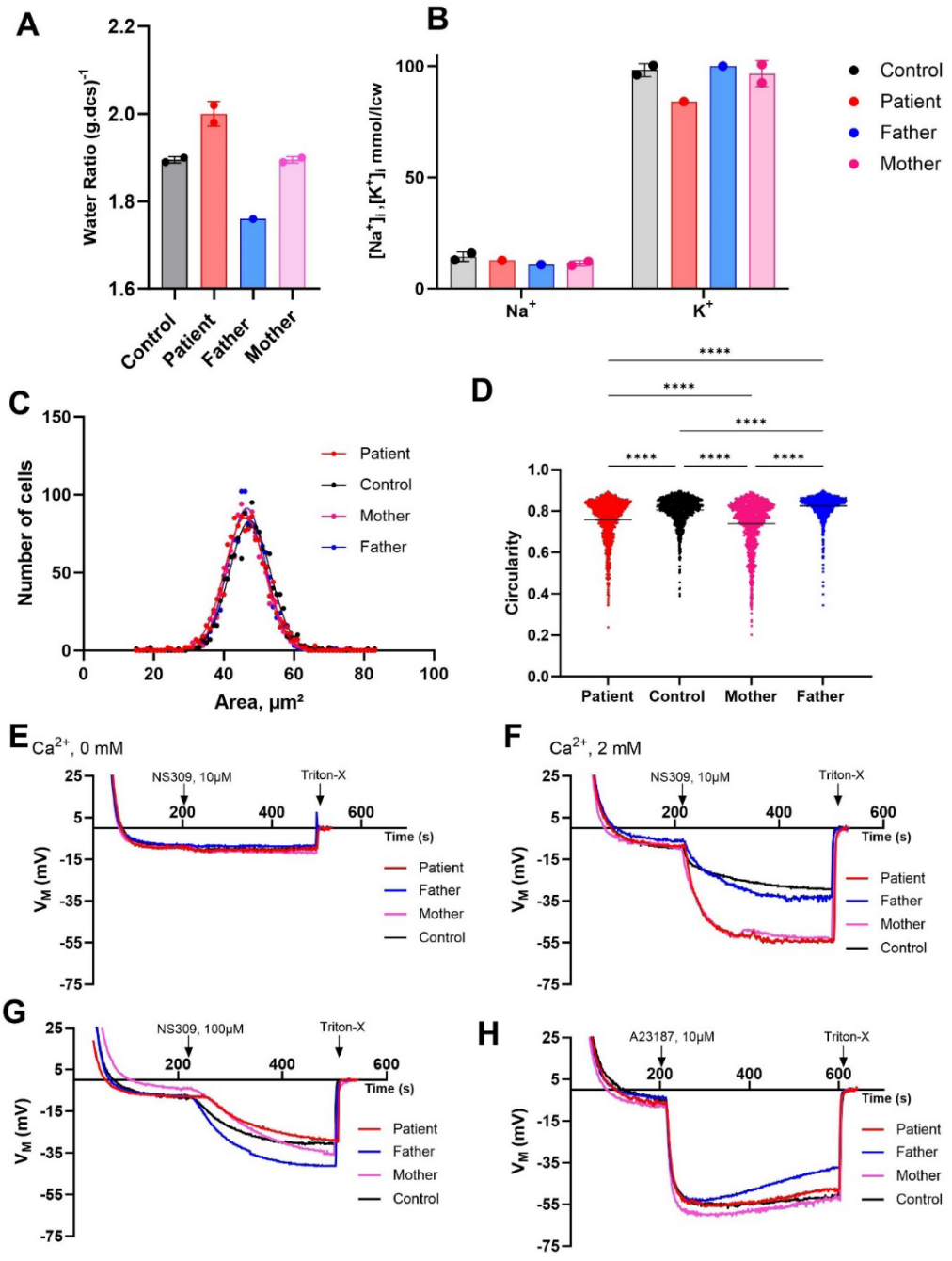

Figure 41: *KCNN4* H340N variant. (A) Intracellular water content of control, patient, father, and mother blood samples. (B) Intracellular Na^+ and K^+ contents (in mmol/lcw). Histograms represent means ± SD of experimental replicates, with n=2 or 1. (C) surface area, (D) circularity. Number of analyzed cells for control: 1224, for patients: 1264, mother: 1192, and father: 1234. Statistical difference was assessed using one-way ANOVA, *p<0.05 ****p<0.0001. (E-H) Membrane potential measurements of *KCNN4* H340N patient (in red), control blood (in black), mother (in pink), and father (in blue), in response to (E) NS309, 10 µM without Ca^{2+} in the extracellular media, (F) NS309,

10 µM with Ca^{2+} in the extracellular media NS309, (G) NS309, 100 µM without Ca^{2+} in the extracellular media, and (H) A23187, 10 µM.

3. R352H

R352H is one of the most common and described variants of KCNN4. It is a pathogenic gain-of-function mutation linked to the position of this residue within in the calmodulin binding domain.

Samples were collected from the proband, his father, and a transport control. The father also carries a heterozygous *PIEZO1* mutation (A1210V). The patients' cells showed a hydration state similar to that of the control. However, the father's cells were dehydrated compared to the control cells. This dehydration could be due to the additional mutation in the *PIEZO1* channel carried by the father. Analysis of cation content revealed identical Na^+ content but a slight decrease in K^+ content in the proband (Figure 42A &B). Morphometric analysis shows increased projected areas in the father and extreme projected areas in the son (control 35.6 ± 4.74 µm², father 43.2 ± 8.1 µm² and son 51.7 ± 10.0 µm², Figure 42C). The increase in the projected area is accompanied by a significant decrease in the circularity index (Control 0.86 ± 0.06, Father 0.80 ± 0.12 and son 0.81 ± 0.10), which may be related to the numerous aberrant shapes on the smears (Figure 42D). Experiments carried out with the MBE method show the consequences of this mutation on the sensitivity of the Gárdos channel to Ca^{2+}. Indeed, the three different conditions used with NS309 as Gárdos channel activator showed a rapid and very pronounced hyperpolarization (Figure 42E, F &G). This was confirmed looking on hyperpolarizations obtained with A23187 (Figure 42H). The mutation clearly affects the calcium sensitivity of the Gárdos channel, which probably accelerates the aging process and eventually a fast removal of cells from the circulation.

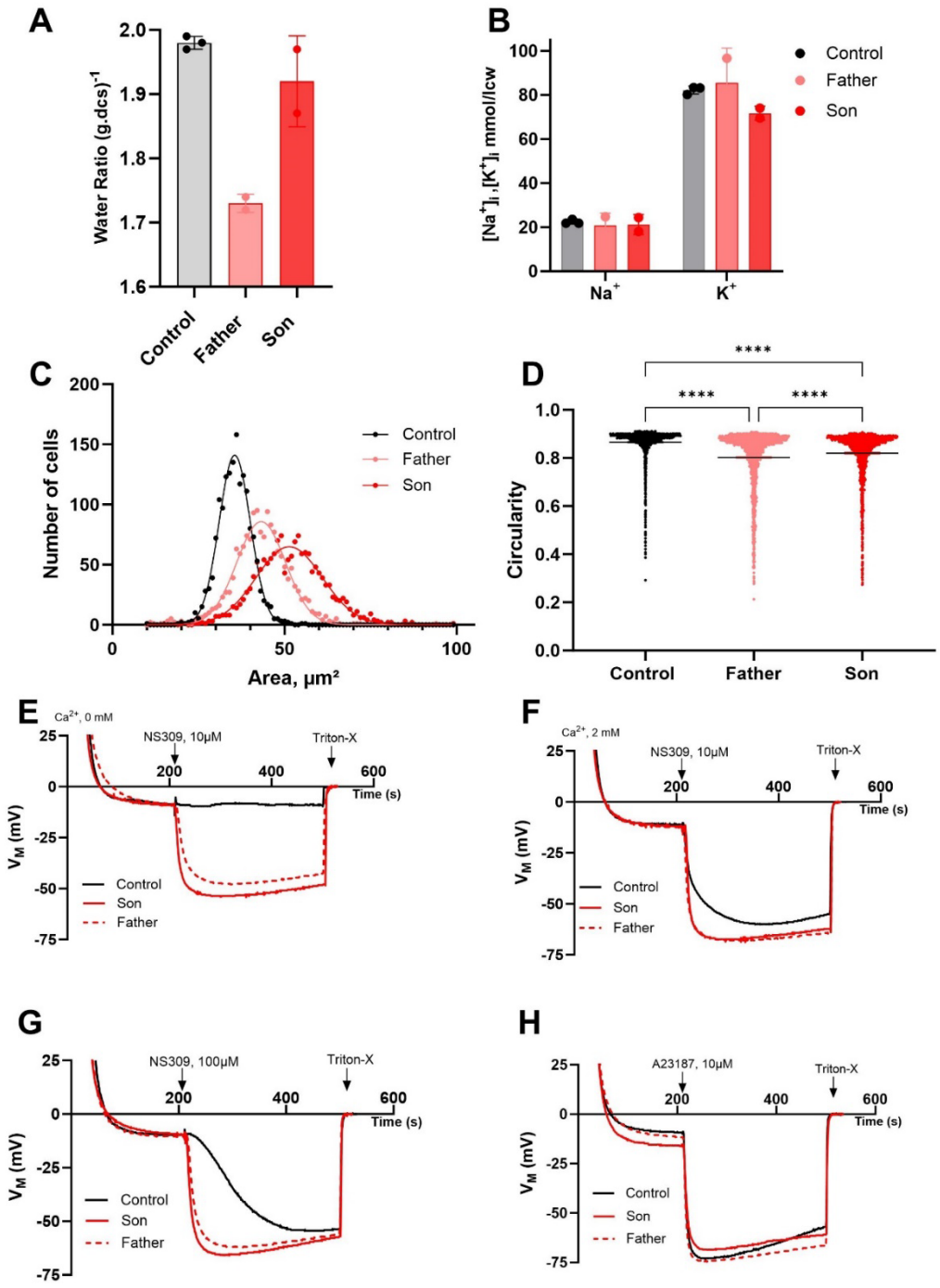

Figure 42: *KCNN4* R352H variant. (A) Intracellular water content of control, father, and son blood samples. (B) Intracellular Na^+ and K^+ contents (in mmol/lcw). Histograms represent means ± SD of experimental replicates, with n=2 or 3. (C) surface area, and (D) aspect ratio. Number of analyzed cells for control: 1611, for the father: 1567, and the son: 1577. Statistical difference was assessed using the one-way ANOVA ***p<0.001, ****p<0.0001 (E-H) Membrane potential measurements of *KCNN4* R352H patients (in red; father: dashed lines, son: plain lines), and control (black), in response to (E) NS309, 10 µM without Ca^{2+} in the extracellular media, (F) NS309, 10 µM with Ca^{2+} in the extracellular media NS309, (G) NS309, 100 µM without Ca^{2+} in the extracellular media, and (H) A23187, 10 µM.

4. S386N

Little is known about position S386 in KCNN4; we only know that position S387 may have a benign mutation (S387R) and that the region 368-386 is a partially modeled or an unmodeled region of KCNN4 (UniProt). MBE results showed the same profiles of membrane potential variations between S386N patients and the corresponding controls, except for the condition of NS309 (10 μM) with Ca^{2+} (2mM) in the medium (Figure 43B). These results may suggest that the S386N mutation is a gain-of-function, Ca^{2+}-sensitive mutation, but a largely benign one. The morphological parameters showed exactly the same profiles of S386N and the corresponding control (Figure 43A-B). The S386N mutation is probably not pathogenic and leads to mild hemolysis, or the origin of the proband's health problems is related to another undiagnosed pathology.

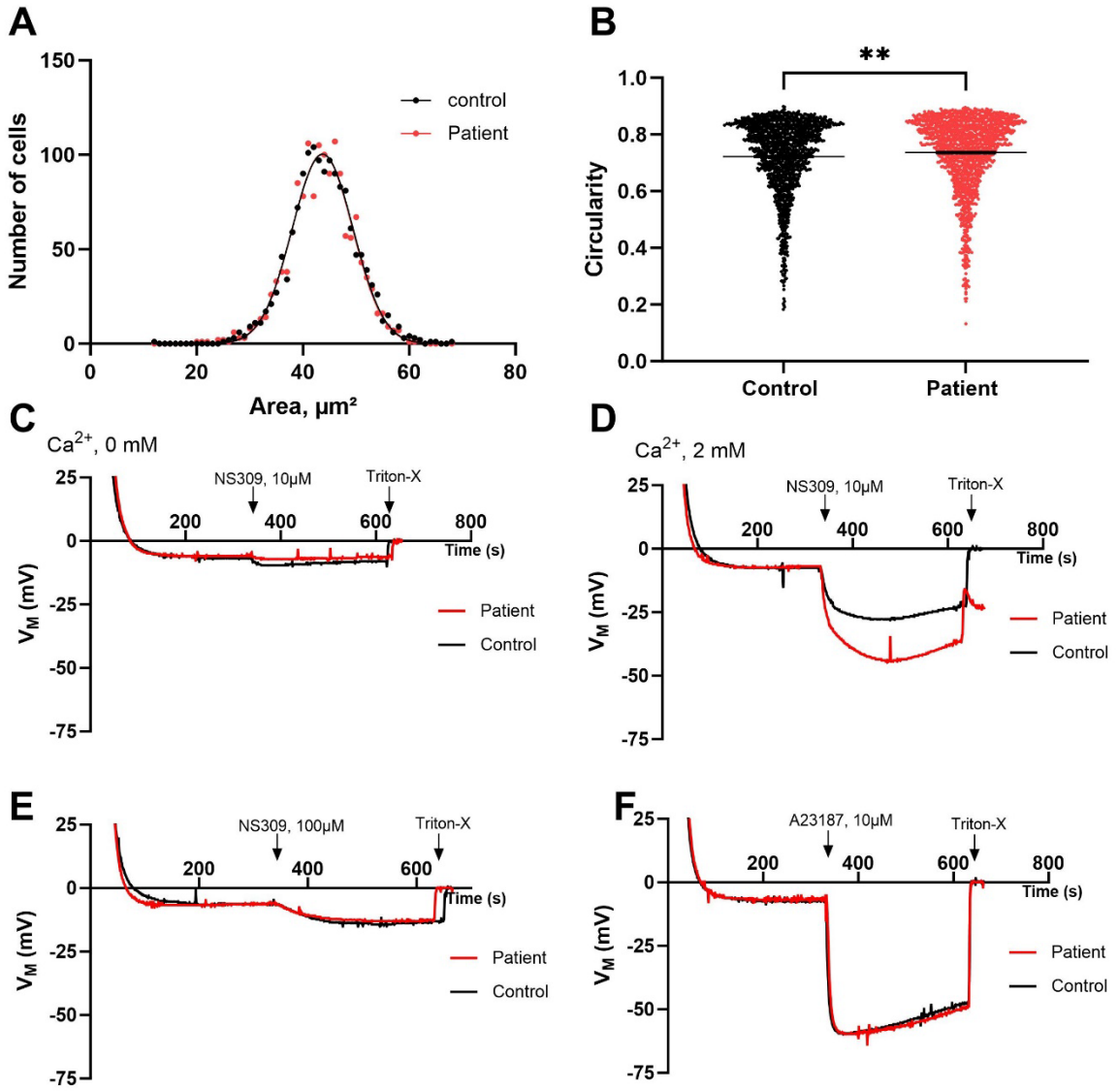

Figure 43: *KCNN4* S386N variant. (A, B) are parts of the morphometric study, (A) surface area, and (B) circularity. Number of analyzed cells for control: 1466, for patients: 1447. Statistical difference was assessed using the unpaired t-test **p<0.01, ***p<0.001. (C-F) Membrane potential measurements of *KCNN4* S386N patient (in red) and control blood (in black) in response to (C) NS309, 10 µM without Ca^{2+} in the extracellular media, (D) NS309, 10 µM with Ca^{2+} in the extracellular media NS309, (E) NS309, 100 µM without Ca^{2+} in the extracellular media, and (F) A23187, 10 µM.

3. Overall recap of the studied KCNN4 mutations

To conclude this section, we chose to present a summary of the NS309 (100 µM- 0mM Ca^{2+}) experiments performed on KCNN4 variants located in (or near) the CaM binding domain. The result indicated that mutations in this region lead to an overactivation of the Gárdos channel (Figure 44). The S314P, A322V, and R352H mutations resulted in enhanced hyperpolarizations, whereas the H340N and S386N mutations had no effect on the hyperpolarization magnitudes due to the increased sensitivity of the Gárdos channel to Ca^{2+}. This could be explained by the fact that H340N and S386N are apparently benign mutations, as explained above, and that the other mutations, are likely to be gain-of-function mutations. An in-depth structure-function analysis would be valuable for the eventual prediction of the consequences of future mutation discoveries.

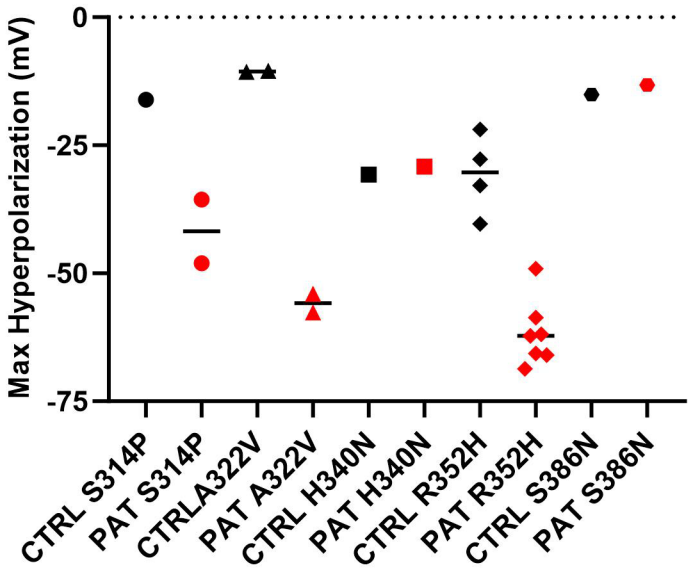

Figure 44: Chart to compare the differences in the maximal hyperpolarizations obtained for control samples and *KCNN4* variants located in or near the CaM-binding domain. Hyperpolarizations are in response to NS309, 100µM. A279D, H340N, R352H, and S386N are variants studied during my Ph.D. S314P, A322V, and other R352H variants are studied in the laboratory before my arrival. Controls are represented in black, and variants are represented in red.

IV. Discussion

The majority of treated variants were heterologous for the mutations detected by genetic exploration. Sometimes, variants had only a heterologous variant of *KCNN4* or *PIEZO1*, or even an association of another mutation, such as *PIEZO1* mutants associated with β-Thalassemia, sickle cell disease, or spectrin mutations. The results suggest that pathologies may result from a cumulative effect of different mutations. The consequences of *KCNN4* or *PIEZO1* variants could extend to tissues other than the RBCs. Given the roles of PIEZO1 in a wide range of tissues, gain-of-function mutations may lead to diverse pathogenicity, complicating the understanding of the disease. Similarly, mutations in the Gárdos channel are rarely associated with dehydration, but the anemia can still be very severe.

Regarding the use of Yoda1 to study KCNN4 variants, we suggest that this is not an appropriate way. Yoda1 can modulate the activity of the PIEZO1 channel and has no effect on the kinetics of activation of Gárdos channel variants.

In addition, we had a technical problem with the measurements of K^+ by flame photometry, since the range of the detected intracellular content of K^+ was found to be lower in all the samples compared to the range we got previously. We still don't know the reason for these discrepancies, but we can assume the comparisons between patients and samples are valid, since the error is applied to all the samples and the calibration curves are still linear within the concentration range of the samples.

The clinical heterogeneity, vague symptoms, and lack of specific diagnostic markers make the diagnosis of Gárdos channelopathy challenging (Fermo et al., 2020), because a large number of treated patients had mutations in different genes at the same time, with the mutations being heterozygous.

Nevertheless, the MBE method has proven to be effective in detecting changes in channel activity in the case of PIEZO1 and Gárdos channels. A major limitation of these experiments is that they were all carried out on blood samples, that have already been fragilized by transport (Makhro et al., 2016b), and one might wonder whether this procedure does not cause the most affected cells in the sample to disappear. Since RBCs do not have the ability to replace their protein repertoire, it is very likely that the changes they have undergone (morphology, ion content, oxidation level linked in particular to the inflammatory process, etc.) will have an impact on the quality of the

samples. Another difference between the different experiments presented in this study, is that the morphometric studies, intracellular water, Na^+, and K^+, were performed on whole blood without any washing step. For the MBE measurements, blood samples were washed at least thrice, and these washing steps, performed by centrifugation at high speeds, could be the reason for the elimination of the most fragile/hemolyzed cells from the total blood population. In addition, the use of protein-free solutions to wash blood samples creates an environment that is completely different from normal plasma. This factor may induce rapid cell dehydration that may affect membrane potential measurements.

What will be most interesting is to establish a protocol on a European scale to study blood samples with variants; as soon as there's a diagnostic of a variant, physiological and morphological tests should be carried out directly on fresh blood. These series of experiments are very important for clinicians to find characteristics of VUS, and to help understand and classify variants.

Chapter III- Sickle Cell Disease and cation permeabilities

I. Introduction

As described in the introduction, the permeability of erythrocytes from patients with sickle cell disease (SCD) is significantly different from that of normal individuals. The nominal cationic permeability is higher than that of normal cells (Vandorpe et al., 2010; Ma et al., 2012) and is characterized by an increased membrane current upon deoxygenation and increased intracellular acidification (Browning et al., 2007). The cation conductance triggered by deoxygenation is permeable to Ca^{2+} (Lew and Bookchin, 2005), which eventually activates the Gárdos channel, leading to dehydration of SS RBCs, thereby increasing the intracellular concentration of HbS and then the propensity of HbS to polymerize. All of these steps contribute to the production of denser sickle cells up to irreversible sickle cells with obvious membrane defects. Furthermore, vaso-occlusion is a consequence of the alteration in membrane integrity, which renders the RBCs more sticky (Brugnara, 2018; Wadud et al., 2020). The altered permeability of HbSS cells was found to be linked to three membrane transport systems. Two of them are present in the membrane of healthy erythrocytes with very low basal activity: the Gárdos channel (Rhoda et al., 1990) and the KCl cotransporter (Gibson et al., 1998). More importantly, a third transporter that behaves as a non-selective cation conductance and usually called P_{Sickle}, is highly active in deoxygenating HbSS RBCs (Mohandas et al., 1986; Joiner et al., 1993). P_{Sickle} is defined as the deoxygenation-induced non-selective cation channel, likely activated by HbS polymerization (Mohandas et al., 1986). Several studies were conducted to characterize and to try to identify the nature of P_{Sickle}. Albeit the triggering of P_{Sickle} is clearly linked to deoxygenation processes, the regulatory pathways of such phenomenon are still elusive. The identification of PIEZO1 at the RBC membrane and its mechanosensitive nature clearly presented it as a potential candidate for all or part of the phenomenon called P_{Sickle} (Ma et al., 2012; Wadud et al., 2020). Interestingly, P_{Sickle}, like PIEZO1, is permeable to Ca^{2+} (Saotome et al., 2018; Zhao et al., 2018). The sensitivity of P_{Sickle} (Wadud et al., 2020), as well as the deoxygenation-activated cation conductance, sensitive to Gd^{3+} and GsMTx-4 (Vandorpe et al., 2010; Bae et al., 2011; Wadud et al., 2020), points out its

mechanosensitive nature. The heterozygous state of HbS has been correlated with partial protection against severe malaria (Allison, 1954; Malaria Genomic Epidemiology Network and Malaria Genomic Epidemiology Network, 2014).

The recent discovery that the TRPV2-type channel is not only present in a significant number of copies in the membrane of RBCs (Karayel et al., 2020), but also that activation of this channel causes a significant alteration in the shape and filterability of RBCs (Belkacemi et al., 2021; Flormann et al., 2022), led to the idea of testing the consequences of the activation of such a channel in the case of SCD. Indeed, TRPV2 presents some features of a mechanosensitive non-selective cation channel with a high permeability for Ca^{2+} (Egée and Kaestner, 2021). Known TRPV2 activators include various cannabis-derived molecules such as CBD and Δ^9-THC. As these compounds are being studied for their analgesic properties, it was interesting to determine to what extent they could affect the permeability parameters of healthy or sickle RBCs.

The aim of this chapter is to illustrate my contribution to the understanding of the non-selective cation permeability of sickle RBCs. The chapter is divided into two parts corresponding to two articles. The first one deals with the consequences of activation and inhibition of PIEZO1 in SCA patients, while the second focuses on the effects of Δ^9-THC activation of TRPV2 in healthy and SCA patients.

The first part of the chapter relates a collaborative work investigating the role of PIEZO1 in RBC sickling. For that, PIEZO1 was activated using Yoda1 and inhibited by GsMTx-4 on SS RBCs, and sickling propensity and rheological parameters were monitored by Oxygenscan, RBC adhesion to endothelium and membrane potential variations by MBE method (Nader et al., 2023). In Roscoff, we followed membrane potential changes upon activation of PIEZO1 in SS RBCs under oxygenated and deoxygenated conditions.

In the second part of the chapter, we used Δ9-THC to activate TRPV2 also on SS RBCs. The main originality of this work lies in the joint use of different approaches (patch-clamp, measurement of membrane potential variation, combined with intracellular calcium concentration monitoring). This work was the fruit of a secondment realized in Roscoff, joining the efforts of 4 ESRs of the ITN-consortium EVIDENCE.

II. Results

A. PIEZO1 and SCD

1. Published article

Check for updates

Received: 3 January 2023 | Accepted: 28 March 2023

DOI: 10.1111/bjh.18799

ORIGINAL PAPER

Piezo1 activation augments sickling propensity and the adhesive properties of sickle red blood cells in a calcium-dependent manner

Elie Nader[1] | Nicola Conran[2] | Flavia C. Leonardo[2] | Aline Hatem[3] | Camille Boisson[1,4] | Romain Carin[1] | Céline Renoux[1,4] | Fernando F. Costa[2] | Philippe Joly[1,4] | Pamela L. Brito[2] | Sofia Esperti[1,5] | Joelle Bernard[4] | Alexandra Gauthier[1,6] | Solene Poutrel[1,7] | Yves Bertrand[6] | Caroline Garcia[4] | Sara T. O. Saad[2] | Stéphane Egée[3] | Philippe Connes[1]

[1]Laboratory LIBM EA7424, Vascular Biology and Red Blood Cell Team, University of Lyon, Lyon, France

[2]Hematology and Transfusion Center, University of Campinas, Campinas, Brazil

[3]Sorbonne Université, CNRS, UMR 8227 LBI2M, Station Biologique de Roscoff SBR, Roscoff, France

[4]Service de Biochimie et Biologie Moléculaire, Laboratoire de Biologie Médicale Multi-site, Hospices Civils de Lyon, Lyon, France

[5]Erytech Pharma, Lyon, France

[6]Institut d'Hématologique et d'Oncologique Pédiatrique, Hospices Civils de Lyon, Lyon, France

[7]Service de Médecine Interne, Hôpital Edouard Herriot, Hospices Civils de Lyon, Lyon, France

Correspondence
Philippe Connes, Laboratory LIBM EA7424, Vascular Biology and Red Blood Cell team, University of Lyon, France.
Email: pconnes@yahoo.fr

Nicola Conran, Hematology and Transfusion Center, University of Campinas, São Paulo, 13083-878SP, Brazil.
Email: conran@unicamp.br

Funding information
Fundação de Amparo à Pesquisa do Estado de São Paulo, Grant/Award Number: 2020/06133-6

Summary

Haemoglobin S polymerization in the red blood cells (RBCs) of individuals with sickle cell anaemia (SCA) can cause RBC sickling and cellular alterations. Piezo1 is a mechanosensitive protein that modulates intracellular calcium (Ca^{2+}) influx, and its activation has been associated with increased RBC surface membrane phosphatidylserine (PS) exposure. Hypothesizing that Piezo1 activation, and ensuing Gárdos channel activity, alter sickle RBC properties, RBCs from patients with SCA were incubated with the Piezo1 agonist, Yoda1 (0.1–10 μM). Oxygen-gradient ektacytometry and membrane potential measurement showed that Piezo1 activation significantly decreased sickle RBC deformability, augmented sickling propensity, and triggered pronounced membrane hyperpolarization, in association with Gárdos channel activation and Ca^{2+} influx. Yoda1 induced Ca^{2+}-dependent adhesion of sickle RBCs to laminin, in microfluidic assays, mediated by increased BCAM binding affinity. Furthermore, RBCs from SCA patients that were homo–/heterozygous for the rs59446030 gain-of-function Piezo1 variant demonstrated enhanced sickling under deoxygenation and increased PS exposure. Thus, Piezo1 stimulation decreases sickle RBC deformability, and increases the propensities of these cells to sickle upon deoxygenation and adhere to laminin. Results support a role of Piezo1 in some of the RBC properties that contribute to SCA vaso-occlusion, indicating that Piezo1 may represent a potential therapeutic target molecule for this disease.

KEYWORDS
adhesion molecule, calcium influx, erythrocyte, rheology, vaso-occlusion

INTRODUCTION

Sickle cell disease (SCD) is a group of inherited disorders, caused by mutations in the β-globin gene, where sickle cell anaemia (SCA, HbSS) constitutes the homozygous form of SCD. SCD is characterized by the production of an abnormal haemoglobin (Hb), called HbS, which may polymerize when deoxygenated, causing mechanical distortion (i.e. sickling) of

Elie Nader and Nicola Conran share the same position.

Stephane Egee and Philippe Connes share the same position.

© 2023 British Society for Haematology and John Wiley & Sons Ltd.

red blood cells (RBCs).[1] Sickled RBCs are poorly deformable and very fragile, whereby the pathophysiological changes incurred from these alterations result in several acute and chronic complications, including enhanced intravascular and extravascular haemolysis, anaemia, frequent painful vaso-occlusive episodes, auto-splenectomy, acute chest syndrome, priapism, pulmonary hypertension, leg ulcers, nephropathy, retinopathy, hepatopathy, osteonecrosis and stroke.[2,3]

Activation of the Gárdos pathway upon deoxygenation has been shown to play a key role in the dehydration of RBCs from SCA patients, as well from patients with other SCD genotypes (HbSC for instance), further increasing the propensity of HbS to polymerize and RBCs to sickle.[4] Increased RBC Ca^{2+}, due to permeability caused by deoxygenation and sickling, causes the loss of K^+ through the Gárdos channel. This increased Ca^{2+} influx, also known as P_{sickle}, is considered to be the manifestation of a non-selective cation conductance for monovalent and divalent cations such as Na^+, K^+, Rb^+, Ca^{2+} and Mg^{2+}.[5–7] At this time, the protein (or proteins) that mediates P_{sickle} has not been identified, but the inhibitory effect of *Grammastola spatulata* mechanotoxin-4 (GsMTx4) suggests that P_{sickle} could be a mechanosensitive protein,[8,9] and it has been proposed that Piezo1 could be a good candidate for P_{sickle}.[8,10,11] Piezo1 (also known as FAM38A) is a protein with mechanosensitive properties that is involved in the cellular influx of calcium (Ca^{2+}). Genetic mutations, considered as gain of function, affect Piezo1 deactivation and thus increase its opening time, leading to an uncontrolled influx of Ca^{2+} that will secondarily activate the Gárdos channel. Such mutations have been associated with hereditary xerocytosis, explaining the characteristic dehydrated state of RBCs in this disease.[10,12] Indeed, one could speculate on a role for Piezo1 in RBC sickling in SCA; slight mechanical deformation, compatible with that encountered by RBCs in the circulation, can produce robust cellular Ca^{2+} entry that is strictly dependent on Piezo1 expression.[11,13] SCA pathophysiology is characterized by the occurrence of continuous vaso-occlusive processes in the microcirculation that result from a complex interplay between altered blood rheology, inflammatory processes and the adhesion of RBCs, leukocytes and platelets to each other and to the endothelium.[14] While sickle RBCs display an augmented expression of multiple cell surface adhesion molecules,[15] modifications in the membrane topography induced by the accumulation of Ca^{2+} in sickle RBCs could be accompanied by increased adhesiveness,[16] even at a concentration below the threshold required for cell dehydration. A recent study found that Piezo1 activation on sickle RBCs could induce Ca^{2+} entry into cells and increase phosphatidylserine (PS) exposure.[17] While calcium accumulation has been reported to promote intercellular adhesion interactions between red blood cells under conditions of strength consistent with those encountered within the circulation,[18] the impact of Ca^{2+} accumulation in RBCs on adhesion to endothelial cells/extracellular matrix ligands is still unknown. We hypothesize that Piezo1 could, thus, be involved in the modulation of sickle RBC properties such as cell sickling and adhesive properties.

The aim of this project was to characterize the role of Piezo1 and ensuing Gárdos channel activity in RBC sickling and adhesion in SCA. We used pharmacological tools to inhibit or activate Piezo1 in sickle RBCs, in the presence of conditions mimicking shear stress and/or deoxygenation, and investigated the consequences of channel activity modulation on the rheological properties, sickling, senescence markers, membrane potential and adhesive properties of sickle RBCs. We also screened frequent polymorphisms of the *PIEZO1* gene in SCA patients and tested for their associations with blood rheological parameters.

METHODS

SCA patients

Patients (HbSS genotype) were recruited, with informed consent, from Hospices Civils de Lyon and Institut d'Hématologie et d'Oncologie Pédiatrique de Lyon, France, and from the Hematology Center, University of Campinas, Brazil. Healthy controls participated in the study after giving written informed consent. All subjects were in clinical steady-state at the time of the study; that is, without experiencing any vaso-occlusive crisis or other acute medical complication within the last 2 months, and without any blood transfusions for at least 3 months before inclusion. The study was conducted in accordance with the guidelines set by the Declaration of Helsinki and approved by the Regional Ethics Committees (L14-127, Université de Lyon; 4.649.745, University of Campinas).

Preparation and treatment of red blood cells

RBCs from SCA patients (SS RBCs) were separated from peripheral blood samples (collected in citrate) by centrifugation (800 *g*, 10 min, 20°C). RBCs were washed in PBS 1×, and RBC pellets were resuspended in PBS buffer containing 2.5 mM Ca^{2+} and incubated (30 min, 37°C) with Yoda1 (Sigma Aldrich or Saint-Quentin-Fallavier; 0.1–10 μM, depending on the assay), a Piezo1 agonist, or GsMTx4 (Sigma Aldrich; 10 μM), a Piezo1 antagonist, or vehicle (dimethyl sulfoxide, DMSO; equivalent dilution) before assays. In some assays, cells were preincubated with BAPTA AM (Tocris; a cell-permeable calcium chelator; 10 μM) for 30 min, or adhesion molecule neutralizing antibodies (25 μg/mL anti-BCAM [AF148]; 10 μg/mL anti-VLA4 [clone 2B4], R&D Systems). All assays were performed on cells in the continued presence of agonists/antagonists/inhibitors/antibodies following pre-incubation.

Flow cytometry

Following the 30 min incubations with Yoda1 or GsMTx4, PS exposure on the outer membrane leaflet of the RBCs was

13652141, 2023, 3, Downloaded from https://onlinelibrary.wiley.com/doi/10.1111/bjh.18799 by Portail BibCNRS INSB, Wiley Online Library on [05/11/2025]. See the Terms and Conditions (https://onlinelibrary.wiley.com/terms-and-conditions) on Wiley Online Library for rules of use; OA articles are governed by the applicable Creative Commons License

evaluated using Annexin V-FITC binding. RBC suspensions (in 0.4% Hct in PBS containing 2.5 mM Ca^{2+}) were protected from light and incubated for 30 min at room temperature (RT) with Annexin V-FITC (1:200 dilution, Beckman Coulter). As a PS-negative control, cells were incubated in the presence of 5 mM EDTA. Immediately after incubation, samples were diluted and analysed by FACS (BD Accuri C6 or BD Calibur). PS exposure was measured in the FITC channel (with an excitation wavelength of 488 nm and an emission wavelength of 530 nm), according to the manufacturer's instructions. The RBC surface expressions of CD47, CD49 and BCAM were also evaluated by flow cytometry (incubations, as above) using the anti-CD47-PE (1:33 dilution, Miltenyi Biotec), or anti-CD49-PE (clone ALC1/1; Abcam) and/or anti-CD239(BCAM)-APC (clone REA276, 1:11 dilution Miltenyi Biotec) antibodies. For each sample, 50 000 events were acquired and gated for the appropriate forward scatter (FSC)/ side scatter (SSC).

Intracellular calcium (Ca^{2+}) measurement

Intracellular RBC Ca^{2+} level was determined using Fluo3/AM. RBC suspensions (0.4% Hct) were incubated for 30 min at RT in the dark with 10 µM of Fluo3/AM (Biotium) probe. The samples were then analysed using flow cytometry, according to the manufacturer's instructions (BD Accuri C6). The median fluorescence intensity (MFI) of 50 000 gated events was recorded to quantify Ca^{2+} levels.

Microfluidic adhesion assays

RBC adhesion and rolling on laminin-coated microchannels (400 µm-wide microchannels, Cellix Ltd) were observed using a microfluidic platform (Cellix Ltd). Biochip channels were coated with 4 µg/mL human laminin (LN, from human placenta, Sigma Aldrich) for 2 h at RT. The LN ligand concentration was chosen based on standardization assays, employing ligand concentrations of 2–10 µg/mL (data not shown). Non-specific binding sites on channels were then blocked with 1% (w/v) BSA (30 min, RT) and chips were stored in a humidified chamber for use in assays within 1 h. After treatments, cell suspensions were loaded sequentially, onto microchannel entry wells, and a shear stress of 0.25 dyn/cm^2 applied for >3 min (ExiGo Pump Pulse-Free Microfluidic Syringe Pump). Images for each channel, in 3 fields, were acquired (1 per second) for video manufacture using a Zeiss microscope (×40 lens) and Exi Blue Cooled camera (Qimaging). Numbers of cells rolling along the chip (defined as a significant decrease in cell velocity through the channel, to 50% or less) and adhered to the chip were evaluated in 3 fields at the time of 180 s (3 min) post cell loading. The optimal perfusion time and shear stress for the assay were standardized previously and adapted to the current study conditions.[19]

Ektacytometry

After the 30 min incubations with the drugs modulating Piezo1 activity, RBC deformability was measured under an oxygen gradient by oxygenscan ektacytometry, as previously described.[20–22] A volume of 50 µL of blood, standardized to a fixed total RBC count of 200×10^6, was mixed with 5 mL of Oxy-Iso polyvinylpyrrolidone (PVP) suspension with a mean viscosity of 28–30 cP (Mechatronics, The Netherlands) and osmolality of 282–286 mOsm/kg. The suspension was sheared at 30 Pa and 37°C while the oxygen partial pressure (pO_2) was gradually decreased from 160 to 20 mm Hg (deoxygenation) and then returned to normoxic values. The diffraction pattern was analysed by computer to determine the maximum RBC deformability in normoxia (EImax), the minimum RBC deformability reached during deoxygenation (EImin), and the oxygen partial pressure at which RBC start to sickle (i.e. the Point of Sickling, PoS). PoS is defined as a decrease of at least 5% of EImax during deoxygenation.[20–22]

Membrane potential measurements

The CCCP (carbonyl cyanide m-chlorophenylhydrazone) method[23–25] or MBE method (as renamed recently)[26] was used for the monitoring of membrane potential evolution. Briefly, when RBCs are suspended in nominally buffer-free solution in the presence of the CCCP protonophore (10 µM), changes in extracellular pH reflect membrane potential changes since protons are kept at equilibrium across the membrane. The membrane potential (V_M) can, thus, be estimated from:

$$V_M = 61.51\,\text{mV} \cdot \left(\text{pH}_i - \text{pH}_o\right).$$

Due to the high red cell buffer capacity, the intracellular pH (pH_i) remains constant (at about 7.2) throughout an experiment and can be estimated as the pH of the solution after lysis with Triton™ X-100 at the end of the experiment. Regarding the experimental procedure, 2900 µL of experimental solution containing 20 µM of CCCP were heated to 37°C under constant magnetic stirring. For each experiment, 100 µL of packed RBCs (99% hct) were added, to reach a final cytocrit of 3.3%. All inorganic compounds were added as stock solution 1000× in DMSO. The final concentration of DMSO never exceeded 0.3%, a concentration that has no effect on either fluxes or membrane potential. Extracellular pH was measured using a G200 pH electrode (Radiometer) coupled to a Red Rod 200 reference electrode (Radiometer) and a PHM210 pHmeter (Radiometer). Sampling and acquisition were done with an electrode amplifier (EA-BTA, Vernier) at a rate of 1 measurement per second connected to an AD LABQUEST Mini interface (Vernier) with a resolution of 0.01 pH unit. The data were visualized and analysed with the Logger Lite software (Vernier). At the end of each experiment, Triton X-100 detergent (1% in 3 M NaCl) was added,

13652141, 2023, 3, Downloaded from https://onlinelibrary.wiley.com/doi/10.1111/bjh.18799 by Portail BibCNRS INSB, Wiley Online Library on [05/1/2023]. See the Terms and Conditions (https://onlinelibrary.wiley.com/terms-and-conditions) on Wiley Online Library for rules of use; OA articles are governed by the applicable Creative Commons License

causing total cell lysis and a resulting solution that attains the intracellular pH.

Next-generation sequencing

Genomic DNAs from 50 SCA patients were tested by next-generation sequencing (NGS) sequencing using a custom design based on a SeqCap EZ Solution-Based Enrichment strategy (Roche NimbleGen). Targeted sequencing capture probes were designed by Roche NimbleGen, in order to sequence the coding sequences (exons ±30 pb) of the *PIEZO1* gene (NM_001142864). For each sample, 100 ng of high quality genomic DNA was used. Library preparation was performed with the Kapa HyperPlus Kit for Illumina platforms (Kapa Biosystems). The manufacturer's DNA sample preparation protocol for Roche NimbleGen SeqCap EZ Library (Roche, SeqCap-EZ_UGuide_v5p0) was followed, using dual index adapters. Pre-enrichment pools were performed by equimolarly pooling 24 samples. The patients were further sequenced on a MiSeq® sequencer using the MiSeq reagent kit v2 500 cycles (Illumina). FASTQ files (8 per patient) were uploaded and bioinformatic analyses were further performed using an academic pipeline.

For each sample, read pairs were first trimmed using trimmomatic v 0.33.[27] Then, reads were aligned against the hg19 version of the human genome using BWA-MEM v 0.7.12,[28] producing a BAM file for each sample, which was indexed and sorted with samtools v 1.3.1.[29] This last then underwent several treatments: (i) duplicate marking was performed by PicardTools MarkDuplicates v 1.138 (Picard Toolkit, 2018); (ii) indel realignment and (iii) nucleotide recalibration were done using respectively GATK IndelRealigner and GATK BaseRecalibrator.[30] FASTQ and BAM metrics were collected using respectively FastQC[31] and PicardTools (Picard Toolkit software, 2018). The variant calling was performed using GATK HaplotypeCaller,[30] producing a genomic VCF for each sample. The genotyping was performed using GATK GenotypeGVCFs,[13] merging all the samples in a unique VCF. Variants normalization and annotation were respectively handled by GATK LeftAlignAndTrimVariants[11] and the snpEff/SnpSift toolbox.[32] VCF metrics were collected using snpEff/SnpSift.[32] DeCovA, an in-house script, was used for copy number variant detection.[33] Identitovigilance process was done using SNPxPlex technology. Only frequent (> 10% in the SCA patients) single nucleotide variations (SNV) were selected. The PoS and RBC PS exposure were also measured in these patients.

Data analysis

Data are depicted as means±SEM; normal distribution of data was confirmed, or not, and groups were statistically compared using paired *t*-tests or one way RM ANOVA completed by Friedman multiple comparison test, Sidak's multiple comparison test or Dunn's multiple comparison test, as appropriate. Pearson correlation was performed to test the association between PoS and changes in membrane potential following Piezo1 activation. A *t*-test was used to compare healthy individuals with SCA patients. A $p < 0.05$ was considered as significant. GraphPad Prism 7 software was used for statistical analyses.

RESULTS

Piezo1 activity modulates RBC deformability and sickling in SCA

Suspensions of RBCs from SCA patients (SS RBCs) were subjected to pharmacological modulation of Piezo1 channel activity with Yoda1 (Piezo1 agonist) or GsMTx4 (Piezo1 antagonist) as described in Section 2, and RBC deformability and sickling propensity were investigated using oxygen gradient ektacytometry (Figure 1). Figure S1 shows a typical example of the RBC deformability response with both molecules. Piezo1 activation (Yoda1, 10 µM) significantly decreased the deformability of SS RBCs under normoxia and the SS RBCs started to sickle at higher oxygen partial pressures (Figure 1A,C). Similarly, the inhibition of Piezo1 activation with GsMTx4 (10 µM) increased SS RBC deformability in normoxia and lowered the oxygen partial pressure (i.e. PoS) at which the cells started to sickle (Figure 1B,D). Piezo1 activation by Yoda1 incubation (0.1–5 µM; 30 min 37°C) also induced significant visible SS RBC sickling under conditions of flow (0.25 dyn/cm^2), as evaluated microscopically on a microfluidic platform (Figure 1E; cell sickling status was observed for 3 min in 400-µm-wide channels). The deformability (EImax) of RBCs from healthy individuals without SCA (AA RBC, $n = 8$) was higher compared to SCA patients ($p < 0.001$), decreased from 0.63 ± 0.1 to 0.56 ± 0.03 ($p < 0.001$) with Yoda1 (10 µM) and did not change with GSMTx4 (0.62 ± 0.02).

Piezo1 modulates sickle RBC adhesion to laminin in a BCAM-dependent manner

Having confirmed that Piezo1 activation reduces SS RBC deformability and augments sickling, we looked at whether Piezo1 activation could modulate SS RBC adhesive interactions with an extracellular matrix component. SS RBCs were preincubated with Yoda1 (0.1–10 µM; 30 min) and their rolling along and adhesion to laminin (LN) was monitored under conditions of shear stress using a microfluidic flow assay (3 min, 37°C, 0.25 dyn/cm^2; as described in Section 2). Piezo1 stimulation augmented the rolling of SS RBCs and their adhesion to LN-coated microchannels, at the concentration of 0.5 µM Yoda1 (Figure 1F,G; Figure S2C shows representative photographs of rolling and adhered RBCs). In contrast, both the basal rolling and adhesion of AA RBCs to LN was significantly lower than those of SS RBCs (Figure S2A,B), and incubation of AA RBC with 0.5 µM

13652141, 2023, 3, Downloaded from https://onlinelibrary.wiley.com/doi/10.1111/bjh.18799 by Portail BibCNRS INSB, Wiley Online Library on [05/11/2023]. See the Terms and Conditions (https://onlinelibrary.wiley.com/terms-and-conditions) on Wiley Online Library for rules of use; OA articles are governed by the applicable Creative Commons License

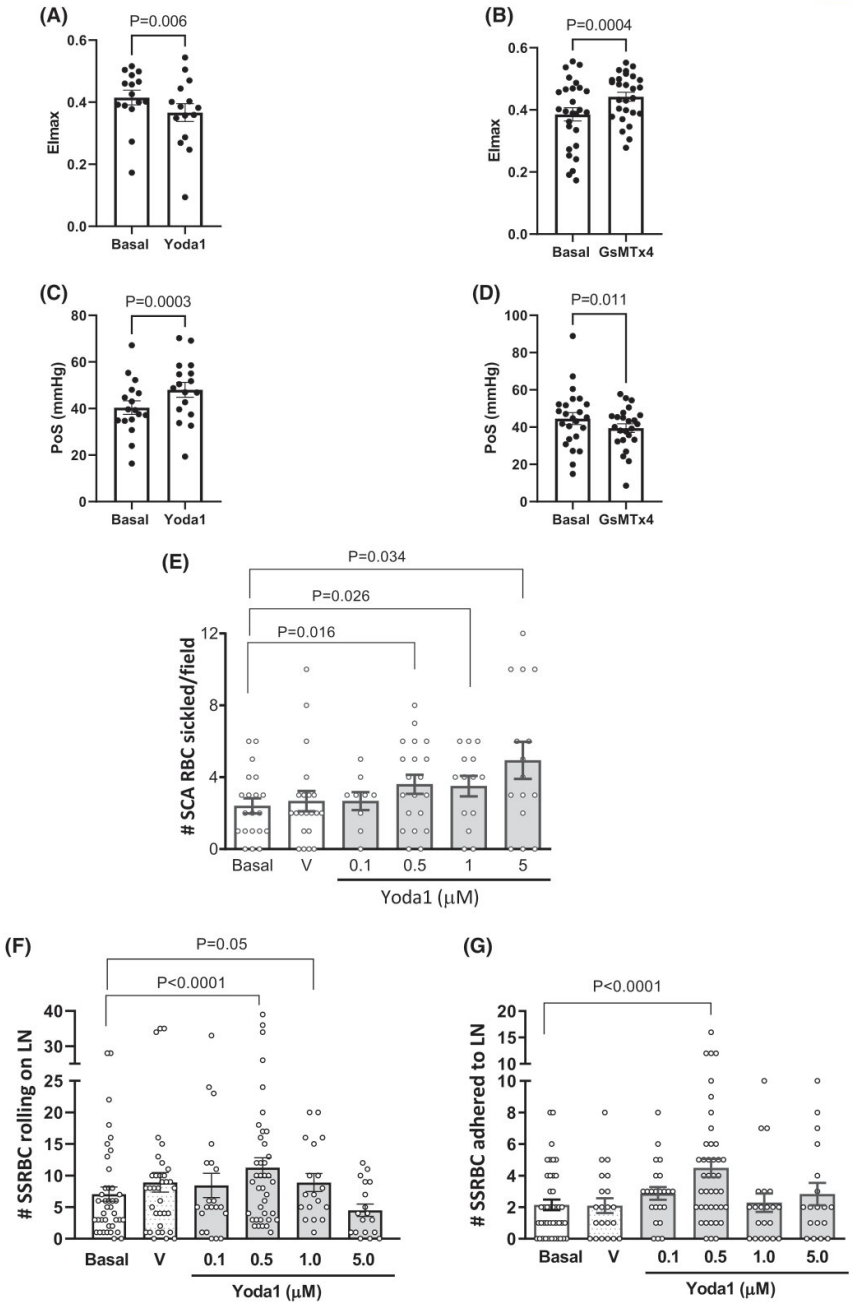

FIGURE 1 Effects of PIEZO1 channel activation and inhibition on sickle RBC deformability, sickling and adhesive properties. (A–D) Oxygenscan ektacytometry was used to measure EImax (maximal RBC deformability in normoxia) and oxygen pressure at which RBCs start to become rigid and change shape (point of sickling, PoS), in response to Piezo1 activation or inhibition. SS RBC were incubated for 30 min with Yoda1 (10 μM, $n = 15, 17$; A and C), or GsTMx4 (10 μM, $n = 27, 24$; B and D) (37°C) before measurement of RBC deformability in normoxia (A and B, respectively) and PoS during progressive deoxygenation (C and D, respectively). p values calculated by paired t-test. (E) Sickling of SS RBC after incubation with DMSO vehicle or Yoda1 (0.1–10 μM, 30 min), observed by light microscopy ($n = 3$–7 patients; three fields per channel). (F–G) Rolling and adhesion of sickle RBCs on laminin; SS RBCs were incubated for 30 min with Yoda1 (0–5.0 μM; 37°C) and the rolling (F) and adhesion (G) of SS RBCs were evaluated on laminin (LN)-coated microchannels using a microfluidic platform, under shear stress of 0.25 dyn/cm^2 (400 μm-wide microchannel; 4 μg/mL LN, 37°C, 2 min) ($n = 6$–12 patients per treatment; three fields per channel). Data are expressed as the number of RBCs observed rolling or adhering per 0.186 μm^2 area. V, DMSO vehicle. For (E–G), p values were calculated by Mixed effects analysis with Sidak's multiple comparison test.

13652141, 2023, 3, Downloaded from https://onlinelibrary.wiley.com/doi/10.1111/bjh.18799 by Portail BibCNRS INSB, Wiley Online Library on [05/11/2023]. See the Terms and Conditions (https://onlinelibrary.wiley.com/terms-and-conditions) on Wiley Online Library for rules of use; OA articles are governed by the applicable Creative Commons License

Yoda1 did not significantly increase their rolling or adhesion (Figure S2A,B; $p > 0.05$).

Flow cytometry showed that, while SS RBCs highly express the basal cell adhesion molecule (BCAM; CD239) on their membrane surface (Figure 2A),[34] the activation of Piezo1 by Yoda1 (0.5–5.0 μM; 30 min) did not significantly alter cell surface expression of this laminin-binding molecule (Figure 2C). Expression of the CD49d subunit of the VLA-4 integrin (an adhesion molecule that binds primarily to fibronectin or VCAM-1) is also increased on SS RBBCs, compared to RBC from healthy controls; however, activation of Piezo1 on SS RBCs by Yoda1 (0.5–5.0 μM) did not significantly alter VLA-4 cell surface expression (Figure 2B,D).

Importantly, co-incubation of the SS RBCs with an antibody that neutralizes the binding activity of BCAM completely abolished the effect of Yoda1 (0.1 and 0.5 μM; 30 min) on SS RBC rolling and adhesion, while an antibody that neutralizes CD49d binding had no effect on these parameters (Figure 2E,F). Data indicate that Piezo1 activation induces SS RBCs adhesion via a mechanism that increases the binding affinity of BCAM, rather than by BCAM expression.

Piezo1 stimulation triggers pronounced membrane hyperpolarization linked to Gárdos Channel activation

Membrane potential measurement showed that Piezo1 stimulation triggers immediate and pronounced membrane hyperpolarization of SS RBCs, suggestive of Gárdos channel activation triggered by Ca^{2+} entry, via a phenomenon that was exacerbated by low oxygen partial pressure (Figure 3A–C). Hyperpolarization was significantly more pronounced under low oxygen partial pressure conditions (Figure 3B) and this hyperpolarization lasted longer (Figure 3C). Consistent with this result, flow cytometry demonstrated a clear effect of Piezo1 activation and inhibition by Yoda1 (10 μM; Figure 3D) and GsMTx4 (10 μM; Figure 3E) on Ca^{2+} influx. Yoda1 also increased Ca^{2+} in AA RBC ($n = 8$) (MFI: 221 ± 10 vs. 251 ± 6; $p < 0.01$), but no significant effect of GTMx4 was observed on AA RBC (231 ± 9). Further experiments showed Ca^{2+} influx was directly associated with the propensity of sickling under decreased O_2 partial pressure (Figure 3F) and subsequent Gárdos channel activation, as demonstrated by co-incubation of SS RBCs with TRAM34, a Gárdos channel inhibitor, albeit no direct measurement of calcium influx kinetics has been conducted in this series of experiments. This Ca^{2+} entry through Piezo1 is sufficient to activate the Gárdos channel as shown by the transient hyperpolarization recorded, where the extent of hyperpolarization triggered by calcium through Piezo1 activation, both in oxy and deoxy conditions, correlated with the susceptibility of RBCs to sickle, as measured by the PoS by oxygenscan (Figure 3G,H).

In additional experiments, SS RBC suspensions were incubated with the cell permeable Ca^{2+} chelator, BAPTA-AM (10 μM, 30 min), before observing Yoda1-induced cellular rolling and adhesion to LM-coated microchannels under shear stress. The chelation of intracellular Ca^{2+} abrogated the enhanced cell adhesion triggered by Piezo1 activation using Yoda1 (0.1 and 0.5 μM), but did not affect cell rolling on laminin (Figure 3I,J).

Piezo1 stimulation induces PS exposure and CD47 expression on sickle RBC

Flow cytometry experiments demonstrated a clear effect of Piezo1 activation by Yoda1 (10 μM) on CD47 expression and on PS exposure on SS RBCs (Figure S3A,B), where CD47 expression was suppressed and PS exposure was augmented. The use of GsMTx4 (10 μM) increased CD47 exposure but had no impact on PS exposure, compared to the control condition (Figure S3C,D). The percentage of RBCs with externalized PS was higher in SS than in AA ($n = 8$) (0.28 ± 0.16; $p < 0.001$) and Yoda1 tended to increase PS exposure in AA RBCs (0.35 ± 0.17; $p = 0.08$). GSTMx4 had no effect on PS exposure in AA RBCs (0.27 ± 0.13). CD47 exposure in AA RBCs (6492 ± 2014) was higher than in SS RBCs ($p < 0.001$). Neither Yoda1, nor GSMTx4 significantly affected CD47 exposure on AA RBCs (6667 ± 2187 and 7476 ± 2594, respectively).

Sickling tendency and RBC PS exposure are greater in patients with the gain of function E756del variant in PIEZO1, compared to those without

Using next generation sequencing, eight frequent SNV were found in SCA patients (rs2911442 [13%], rs7404939 [20%], rs11076706 [23%], rs13333358 [34%], rs35265318 [12%], rs59446030 [13%], rs750038587 [18%], rs1803382 [17%]) in the heterozygous or homozygous state. Of interest, the PoS and the percentages of RBCs with externalized PS were significantly higher in patients with rs59446030 (E756del) in the heterozygous ($N = 7$) and homozygous states ($N = 3$). PoS was 42.3 ± 7.2 and 48.1 ± 6.8 mmHg in SCA patients without and with the gain of function E756del variant in Piezo1, respectively ($p < 0.05$); PS = 2.4 ± 1.8 and 4.2 ± 2.5% of positive RBCs in SCA patients without and with the gain of function E756del variant in Piezo1, respectively ($p < 0.01$). The presence of the other frequent SNV had no effect on RBC rheological properties and biological parameters (data not shown).

DISCUSSION

Piezo1 is a non-selective membrane cation channel, involved in the regulation of RBC hydration status and volume

13652141, 2023, 3, Downloaded from https://onlinelibrary.wiley.com/doi/10.1111/bjh.18799 by Portail BibCNRS INSB, Wiley Online Library on [05/11/2023]. See the Terms and Conditions (https://onlinelibrary.wiley.com/terms-and-conditions) on Wiley Online Library for rules of use; OA articles are governed by the applicable Creative Commons License

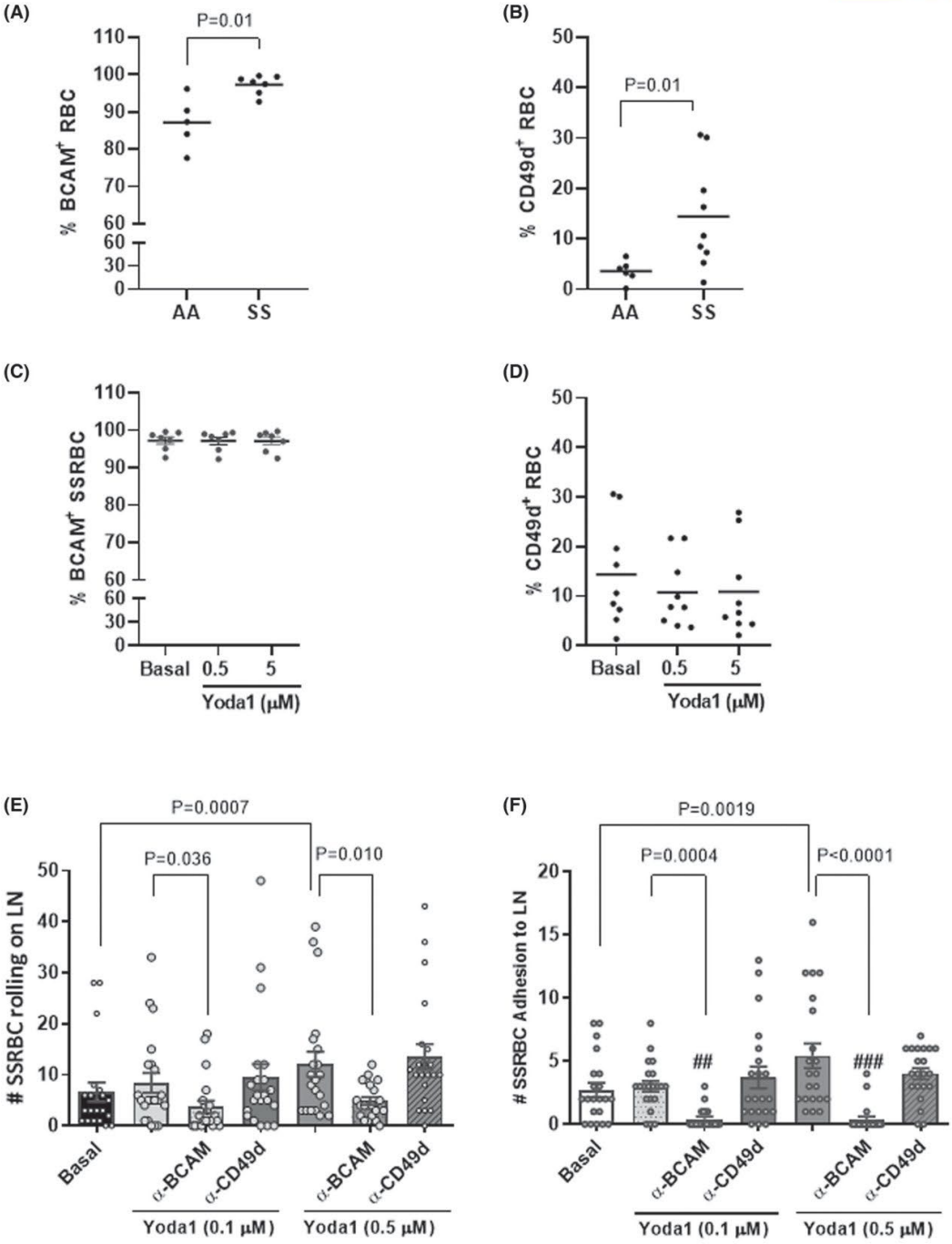

FIGURE 2 Piezo1-mediated activation of sickle red blood cell rolling and adhesion on laminin occurs via a BCAM-dependent mechanism. (A, B) The surface expressions of (A) BCAM (CD239) or (B) CD49d molecules were determined by flow cytometry on 50 000 gated RBC from healthy control (AA; $n=5$) or SCA (SS; $n=7$ and 9, respectively) individuals. In (C, D), SS RBC were co-incubated with Yoda1 (30 min) before determining the cell surface expressions of (C) BCAM and (D) CD49d by flow cytometry. $n=7$ (C) and 9 (D). (E, F) SS RBC ($n=7$) were co-incubated with Yoda1 and antibodies that neutralize the functions of the BCAM or CD49d adhesion molecules, and RBC rolling (E) and adhesion (F) to laminin (LN) were evaluated using the microfluidic assay (400 μm-wide microchannel; 4 μg/mL LN; 0.25 dyn/cm^2, 37°C, 3 min; ≤3 fields per channel/patient). Non-parametric ANOVA, Dunn's multiple comparison test.

13652141, 2023, 3, Downloaded from https://onlinelibrary.wiley.com/doi/10.1111/bjh.18799 by Portail BibCNRS INSB, Wiley Online Library on [05/11/2023]. See the Terms and Conditions (https://onlinelibrary.wiley.com/terms-and-conditions) on Wiley Online Library for rules of use; OA articles are governed by the applicable Creative Commons License

under mechanical constraints.[35] Hereditary xerocytosis, a rare haemolytic anaemia, is demonstrated to be due to gain of function mutations in PIEZO1.[36] Several electrophysiological studies demonstrated that this gain of function phenotype is characterized by a delayed inactivation of Piezo1, accompanied by increased cation permeability.[10,37,38] Vandorpe et al.[39] previously demonstrated that hypoxia activated a Ca^{2+}-permeable cation conductance, which was sensitive to GsMTx-4, a mechanosensitive and stretch-activated ion channel inhibitor, in human and mouse sickle RBCs. Indeed, Brugnara[8] suggested that P_{sickle}, that is, the increase in permeability to Ca^{2+} and other ions occurring during deoxygenation, and sickling, which causes RBCs from SCA patients to become so dehydrated, could be mediated by Piezo1.

Our findings showed that activation of Piezo1 in sickle RBCs, but also in RBCs from healthy individuals, leads to intracellular Ca^{2+} accumulation, while its inhibition caused the opposite in sickle RBCs. Although we did not examine the detailed kinetics of intracellular Ca^{2+} changes using Yoda1 and GSMTx4, our results reinforce the previous findings of Wadud and colleagues.[17] Consequently, the stimulation of Piezo1 caused immediate pronounced membrane hyperpolarization of sickle RBCs, linked to Gárdos channel activation, via a phenomenon that was exacerbated by low oxygen partial pressure. This channel activation, and possibly ensuing RBC dehydration, affected the deformability of RBCs and increased their propensity to sickle when oxygen pressure was reduced. Experiments conducted in AA RBCs also demonstrated that activation of Piezo1 was followed by a decrease in their deformability. Electrophysiological and ektacytometry measurements were also both performed in the same subset of SCA patients and showed significant negative correlations between the degree of RBC membrane hyperpolarization and the PoS under Yoda1 stimulation. A comparison of SCA patients with the gain of function variant in Piezo1 (E756del), to those without, demonstrated a propensity of RBCs to sickle at higher oxygen partial pressure (greater PoS) in the former population, confirming previous findings showing an association between the E756del allele and RBC density in SCA.[40] The use of a Gárdos channel inhibitor (i.e. TRAM34) with the Piezo1 activator (Yoda1) during oxygen gradient ektacytometry measurements restored baseline PoS, indicating that the increased propensity of RBC to sickle during deoxygenation and upon Piezo1 activation was mediated ultimately by Gárdos channel activation. Altogether, these findings support a key role of Piezo1 protein in RBC sickling in SCA that could be mediated by RBC dehydration (although not directly tested in the present study) following Gárdos channel activation. We suspect that alterations in membrane tension and red cell morphology may further activate the mechanosensitive Piezo1 channel, leading to a vicious cycle of cellular dehydration, HbS polymerization and, thereby, cell sickling. Our results also showed that sickle RBCs responded to GsMTx4 without prior stimulation with Yoda1. These findings could indicate that Piezo1 is constitutively active in sickle RBCs and could contribute to their higher nominal calcium concentration compared to healthy RBCs. However, it is worth noting that almost all experiments performed in this study were done under flow/shear stress conditions that could mimic the mechanical stress applied to Piezo1 within the circulation and activate the channel. Furthermore, wall shear stress has been shown to be increased in SCA patients, which could further increase the mechanical constraints that RBCs are subjected to, further increasing Piezo1 activation and subsequent deleterious consequences.[41]

The stimulation of Piezo1 also caused a rise in the number of RBCs positive for PS and a decrease in membrane CD47 level; two changes indicating enhanced RBC senescence. These findings are consistent with a recent study showing that Yoda1 caused an increase in intracellular Ca^{2+} and PS exposure on sickle RBCs, which was inhibited by its antagonist Dooku1 and the Piezo1 inhibitor GsMTx4.[17] Accumulation of Ca^{2+} in RBCs may activate scramblase, causing the disruption of membrane phospholipid asymmetry and the externalization of PS at the outer leaflet of the RBC membrane.[42,43] Additionally, Wadud et al.[17] showed that Yoda1 could induce PS externalization independently of extracellular calcium concentration, suggesting an effect that is not mediated by Piezo1-dependent calcium influx. It should also be mentioned that Yoda1 and GsMTx4 do not exhibit complete specificity towards Piezo1, and may elicit off-target effects, implying that other channels or pathways could be involved in the effects observed. Increased PS externalization and decreased membrane CD47 level have been reported in sickle RBCs,[44] compared to healthy RBCs, indicating accelerated RBC senescence in this disease,[45,46] which may lead to early recognition by macrophages and increased erythrophagocytosis.[46–48] Interestingly, SCA patients with the

FIGURE 3 Effects of Piezo1 activation on membrane hyperpolarization, sickling and adhesion are mediated by direct activation of the Gárdos channel or calcium influx. Changes in membrane potential of SS RBCs (A) following Piezo1 activation by YODA1 (625 nM, $n = 13$ averaged curve ± SEM) in oxy (black) and deoxy (grey) conditions, showing a more pronounced hyperpolarization (B), associated with a decreased pace of repolarization (C) when partial pressure of O_2 is reduced to 10% of nominal air partial pressure (0.8 mg/mL, $n = 13$). (D–E) Calcium influx in SS RBCs following Yoda1 (10 μM) or GsTMx4 (10 μM) incubation was determined by flow cytometry in 50 000 gated RBCs ($n = 23$, 19). (F) Oxygen gradient ektacytometry was used to observe the effect of inhibition of the Gárdos channel with Tram 34 (10 μM) on the point of sickling of SS RBCs incubated with/without Yoda1 (10 μM; 30 min, 37°C, $n = 7$). (G, H) Correlations between RBC membrane hyperpolarization following Piezo1 activation and PoS, both in oxy (G) and deoxy conditions (H). (I, J) Calcium chelation of SS RBCs with BAPTA-AM (10 μM, 30 min) did not significantly affect the Yoda1-induced rolling of cells on laminin (LN) (H), but significantly decreased Yoda1-induced SS RBC adhesion (I), as demonstrated by a microfluidic assay (400 μm-wide microchannel; 4 μg/mL LN; 0.25 dyn/cm^2, 37°C, 3 min; $n = 9$ patients per group, ≤3 fields per channel). Data are expressed as the number of RBC observed per 0.186 μm^2 area. Paired *t*-test, except (F), Friedman multiple comparison test and (I, J), non-parametric ANOVA/Sidak's multiple comparison test.

13652141, 2023, 3, Downloaded from https://onlinelibrary.wiley.com/doi/10.1111/bjh.18799 by Portail BibCNRS INSB, Wiley Online Library on [05/11/2023]. See the Terms and Conditions (https://onlinelibrary.wiley.com/terms-and-conditions) on Wiley Online Library for rules of use; OA articles are governed by the applicable Creative Commons License

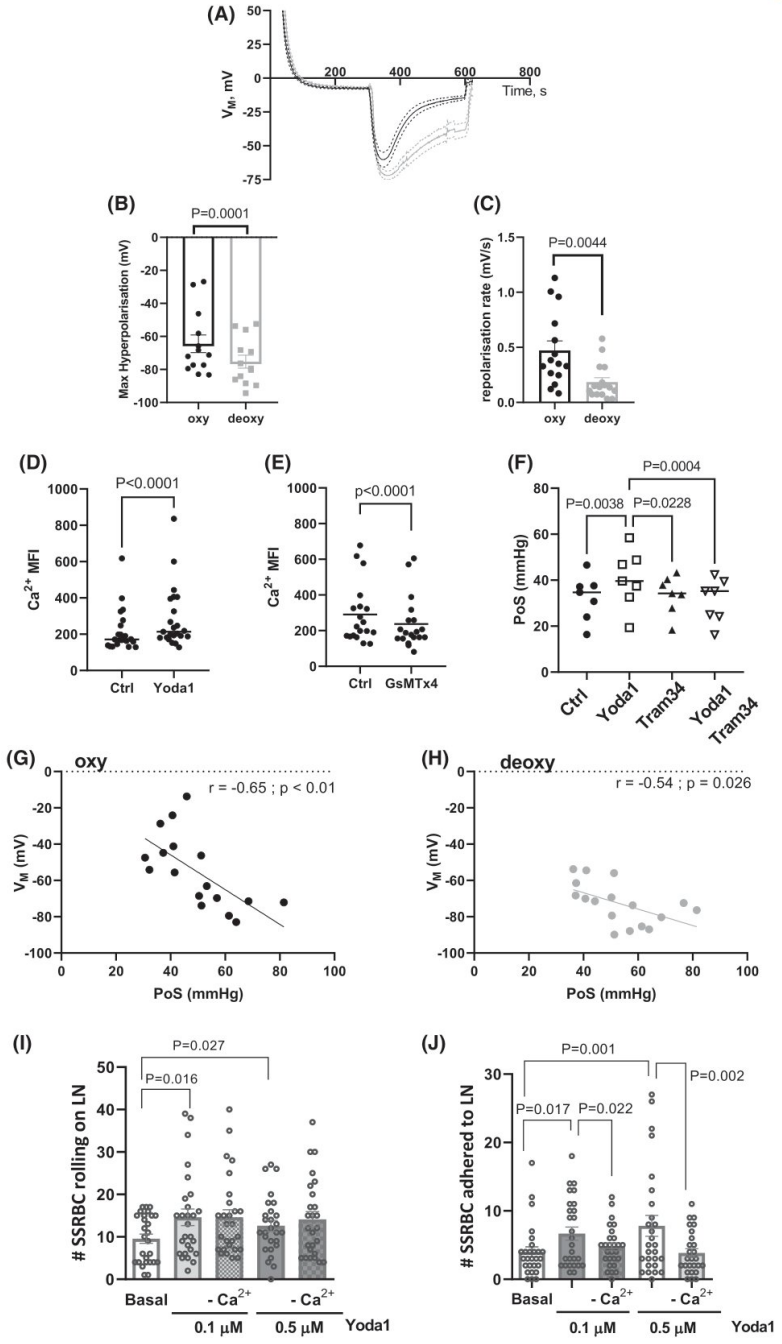

gain of function variant in Piezo1 (E756del) had a greater number of RBCs positive for PS than those without. The membrane phospholipid asymmetry disruption and the resulting membrane blebbing could also favour the release of extracellular vesicles from RBCs, which are known to play a key role in SCD pathophysiology and vascular dysfunction.[45,49]

The present study also explores the effect of Piezo1 activation on RBC adhesion. We found that activating Piezo1 resulted in increased rolling and adhesion of sickle RBCs

13652141, 2023, 3, Downloaded from https://onlinelibrary.wiley.com/doi/10.1111/bjh.18799 by Portail BibCNRS INSB, Wiley Online Library on [05/11/2023]. See the Terms and Conditions (https://onlinelibrary.wiley.com/terms-and-conditions) on Wiley Online Library for rules of use; OA articles are governed by the applicable Creative Commons License

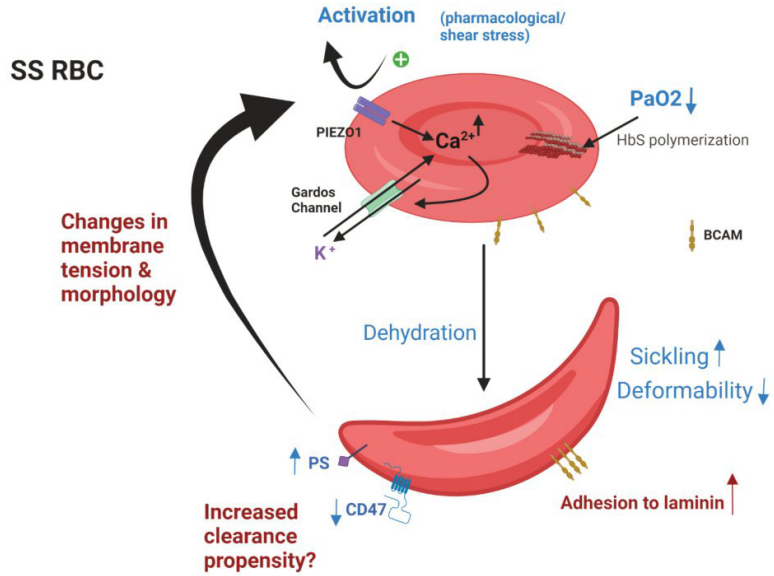

FIGURE 4 Role of Piezo1 in modulating red blood cell (RBC) physiology and function in sickle cell anaemia (SCA). Activation (pharmacological or physical) of Piezo1 on sickle RBCs leads to intracellular calcium influx and probable Gárdos channel activation, with triggering of further calcium influx and potassium efflux, leading to RBC dehydration. These events exacerbate the increased sickling of sickle RBCs and reduced deformability that occurs under lower oxygen pressure (PaO_2). Piezo1 activation also leads to phosphatidylserine (PS) exposure on the RBC surface, possibly facilitating microvesicle production, and reduced expression of CD47, potentially augmenting cell clearance propensity. Furthermore, Piezo1 activation induced the adhesion of sickle RBC to laminin via a mechanism dependent upon BCAM adhesion molecule activation (conceivably mediated by BCAM clustering). Increased sickle RBC adhesiveness can contribute to vaso-occlusive processes. Figure created at Biorender.com. [Colour figure can be viewed at wileyonlinelibrary.com]

to laminin, without any changes in BCAM expression at the RBC membrane level. Increased expression of the Lutheran(Lu)/BCAM glycoproteins, which bind to the laminin α5 chain, has been reported on sickle RBCs and a role for this molecule in the increased adhesive properties of sickle RBCs suggested.[50,51] Furthermore, a more recent study reported that Gárdos channel activation on RBCs triggers cellular senescence and the shedding of glycophorin-C–containing vesicles, resulting in Lu/BCAM and CD44 activation.[52] Importantly, the use of an antibody to neutralize the function of the BCAM molecule decreased the adhesion of Piezo1-stimulated sickle RBCs to laminin, while an antibody that binds to the CD49 integrin subunit, which is also highly expressed on sickle RBCs, had no effect on sickle RBCs adhesion. Although we did not directly measure the effects of BATPA-AM on RBC Ca^{2+} in the present study, our findings suggest that BCAM-dependent adhesion of Piezo1-activated sickle RBCs could also be dependent on intracellular Ca^{2+} accumulation. As Piezo1 stimulation by Yoda1 was not associated with any alteration in RBC surface BCAM expression, we suggest that the increase in the adhesion of SS RBCs to laminin was mediated by BCAM clustering at the cell surface. Indeed, Ca^{2+}-dependent BCAM clustering and consequent adhesion to laminin has recently been described in uninfected RBCs during malaria infection[53] and on sickle RBCs under conditions of oxidative stress.[54] One curiosity of our findings was that we found that activation of SS RBC adhesion to laminin occurred at lower concentrations of Yoda1 than needed to reduce cell deformability and augment sickling. A range of Yoda1 concentrations have been used to activate Piezo1, with recent studies employing between 1 and 10 μM Yoda1 to induce PS exposure on SS RBCs[17] and 1 μM to stimulate integrin-mediated erythroblast adhesive interactions.[55] We postulate that the exacerbated sickling of sickle RBCs that we observed at concentrations of greater or equal to 5 μM Yoda1 may in fact interfere with the ability of the cells to adhere to ligands such as laminin. Notably, it is known that Piezo1 sensitivity to shear stress is dependent on the surrounding lipid environment, and also on the proteins of the extracellular matrix with which Piezo1 channel can interact.[56,57] Clearly, the topology and the Piezo1-protein interaction at the RBCs membrane is still elusive, but the preferential location of Piezo1 channels at the rim of healthy red blood cells[58] suggests that, in the case of aberrant forms (such as upon sickling), this location may be altered and induce different mechanisms or sensitivities to shear stress.

In conclusion, our results demonstrated that Piezo1 activation and the resulting Ca^{2+} accumulation provoke a decrease in sickle RBC deformability and a greater propensity of RBCs to sickle upon deoxygenation via its effects on Gárdos channel activation. In addition, Piezo1 activation increased sickle RBC senescence and RBC adhesiveness in a calcium- and BCAM-dependent manner (Figure 4). Our results strongly support a role of the Piezo1 mechanosensor

13652141, 2023, 3, Downloaded from https://onlinelibrary.wiley.com/doi/10.1111/bjh.18799 by Portail BibCNRS INSB, Wiley Online Library on [05/11/2023]. See the Terms and Conditions (https://onlinelibrary.wiley.com/terms-and-conditions) on Wiley Online Library for rules of use; OA articles are governed by the applicable Creative Commons License

in the alterations in RBC properties that can contribute to vaso-occlusive crises and other complications in SCA and may represent a potential therapeutic target molecule for the treatment of this devastating disease. Nevertheless, our results showed a high variability for most of the parameters studied that could reflect the fact that RBCs from SCA patients are very heterogeneous in properties. Further studies are warranted in larger groups of patients to test the associations between clinical severity, membrane electrophysiological properties, RBC adhesiveness and sickling propensity.

AUTHOR CONTRIBUTIONS

E.N., N.C., S.E. and P.C. designed the study, analysed data and wrote the manuscript. F.C.L. and N.C. performed adhesion experiments. C.B., E.N,. P.L.B., R.C. and S.E. performed rheological and flow cytometry experiments. A.H. and S.E. carried out membrane potential measurements. C.R., P.J., J.B. and C.G. did N.G.S. protocols. A.G., S.P., Y.V., F.F.C. and S.T.O.S. supervised patient diagnosis and management (Lyon and UNICAMP centres). P.L.B. performed flow cytometry. All authors read and approved the final version of the manuscript.

ACKNOWLEDGEMENTS

The authors thank Victoria E. Galvão and Jaqueline Munhoz for assistance with experimental procedures at the UNICAMP centre.

FUNDING INFORMATION

This study was funded by a joint cooperation between Sao Paulo State Funding agency (FAPESP) and Université de Lyon (Grant number; Fapesp 2020/06133-6) and also by grants from the association de recherche sur les pathologies des cellules sanguines and the Club du Globule Rouge et du Fer.

CONFLICT OF INTEREST STATEMENT

The authors report no conflicts of interest relevant to this study.

DATA AVAILABILITY STATEMENT

All raw data are available, upon reasonable request, from the corresponding authors.

ORCID

Nicola Conran https://orcid.org/0000-0001-5726-7919
Céline Renoux https://orcid.org/0000-0002-7263-805X
Philippe Joly https://orcid.org/0000-0002-2351-9441
Philippe Connes https://orcid.org/0000-0002-9232-0268

REFERENCES

1. Pauling L, Itano HA, Singer SJ, Wells IC. Sickle cell anemia a molecular disease. Science. 1949;110(2865):543–8.
2. Kato GJ, Gladwin MT, Steinberg MH. Deconstructing sickle cell disease: reappraisal of the role of hemolysis in the development of clinical subphenotypes. Blood Rev. 2007;21(1):37–47.
3. Ballas SK. Sickle cell disease: classification of clinical complications and approaches to preventive and therapeutic management. Clin Hemorheol Microcirc. 2018;68(2–3):105–28.
4. Brugnara C. Membrane transport of na and k and cell dehydration in sickle erythrocytes. Experientia. 1993;49(2):100–9.
5. Ma YL, Rees DC, Gibson JS, Ellory JC. The conductance of red blood cells from sickle cell patients: ion selectivity and inhibitors. J Physiol. 2012;590(9):2095–105.
6. Browning JA, Staines HM, Robinson HC, Powell T, Ellory JC, Gibson JS. The effect of deoxygenation on whole-cell conductance of red blood cells from healthy individuals and patients with sickle cell disease. Blood. 2007;109(6):2622–9.
7. Cytlak UM, Hannemann A, Rees DC, Gibson JS. Identification of the ca (2)(+) entry pathway involved in deoxygenation-induced phosphatidylserine exposure in red blood cells from patients with sickle cell disease. Pflugers Arch. 2013;465(11):1651–60.
8. Brugnara C. Sickle cell dehydration: pathophysiology and therapeutic applications. Clin Hemorheol Microcirc. 2018;68(2–3):187–204.
9. Vandorpe DH, Rivera A, Shmukler BE, Wohlgemuth JG, Dlott JS, Snyder LM, et al. Trpv1 and trpa1 are not essential for psickle-like activity in red cells of the sad mouse model of sickle cell disease. Blood Cells Mol Dis. 2021;92:102619.
10. Zarychanski R, Schulz VP, Houston BL, Maksimova Y, Houston DS, Smith B, et al. Mutations in the mechanotransduction protein piezo1 are associated with hereditary xerocytosis. Blood. 2012;120(9):1908–15.
11. Cahalan SM, Lukacs V, Ranade SS, Chien S, Bandell M, Patapoutian A. Piezo1 links mechanical forces to red blood cell volume. elife. 2015;4:4.
12. Archer NM, Shmukler BE, Andolfo I, Vandorpe DH, Gnanasambandam R, Higgins JM, et al. Hereditary xerocytosis revisited. Am J Hematol. 2014;89(12):1142–6.
13. Danielczok JG, Terriac E, Hertz L, Petkova-Kirova P, Lautenschlager F, Laschke MW, et al. Red blood cell passage of small capillaries is associated with transient Ca(2+)-mediated adaptations. Front Physiol. 2017;8:979.
14. Nader E, Conran N, Romana M, Connes P. Vasculopathy in sickle cell disease: from red blood cell sickling to vascular dysfunction. Compr Physiol. 2021;11(2):1785–803.
15. Conran N, Embury SH. Sickle cell vaso-occlusion: the dialectic between red cells and white cells. Exp Biol Med (Maywood). 2021;246(12):1458–72.
16. Hebbel RP, Yamada O, Moldow CF, Jacob HS, White JG, Eaton JW. Abnormal adherence of sickle erythrocytes to cultured vascular endothelium: possible mechanism for microvascular occlusion in sickle cell disease. J Clin Invest. 1980;65(1):154–60.
17. Wadud R, Hannemann A, Rees DC, Brewin JN, Gibson JS. Yoda1 and phosphatidylserine exposure in red cells from patients with sickle cell anaemia. Sci Rep. 2020;10(1):20110.
18. Steffen P, Jung A, Nguyen DB, Muller T, Bernhardt I, Kaestner L, et al. Stimulation of human red blood cells leads to Ca2+-mediated intercellular adhesion. Cell Calcium. 2011;50(1):54–61.
19. Dominical VM, Vital DM, Garrido VT, Silveira AA, Olalla-Saad ST, Costa FF, et al. Interactions of sickle red blood cells with neutrophils are stabilized on endothelial cell layers. Blood Cells Mol Dis. 2016;56(1):38–40.
20. Rab MAE, Kanne CK, Bos J, Boisson C, van Oirschot BA, Nader E, et al. Methodological aspects of the oxygenscan in sickle cell disease: a need for standardization. Am J Hematol. 2020;95(1):E5–8.
21. Rab MAE, Kanne CK, Bos J, van Oirschot BA, Boisson C, Houwing ME, et al. Oxygen gradient ektacytometry-derived biomarkers are associated with vaso-occlusive crises and correlate with treatment response in sickle cell disease. Am J Hematol. 2021;96(1):E29–32.
22. Boisson C, Rab MAE, Nader E, Renoux C, van Oirschot BA, Joly P, et al. Methodological aspects of oxygen gradient ektacytometry in sickle cell disease: effects of sample storage on outcome parameters in distinct patient subgroups. Clin Hemorheol Microcirc. 2021;77(4):391–4.
23. Macey RI, Adorante JS, Orme FW. Erythrocyte membrane potentials determined by hydrogen ion distribution. Biochim Biophys Acta. 1978;512(2):284–95.

13652141, 2023, 3, Downloaded from https://onlinelibrary.wiley.com/doi/10.1111/bjh.18799 by Portail BibCNRS INSB, Wiley Online Library on [05/11/2023]. See the Terms and Conditions (https://onlinelibrary.wiley.com/terms-and-conditions) on Wiley Online Library for rules of use; OA articles are governed by the applicable Creative Commons License

24. Bennekou P, Christophersen P. Flux ratio of valinomycin-mediated k+ fluxes across the human red cell membrane in the presence of the protonophore cccp. J Membr Biol. 1986;93(3):221–7.
25. Peres L, Monedero Alonso D, Nudel M, Figeac M, Bruge J, Sebda S, et al. Characterisation of asp669tyr piezo1 cation channel activity in red blood cells: an unexpected phenotype. Br J Haematol. 2021;194(1):e51–e5.
26. Jansen C, Zetterberg M. Descemet membrane endothelial keratoplasty versus descemet stripping automated keratoplasty—outcome of one single surgeon's more than 200 initial consecutive cases. Clin Ophthalmol. 2021;15:909–21.
27. Bolger AM, Lohse M, Usadel B. Trimmomatic: a flexible trimmer for illumina sequence data. Bioinformatics. 2014;30(15):2114–20.
28. Li H. Aligning sequence reads, clone sequences and assembly contigs with bwa-mem. 2013.
29. Li H, Handsaker B, Wysoker A, Fennell T, Ruan J, Homer N, et al. The sequence alignment/map format and samtools. Bioinformatics. 2009;25(16):2078–9.
30. DePristo MA, Banks E, Poplin R, Garimella KV, Maguire JR, Hartl C, et al. A framework for variation discovery and genotyping using next-generation DNA sequencing data. Nat Genet. 2011;43(5):491–8.
31. Andrews S. A quality control tool for high throughput sequence data. http://www.bioinformatics.babraham.ac.uk/projects/fastqc/2010
32. Cingolani P, Patel VM, Coon M, Nguyen T, Land SJ, Ruden DM, et al. Using drosophila melanogaster as a model for genotoxic chemical mutational studies with a new program, snpsift. Front Genet. 2012;3:35.
33. Dimassi S, Simonet T, Labalme A, Boutry-Kryza N, Campan-Fournier A, Lamy R, et al. Comparison of two next-generation sequencing kits for diagnosis of epileptic disorders with a user-friendly tool for displaying gene coverage, decova. Appl Transl Genom. 2015;7:19–25.
34. El Nemer W, Colin Y, Le Van Kim C. Role of lu/bcam glycoproteins in red cell diseases. Transfus Clin Biol. 2010;17(3):143–7.
35. Bozic B, Svetina S. Membrane localization of piezo1 in the context of its role in the regulation of red blood cell volume. Front Physiol. 2022;13:879038.
36. Albuisson J, Murthy SE, Bandell M, Coste B, Louis-Dit-Picard H, Mathur J, et al. Dehydrated hereditary stomatocytosis linked to gain-of-function mutations in mechanically activated piezo1 ion channels. Nat Commun. 2013;4:1884.
37. Andolfo I, Alper SL, De Franceschi L, Auriemma C, Russo R, De Falco L, et al. Multiple clinical forms of dehydrated hereditary stomatocytosis arise from mutations in piezo1. Blood. 2013;121(19):3925–35. S1-12, 3935.
38. Bae C, Gnanasambandam R, Nicolai C, Sachs F, Gottlieb PA. Xerocytosis is caused by mutations that alter the kinetics of the mechanosensitive channel piezo1. Proc Natl Acad Sci U S A. 2013;110(12):E1162–8.
39. Vandorpe DH, Xu C, Shmukler BE, Otterbein LE, Trudel M, Sachs F, et al. Hypoxia activates a Ca^{2+}–permeable cation conductance sensitive to carbon monoxide and to gsmtx-4 in human and mouse sickle erythrocytes. PLoS One. 2010;5(1):e8732.
40. Ilboudo Y, Bartolucci P, Garrett ME, Ashley-Koch A, Telen M, Brugnara C, et al. A common functional piezo1 deletion allele associates with red blood cell density in sickle cell disease patients. Am J Hematol. 2018;93(11):E362–E5.
41. Belhassen L, Pelle G, Sediame S, Bachir D, Carville C, Bucherer C, et al. Endothelial dysfunction in patients with sickle cell disease is related to selective impairment of shear stress-mediated vasodilation. Blood. 2001;97(6):1584–9.
42. Weiss E, Rees DC, Gibson JS. Role of calcium in phosphatidylserine externalisation in red blood cells from sickle cell patients. Anemia. 2011;2011:379894.
43. Bogdanova A, Makhro A, Wang J, Lipp P, Kaestner L. Calcium in red blood cells—a perilous balance. Int J Mol Sci. 2013;14(5):9848–72.
44. de Jong K, Larkin SK, Styles LA, Bookchin RM, Kuypers FA. Characterization of the phosphatidylserine-exposing subpopulation of sickle cells. Blood. 2001;98(3):860–7.
45. Nader E, Romana M, Guillot N, Fort R, Stauffer E, Lemonne N, et al. Association between nitric oxide, oxidative stress, eryptosis, red blood cell microparticles, and vascular function in sickle cell anemia. Front Immunol. 2020;11:551441.
46. Eldakhakhny B, Al Sadoun H, Taleb NB, Nori DA, Helmi N, Ahmed IM, et al. Evaluation of the role of CD47 in sickle cell disease. J Hematopathol. 2021;14(1):31–9.
47. Solanki DL. Erythrophagocytosis in vivo in sickle cell anemia. Am J Hematol. 1985;20(4):353–7.
48. Mamtani M, Sharma M, Amin M, Amin A, Jawahirani A, Kulkarni H. Erythrophagocytosis in sickle cell anemia: statistical evidence for a biological phenomenon. Med Hypotheses. 2007;68(5):1065–70.
49. Garnier Y, Ferdinand S, Garnier M, Cita KC, Hierso R, Claes A, et al. Plasma microparticles of sickle patients during crisis or taking hydroxyurea modify endothelium inflammatory properties. Blood. 2020;136(2):247–56.
50. Udani M, Zen Q, Cottman M, Leonard N, Jefferson S, Daymont C, et al. Basal cell adhesion molecule/lutheran protein. The receptor critical for sickle cell adhesion to laminin. J Clin Invest. 1998;101(11):2550–8.
51. El Nemer W, Gauthier E, Wautier MP, Rahuel C, Gane P, Galacteros F, et al. Role of lu/bcam in abnormal adhesion of sickle red blood cells to vascular endothelium. Transfus Clin Biol. 2008;15(1–2):29–33.
52. Klei TRL, Dalimot JJ, Beuger BM, Veldthuis M, Ichou FA, Verkuijlen P, et al. The gardos effect drives erythrocyte senescence and leads to lu/bcam and cd44 adhesion molecule activation. Blood Adv. 2020;4(24):6218–29.
53. Dalimot JJ, Klei TRL, Beuger BM, Dikmen Z, Bouwman SAM, Mombo-Ngoma G, et al. Malaria-associated adhesion molecule activation facilitates the destruction of uninfected red blood cells. Blood Adv. 2022;6(21):5798–810.
54. Lizarralde-Iragorri MA, Lefevre SD, Cochet S, El Hoss S, Brousse V, Filipe A, et al. Oxidative stress activates red cell adhesion to laminin in sickle cell disease. Haematologica. 2021;106(9):2478–88.
55. Aglialoro F, Hofsink N, Hofman M, Brandhorst N, van den Akker E. Inside out integrin activation mediated by piezo1 signaling in erythroblasts. Front Physiol. 2020;11:958.
56. Lai A, Thurgood P, Cox CD, Chheang C, Peter K, Jaworowski A, et al. Piezo1 response to shear stress is controlled by the components of the extracellular matrix. ACS Appl Mater Interfaces. 2022;14(36):40559–68.
57. Lai A, Cox CD, Chandra Sekar N, Thurgood P, Jaworowski A, Peter K, et al. Mechanosensing by piezo1 and its implications for physiology and various pathologies. Biol Rev Camb Philos Soc. 2022;97(2):604–14.
58. Vaisey G, Banerjee P, North AJ, Haselwandter CA, Mac KR. Piezo1 as a force-through-membrane sensor in red blood cells. elife. 2022;11:e82621.

SUPPORTING INFORMATION

Additional supporting information can be found online in the Supporting Information section at the end of this article.

How to cite this article: Nader E, Conran N, Leonardo FC, Hatem A, Boisson C, Carin R, et al. Piezo1 activation augments sickling propensity and the adhesive properties of sickle red blood cells in a calcium-dependent manner. Br J Haematol. 2023;202(3):657–668. https://doi.org/10.1111/bjh.18799

13652141, 2023, 3, Downloaded from https://onlinelibrary.wiley.com/doi/10.1111/bjh.18799 by Portail BibCNRS INSB, Wiley Online Library on [05/11/2023]. See the Terms and Conditions (https://onlinelibrary.wiley.com/terms-and-conditions) on Wiley Online Library for rules of use; OA articles are governed by the applicable Creative Commons License

The results suggested an increased activation of the Gárdos channel in deoxygenated SS (Figure 3A in the article) since the hyperpolarization was more pronounced (Figure 3B in the article) and lasted longer (Figure 3C in the article) when the media was deoxygenated. Following this, flow cytometry results assessed that intracellular Ca^{2+} was significantly increased upon activation of the PIEZO1 channel with Yoda1 (Figure 3D in the article). In addition, Ca^{2+} levels were significantly decreased after inhibition of the PIEZO1 channel with GsMTx-4 toxin (Figure 3E in the article). Panel F of Figure 3 showed that the inhibition of Gárdos channel by Tram34 reversed the loss of deformability initially caused by Yoda1, indicating by such that the increased propensity of RBC to sickle during deoxygenation and upon PIEZO1 activation was ultimately mediated by Gárdos channel activation. The extent of hyperpolarization dependent on the Gárdos channel activation correlated both in oxygenated and deoxygenated conditions with the susceptibility of RBCs to sickle, as measured by the PoS by oxygenscan (Figure 3 G-H in the article). In the article, the oxygen-gradient ektacytometry study showed that PIEZO1 activation significantly decreased sickle RBC deformability and augmented the sickling propensity. This article also revealed that Yoda1 induced a Ca^{2+}-dependent adhesion of sickle RBCs to laminin, mediated by increased BCAM binding affinity. Altogether, these findings shed light on a potential key role of the PIEZO1 protein in SCA sickling, which may be mediated by RBC dehydration following Gárdos channel activation (Gibson and Stewart, 2023).

2. Unpublished results

In addition to the results reported in the paper, additional experiments were performed.

First, the results shown in the article did not include control experiments of healthy cells exposed to Yoda1 in oxygenated and deoxygenated conditions. Figure 45, shows the comparison of maximal hyperpolarizations (panel A) and repolarization rates (panel B) of healthy RBCs between oxygenated and deoxygenated conditions. The results clearly show no differences, indicating that the oxygenation state does not affect the behavior of healthy RBCs, and that deoxygenation only affects sickle RBCs.

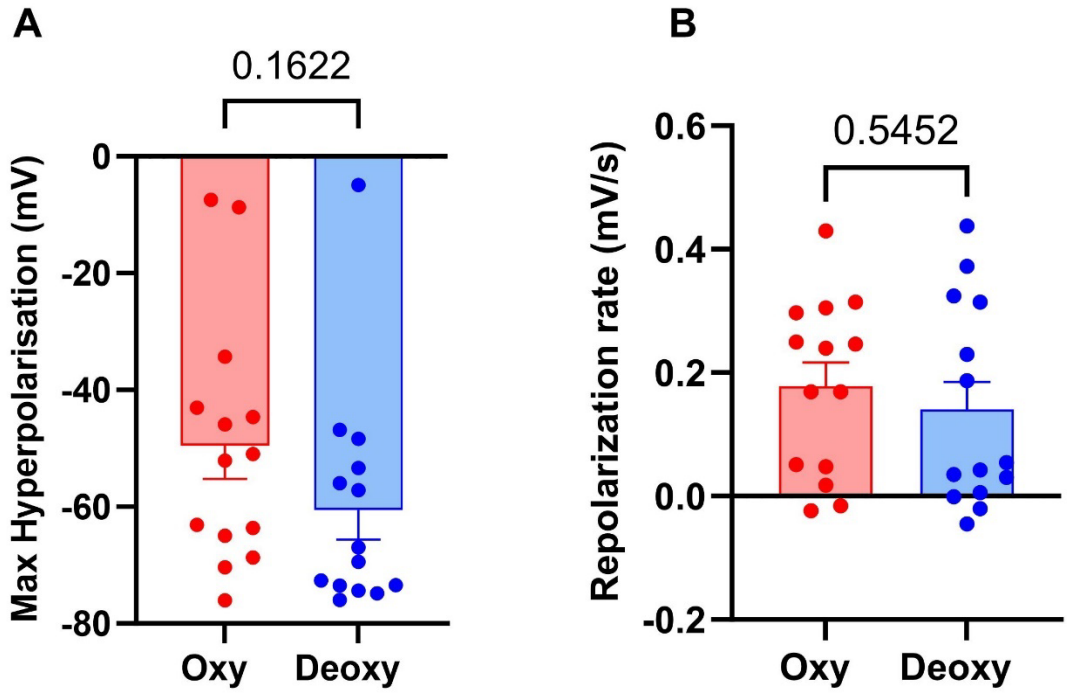

Figure 45: Yoda1-effects are not oxygen-dependent in healthy RBC. (A) comparison of the maximal hyperpolarization, and (B) the repolarization rate, showing no significant difference between oxygenated (in red) and deoxygenated (in blue) conditions. The statistical test is paired t-test. Histograms represent means ± SEM, n=14.

Knowing that the Gárdos channel is activated by intracellular Ca^{2+}, it was also necessary to test the effects of NS309 on these cells. By shifting the Ca^{2+} sensitivity of the Gárdos channel, NS309 proved to be a powerful pharmacological agent for studying K^+ movements via the Gárdos without altering intracellular Ca^{2+} concentrations.

Cells from sickle cell patients are known to have a higher basal Ca^{2+} content than those found in normal cells (Eaton et al., 1973). Moreover, the effects of GsMTx-4 on Ca^{2+} content in sickle cell anaemia patients clearly show that a 15-minute incubation with this inhibitor is sufficient to significantly reduce intracellular Ca^{2+} concentration in sickle cell anaemia patients.

While under oxygenated conditions the effects of NS309 (10µM) are similar to those observed in normal cells, abrupt deoxygenation causes a significant more pronounced hyperpolarization in SS RBCs (Figure 46A-C) in a Ca^{2+}- free media. Remarkably, pronounced deoxygenation does not trigger a more pronounced hyperpolarisation in healthy cells, with only a slight hyperpolarization.

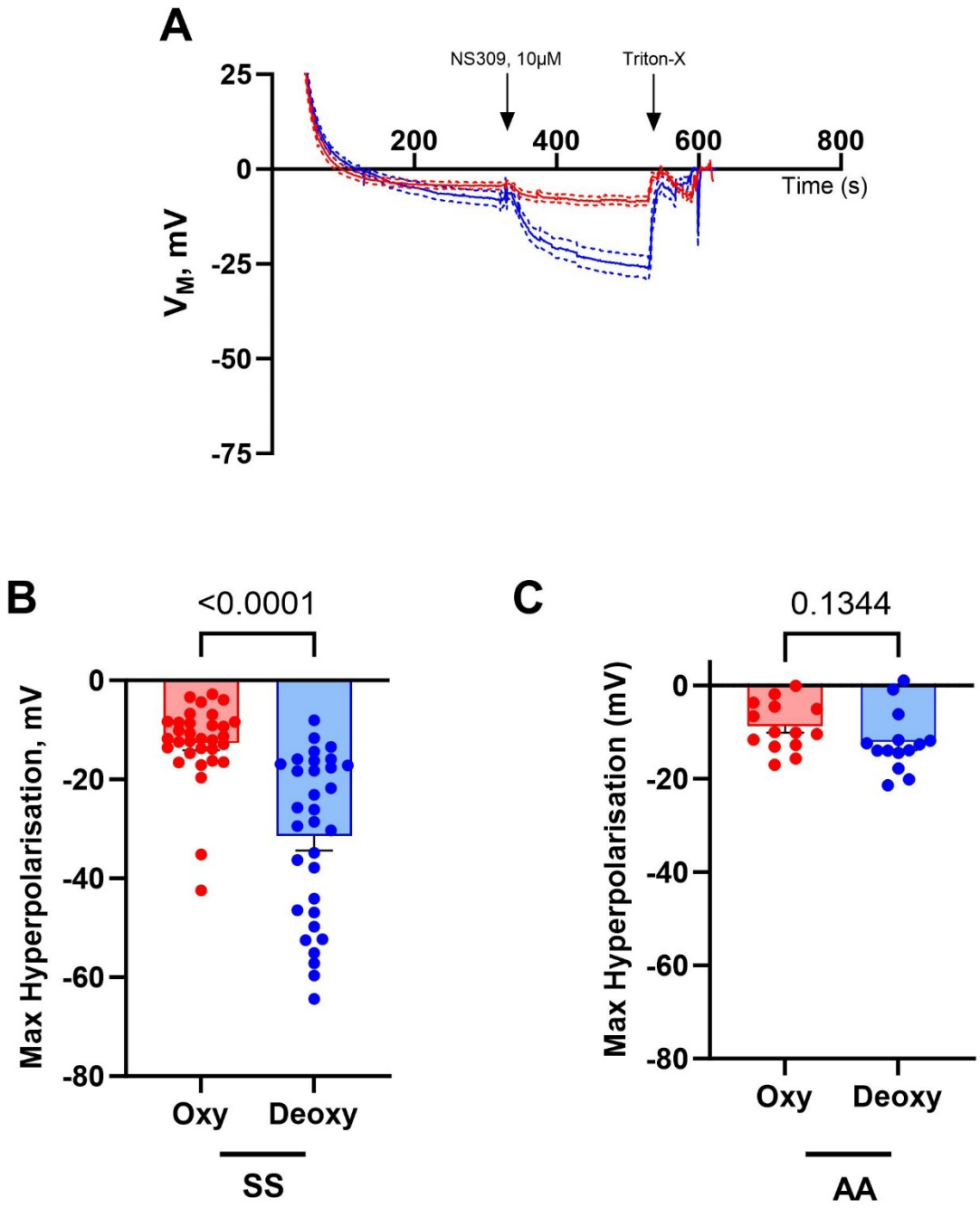

Figure 46: Changes in membrane potential of SS RBCs following Gárdos channel activation by NS309 (10 µM) (A) Mean MBE traces (n =32, averaged curve ± SEM) in oxy (red) and deoxy (blue) conditions, showing a more pronounced hyperpolarization. Dashed lines represent SEM envelopes of the curves (B) Maximum hyperpolarization in SS red cells in oxygenated and deoxygenated conditions (partial pressure of O_2 is reduced to 10% of nominal air partial pressure (0.8 mg/mL, n = 32)). (C) The difference in response to NS309 is absent in normal AA red cells, where no hyperpolarizations occurred (n=14). Paired student's t-test was performed. Histograms represent means +SEM.

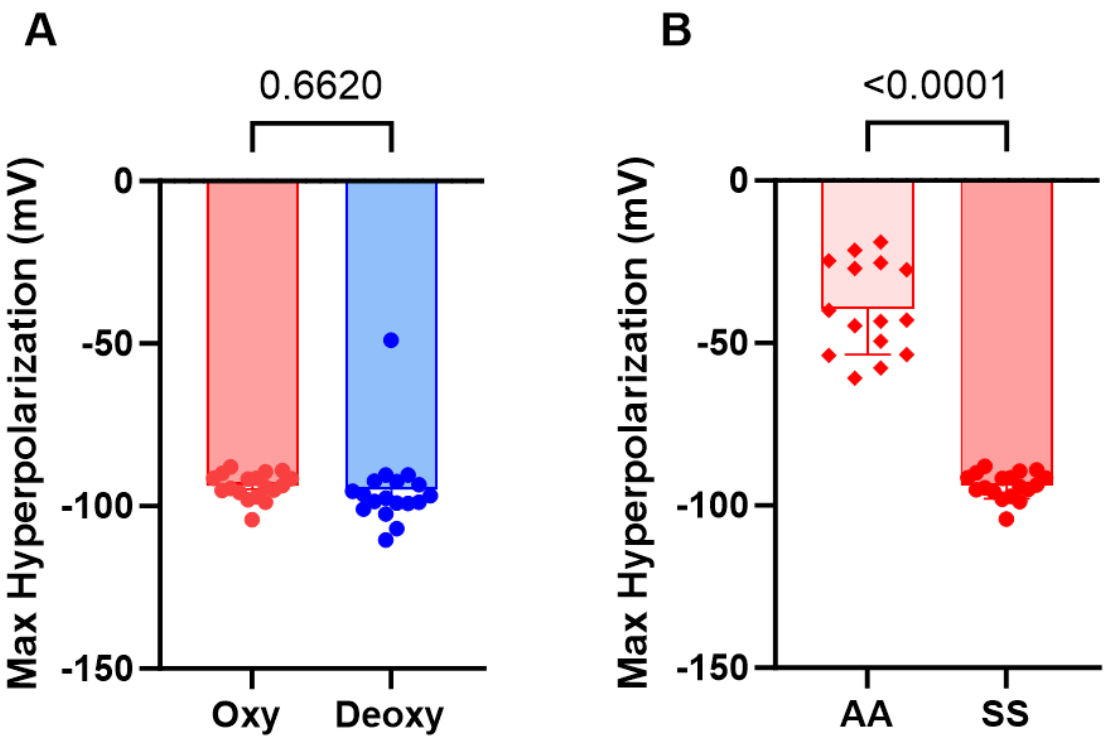

Figure 47: Maximum hyperpolarization using 10 µM of NS309 with the presence of Ca^{2+} (2mM) in the extracellular media. A. Comparison of the maximal hyperpolarization values reached by SS RBCs between oxygenated (in red) and deoxygenated (in blue) conditions. Statistical difference was assessed using a paired t-test, n=18. Histograms are means +SEM, n=18. B. Comparison of the maximal hyperpolarization values reached in oxygenated conditions between AA and SS RBCs. Statistical difference in this case was assessed using an unpaired t-test. n= 15 for AA cells, and n= 18 for SS cells.

The difference in hyperpolarization recorded with NS309 in a Ca^{2+}- free media, was not observed in the presence of 2 mM of Ca^{2+} in the extracellular media (Figure 47A). This may be due to a maximal state of hyperpolarization reached whenever Ca^{2+} is present in the media, leading to automatic and maximal activation of the Gárdos channel whenever PIEZO1 is open, especially in SS RBCs, which are usually more loaded with Ca^{2+}. This is why, the study of the activation of the Gárdos channel with NS309 could be more valuable in the absence of Ca^{2+}, because it strongly reflects the difference of the activation between oxygenated and deoxygenated conditions of sickle RBCs.

However, it is noteworthy to observe the significant difference in the maximal hyperpolarization between normal and sickle RBCs, when using NS309, 10 µM with the presence of Ca^{2+} in the extracellular medium in oxygenated condition (Figure 47B). This is presumably linked to the fact

that SS RBCs are initially more loaded in Ca^{2+} than normal cells. As a consequence, the usage of NS309 with the presence of Ca^{2+} in the extracellular media, shifts the Gárdos sensitivity towards its maximal activation levels, even at the oxygenated conditions. This could be the main reason for the non-significant difference between oxygenated and deoxygenated conditions in Figure 47A.

We also tried to inhibit the effects of Yoda1 in sickle cells using GsMTx-4. Figure 48A shows the membrane potential traces of one patient's RBCs, representative of the results obtained. Nevertheless, it is noteworthy that the inhibition was really variable, in both oxygenated (Figure 48B) and deoxygenated (Figure 48C) conditions. Therefore, we think that GsMTx-4 is not an optimal inhibitor of PIEZO1 and alternatives should be found. For now, no satisfactory conclusions can be drawn from this experiment. Knowing that GsMTx-4 interferes with membrane phospholipids, we can hypothesize that the phospholipid and cholesterol content of SS RBCs may alter the efficiency of GsMTx-4 in some patients. Further measurements in SS RBCs could help to clarify this hypothesis.

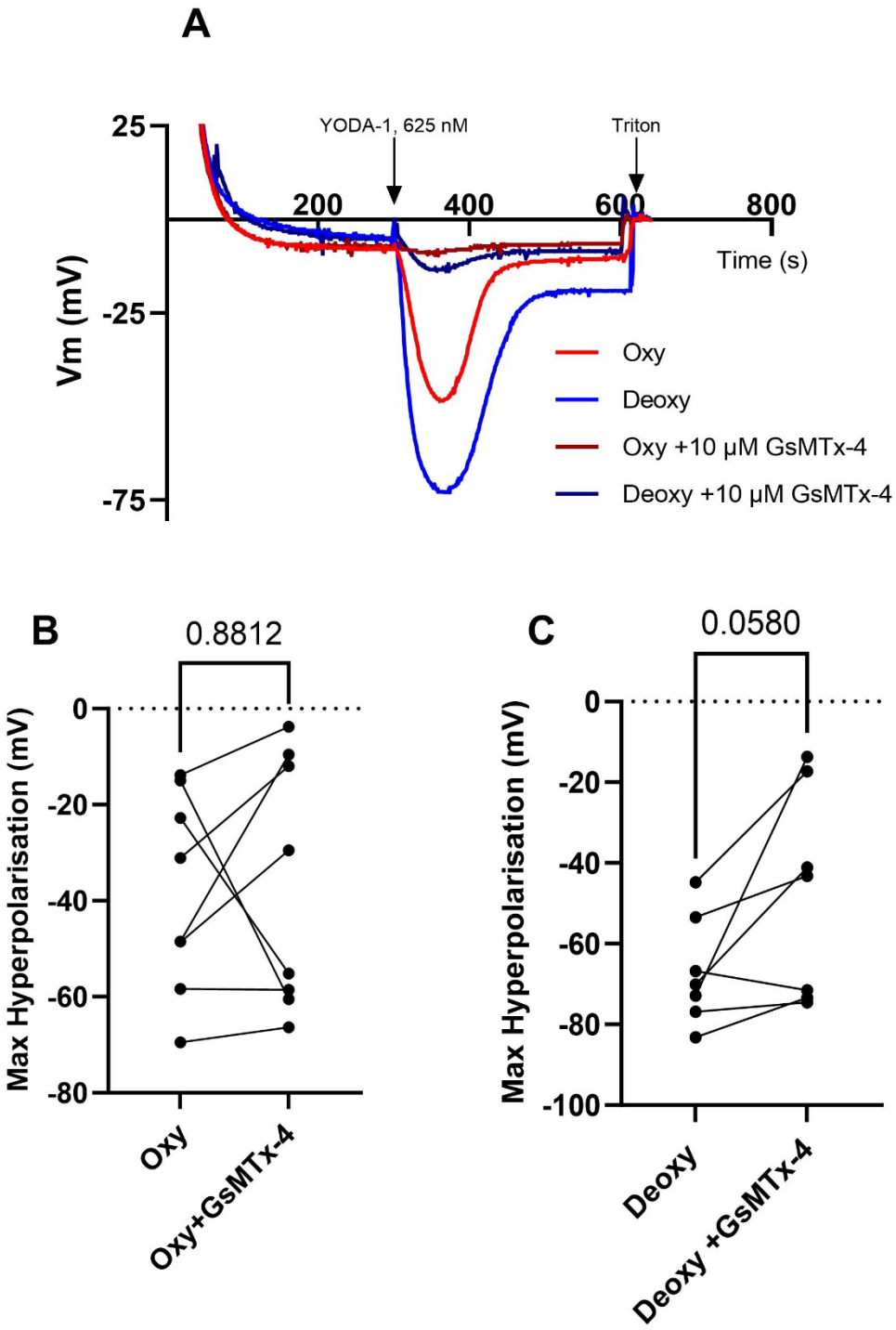

Figure 48: The inhibition of Yoda1-effects by GsMTx-4 in Sickle Cells. (A) Representative traces showing the inhibition of Yoda1 (625 nM-oxy and deoxy) effects by using GsMTx4. (B,C) Statistical comparison between the maximal hyperpolarizations in response to Yoda in the presence or absence of GsMTx4 (10 µM) in oxygenated conditions (B), and deoxygenated conditions (C).

B. **TRPV2 and SCD**

1. Published article

Check for updates

Received: 26 June 2023 | Revised: 31 August 2023 | Accepted: 9 September 2023

DOI: 10.1002/ajh.27109

CORRESPONDENCE

Adverse effects of delta-9-tetrahydrocannabinol on sickle red blood cells

To the Editor,

Sickle Cell Disease (SCD) is characterized by the presence of an abnormal hemoglobin HbS that crystalizes in deoxygenated conditions, causing the sickling of red blood cells (RBCs). During deoxygenation, increased RBC cation conductance, especially of Ca^{2+}, has been shown to promote RBC dehydration through Gárdos channel activation, hence increasing RBC sickling. Thus, any pathway that may increase Ca^{2+} represents a threat to the lifespan of the sickle RBCs within the circulation. Notably, Piezo1 has been recently demonstrated to play a role in the increased Ca^{2+} entry observed in sickle RBCs.[1] Furthermore, the presence of the transient receptor potential channel vanilloid type 2 (TRPV2) in RBCs has also been validated,[2] opening immediate questions on its physiological relevance for RBC life. TRPV2 channels share several features with Piezo1 such as mechanosensitivity as well as a strong permeability for calcium ions.[3] More importantly, it can be activated by Δ^9-tetrahydrocannabinol (Δ^9THC) even in RBCs.[4] The instantaneous changes in cell shape and filterability that occur upon Δ^9THC stimulation in normal RBCs[4] have led us to wonder what could happen to sickle RBCs, which are even more susceptible to alterations of shape and deformability.

Figure 1A shows whole-cell current traces of normal (AA) and sickle (SS) RBCs before and after stimulation with 80 μM Δ^9THC. While AA RBCs display a conductance below 0.5 nS (Figure 1A—left panel, B),[5] SS RBCs exhibit a three times higher conductance as already demonstrated in other SCD studies (Figure 1A,B).[6] Furthermore, despite both cell types respond positively to Δ^9THC, the magnitude of the response obtained for SS RBCs is much more pronounced with an average conductance of 2.3 ± 0.5 nS ($n = 10$) compared with AA cells (0.7 ± 0.2 nS, $n = 4$). Importantly, not all cells tested in both groups respond to Δ^9THC stimulation, showing again the heterogeneity of the RBC population.[4] Nevertheless, the percentage of responding RBCs in the SS group is much higher than the percentage observed in the control cells (20% vs. 47% $n = 4$ out of 20 and $n = 10$ out of 21 respectively) (Figure 1A). When monitored by the Macey–Bennekou–Egee (MBE) method, the addition of Δ^9THC causes only a very small change in membrane potential of AA RBCs (−3.75 ± 0.7 mV, $n = 12$, Figure 1C,D), whereas the same concentration of Δ^9THC triggers a highly significant hyperpolarization of −16.3 ± 1.5 mV in SS RBCs ($n = 35$, $p < .001$, Figure 1C,D). This hyperpolarization is strictly dependent on oxygen, as once the oxygen of the experimental media is decreased, with levels of oxygen reduced to 0.8–1 mg/L (O_2 partial pressure: 19.6–24.5 mmHg) only, the hyperpolarization was enhanced, reaching −28.4 ± 2.3 mV ($n = 20$, Figure 1C,D). The observed hyperpolarizations are accounted for an increased activity of the Gárdos channel because all are prevented by preincubation with charybdotoxin (100 nM, Figure 1D). It is noteworthy that the resting membrane potential of sickle RBCs is on average less electronegative than AA cells (Figure 1E) and that such a difference may be related to a different aging process (120 days vs. 15–20 days, respectively).

The possibility that the copy number of TRPV2 channels in SS RBCs is higher than in control cells was tested by western blot on two different controls and three patients (Figure 1F). No difference in expression could be detected between the two populations, indicating that the differences in response between the two populations are likely to be related to the differential ability of TRPV2 to drive Ca^{2+} entry. The Gárdos channel is strictly dependent on the intracellular Ca^{2+} concentration, which affects not only its gating but also more precisely its open probability.[7] Therefore, it was necessary to determine whether the Ca^{2+} movements were similar between the two cell populations. To this end, the Ca^{2+} content in RBCs after stimulation with Δ^9THC was assessed by flow cytometry using Fluo-4 fluorescence intensity. As expected, SS RBCs have a higher Ca^{2+} content than AA cells at the resting state (Figure 1G,H). Thus, the mean fluorescence intensity of Fluo-4 is significantly higher ($p = .04$, Suppl. Figure 1) for SS compared with AA RBCs (Figure 1G, gray and black traces respectively). Moreover, when the cells are subjected to Δ^9THC stimulation, not only is the number of responding RBCs higher in SS, but so is the intensity of the measured fluorescence (Figure 1G, purple and red traces and Figure 1H). Importantly, it should be noted that this increase in $[Ca^{2+}]_i$ affects more the SS cells compared with the AA RBCs because only 25% are positive for high Ca^{2+} content compared with almost 50% of SS RBCs (Figure 1H). This finding is consistent with the results obtained by the patch-clamp technique (Figure 1A,B) or the MBE method (Figure 1C). Indeed, only 20% of the control RBCs were responsive to Δ^9THC compared with 47% of the SS RBCs in the whole-cell configuration of the patch-clamp technique. More importantly, the MBE method measures the average change in membrane potential of a whole population of cells. The response obtained is affected by the capacity of all the population to react simultaneously to the stimulus. It is therefore likely

 © 2023 Wiley Periodicals LLC.

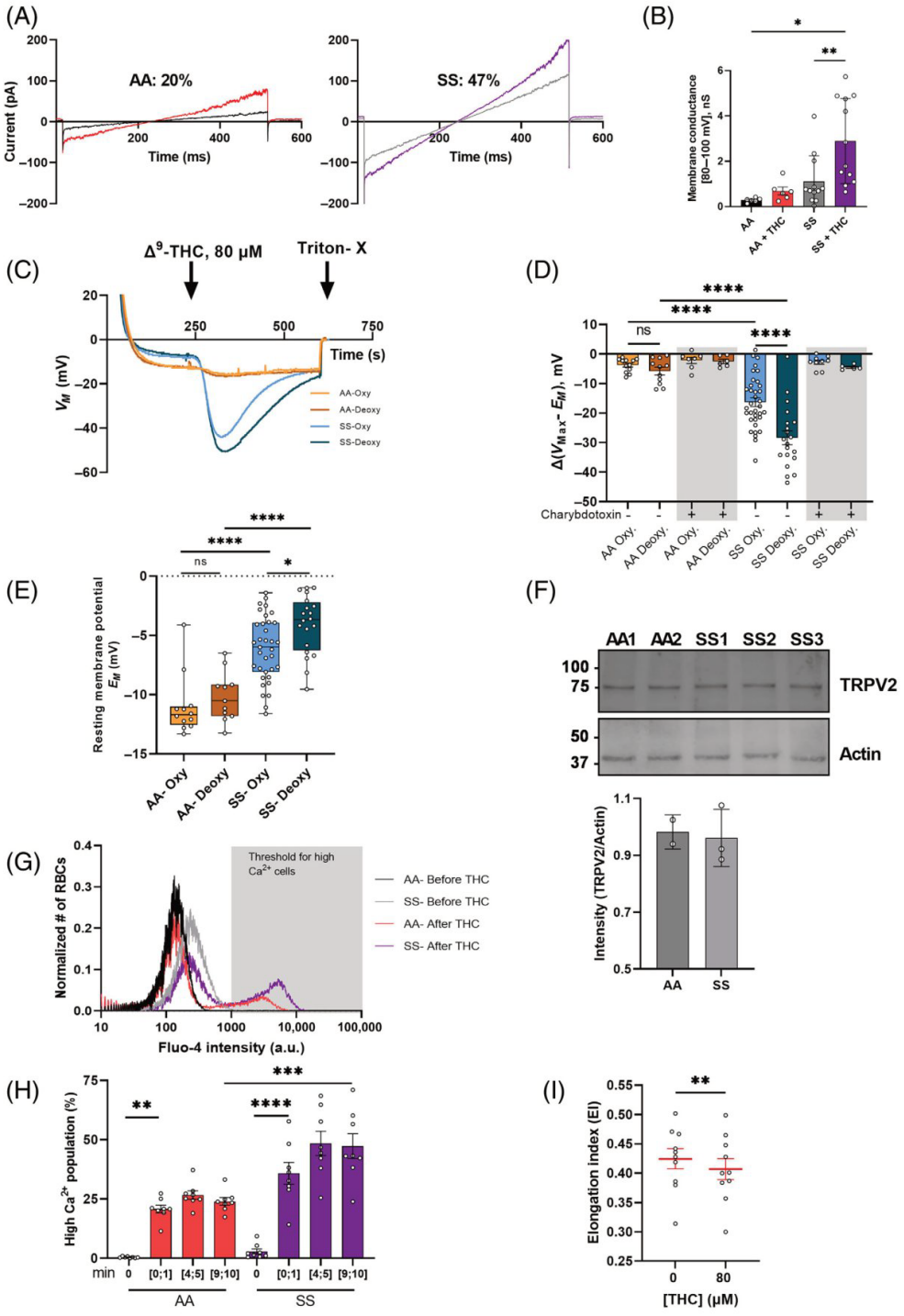

FIGURE 1 Legend on next page.

10968652, 0, Downloaded from https://onlinelibrary.wiley.com/doi/10.1002/ajh.27109 by Portail BibCNRS INSB, Wiley Online Library on [05/11/2023]. See the Terms and Conditions (https://onlinelibrary.wiley.com/terms-and-conditions) on Wiley Online Library for rules of use; OA articles are governed by the applicable Creative Commons License

that the large difference observed between the two populations (AA vs. SS) is also partly due to the susceptibility of all or part of the cell population to respond to Δ^9THC. Finally, Gárdos channel activity, measured by the extent of hyperpolarization, is dependent on other conductance pathways in the cell, in particular chloride, which counteracts the efflux of K^+ (from an electrical point of view), but also on the capacity of the cell to limit the intracellular Ca^{2+} increase by the action of the Ca^{2+}-pump (PMCA). To investigate the potential effects of Δ^9THC on RBC deformability, ektacytometry tests were practiced. The results revealed a significant loss of SS deformability (Figure 1I) in response to Δ^9THC without any effect on normal AA cells (data not shown).

From all presented data, we can conclude that:

1. RBCs from SCD patients are more responsive to acute Δ^9THC stimulation compared with control RBCs without any difference in the copy number of TRPV2 channels. The immediate consequences of this reactivity to Δ^9THC are a rapid and prolonged increase in intracellular Ca^{2+} concentration, which—in contrast to healthy RBCs—reaches and exceeds the threshold for activation of the Gárdos channel. The latter stays open long enough to presumably cause a substantial loss of potassium, overcompensating the volume increase caused by the sodium entry through TRPV2 and thus the propensity to sickle by increasing the intracellular hemoglobin concentration. This enhanced responsiveness of SS cells can be due to the increased basal levels of Ca^{2+} in these cells, making the threshold of Gárdos activation easier to attain. In addition, we speculate about a role of difference in cellular age between these two cell types, because SS cells are usually removed earlier from the circulation than the average 120 days for AA cells. Finally, the slower activity of PMCA in SS cells can also provoke delayed Ca^{2+} effects.[8]
2. The heterogeneity observed in Δ^9THC responses clearly raises the question of the relationship between RBCs ion channel response and the age of the cells within the circulation. The physiological environment of sickle RBCs is disturbed by increased oxidative stress, coupled with nitric oxide and change in ions' balance. This likely could change the activity of various channels, which makes it interesting for future investigations.

The present results were obtained with a high Δ^9THC concentration, above regular levels detected in blood of daily smokers.[9] Nevertheless, upon puff on the cannabis cigarette, RBCs may encounter an acutely high Δ^9THC concentration peak in the lungs. This raises a further question in the perspective of recent and very encouraging results on the use of cannabinoid derivatives (CBD) for the treatment of pain associated with the disease,[10] as well as studies showing that daily cannabis users with SCD had worse pain episode severity scores than others, yet they were associated with a lower rate of hospital admission and emergency room visits.[11] Thus, a longitudinal clinical study would be timely and relevant to shed light on this risk.

FUNDING INFORMATION

This work received funding from the European Union Horizon 2020 Research and Innovation Program under the Marie Skłodowska-Curie grant agreement No 860436—EVIDENCE.

CONFLICT OF INTEREST STATEMENT

The authors declare no conflicts of interest.

DATA AVAILABILITY STATEMENT

Requests for data should be sent to the corresponding author at egee@sb-roscoff.fr.

FIGURE 1 Transient receptor potential channel vanilloid type 2 (TRPV2) activation in SS and AA red blood cells (RBCs). (A) Raw traces of current amplitude (pA) were recorded using patch-clamp from healthy controls (AA cells), $n = 4$ (left panel), before Δ^9-tetrahydrocannabinol (Δ^9THC) (black trace) and after 80 μM of Δ^9THC (red trace), and from sickle patients (SS cells), $n = 10$ (right panel), before Δ^9THC (gray trace) and after 80 μM of Δ^9THC (purple trace). The percentage of responding cells is indicated for each type of cells in both panels of (A). (B) Differences in membrane conductance (nS) before and after Δ^9THC application, calculated at positive voltages (between 80 and 100 mV) in AA and SS cells (paired *t*-test, $^{**}p < .01$). (C) Representative traces for the variations of membrane potential after injection of Δ^9THC (80 μM) in AA oxygenated cells (orange trace), AA deoxygenated cells (brown trace), SS oxygenated cells (light blue trace), and SS deoxygenated cells (dark blue trace). (D) Statistical comparison of the hyperpolarization magnitudes reached at different conditions with and without inhibiting the Gárdos channel with charybdotoxin. $N = 12$ for AA oxygenated cells, $N = 11$ for AA deoxygenated cells, $N = 7$ for AA oxygenated cells with charybdotoxin, and $N = 7$ for AA deoxygenated cells with charybdotoxin; $N = 33$ for SS oxygenated cells, $N = 19$ for SS deoxygenated cells, $N = 8$ for SS oxygenated cells with charybdotoxin, and $N = 5$ for SS deoxygenated cells with charybdotoxin. Hyperpolarization magnitudes (mV) are obtained after the deduction of resting membrane potential (E_M) from the maximal hyperpolarization (V_{Max}) reached at each condition. (E) Resting membrane potentials, obtained at different conditions before the application of Δ^9THC (80 μM). $N = 12$ for AA oxygenated cells, $N = 11$ for AA deoxygenated cells, $N = 35$ for SS oxygenated cells, and $n = 20$ for SS deoxygenated cells. (F) Western blot showing the expression of TRPV2 and actin (as loading control) in healthy donors (AA1 and AA2), and SCA patients (SS1, SS2, and SS3) (top panel), and the quantitative comparison of band densities (ratio TRPV2/actin) on western blots from AA ($N = 2$) and SS cells ($N = 3$) (bottom panel). (G) Representative normalized histograms of Fluo-4 intensity in high Ca^{2+} population of AA cells without Δ^9THC (black trace), SS cells without Δ^9THC (gray trace), AA cells with 80 μM of Δ^9THC (red trace), and SS cells with 80 μM of Δ^9THC (purple trace). (H) Quantitative analysis of AA and SS RBCs with high Ca^{2+} in response to 80 μM of Δ^9THC, $N = 8$ for all conditions. All histograms represent means ± SEM. Statistical difference was assessed using two-way analysis of variance. (I) Elongation index (EI) in response to Δ^9THC stimulation in patients' RBCs (paired *t*-test, $^{*}p < .05$; $^{**}p < .01$; $^{***}p < .001$; $^{****}p < .0001$). In the legend, "n" refers to the number of individual cells that could be patched using patch-clamp technique and "N" refers to the number of experiments of a cell population.

10968652, 0, Downloaded from https://onlinelibrary.wiley.com/doi/10.1002/ajh.27109 by Portail BibCNRS INSB, Wiley Online Library on [05/11/2023]. See the Terms and Conditions (https://onlinelibrary.wiley.com/terms-and-conditions) on Wiley Online Library for rules of use; OA articles are governed by the applicable Creative Commons License

Aline Hatem[1,2], Sofia Esperti[3], Nicoletta Murciano[4,5], Min Qiao[5,6], Maria Giustina Rotordam[4], Nadine Becker[4], Elie Nader[3], Felix Maurer[6], Laurent Pérès[1,2], Guillaume Bouyer[1,2], Lars Kaestner[5,6], Philippe Connes[3], Stéphane Egée[1,2]

[1]*Sorbonne Université, CNRS, UMR8227 LBI2M, Station Biologique de Roscoff, Roscoff, France*
[2]*Laboratory of Excellence GR-Ex, Paris, France*
[3]*Laboratory LIBM EA7424, Vascular Biology and Red Blood Cell Team, University of Lyon, Lyon, France*
[4]*Research and Development, Nanion Technologies, Munich, Germany*
[5]*Theoretical Medicine and Biosciences, Saarland University, Homburg, Germany*
[6]*Experimental Physics, Saarland University, Saarbrücken, Germany*

Correspondence
Stéphane Egée, UMR8227 LBI2M Sorbonne Université-CNRS, Station Biologique de Roscoff, Place Georges Teissier, 29680 Roscoff, France.
Email: egee@sb-roscoff.fr

Aline Hatem, Sofia Esperti, Nicoletta Murciano, Min Qiao contributed equally to this study and should be considered as first co-authors.

ORCID

Aline Hatem https://orcid.org/0009-0000-2944-9037
Sofia Esperti https://orcid.org/0009-0000-9665-2430
Nicoletta Murciano https://orcid.org/0000-0002-8046-7297
Min Qiao https://orcid.org/0000-0002-2734-6824
Elie Nader https://orcid.org/0000-0002-6054-2456
Felix Maurer https://orcid.org/0000-0002-6459-1204
Laurent Pérès https://orcid.org/0000-0001-6016-4785
Guillaume Bouyer https://orcid.org/0000-0002-5808-0539
Lars Kaestner https://orcid.org/0000-0001-6796-9535
Philippe Connes https://orcid.org/0000-0002-9232-0268
Stéphane Egée https://orcid.org/0000-0002-6195-4639

REFERENCES

1. Nader E, Conran N, Leonardo FC, et al. Piezo1 activation augments sickling propensity and the adhesive properties of sickle red blood cells in a calcium-dependent manner. *Br J Haematol*. 2023;202:657-668. doi:10.1111/bjh.18799
2. Belkacemi A, Trost CF, Tinschert R, et al. The TRPV2 channel mediates Ca^{2+} influx and the Δ9-THC-dependent decrease in osmotic fragility in red blood cells. *Haematologica*. 2021;106(8):2246-2250. doi:10.3324/haematol.2020.274951
3. Egée S, Kaestner L. The transient receptor potential vanilloid type 2 (TRPV2) channel—a new druggable Ca^{2+} pathway in red cells, implications for red cell ion homeostasis. *Front Physiol*. 2021;12:677573. doi:10.3389/fphys.2021.677573
4. Flormann D, Qiao M, Murciano N, et al. Transient receptor potential channel vanilloid type 2 in red cells of cannabis consumer. *Am J Hematol*. 2022;97(5):E180-E183. doi:10.1002/ajh.26509
5. Egée S, Lapaix F, Decherf G, et al. A stretch-activated anion channel is up-regulated by the malaria parasite plasmodium falciparum. *J Physiol*. 2002;542(3):795-801. doi:10.1113/jphysiol.2002.022970
6. Browning JA, Staines HM, Robinson HC, Powell T, Ellory JC, Gibson JS. The effect of deoxygenation on whole-cell conductance of red blood cells from healthy individuals and patients with sickle cell disease. *Blood*. 2006;109(6):2622-2629. doi:10.1182/blood-2006-03-001404
7. Dunn PM. The action of blocking agents applied to the inner face of Ca^{2+}-activated K^+ channels from human erythrocytes. *J Membrane Biol*. 1998;165(2):133-143. doi:10.1007/s002329900427
8. Gopinath RM, Vincenzi FF. ($Ca^{2++}Mg^{2+}$)-ATPase activity of sickle cell membranes: decreased activation by red blood cell cytoplasmic activator. *Am J Hematol*. 1979;7(4):303-312. doi:10.1002/ajh.2830070402
9. Huestis MA. Human cannabinoid pharmacokinetics. *Chem Biodivers*. 2007;4(8):1770-1804. doi:10.1002/cbdv.200790152
10. Cherukury HM, Argueta DA, Garcia N, et al. Cannabidiol attenuates hyperalgesia in a mouse model of sickle cell disease. *Blood*. 2023;141(2):203-208. doi:10.1182/blood.2022016382
11. Curtis SA, Brandow AM, DeVeaux M, Zeltermam D, Devine L, Roberts JD. Daily cannabis users with sickle cell disease show fewer admissions than others with similar pain complaints. *Cannabis Cannabinoid Res*. 2020;5(3):255-262. doi:10.1089/can.2019.0036

SUPPORTING INFORMATION

Additional supporting information can be found online in the Supporting Information section at the end of this article.

10968652, 0, Downloaded from https://onlinelibrary.wiley.com/doi/10.1002/ajh.27109 by Portail BibCNRS INSB, Wiley Online Library on [05/11/2023]. See the Terms and Conditions (https://onlinelibrary.wiley.com/terms-and-conditions) on Wiley Online Library for rules of use; OA articles are governed by the applicable Creative Commons License

-Supplementary Material- ajh27109-sup-0001-supinfo

A. Supplementary Figures

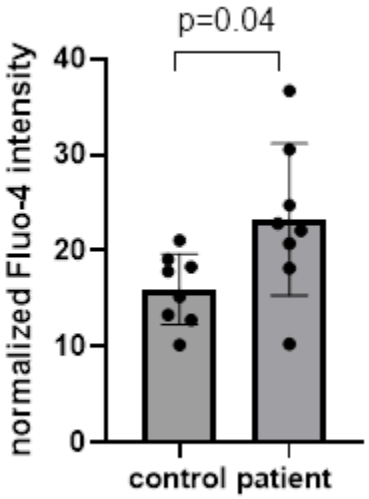

Supplementary Figures. **1**. Statistical comparison of the Fluo-4 intensity before THC stimulation between AA and SS cells. Values are normalized and statistical comparison is assessed using paired Welch's *t*-test. N=8.

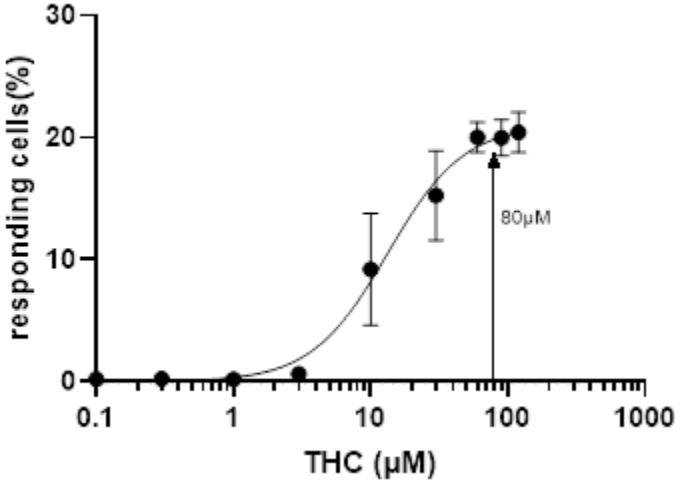

Supplementary Figures 2. Dose-response effects of THC in healthy RBCs. The curve shows the percentage of responding cells in response to different concentrations of Δ^9THC after 1 minute of incubation. (N=4).

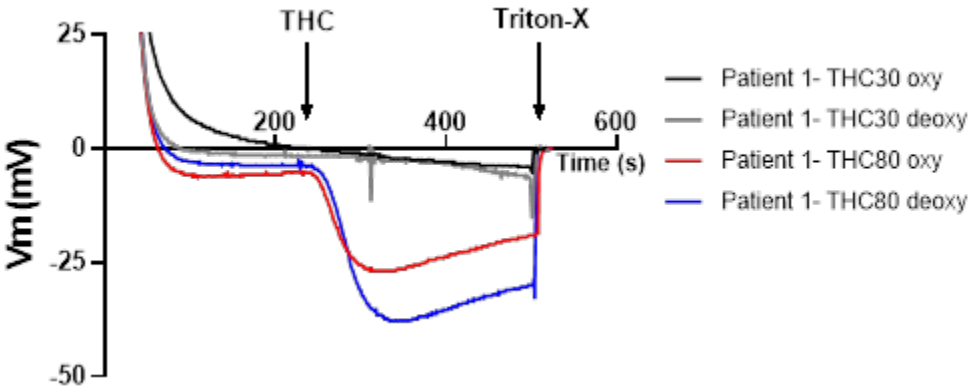

Supplementary Figures 3.MBE traces from a random patient under different THC concentrations in oxygenated and deoxygenated conditions.

2. Unpublished results

THC is one of the chemicals commonly dissolved in ethanol. Therefore, we did control experiments to make sure that the effects were due to THC only. Indeed, ethanol was not able to trigger any hyperpolarization, unlike THC (Figure 49).

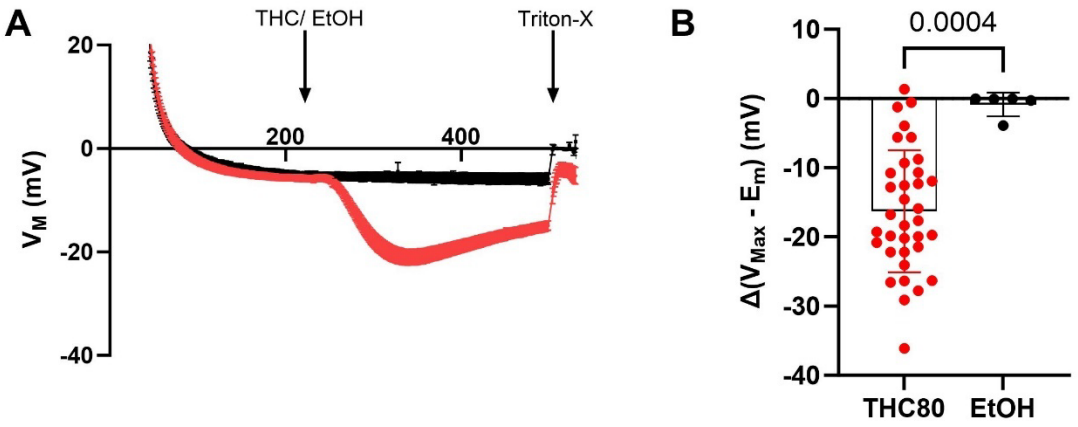

Figure 49: Ethanol has no effects on SS RBCs. A. Mean MBE ± SD traces of SS cells stimulated with THC (red trace, 80 µM, oxygenated condition n=35) or solvent (black trace, EtOH, oxygenated condition, n=5). B. Statistical comparison of changes in membrane potentials. Statistical test is unpaired t-test.

Experiments were done using 30 and 80 µM of THC. Only experiments with 80 µM THC were presented in the published manuscript. 30 µM was clearly sufficient to ensure calcium entry into the cells. However, we chose 80 µM because at this concentration we start to reach the plateau of responding cells for Ca^{2+} measurement by flow cytometry (Suppl. Figure 2). Second, the results were more variable when it came to measuring membrane potential variations, where we should remember that this is an indirect effect that we record through the development of the hyperpolarization generated by the activation of the Gárdos channel. Thus, we could detect a higher TRPV2 activation in response to THC using 80 µM (Suppl. Figure 3). Below are the results of the experiments with 30 µM THC. As we can see in Figure 50, Ca^{2+} influx measurements by flow cytometry results at 30 µM THC (panels A and B) were comparable to the results obtained at 80 µM. Same for MBE experiments, the only significant difference was between oxygenated and deoxygenated sickle RBCs (Figure 50C). Finally, using the patch-clamp technique, a significant difference was recorded in sickle cells at positive voltages (panel D, SS (+)) but not at negative voltages (panel D, SS (-)), indicating that the activation of TRPV2 induced an increase in the outward currents, probably due to Gárdos channel activation, only in SS RBCs (Figure 50D).

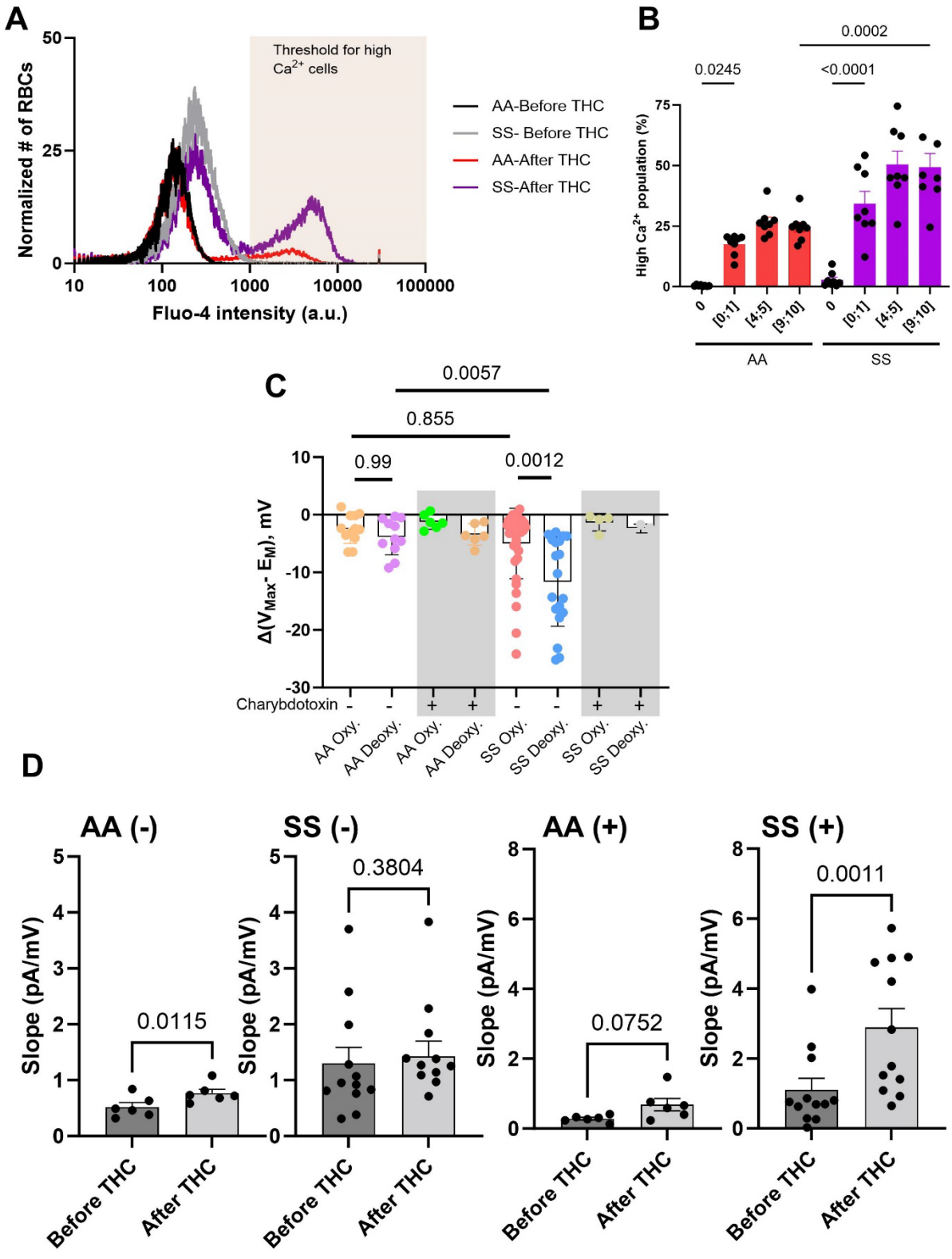

Figure 50: TRPV2 evaluation using THC at 30 µM. (A-B) Flow cytometry results A. Normalized representative curve of SS and AA cells before and after stimulation with THC. B. Statistical

comparison in time of calcium entry in both AA and SS cells. Statistical test is one-way-ANOVA (C) Statistical comparison of the hyperpolarization magnitudes reached at different conditions with and without inhibiting the Gárdos channel with charybdotoxin. N = 12 for AA oxygenated cells, N = 11 for AA deoxygenated cells, N = 6 for AA oxygenated cells with charybdotoxin, and N = 6 for AA deoxygenated cells with charybdotoxin; N = 33 for SS oxygenated cells, N = 19 for SS deoxygenated cells, N = 4 for SS oxygenated cells with charybdotoxin, and N = 3 for SS deoxygenated cells with charybdotoxin. Statistical difference was assessed using one-way ANOVA. (D) Slope comparison of patch-clamp recordings of positive voltages (+; between +80 and +100 mV), and negative voltages (-; between -80 and -100 mV) in AA cells (n=6), and SS cells (n=12). A paired t-test to attest statistical differences.

III. Chapter discussion and conclusion

In this chapter, we illustrated the roles of two different non-selective cation channels in the manifestation of Sickle Cell Disease. We demonstrated that both PIEZO1 and TRPV2 channels could be key players in the characteristic increased cation permeability in sickle cells.

We showed that the activation of PIEZO1 by Yoda1 induced a more pronounced activity of the Gárdos channel, probably with a more pronounced dehydration. Unfortunately, we didn't measure dehydration in this study. The extent of hyperpolarization reached after Gárdos channel activation, was correlated with the point of sickling (PoS) in sickle cells, showing that the activation of PIEZO1 augments the sickling propensity. Importantly, the inhibition of PIEZO1 by GsMTx-4 reversed this effect. The same study showed that HbSS RBCs have an increased activation of the Gárdos channel under deoxygenated conditions. This is a demonstration that the PIEZO1-KCNN4 tandem is overactivated in sickle cells, and is sensitive to the oxygenation state. This made us suggest that PIEZO1 could be involved in P_{Sickle} phenomenon. Going back to the MBE method, the recorded hyperpolarizations represent the average cell behavior. Here, the important heterogeneity of the HbSS RBC population may be the reason behind the exacerbated hyperpolarizations. HbSS RBCs have a higher fraction of young cells whose calcium content may differ from that of the oldest cells. This may explain why HbSS RBCs show more currents in deoxygenated conditions; these populations may have cells with a calcium content high enough to cross the activation threshold of the Gárdos channel more rapidly. This explanation could be the most valid, especially since in the NS309 (10 µM) without extracellular calcium (Figure 46), the difference cannot be attributed to a massive influx of calcium into the cells linked to deoxygenation, but rather to the variation in the age of the cell population in sickle blood.

In the second part of this chapter, we showed that the stimulation of TRPV2 by Δ^9-THC resulted in increased activity of the Gárdos channel in SS RBCs compared to healthy RBCs. In addition, we showed that TRPV2 activity in SS RBCs was oxygenation-sensitive, which made us recall to the activation of P_{Sickle} in hypoxic conditions.

Both PIEZO1 and TRPV2 are mechanosensitive, non-selective cation channels in the RBC membrane. We demonstrated that they could potentially be overactivated in HbSS RBCs. Once triggered, their activities were exacerbated under deoxygenated conditions. This could be a clue that P_{Sickle} is a phenomenon involving several channels that act together and have a common effect. We cannot assert this hypothesis, especially because the experiments were often undirect; we manipulated the subsequent activation of the Gárdos channel rather than directly inhibiting TRPV2 or PIEZO1 themselves. Further molecular evidence is needed to establish the true identity of P_{Sickle}.

Chapter IV- Alectinib and RBCs

I. Foreword

Several recent reports in the literature indicate that the second-generation of ALK inhibitors, Alectinib, albeit highly efficient against non-small cell lung cancers (NSCLC), invariably induces subclinical hemolysis, which is presumably caused by acanthocytic deformation and splenic trapping of erythrocytes as observed during hematological follow-up post-treatment (Yuan et al., 2020; Kuzich et al., 2021). In this context, Dr. Wassim El Nemer, scientific director at EFS-Marseille, was contacted by oncologists, who wondered what could be the cause of such a systematic change in shape, which is usually associated with non-compensated anemia. Thus, on the assumption that there is a real possibility that the shape change originates from altered ion movements at the membrane, Dr. Wassim El Nemer suggested that we test this hypothesis.

II. Introduction

ALK inhibitors are anti-cancer drugs that target tumors with variations of anaplastic lymphoma kinase (ALK). They belong to the family of tyrosine kinase inhibitors, which act by inhibiting proteins implicated in the abnormal growth of tumor cells. The current approved ALK inhibitors work by binding to the ATP pocket of the abnormal concerned ALK protein to block its access to energy and deactivate it. Non-small cell lung cancers (NSCLCs) commonly exhibit ALK rearrangement. This category of cancer affects more particularly patients who never or lightly smoked, with adenocarcinoma histology, very young patients, and female patients. Thus, these high-risk populations are systematically tested for EML4-ALK translocations or mutations and treated with ALK inhibitors in the frame of personalized cancer therapy. Crizotinib constituted the first approved ALK inhibitor by the US Food and Drug Administration (FDA) and by the European Medicines Agency (EMA) with the only inconvenient that patients developed Crizotinib-resistance within the first 12 months. Alectinib is a highly selective ALK inhibitor that was shown to be active against Crizotinib-resistant cases. It demonstrated a safety profile and yielded a robust treatment response (Sullivan and Planchard, 2016).

As mentioned in the forewords, severe hemolytic anemia under treatment associated with reticulosis and shape changes (anisopoikilocytosis, spheroacanthocytosis, acanthocytosis) of

circulating RBCs is usually observed during treatment (Yuan et al., 2020; Kuzich et al., 2021; Kunz et al., 2022; Legland Ép Dejean et al., 2022; Misawa et al., 2023).

Thus, a series of samples from patients under Alectinib treatment were obtained to test the hypothesis that the shape change is associated with upregulated ion channel activity leading to dehydration and is involved in the rapid removal of RBCs from the circulation. In parallel, several tests were performed on normal RBC treated *in-vitro* to look for short and mid-term shape responses.

III. Results

A. RBCs from patients treated with Alectinib

Seven blood samples from patients treated with Alectinib were sent to Roscoff, systematically associated with a control sample. All the patients were treated with Alectinib for lung cancer and followed up at the Hospital of Marseille. Table 10 shows the date of withdrawal, the age of the patients, and the hematocrit on arrival to assess that the transportation of the samples did not induce any massive hemolysis.

Table 10: Summary about the received blood samples of patients treated with Alectinib (N.A. means not available).

Date	**Patient age**	**Hematocrit upon arrival of samples**
18/11/2022	6 years	Patient: 38.4% Control: 44.6%
09/01/2023	8 months	Patient: 36.5% Control: 43.9%
16/01/2023	33 years	Patient: 29.5% Control: 44.6%
06/02/2023	N. A.	Patient: 43.8% Control: 44%
15/02/2023	N. A.	Patient: 39.5% Control: 45.4%
19/05/2023	62 years	Patient: 42.85% Control: 46.97%
23/11/2023	63 years	N. A.

In order to simplify the chapter's organization, all experiments are shown with a representative experiment (one patient taken randomly among the 7 samples received).

Upon arrival, we measured the hematocrit of almost all the blood samples to ensure that there was no massive hemolysis during transport, and to compare these values with those obtained during the hospital visit of the patient at the time of sampling. No specific hemolysis linked to transportation was observed. However, the hematocrit of the patient samples was systematically lower than that of to the control (n=6, p=0.013) (Figure 51).

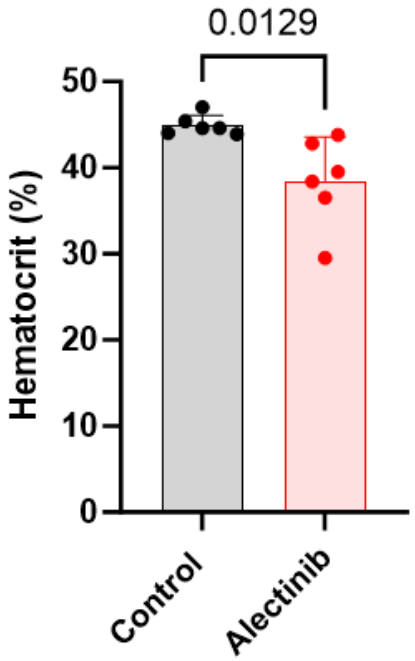

Figure 51: Hematocrit of control cells and Alectinib-treated patient cells. Statistical difference was assessed using the unpaired t-test.

1. **Cell imaging, and morphological characterization**

Live images obtained on fresh cells suspended in NECM-BSA medium showed a large number of cells with abnormal shapes compared to the discocytes observed in the control sample (Figure 52). The population of patient RBCs presents a significant number of echinocytes and acanthocytes (> 70%).

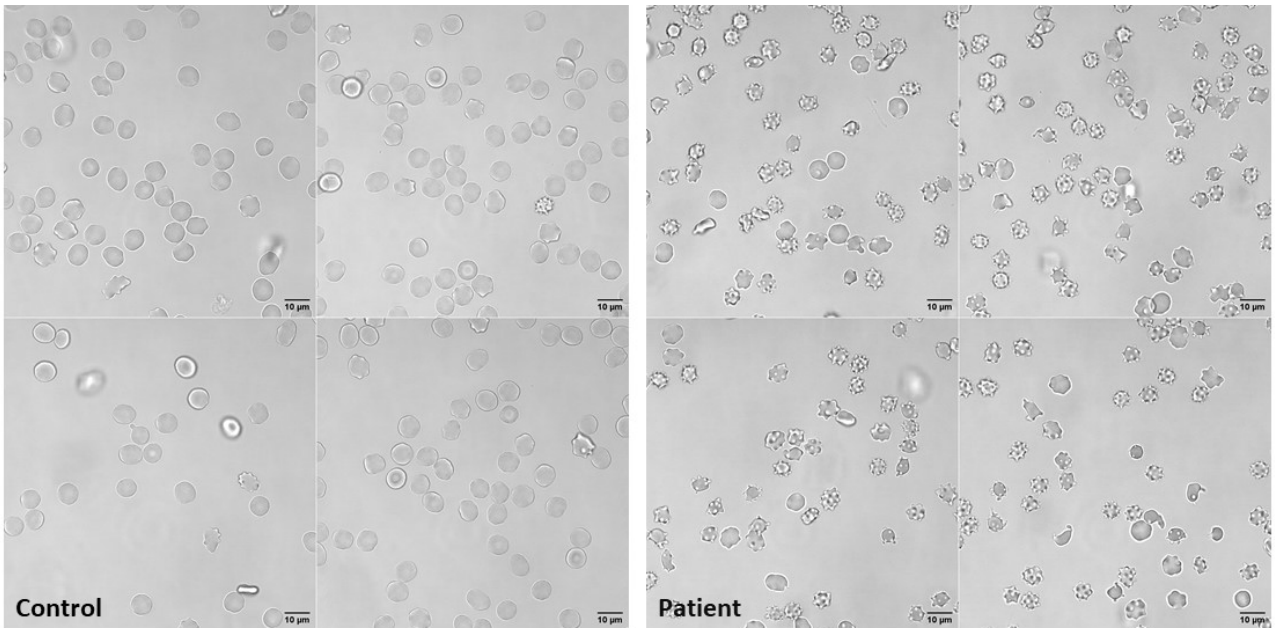

Figure 52: Brightfield images of RBCs from control and Alectinib-treated patient upon arrival (received the 23/11/2023). The left panel is 4 random fields from control cells and the right panel corresponds to 4 random fields obtained on patient cells. Cells were suspended in NECM-BSA and images were taken of cells on polylysine-coated coverslips.

Morphometric analyses realized on fixed smears (Figure 53) confirmed this observation, with almost the entire population of patient cells showing echinocytosis/acanthocytosis. However, it must be considered that smears and fixation can profoundly modify the morphology, worsening the results obtained in live imaging (Simionato et al., 2021).

In this case, it would have been judicious to check the number of cells/mL, as the hematocrit is a volume estimate.

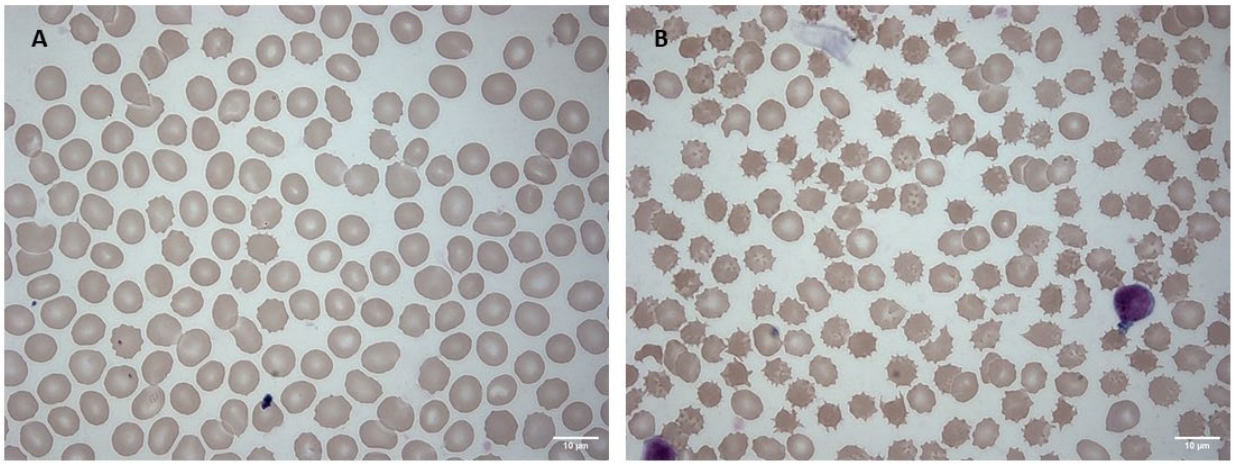

Figure 53: Blood smears fixed with methanol and stained with Giemsa coloration of control and Alectinib-treated patient cells on arrival. (A) control blood and the (B) patient blood.

The morphological analysis confirms the observations made on live cells or initial observation of smears. The projected surface area is significantly reduced in patient cells (e.g. patient received on 18/11/2022). (Figure 54A) (32.5 µm² ± 5.3 vs 38.4 µm² ± 4.6, n= 1519 and 1510, respectively). This apparent cell shrinkage is associated with a considerable number of abnormal shapes, as shown by the spread of points on the cell circularity graphic (Figure 54B).

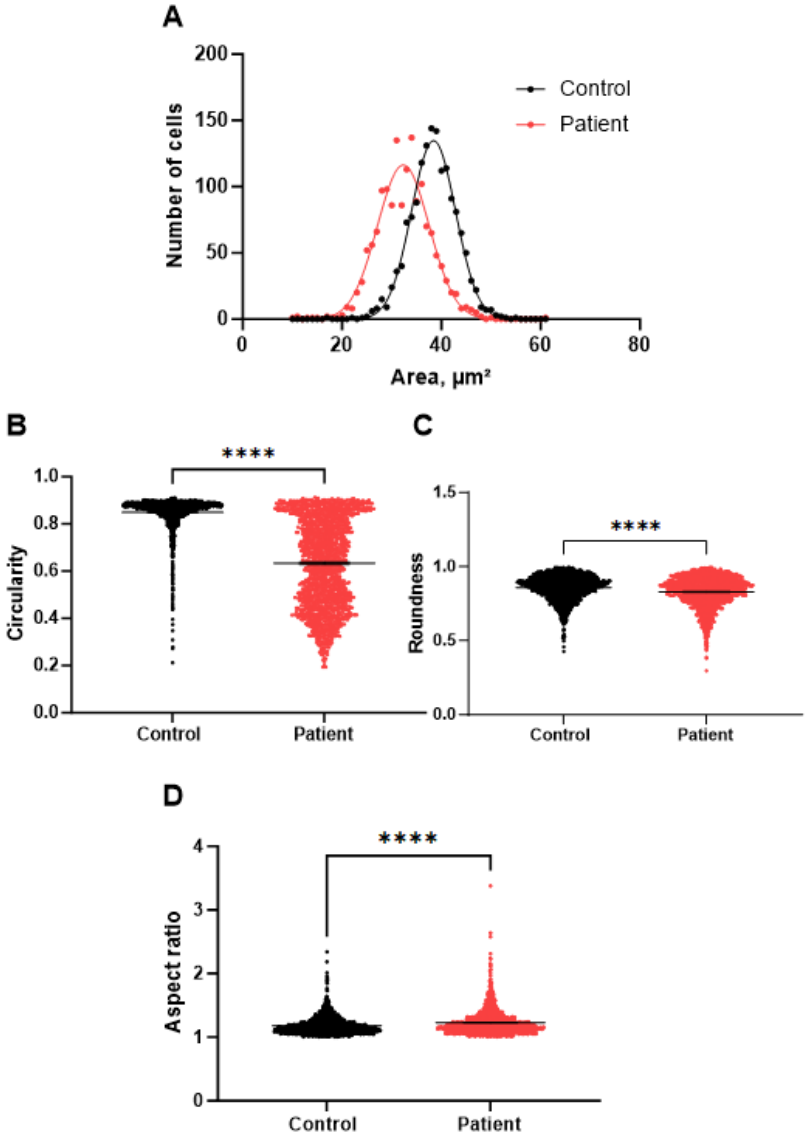

Figure 54: Morphological characteristics of RBCs from one patient (received 18/11/2022) treated with Alectinib. Comparison between control (black) and patient (red) of the projected area (A), circularity (B), roundness (C), and aspect ratio (D). Statistical difference was assessed using the unpaired t-test. **** p<0.0001 Control cell n=1510, Patient cells n=1519).

2. Membrane potential monitoring with MBE method

To determine whether the cell shrinkage is accompanied by a massive efflux of K^+ and Cl^-, enhanced after Alectinib treatment, channel activity was challenged using the MBE method. First, PIEZO1 was stimulated by promoting its activity with Yoda1 (625 nM) (Figure 55A). The hyperpolarization induced by Yoda1 reached a higher hyperpolarization magnitude in patient cells compared to control cells (6 out of 7 samples) (Figure 55A). Knowing that Yoda1 stimulates Ca^{2+} entry through PIEZO1, this indicates that a faster and/or stronger Ca^{2+} entry occurred, or that Gárdos channel has an increased sensitivity to Ca^{2+}. The speed of hyperpolarization is similar between control and patients. Due to the extended hyperpolarization, K^+ efflux probably lasts longer.

The shift in the Ca^{2+} sensitivity of the Gárdos channels with NS309 (Figure 55B,D) shows that when this compound is used at 100 µM with a low extracellular calcium concentration (0 mM) or at 10 µM with a physiological calcium concentration (2 mM), larger hyperpolarizations develop (6 out of 7 samples), indicating that the intracellular calcium concentration is certainly higher in the patient cells compared to control cells, albeit a higher Ca^{2+} sensitivity of patient Gárdos channel cannot be ruled out.

However, as mentioned above, shrinkage upon Gárdos channel activation or any K^+ efflux implies an additional chloride efflux. In RBCs, this is usually considered to be rate-limiting. To test the contribution of Cl^- to the observed phenomenon, cells were treated just before experiment (1-2 min) with 10 µM of NS3623 (Bennekou et al., 2001, 2003). Contrary to previous observations, patient and control cells responded similarly upon inhibiting the chloride conductance, using NS3623. With a chloride conductance inhibited by more than 98% at this concentration, this would indicate that the difference of hyperpolarization extent obtained without NS3623 is probably due to a change in chloride conductance, with patient cells having an overall reduced nominal anionic permeability. This was confirmed when we induced the hyperpolarization with A23187, a Ca^{2+} ionophore that causes a maximal Gárdos channel activation; patient cells reached the same magnitude of hyperpolarization with and without NS3623, contrary to the control cells in which the inhibition of chloride conductance, generated a bigger hyperpolarization (Figure 55E).

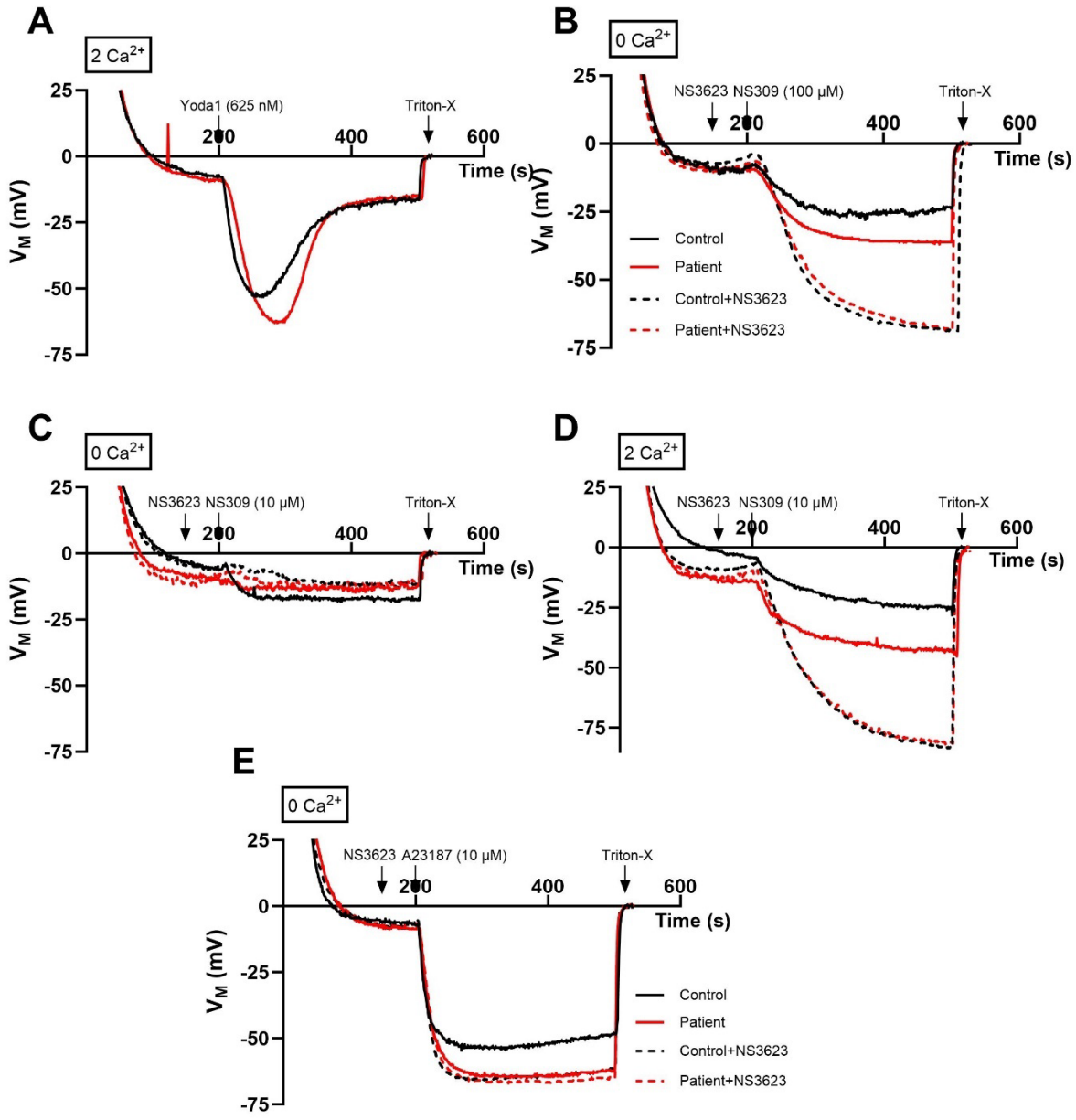

Figure 55: Representative MBE traces of a patient treated with Alectinib. (A) in response to Yoda1 (625 nM) with 2 mM of Ca^{2+} in the media, (B) NS309 (100 µM) without Ca^{2+} in the medium, (C) NS309 (10 µM) without Ca^{2+} in the media, (D) NS309 (10 µM) with 2 mM of Ca^{2+} in the medium, and (E) with A23187 (10 µM) without Ca^{2+} in the media. Patients are represented in red and controls in black. The solid lines represent experiments performed without NS3623 in the extracellular media, and the dashed lines represent experiments with NS3623 (10 µM) in the extracellular media.

To summarize this experimental part, we statistically compared the difference in the magnitude of hyperpolarization between control and patients using different hyperpolarizing molecules (Figure 56). Indeed, as shown in the representative graphics (Figure 55), patient cells showed higher hyperpolarizations in almost all cases (6 out of 7 patients). In Figure 56 below, the red points

represent an outlier patient sample among the seven we have tested (15/02/2023). The corresponding values of this sample were excluded from the statistical test. Unfortunately, experiments with NS3623 were not performed on all patients, so we did not include statistics with the NS3623 part.

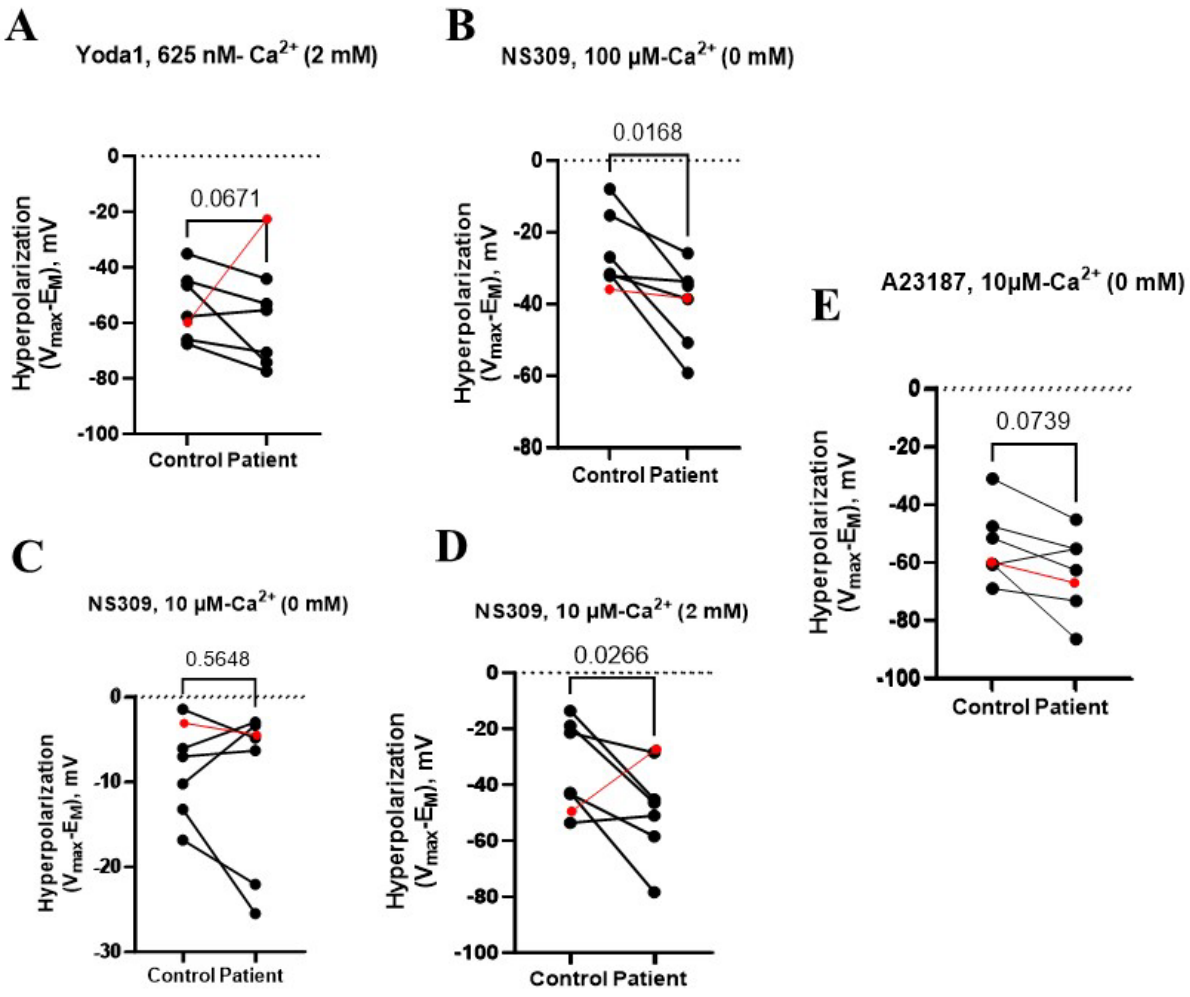

Figure 56: Membrane potential variations of Alectinib-treated patients. (A) in response to Yoda1 (625 nM) with 2 mM of Ca^{2+} in the medium, (B) NS309 (100 µM) without Ca^{2+} in the medium, (C) NS309 (10 µM) without Ca^{2+} in the medium, (D) NS309 (10 µM) with 2 mM of Ca^{2+} in the medium, and (E) with A23187 (10 µM) without Ca^{2+} in the medium. Only one patient was excluded. Statistical differences are assessed by paired t-test, n=6. The red points correspond to values obtained with the outlier patient (15/02/2023), and were not included in the statistics.

3. Ca^{2+} imaging

To determine whether the change in Ca^{2+} permeability leads to a massive efflux of K^+ and Cl^- is the reason for the enhanced hyperpolarizations observed in the MBE method, we tested the intracellular Ca^{2+} content in each condition to understand whether Alectinib acts by inducing a Ca^{2+} entry. Curiously, patient red cells treated with Alectinib were less loaded with Ca^{2+} than control RBCs (Figure 57). This result indicates that the shape changes, greater hyperpolarizations, and altered ion content, were not seemingly due to an Alectinib-induced Ca^{2+} entry.

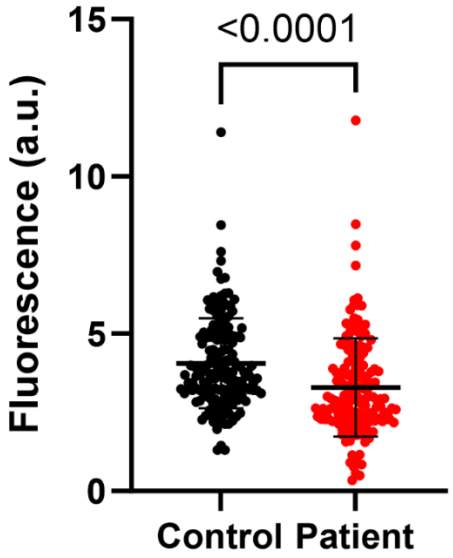

Figure 57: Ca^{2+} imaging of control and patient red cells (received 16/01/2023). Fluorescence measurement of control and patient RBCs, stained with Fluo-4. Values are represented as means ± SD. Statistical differences were assessed using an unpaired t-test.

4. Intracellular content of water, Na+, and K+

Previous experiments clearly show that treatment with Alectinib affects not only shape but also, probably directly or indirectly, membrane transport.

To determine whether the alteration in shape is accompanied by an alteration in the water status of the cells, measurements of water content combined with measurements of intracellular Na^+ and K^+ concentrations were performed. Given that the cells were not always transported under the same conditions (duration), it is difficult to average the water, K^+, and Na^+ content parameters.

Figure 58 shows all the results obtained from the 7 patient samples received to date. 4 out of 7 patient samples showed pronounced dehydration, in line with what had been concluded from the morphometric analyses (Figure 54). Surprisingly, the three others were slightly overhydrated compared to control cells. Measurements of intracellular Na^+ and K^+ content, expressed here as concentration, show a lowering trend in intracellular Na^+ and a constant or even slightly higher intracellular potassium concentration.

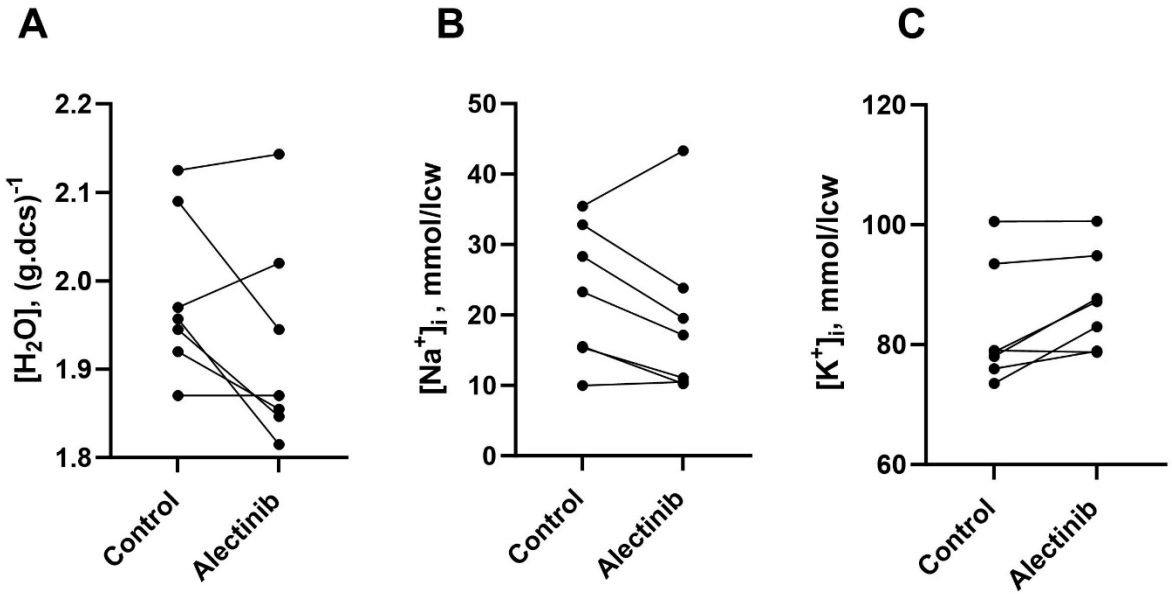

Figure 58: Intracellular water content, Na^+, and K^+ in Alectinib-treated patients (A) Water content, (B) intracellular Na^+ content, and (C) intracellular K^+ content. Each pair belongs to a patient and the control sent in the same date.

B. ***In-vitro* effects of Alectinib on healthy RBCs**

Due to the dramatic shape changes observed in patients treated with Alectinib, it was important to understand whether these shape-changing effects are rapid or develop gradually over time. To determine this, we performed a series of experiments in which we incubated normal RBCs *in vitro* with Alectinib.

1. Cell imaging

While incubation of cells with DMSO (control vehicle) for 60 minutes does not alter RBCs shape, Alectinib (300 nM or 1 μM) induced echinocyte formation in less than 5 minutes in a dose- and time-dependent manner (Figure 59). These concentrations were chosen because Alectinib is usually given to patients twice a day at doses ranging between 141-1944 ng/mL (292-4028 nM) for each administration (Groenland et al., 2021).

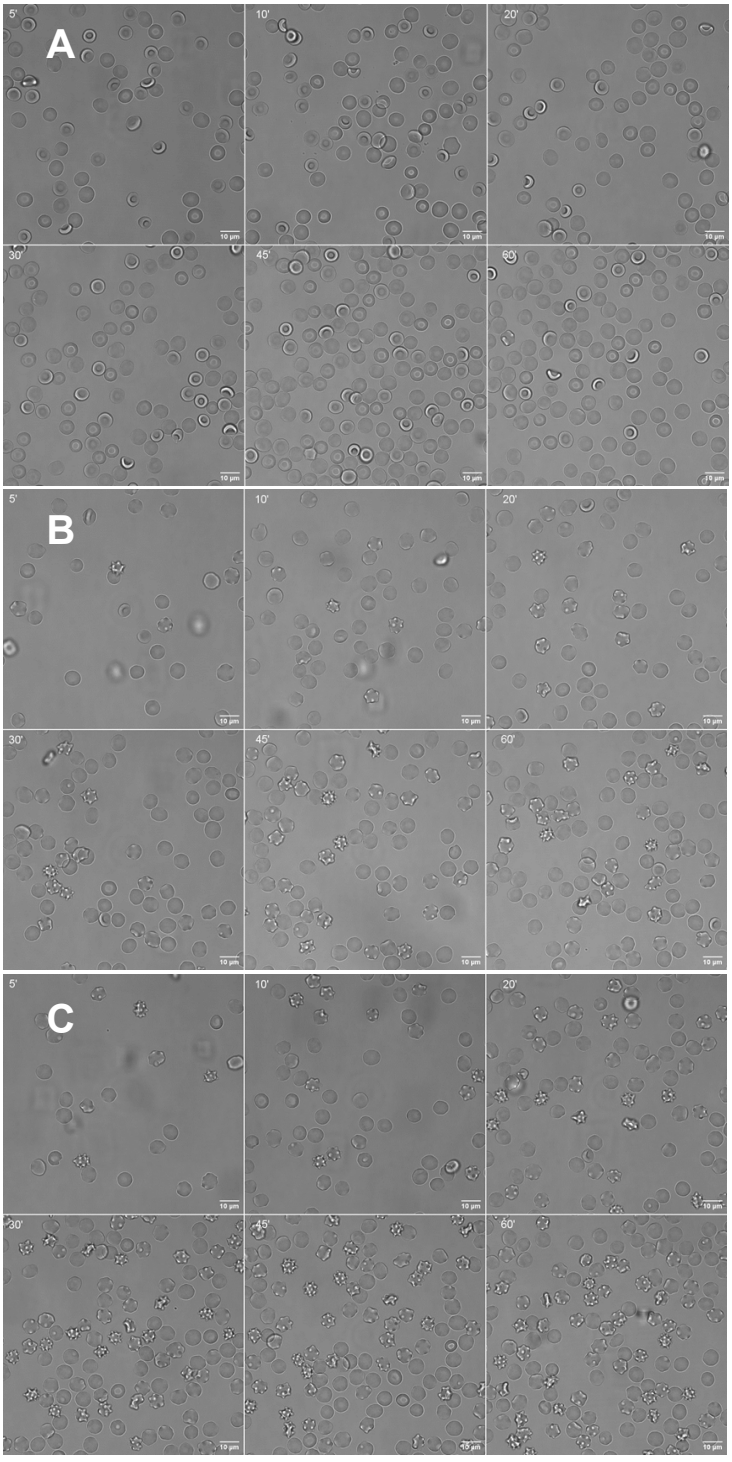

Figure 59: Brightfield images of normal RBCs perfused with (A) DMSO, (B) Alectinib (300 nM), and (C) Alectinib (1 µM) for 1 hour, in NECM-BSA. Alectinib/DMSO were perfused at 0'.

2. Intracellular content of water, Na^+, and K^+

To determine whether this alteration in shape was accompanied by drastic changes in the water and ionic status of the RBCs, the cells were incubated in their autologous plasma for 15 minutes, 24 H, and 48 H in the presence or absence of Alectinib. Similar to cells from patients treated with Alectinib, cells treated *in vitro* with Alectinib (10 µM) showed a similar water content as cells treated with DMSO (control vehicle), but a drastic decrease in Na^+ and K^+ content after 15 mins and 24 hours of exposure to Alectinib.

The experiment was extended to 48 hours, at which point there was no difference, but this provides us with important information because it is likely that at 48 hours the cells, including the control cells, are in a state of energetic exhaustion (Figure 60).

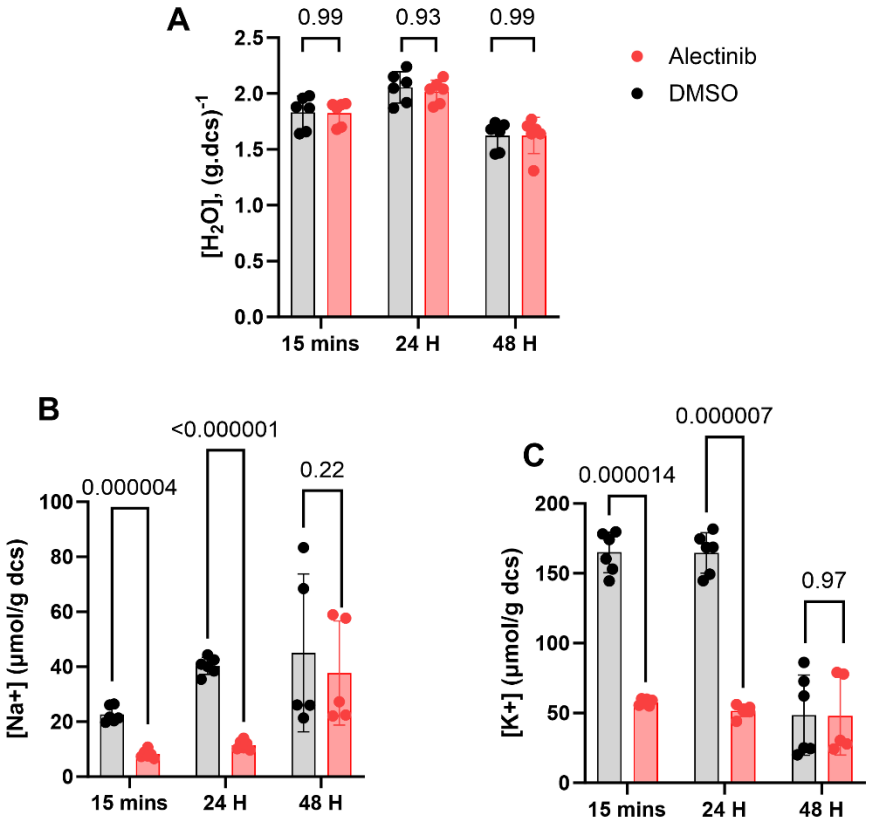

Figure 60: Comparison of intracellular water, Na^+, and K^+ contents of healthy cells treated with 10 µM Alectinib (in red) or DMSO (in black) for 15 mins, 24H, and 48H. (A) Water content, (B) intracellular Na^+ content, and (C) intracellular K^+ content. n=5 in all cases. Statistical comparison was assessed using a multiple unpaired t-test.

3. Membrane potential monitoring with MBE method

Consistent with what we observed on patient cells, stimulation with NS309 of cells incubated with Alectinib developed a more pronounced hyperpolarization than the one incubated with DMSO (control vehicle) or Crizotinib, another inhibitor of ALK, a first generation that does not affect RBC shape or lead to blood anemia side effect (Figure 61).

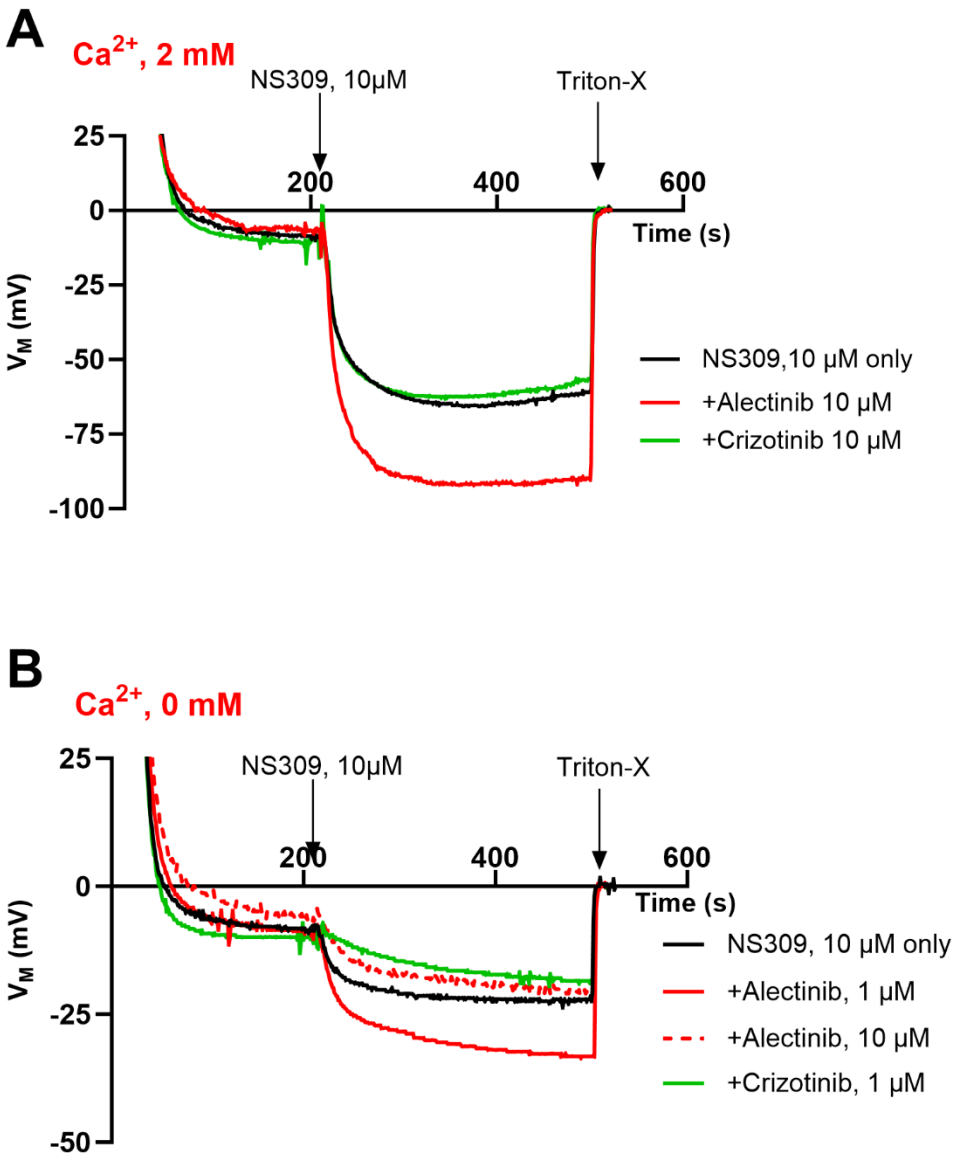

Figure 61: MBE experiments on healthy RBCs pre-treated with Alectinib or Crizotinib for 15 minutes. The used hyperpolarizing molecule is NS309, 10 µM with or without 2mM of Ca^{2+} in the extracellular media (Ca^{2+}, 2 mM and Ca^{2+}, 0 mM respectively).

4. Ca^{2+} imaging

Treatment of RBCs with Alectinib (1 µM) did not alter the Ca^{2+} content compared to RBCs treated with DMSO only (Figure 62).

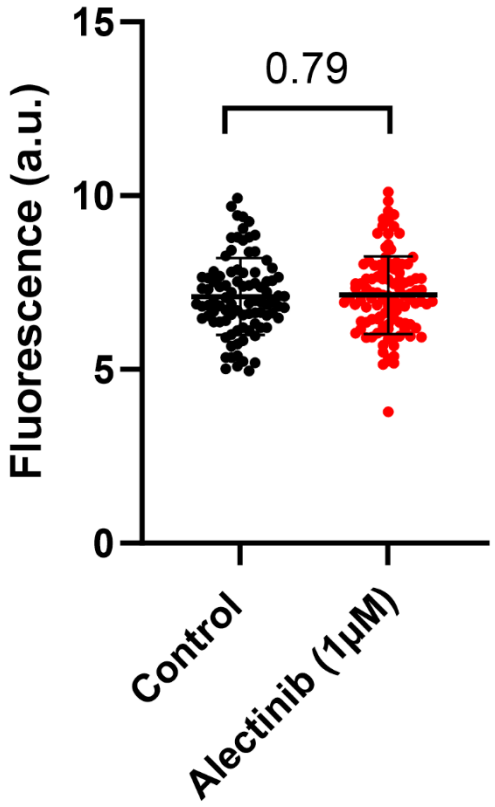

Figure 62: Ca^{2+} imaging of control and healthy RBCs treated with Alectinib. Fluorescence of control cells (treated with DMSO) and healthy RBCs treated with Alectinib (1 µM) for 20 minutes. Values are represented as means ± SD. Statistical differences were assessed using an unpaired t-test.

C. **Results summary**

In Table 11 below, we summarized the main findings we obtained in different parts of this study. RBCs from patients treated with Alectinib were in general dehydrated, with smaller area and shape alteration (mainly acanthocytes). In addition, RBCs from patients treated with Alectinib showed a decreased content of Na^+ and an increased content of K^+, with higher hyperpolarization magnitudes in response to various hyperpolarizing molecules. The discrepancy between the results obtained from RBCs of patients treated with Alectinib and healthy RBCs exposed to Alectinib suggests that the method of exposing cells to compounds to mimic the effects of that compound, may not be the best approach.

Table 11: Summary comparison of RBCs from patients treated with Alectinib and healthy RBC treated with Alectinib (responses are judged compared to control).

	RBCs from Alectinib-treated patient	**Healthy RBCs treated with Alectinib**
Hematocrit	Systematically lower	*Not measured*
Water content	4/7 dehydrated	No effect (10 µM, over 48H)
Na^+ content	Mainly slight decrease	Huge decrease (10 µM, from 15 min)
K^+ content	Stable or slight increase	Huge decrease (10 µM, from 15 min)
Ca^{2+} content	Slightly lower than control	No effect (1 µM)
Morphology	Majority of acanthocytes	Many acanthocytes (from 300 nM, 1H treatment)
Surface area	Smaller	*Not measured*
Circularity	Smaller (acanthocytes)	*Not measured*
Roundness	Slightly smaller	*Not measured*
Aspect ratio	Higher	*Not measured*
PIEZO1 stimulation (Yoda1, 625 nM)	Increased hyperpolarization	*Not measured*
Gárdos channel stimulation (NS309, 10 &100 µM)	Increased and longer hyperpolarization	Increased and longer hyperpolarization
Gárdos channel stimulation (A23187, 10 µM)	Increased and longer hyperpolarization (difference abolished with NS3623)	*Not measured*

IV. Discussion

The high percentage of echinocytes observed in confocal microscopy and blood smears (Figures 52-53) and the results obtained in morphological and electrophysiological studies are tightly linked (Figures 54-55).

Alectinib may act by increasing the permeability of the Gárdos channel in the membrane of RBCs *via* a mechanism still undefined. MBE results showed that Alectinib may make the Gárdos channel more sensitive to Ca^{2+}, and in this case, this could be an alteration that affects the role of calmodulin. Calcium levels might be sufficient to trigger vesiculation and PS exposure. Morphological studies could indicate that Alectinib induces alterations in the cytoskeleton and the cellular shape.

Nevertheless, the results obtained in the MBE method after the inhibition of the Cl^- permeability with NS3623 favors the hypothesis that Alectinib induces changes in the chloride permeability in RBCs; The same response of patient and control in response to Alectinib after hyperpolarization with A23187 (Figure 55E) could mean that the difference between patient and control cells differed only in their Cl^- conductance; control cells had a higher Cl^- conductance than patient cells.

Alectinib may alter the activity of Band 3, which would induce abnormalities in cell shape, notably microvesiculation and echinocyte formation, a reduced cell volume, and eventually hemolysis. Given this result, we thought that it could be important to test Band 3 functionality. Therefore, as part of EVIDENCE, I went to Marseille for a secondment to test Band 3 in RBCs exposed to Alectinib. I performed flow cytometry tests with EMA and BRIC6: BRIC6 is an antibody used to check the presence of Band 3 on the membrane of RBCs. The EMA (eosin 5-maleimide) test allows the investigation of the oligomeric state of Band 3 in the RBC membrane. Preliminary results show that the number of Band 3 as well as the level of oligomerization are similar between control and *in-vitro* RBCs exposed to Alectinib. Nevertheless, the stainings were not fully optimized and should be repeated on patient cells and *in-vitro* Alectinib-treated RBCs.

At the same time, our collaborators in Marseille conducted observations on patients treated with Alectinib: They tested the effects of Alectinib on late erythropoiesis by adding it *in-vitro* to CD34+ cells, undergoing erythroid differentiation. Their results showed that cell proliferation was strongly

inhibited, and the differentiation process was slowed down. This observation raised the question of whether the effect of Alectinib might also be central by affecting the erythropoiesis process.

V. Perspectives

As a next step, we are planning to test the functioning of the NaK pump with our collaborators in Marseille. In addition, further characterization of the cytoskeleton and Band 3 needs to be revisited. Considering that Alectinib is a kinase inhibitor, and of course quite selective, it cannot be excluded that some important phosphorylations are inhibited, thus threatening the stability of the membrane/cytoskeleton of patient RBCs. Thus, it would be very pertinent to realize a phosphoproteome of RBCs. Eventually, shape examinations have shown tremendously abnormal shapes, so it would interesting to i) determine the age of the cells to discover their exact lifespan and ii) to determine if these patients have a higher propensity to form exovesiculation leading to membrane loss and then increased sphericity, that comprise their survival within the circulation.

General Discussion and Conclusion

I. Discussion

The aims of the thesis, carried out as part of the ITN-MSCA EVIDENCE consortium, were to better characterize the role of cationic conductance pathways in erythrocytes under physiological and pathological conditions. As stated in the introduction of the thesis, at the beginning of this work, only two cation channels had been unambiguously identified in the membrane of red blood cells, namely the calcium-dependent potassium channel or Gárdos channel (Hoffman et al., 2003) and the PIEZO1 channel (Zarychanski et al., 2012). However, in 2021, the TRPV2 channel was added to the family of non-selective cation channels present and potentially active in this cell type (Belkacemi et al., 2021). Finally, despite the progress made in progenitor culture (Gautier et al., 2020), which makes it possible to avoid contamination by other cell types during these studies (Minetti et al., 2013), combined with transcriptomic (An et al., 2014) or proteomic studies (Gautier et al., 2016, 2018), today we have only a very fragmented picture of the role of channels in human red blood cell function. Indeed, numerous studies reported pharmacological or experimental evidence for cationic channels (mostly non-selective and permeable to Ca^{2+}), reviewed by Kaestner *et al.* 2020 (Kaestner et al., 2020).

In this context, the studies carried out focused on the three formally identified channels: the Gárdos channel, the PIEZO1 channel, and the TRPV2 channel. Given the deformability of erythrocytes, not only in the capillaries (Cahalan et al., 2015) but also during splenic filtration (Deplaine et al., 2011), it is clear that a channel such as PIEZO1, with its proven intrinsic mechanosensitive properties (Wang and Xiao, 2018), is a prime target for this study. Indeed, RBCs have unique membrane and cytoskeletal properties that allow them to withstand enormous shear stress through deformation: a high surface-area-to-volume ratio, their membrane having the highest cholesterol/lipid ratio of any biological membrane (Subczynski et al., 2017), and a submembranous network of cytoskeleton connecting filaments to transmembrane proteins (Fowler, 2013). These elements confer to the RBCs the deformability property that allows them to flow and bend into the narrowest capillaries.

Our initial finding that Dooku1 can activate, rather than just inhibit, the effects of Yoda1 (Evans et al., 2018) is certainly based on these unique properties of RBCs and their membrane environment. However, only three molecules are recognized for their ability to block mechano-sensitive channels or mechano-transduction signalling: gadolinium and other trivalent lanthanides, ruthenium red, and the spider toxin GsMTx-4. Although not yet fully understood, the acknowledged mode of action of these three compounds is more directly related to their effects on the membrane than actually on the transporters themselves. Recent studies suggest that these molecules compromise the membrane by increasing its modulus, which indicates that the membrane becomes more rigid (Reyes-Pardo and Sánchez-Herrera, 2019). These compounds act through different mechanisms and in a non-specific manner, each showing a preference for a specific cell subpopulation, depending on their cell size. More interestingly, even GsMTx-4 does not interfere with the channel itself but alters the membrane properties through its insertion into the membrane (Gnanasambandam et al., 2017). In this sense, the first chapter of this thesis highlighted the need for a new and specific inhibitor of PIEZO1.

In terms of the properties conferred by the erythrocyte membrane, membrane proteins and membrane lipids interact in a complex and reciprocal biophysical manner: membrane proteins can exert a force on the lipid bilayer, generating local curvatures depending on their hydrophobic surface. To counteract this effect, lipids in the bilayer can exert a force on the membrane protein (Lee, 2004; Andersen and Koeppe, 2007) and can interact at various levels with the proteins present in the membrane (Brown, 2017). Lipids constitute an important part of membrane composition, and the lipid composition of each membrane differs depending on the function of that membrane (Harayama and Riezman, 2018). As explained in the introduction, lipids influence the activity of membrane transporters. For example, the activity of the NaK-ATPase pump in rat RBCs is strictly dependent on the fatty acid composition of the membrane (Bloj et al., 1973). In another cell type, HEK 293, which expresses the rat serotonin transporter-1, the activity of this transporter was reduced after cholesterol depletion. In contrast, cholesterol replenishment restored the activity of this transporter (Scanlon et al., 2001). The effect of cholesterol on the activity of ion channels and transporters is complex (Stieger et al., 2021). In an important finding, Ridone and colleagues demonstrated that PIEZO1 forms clusters in the plasma membrane whose size and density are reduced upon cholesterol depletion (Ridone et al., 2020). This finding assesses that cholesterol controls the organization of PIEZO1 clusters in the membrane, which was expected

knowing that PIEZO1 is activated *via* a force-from-lipid procedure (Cox et al., 2016; Syeda et al., 2016), suggesting that blades and helical beams of PIEZO1 may transfer mechanical forces from lipids to the pore via a lever-like mechanism (Wang et al., 2018). This paradigm suggests that the ion channel is gated by mechanical perturbations in the surrounding lipid layer (Teng et al., 2015). This "force-from-lipid" is not the only gating mechanism proposed to activate the mechanosensitive channels; the "force-from-filament" also known as "force-from-tether", is the other model that suggests that the gating of mechanosensitive channels occurs through a tether that directly or indirectly connects the channel to the cytoskeleton or the cytoskeleton-associated proteins that transmit the force and activate the mechanosensitive channels (Ranade et al., 2015; Zhang et al., 2015; Chuang and Chen, 2022). For example, the "force-from-filament" activation PIEZO1, happens via Matrigel or collagen IV- mediated pulling force (Gaub and Müller, 2017) and through sensitization by non-muscle myosin II-dependent actin contractility (Bavi et al., 2019). The first finding by Gaud and Muller demonstrates that the extracellular elements are important for mechanical activation of PIEZO1, and the second finding by Bavi proves that force from substrate deflection, which affects membrane tension and cytoskeletal stress, is crucial for PIEZO1 activation. Such behavior may also explain why in some pathologies not associated with any mutation in PIEZO1, cation leak and thus alteration of the ion gradient is observed. Indeed, PIEZO1 channel adopts a non-uniform distribution on the red blood cell surface, with a bias towards the biconcave "dimple" (Božič and Svetina, 2022; Vaisey et al., 2022).

Nevertheless, both the "force-from-lipid" and "force-from-filament" paradigms are valid, and they probably work in concert to ensure the opening of mechanosensitive channels such as PIEZO1 (Cox et al., 2019). This was equally suggested by a recent study that claims that PIEZO1 clusters increase in abundance in regions of higher membrane tension and lower curvature, and interact with the spectrin cytoskeleton in both resting and activated states, demonstrating a link between plasma membrane tension gradients, curvature, and the cytoskeleton (Dumitru et al., 2021). In PIEZO1, the interaction of surrounding lipids and cytoskeletal elements with the channel itself is revealed by the protein stomatin-like protein 3 (STOML3), which is one of the proteins associated with PIEZO1 and lowers its activation threshold (Poole et al., 2014). Cholesterol could act at the level of this protein to modulate the activity of the channel (Short, 2020). The importance of the surrounding medium is clearly exemplified in the recent work of Yamaguchi et al. in 2021 (Yamaguchi et al., 2021), which shows that although RBCs with PIEZO1 mutations exhibited a

dehydrated phenotype, the activity of V598M, F681S or R808Q in response to stretch was not significantly different from that of WT channels when expressed in the HEK293 cell line.

Studying the effects of cholesterol on channel physiology seemed fundamental because this molecule stiffens and thickens biological membranes. During my Ph.D., we attempted to alter membrane cholesterol content using methyl-β-cyclodextrin (MBCD). Our primary results showed that incubation of cells with MBCD led to an enhancement of cellular hyperpolarization in response to Yoda1, 100 nM (Figure 63A). However, the results were variable and not homogeneous (Figure 63B). We believe that this is mainly due to our lack of expertise in this area. In fact, MBCD is supposed to deplete the membrane from cholesterol, but we did not check the efficacy of such a depletion. Knowing the importance of phospholipid membrane dynamics at the red blood cell membrane, it would be relevant to address this caveat in our experiments. Indeed, there are four stable submicrometric lipid domains enriched in either cholesterol, sphingomyelin, ganglioside 1, or phosphatidylcholine in RBCs (Conrard et al., 2018). Their distribution across the membrane corresponds to a specific area of curvature and may play a role in the ability of PIEZO1 to be activated. More attention should be paid to these elements in the coming years, especially since the distribution of PIEZO1 channels on the membrane is not at all random, with a preferential distribution at the rim (Vaisey et al., 2022).

In general, cholesterol depletion using MBCD is known to slow the activation and the inactivation of PIEZO1 in response to mechanical force by decreasing its pressure sensitivity (Short, 2020). Our results differ from what is commonly known in the literature about MBCD in terms of slowing down the activation but are consistent with the idea that MBCD slows the inactivation process. Cholesterol depletion alters the viscoelastic properties of the membrane; cholesterol forms links between PIEZO1 clusters, making their activation easier and faster; when cholesterol is depleted from the membrane, connections and synchronization between PIEZO1 clusters are disrupted resulting in slower activation and inactivation (Short, 2020).

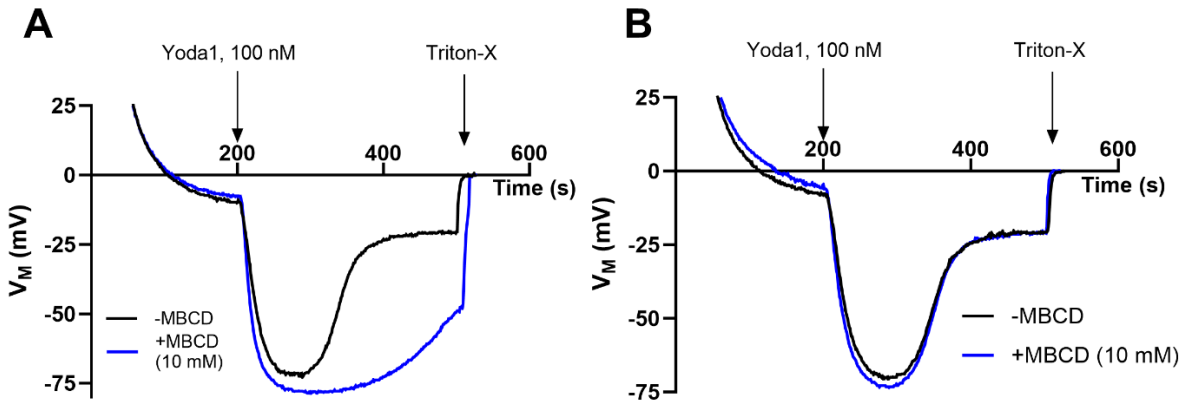

Figure 63: Depletion of cholesterol from healthy RBCs using MBCD. (A) An experiment where MBCD enhanced the hyperpolarization in response to Yoda1 (100 nM). (B) An experiment where the pre-incubation with MBCD didn't cause any change to hyperpolarization magnitude caused by MBCD. Traces in blue represent experiments where RBCs were preincubated with MBCD (10 mM) for 30 mins at 37°C. Traces in black represent control experiments, where cells that are not preincubated with MBCD where challenged with Yoda1, 100 nM. The experimental media was Ringer solution supplemented with 2 mM of Ca^{2+}.

Cholesterol depletion from membranes shares a common consequence with the gain-of-function mutations of the PIEZO1 channel in the patient cells: PIEZO1 gain-of-function mutations leading to xerocytosis are characterized by a delayed inactivation of the channel, just as cholesterol depletion enhances this slow inactivation in mutant PIEZO1 cases (Ridone et al., 2020). In addition, a recent study showed that several cases of hereditary spherocytosis (HS), caused mainly by mutations in membrane and cytoskeletal proteins such as Band 3, Ankyrin, Spectrin A and B, and protein 4.2, all show an increase in cation permeability due to PIEZO1 activation (Vandorpe et al., 2021a). This strongly suggests that PIEZO1 (if PIEZO1 is the sole channel responsible for this apparent cation leak) mediates or contributes significantly to the increased cation permeability in HS RBCs. Of note, in an interesting publication, Bruce *et al.* showed in a study involving 11 pedigrees that when the Band 3 protein undergoes substitution mutations, it is converted from an anion exchanger to an unregulated cation channel (Bruce et al., 2005). This observation was further modeled to understand how mutations in the Band 3 helices lead to the transformation of an anion exchanger into a leaky cation channel, permeable to Na^+ and K^+ (Barneaud-Rocca et al., 2013). Chapter II, which deals with variants of PIEZO1 or Gárdos channels sent by clinicians, reinforces the idea of the need to establish a systematic functional experimental repertoire to study and understand all the mutations discovered thanks to genetic approaches. In fact, the variants of

unknown significance (VUS) predicted *in silico* could be benign and have no effect on the proteins. This makes diagnosis by functional assays mandatory to understand each mutation individually (Kaestner and Bianchi, 2020). Furthermore, as we saw in Chapter II, these uncharacterized mutations were often associated with other complications in the patients themselves or in their families. In such cases, the initially benign mutation could be aggravated by its association with other diseases, such as β-thalassemia, SCD, etc., but also with mutations in the heterozygous state that are normally asymptomatic or without consequence. Obviously, these carriers of multiple mutations deserve very special attention. Although they are not currently associated with any role in the structure or stability of the red cell membrane, ion channels, despite their limited number, play a role because of their transmembrane properties. Furthermore, it is noteworthy that PIEZO1 is expressed in several tissues of the body, and not only in RBCs (Murthy et al., 2017). Interestingly, the only symptom these patients had was anemia, showing that in these cases, gain-of-function mutations in PIEZO1 had deleterious effects only on RBCs, emphasizing the idea of the uniqueness of RBCs and that they should be considered separately in any study, as said in Chapter I.

As a solution to Chapter II, we suggest that each case should be carefully studied separately, taking into account the family's history of diseases. Functional studies should preferably be performed immediately on fresh blood withdrawn from the patient and the close relatives. Our work has shown that phenotypic and electrophysiological tests could be used as functional tests after variant discovery as a functional validation strategy of the discovered VUS. Genetic tools and big data (NGS, proteomics…) do not allow to study of the activity of the discovered ion channels. Otherwise, functional studies usually focus on the patch-clamp technique, which in its whole-cell configuration, gives an idea of the global currents throughout the cells, without knowing, in some cases, which channel is specifically activated. In addition, patch-clamp recording in its single-channel configuration is challenging and time-consuming due to the small number of copies of cation channels across the membrane. In this sense, the development and improvement of automatic patch-clamp devices is and will be a major advantage for the development of rapid test protocols on cell populations that are, after all, very heterogeneous in pathological cases (Rotordam et al., 2019; Crew et al., 2023). Furthermore, the activity of cation channels is generally hindered by the predominant chloride conductance of the erythrocytes. The originality of my thesis was the use of the MBE method along with other techniques to study the activity of different cation

channels. We have used pharmacological tools to activate or inhibit specific ion channels under specific and defined conditions. This can be done by creating artificial membrane hyperpolarizations using these pharmacological tools. The MBE method allows us to instantly visualize hyperpolarizations due to K^+ efflux. This is due to Gárdos channel activation. In other words, what we mainly see in the MBE method is only the Gárdos channel activation. In addition, during the MBE experiment, the RBCs are subject to an indeterminate (albeit constant) shear stress linked to the rotation in the thermostatically-controlled beaker of the experiments. It could be advantageous to quantify the magnitude of this applied shear stress for better interpretation of the experiment. Another limitation of this method is that it measures the average behavior of the cell population. In most cases, this is not a problem if the entire population responds at the same speed in the same order of magnitude. However, some cases, as it was for the study of SS RBCs (and TRPV2), given the inter-individual variability of the cells present and the heterogeneity of the patients, it was likely that the response will not be observed if the stimulation is progressive or slower for certain cells. The experiments used in this thesis, such as MBE, flow cytometry, morphological analysis, and water and ions contents, are done *in-vitro* where they undergo necessarily a deviation of their physiological reality, first of all due to sampling and handling of the cells in the testing tube. As soon as the blood is withdrawn and collected through a tube, RBCs change environment and are no longer subject to the same constraints. *In-vivo* study would be necessary, although this seems unrealistic at present. The solution could be the performance of *ex-vivo* analysis, typically through microfluidics schemes that mimics blood vessels' conditions. On another note, the morphological analysis of RBCs on blood smears may not reflect the physiological reality of RBCs since it is just a classical 2D characterization. A 3D morphological characterization of RBCs could be more specific and adapted (Simionato et al., 2021).

Nevertheless, the real limitation to conducting such a cross-sectional study is the access to samples. On the one hand, it is difficult to extend studies to patients awaiting diagnosis, and on the other hand, it is sometimes difficult to ensure an efficient transport of the samples that does not alter the responses of the cells to the different tests performed. Indeed, once collected, control samples and patient samples can be completely different. With respect to membrane transport, we know very well that temperature affects the activity of the pumps, and hence their ionic content and hydration status. Furthermore, patient cells are often more fragile and, by their definition, have a shorter lifespan, so how can we unambiguously compare cells with different age distributions? Since red

blood cells can never replace their proteins once they are in the circulation, how can we be sure that the proteins in the membrane are truly functional? It is likely that the number of copies of functional PIEZO1 or Gárdos channels in the membrane decreases with age.

When we talk about pathologies involving the dysregulation of cation conductance, it is difficult to ignore sickle cell anemia, with an estimated number of almost 60,000 patients in Europe. In 2023, the number of cases is estimated to have increased by 50% in 10 years (more than 400 births affected per year in France). It is therefore important to seek a better characterization of the P_{sickle} phenomenon, which is to some extent responsible for the dehydration and eventual irreversible sickling of RBCs (Lew and Bookchin, 2005). P_{Sickle} is defined as the deoxygenation-induced increase of non-selective cation permeability (Vandorpe et al., 2010). Importantly, HbSS are known to be more rigid (Li et al., 2017a), and to have a higher basal Ca^{2+} content (Eaton et al., 1973). Once Ca^{2+} entry *via* the P_{Sickle} pathways exceeds the activation threshold of the Gárdos channels, this triggers rapid KCl and water loss (Lew et al., 2002). These factors call into question again the interplay between membrane rigidity and non-selective cation conductance. In Chapter III, we demonstrated the relationship between the activation of two non-selective cation channels (PIEZO1 and TRPV2) and sickling events (Hatem et al., 2023; Nader et al., 2023). The activity of these two channels was shown to be oxygen-dependant, as deoxygenation performed in the MBE method enhanced hyperpolarizations in response to corresponding activators. This finding is important because it could bring us closer to the idea that P_{Sickle} is not just the up-regulation of a single transporter, but rather the concomitant activation of several non-selective cation channels. While it is clear that deoxygenation remains the primary driver, the relationship between this phenomenon and channel activity has yet to be determined. Interestingly, it has been shown that the activity of cation channels in cell-attached human or mouse HbSS cells triggered by deoxygenation and sensitive to inhibition by GsMTx-4, dipyridamole, and DIDS, a common feature of P_{sickle}, is also inhibited by carbon monoxide (Vandorpe et al., 2010). This observation clearly demonstrates a direct relationship between the tensed or relaxed state of hemoglobin and the activity of the channels. Considering that elevated O_2 promotes the strengthening of band 3–ankyrin interactions, thereby stabilizing the erythrocyte membrane during its turbulent flow from the lungs into the capillary beds, and that hypoxia (Stefanovic et al., 2013) leads to the disruption of this important membrane-cytoskeleton bridge, allowing the deoxygenated RBCs to move more efficiently through narrow capillaries during their transit back to the lungs (Chu et al., 2016), this

raises the question to what extent ion channels might not themselves be sensitive to such a phenomenon, or at least to the destabilization of the membrane or membrane complexes.

We suggest that PIEZO1 and TRPV2 could be involved in P_{Sickle} although further studies are needed, in particular to identify the molecular identity of this channel. An experiment is lacking in this field; we should have placed the cells in deoxygenated media, activated PIEZO1 or TRPV2, and checked under the microscope whether or not they undergo sickling or simply dehydration associated with activation of the Gárdos channels triggered by Ca^{2+} entry. In the deformability test that we performed with Oxygenscan, we only obtained the critical level of oxygen around which cells start to lose their deformability, using Yoda1, Δ^9-THC, and GsMTx4. The results obtained using this technique could be biased, especially when using Yoda1 at 10µM, because even at low concentrations (625 nM), Yoda1 is able to induce a rapid and irreversible Ca^{2+} entry that dehydrates even normal cells (see Chapter I). We should have harmonized the concentrations of Yoda1 used in this study between the different types of studies carried out in the three different laboratories (PIEZO1-SCD). In fact, we stress that 10 µM of Yoda1 constitutes huge amounts for RBCs; if this concentration is acceptable for other cell types, using these amounts for RBCs is harmful. It is worth noting that in another series of experiments on RBCs, Conrard and colleagues, incubated the cells with 500 nM of Yoda1 for only 20 seconds, and then washed the cells to get rid of this molecule (Conrard et al., 2018). This is consistent with the results of Ca^{2+} imaging results we have obtained using Yoda1 at 625 nM, where we see that Yoda1 generates a maximum fluorescence intensity within only 5 minutes (see Chapter I).

On the other hand, we need to go further to find the link between TRPV2 and SCD. In our study, we showed that SS RBCs are more reactive in response to Δ^9-THC, even though they express the same levels of TRPV2 protein on their membrane. There are several possible explanations for this higher activity, which may ultimately be concomitant. First, SS RBCs have higher basal levels of Ca^{2+} (Eaton et al., 1973), which lowers the required Ca^{2+} entry to reach the threshold for Gárdos channel activation. Such an assumption is fully consistent with the observations that the extent of hyperpolarization is much more pronounced in SS compared to AA cells, as well as a higher outward current in patch-clamp recordings upon THC stimulation. Moreover, flow cytometry experiments clearly showed a higher Ca^{2+} entry via TRPV2 in HbSS cells. We thought that this could be related to the age of cells since normal RBCs can live up to 120 days but SS RBCs only

live for about 10 to 20 days (Inusa et al., 2019). Hence, TRPV2 might be more functional in young RBCs. Nevertheless, the hypothesis of a difference in downstream response due to a differential Ca^{2+} extrusion rate *via* the PMCA might be valid too, given the fact that PMCA activity is known to be lower in SS RBCs (Gopinath and Vincenzi, 1979; Niggli et al., 1982) and probably linked to ATP exhaustion. This can extend the time of free Ca^{2+} activity in the cells and this is why we observe higher hyperpolarizations. Finally, it is clear that one of the ultimate targets of calcium is PKC. It is clear that numerous publications report an essential role in the alteration of PKC-dependent phosphorylation in SS red blood cells (cytoskeleton proteins, membrane ion and glucose transport, etc.) (George et al., 2010; Soderblom et al., 2013). Concerning the levels of THC used in the study (80 µM) and according to the literature, a concentration of 30 µM of THC was sufficient to activate TRPV2 in human RBCs (Flormann et al., 2022) and in mouse RBCs (Belkacemi et al., 2021). We took this concentration as a reference and determined the dose-response curve for this concentration. We carried out experiments at 30 µM and 80 µM. 30 µM was clearly sufficient to guarantee calcium entry into the cells. However, we chose 80 µM because at this concentration we start to reach the plateau of responding cells (Supp.Fig.1 in Chapter III, part B). Second, the results at 30 µM were more variable when it came to measure membrane potential variations, where we should remember that this is an indirect effect that we are recording through the development of the hyperpolarization generated by the activation of the Gárdos channel. So likely, we could detect a higher TRPV2 activation in response to THC using 80 µM (Supp.Fig. 3 in Chapter III part B). This concentration of THC was nevertheless higher than THC values found usually in the blood of smokers; In smokers' blood, THC levels rise and peak at 10 minutes often at levels around 84.3 to 162 ng/mL in whole blood, depending on the person and dose (Huestis, 2007). These values correspond to concentrations of THC between 0.26 and 0.5 µM in the blood given the molar mass of THC which is 314.45 g/mol. THC concentrations we used in our study were two orders of magnitude higher, and in general, they can't be found *in-vivo*. Nevertheless, 80 µM of THC, and more, can be considered as an acute dose that could probably be reached in the lungs of smokers. This is known, because inhalation of marijuana smoke produces lung tissue concentrations of THC that were 8-10 times higher than those measured in the blood suggesting high local exposure (Sarafian et al., 2006). In that case, we can assume or speculate that some of the RBCs close to the lungs may encounter high exposition to THC. At the very least, this initial study could encourage clinicians to take a closer look at the relationship

between the severity of vaso-occlusive crisis (in terms of pain and clinical consequences) and regular cannabis use. In this study, we decided to use a much higher concentration (80µM) than that commonly found in cannabis users in order to simulate an acute stimulation. However, as stated within the text, this concentration may be locally close to the one we used, implying that part of the red blood cell population could be affected and thus premature sickling linked to erratic activation of the Gárdos channel, which could also exacerbate dehydration of the RBCs. In addition, with around thirty patients, the experiments showed a certain variability in responses to THC, which would require a more in-depth clinical study. Thus, we have no clue about why cannabis consumer may experience increased pain albeit the known analgesic properties of cannabinoid, but one can imagine that if adverse effects occurs it may enhance the severity of the crisis only due to the resilience to pain and the postponed entrance to emergency room.

Returning to the molecular level, TRPV2 has recently been suggested to be involved in the dissipation of the cation gradient in storage-lesion events (Murciano and Kaestner, 2023); in fact, the deterioration of blood quality during storage is a common public health issue (Recktenwald et al., 2022). To counteract the transfusion of deteriorated blood samples, quality control of stored red blood cells was suggested (Lopes et al., 2023). Nevertheless, we see that research topics concerning mechanosensitive non-selective cation channels in RBCs are in general more focused on PIEZO1 and its roles. The presence of TRPV2 in mice and human RBCs was only confirmed in 2021 (Belkacemi et al., 2021) and global interest in the comprehension of the role of TRPV2 in RBCs followed (Egée and Kaestner, 2021; Flormann et al., 2022).

Finally, it is interesting to note that although these two channels (PIEZO1 and TRPV2) have been formally identified in the membranes of red blood cells, other ion channels or conductances that could represent a cation permeability pathway have at least been identified, at least pharmacologically. The VDAC channel could also represent a pathway capable of generating a significant flux (Bouyer et al., 2011), especially since the complex it forms with ANT and TSPO2 has recently been highlighted in the release of ATP by red blood cells (Marginedas-Freixa et al., 2018), in addition to the probable role of pannexins (Locovei et al., 2006).

Furthermore, evidence that the red blood cells from sickle cell patients possess a significant number of potentially activatable NMDA receptor channels remains to be explored (Hegemann et al., 2020). Finally, the recently proposed hypothesis that red blood cells can acquire proteins

(including the TRPC6 channel) as they pass through the splenic slit is very tempting to explore (Hertz et al., 2023). Indeed, sickle cell red blood cells, may have an increased transit time in the spleen due to their increased membrane rigidity, favoring membrane fusion acquisition of membrane proteins contained in spleen-dwelling microvesicles.

II. Conclusion

Taken together, the different studies included in this thesis, contribute to the understanding of cation permeabilities under physiological and pathophysiological conditions. Finally, all these results question the specificity of erythrocytes in terms of cation permeability and biophysical membrane properties compared to other cell types and, more importantly when mechanosensitive pathways are involved in such ion movements.

III. Perspectives

Overall, the results of this Ph.D. have opened new horizons to understanding the non-selective cation channels in RBCs, their activation, their roles, and their complex interplay with other factors that characterize RBCs such as the lipid composition of the membrane.

In the discussion part of this thesis, we have evoked the tight correlation between membrane lipid composition and channel activation. It would be judicious to establish a lipidomic profiling of the RBCs membranes, especially of those from patients treated with Alectinib or from patients with PIEZO1 and KCNN4 variants.

In addition, our MBE method relies on a homogeneous response of the entire population of tested cells. This could bias the results we obtain in this type of experiment for example, as we explained in the case of SS RBCs where sickle cells are younger than normal RBCs. For this reason, the separation of cells according to their density and thus their age could be a key to start understanding the activity of cation channels in each of the populations. This highlights the importance of studying the aging process *in vitro* and *in vivo* and how NSCs are involved in it. Furthermore, abnormal ferroptosis was found to damage the development of RBCs by disrupting systemic iron homeostasis, leading to erythropoiesis suppression and anemia. Thus, targeting ferroptosis, which is an iron-dependent cell death pathway, has been suggested as a new therapeutic potential for blood-cell-related diseases (Chen et al., 2022). We believe that investigating the role of ferroptosis

during aging could be of interest, especially if it interferes with the activity of cation channels at the end of the life of the RBCs.

Finally, the study of channel mutations using progenitor cells (CD34+) is one of the perspectives that could help to understand the fundamental role of each of the channels in the normal development of RBCs.

Appendix 1: Blood smears of Piezo1 and KCNN4 variants

In this Appendix, we placed the images of blood smears that correspond to PIEZO1 and KCNN4 variants presented in Chapter III.

A. **PIEZO1 variants**

R2019H (A: Control- B: Patient)

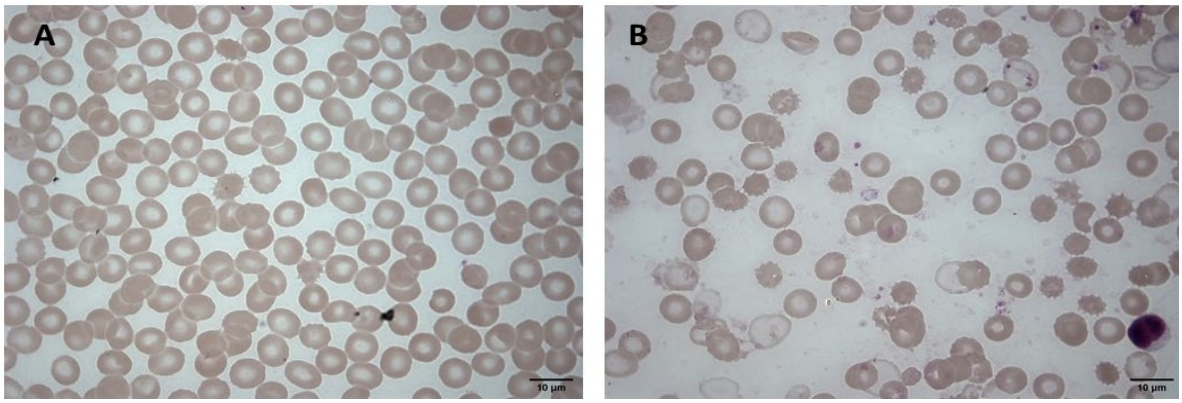

L1697F+A344V (A: Control- B: Patient)

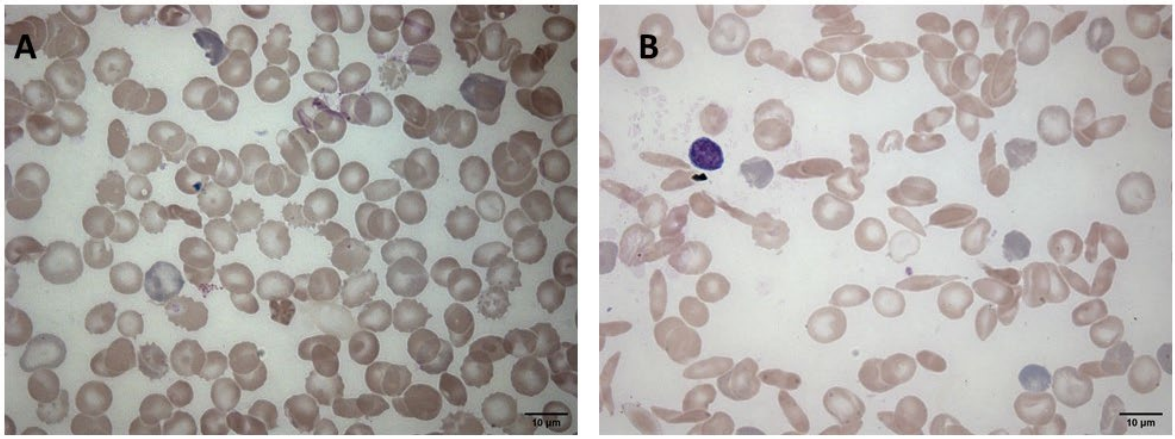

L1708Q (A: Control- B: Patient- C: Father- D: Mother)

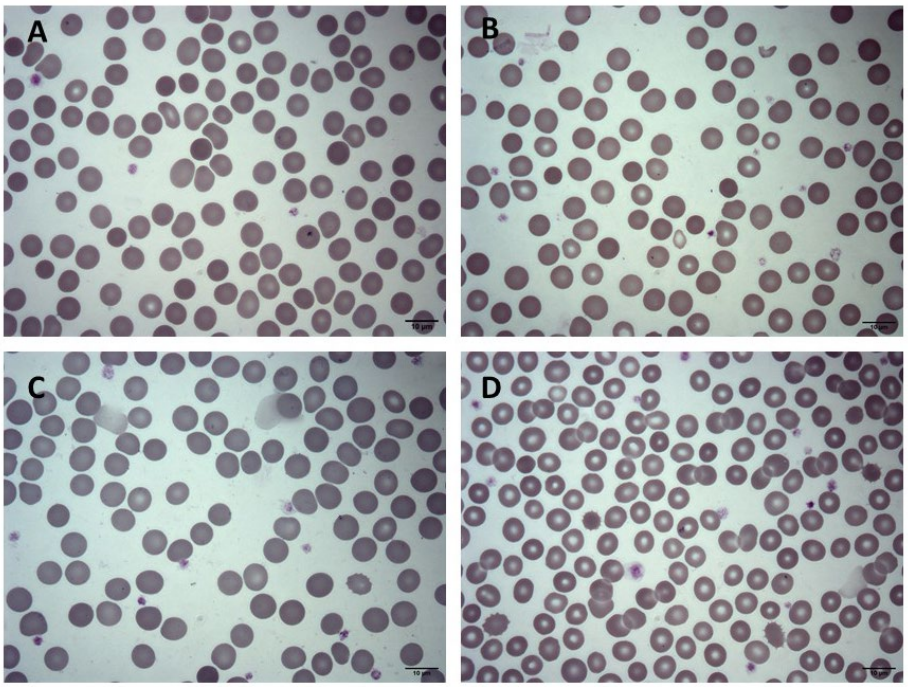

P2282A (A: Control- B: Patient)

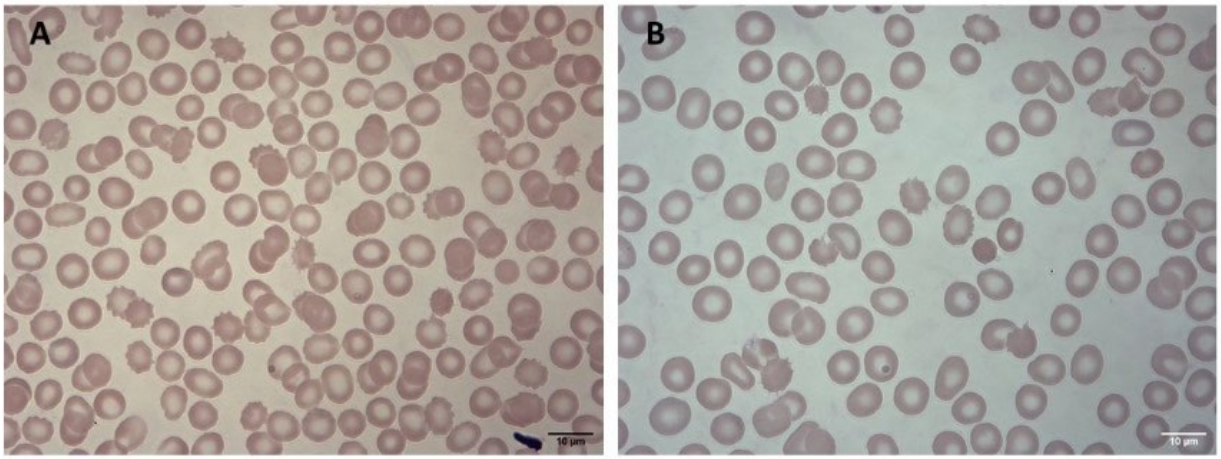

Unknown 4 (Piezo1 + β-Thalassemia) (A: Control- B: Patient- C: Control β-Thalassemia- D: Mother)

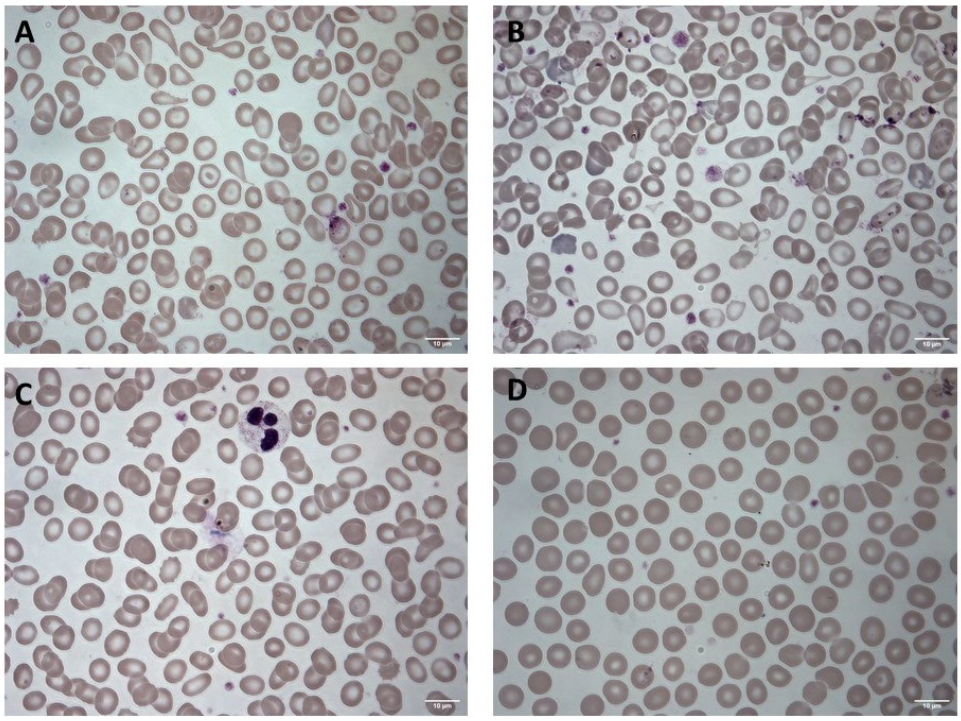

Unknown 1 (A: Control- B: Patient)

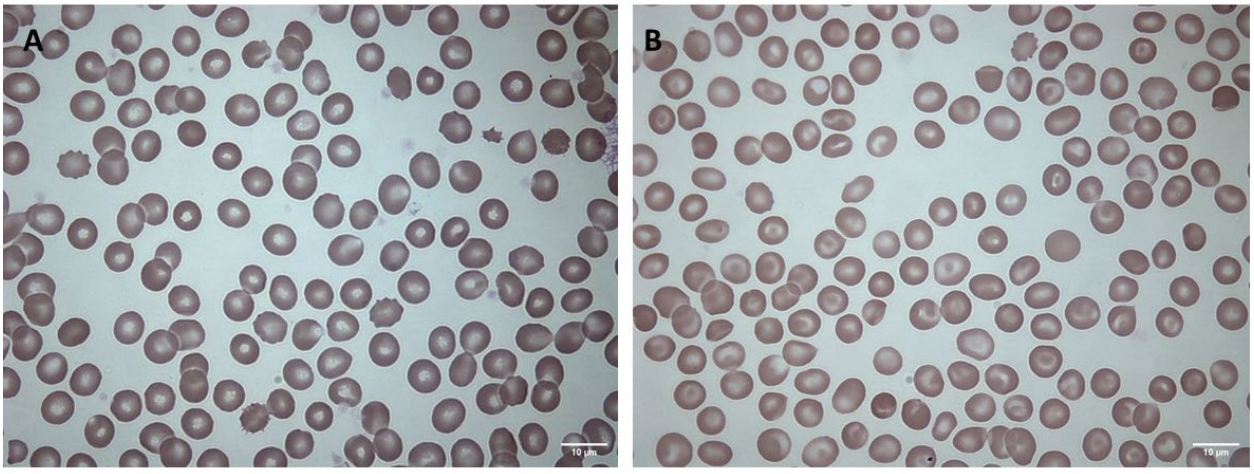

Unknown 2 (No control, patient only)

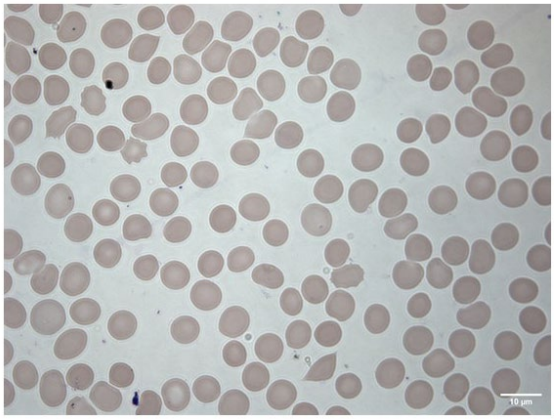

S1726T (Control CR- B: Control MZ- C: Patient AG- D: Patient GK- E: Patient RK)

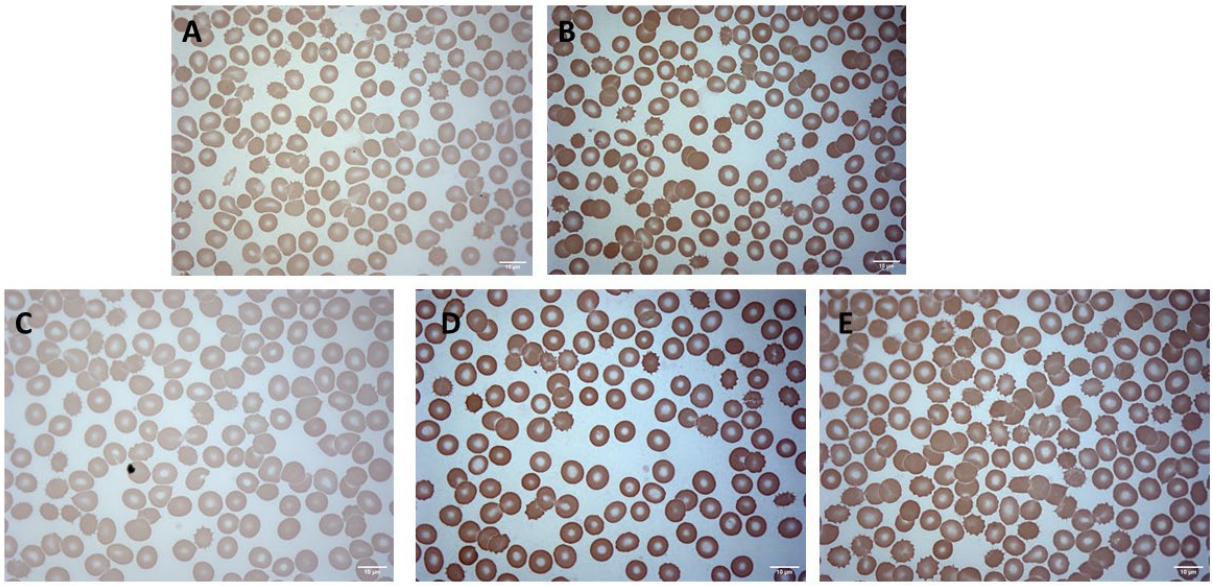

Unknown 3 (A: Control- B: Patient)

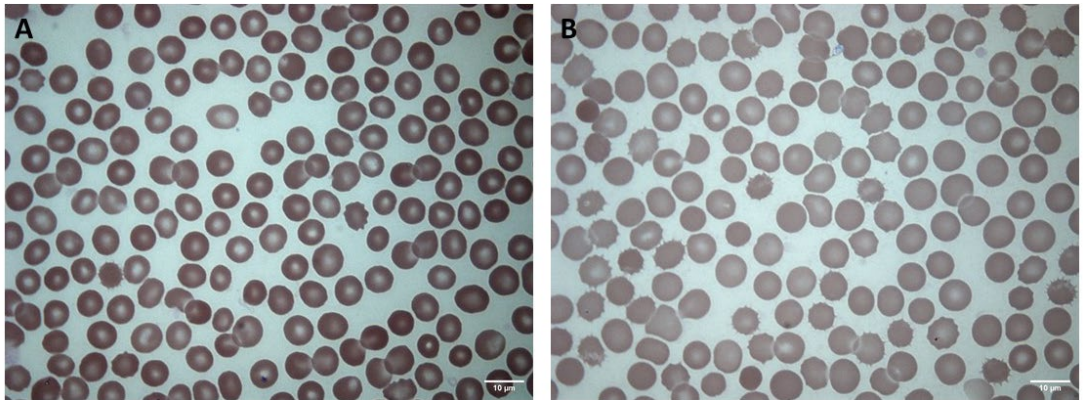

Y2143C (A: Control- B: Patient- C: Father- D: Mother)

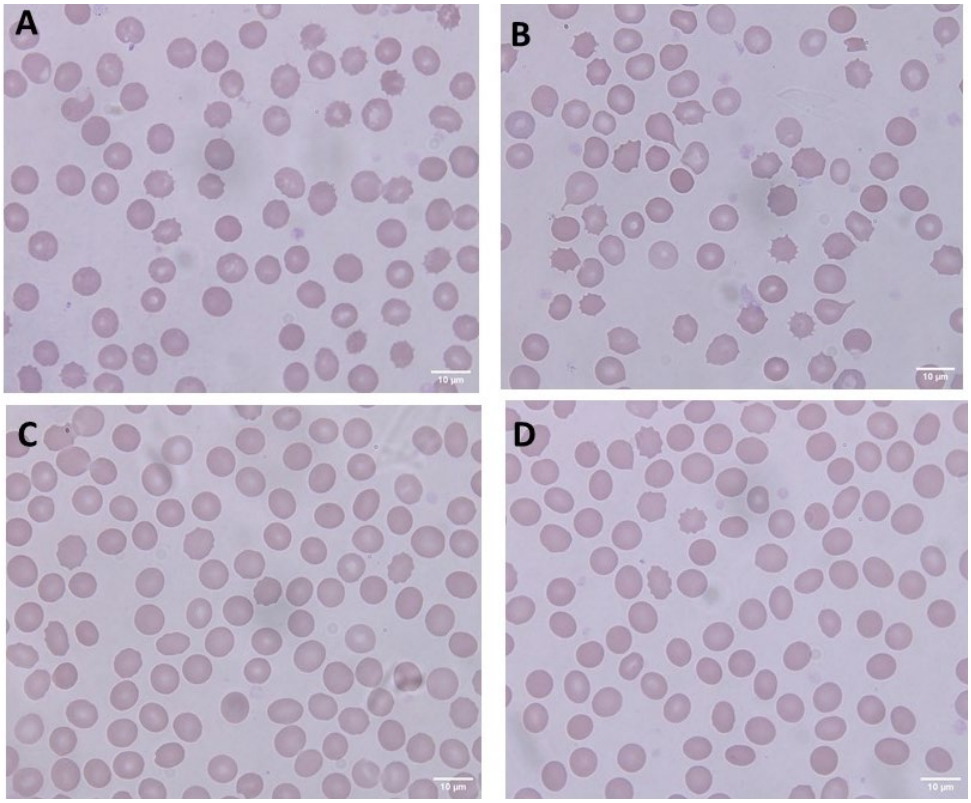

B. **KCNN4 variants**

S386N (A: Control- B: Patient)

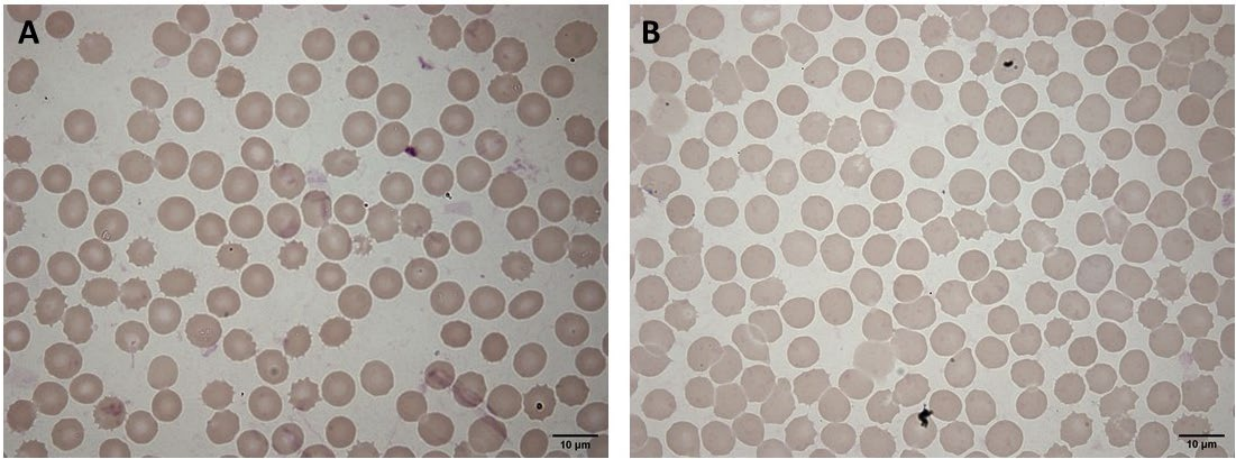

R352H (A: Son- B: Father)

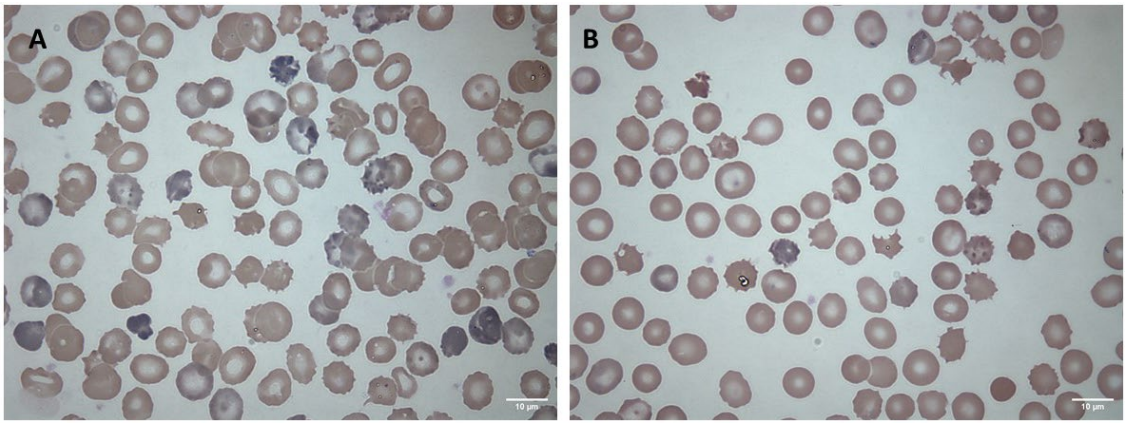

Unknown (A: Control- B: Patient)

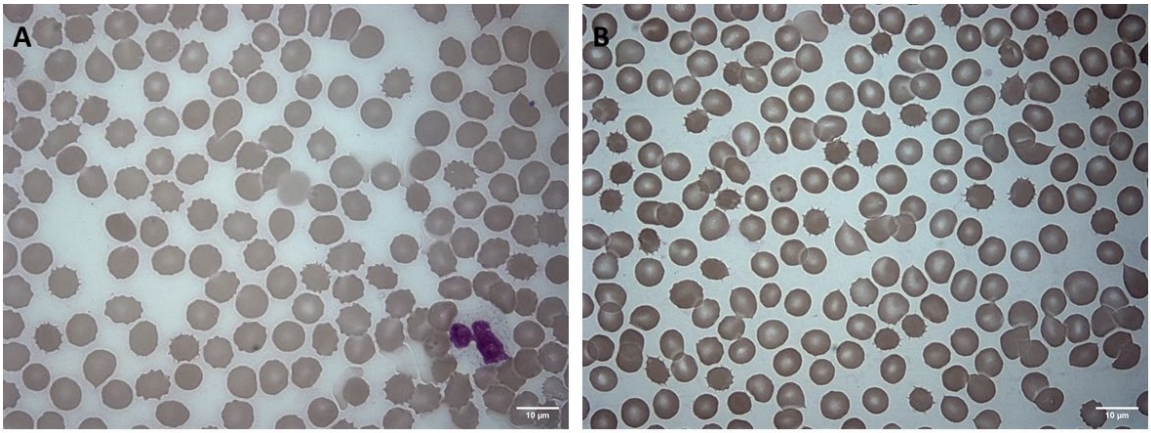

A279D (A: Control- B: Patient)

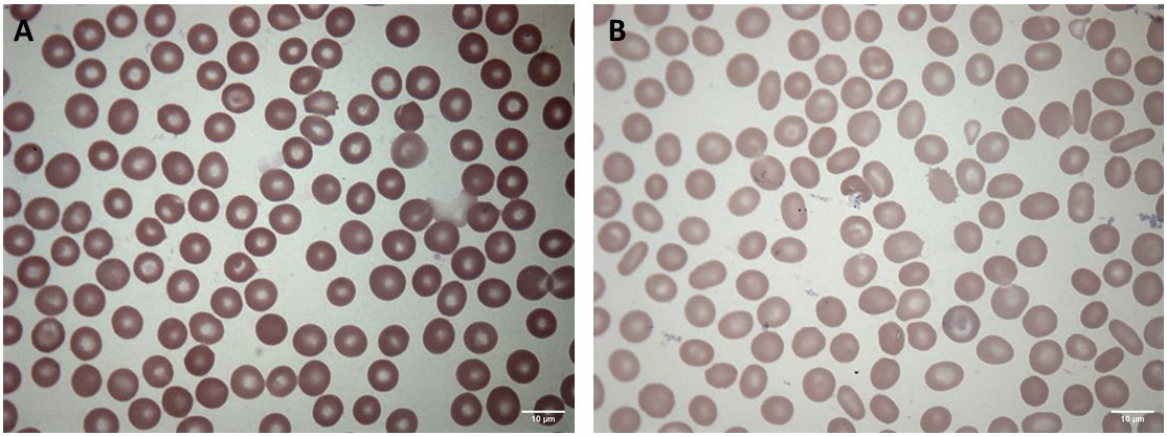

H340N (A: Control- B: Patient- C: Father- D: Mother)

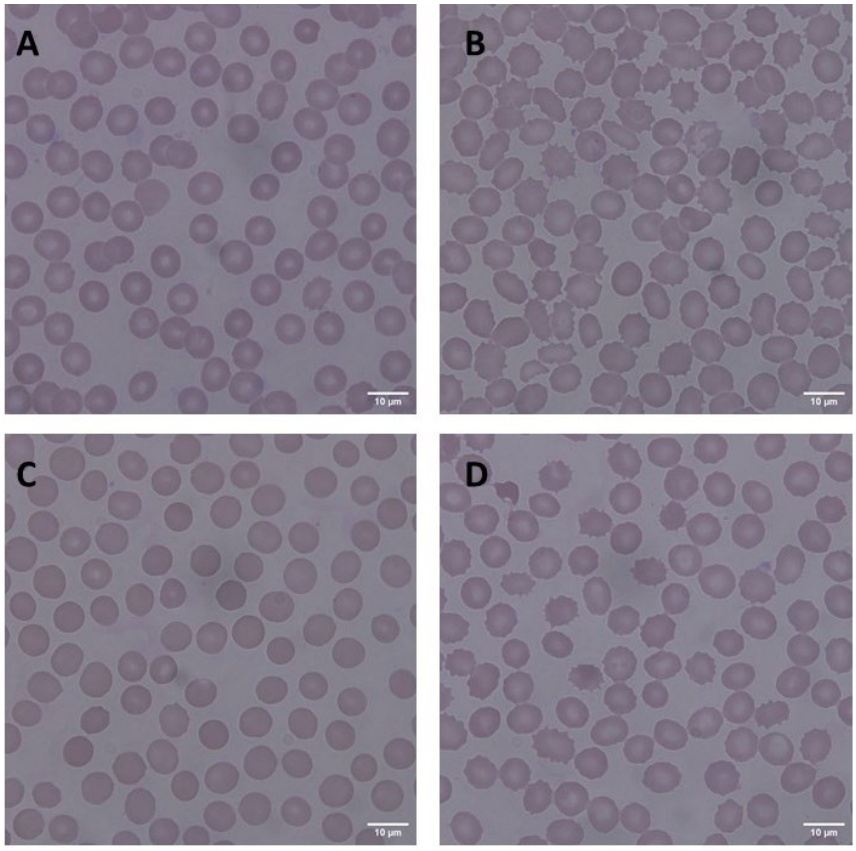

Appendix 2: Science Is Wonderful!

Science is Wonderful! is a science fair organized once per year by the European Commission (Directorate-General for education, youth, sport, and culture- Unit EAC.C.2-MSCA) in Brussels-Belgium. This fair attracts around 4000 primary and secondary school pupils every year, giving them the chance to engage with over 100 international scientists, learn more about their work, and explore research careers. Science is Wonderful! celebrates the value and impact of EU-funded research. Every year, a call for projects is open for MSCA fellows, alumni, and projects to showcase and engage their research. The call is open for two types of activities:

1. The Science is Wonderful! fair

2. The Science is Wonderful! competition

1. For the Science fair, I made a proposal for a stand called "What's in our blood?" with the slogan "Healthy blood, healthy you". My project included three types of hands-on experiments to teach the pupils about the blood components, blood circulation, and shapes of RBCs. Amongst more than 140 proposals, only 43 projects were selected for the fair, including mine! In addition, I was selected as one of Science is wonderful! 2023 ambassadors, and the hands-on experiments I created were filmed professionally and will be published on the EU's website in January 2024 (Figure A).

2. The competition gives the chance to primary or secondary school teachers to find and collaborate with an MSCA researcher to generate an interactive learning resource. A platform was created by the organizers where teachers could match with researchers, develop a common project together, submit it, and get famous. I collaborated with Dr. Katerina Kapodistria, a secondary school teacher in Athens-Greece. The idea was to develop a game around blood typing. The final game we created was about a crime scene investigation. Over 500 researchers and teachers took part in the competition with more than 100 submitted proposals. Three proposals were only selected! Gladly my proposal with Katerina won the competition! Our proposal was professionally produced by the European Commission's Directorate-General for Education, Youth, Sport, and Culture and translated into the EU's 24 official languages. It consists of a video that I filmed professionally in Brussels (Figure B), and two printable assets that I invented (the documents below); The video and the printable assets will be released on the official site of the EU in 2024: the first asset is

dedicated to the students with the quizzes and story-telling of the crime scene. The second is dedicated to the teachers to help them organize the experiment in the classroom and with the answers to the quizzes. They were published on the 16th of February on the EU website https://audiovisual.ec.europa.eu/en/video/I-253456

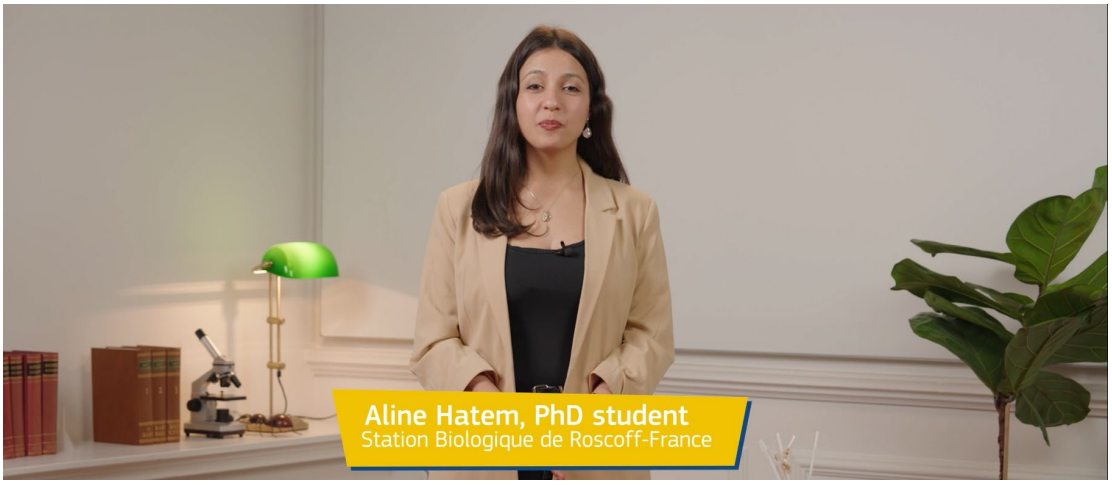

Figure A: Screenshot from "What's in our blood" experiment video.

Figure B: Screenshot from "Crime scene investigators: catch the murderer".

Printable assets of "Crime scene investigators: catch the murderer" project with EU (Students and teachers' versions)

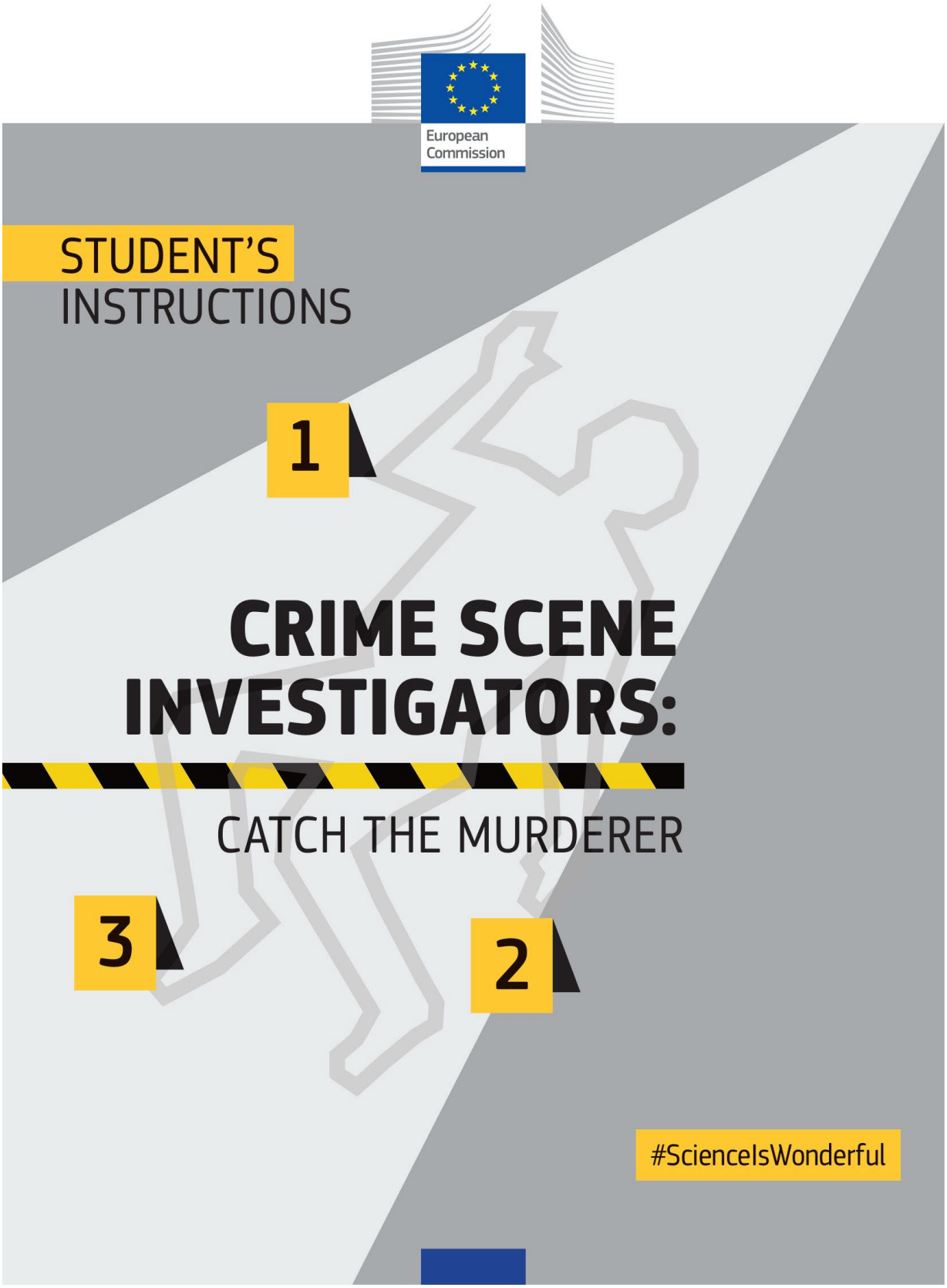
European Commission
STUDENT'S INSTRUCTIONS
1
CRIME SCENE INVESTIGATORS:
CATCH THE MURDERER
3
2
#ScienceIsWonderful

CRIME SCENE SCENARIO

1

On a cold December night, Mr. Jeffrey B. was sitting by the chimney when he suddenly heard a noise in the apartment of his absent neighbors. He went to investigate and was surprised to find a burglary in progress that was taking place.

The thief was frightened by the presence of the victim and attacked him. In his haste, the criminal cut his arm on the broken window through which he had entered the flat. A small piece of clothing stained with the criminal's blood was taken from the scene of the crime. A weapon with a blood sample was also found at the scene. Three suspects were identified who either knew the victim or had been seen in the area before the body was discovered.

You are a criminologist working for the Crime Laboratory of the Ministry of Justice. You are called to the scene of the crime. Your task is to analyze the two samples found at the crime scene and to investigate if A. the weapon found is the murder weapon and B. who the killer is.

3

Good luck detective!

2

#ScienceIsWonderful

CRIME SCENE PLAN

victim :
Mr. Jeffrey B

1

2

3

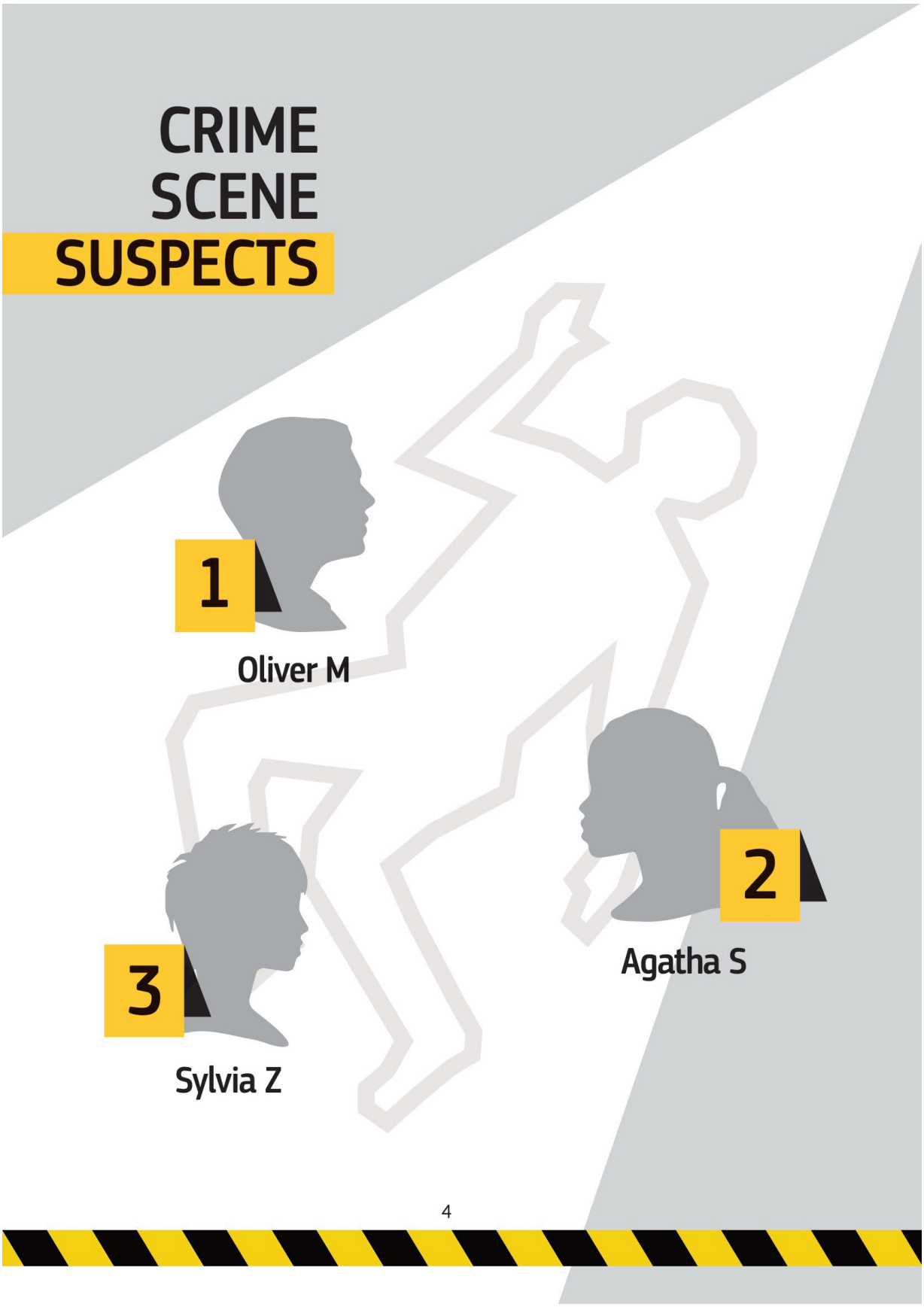
CRIME
SCENE
SUSPECTS
1
Oliver M
2
Agatha S
3
Sylvia Z

PRE-LAB QUESTIONS

1 What does a person's blood type tell you? Be specific.

2 Complete the table below. Use your biology text for reference.
Hypothesize the reactions with anti-serums.
Clumping will indicate a (+) reaction.

Clumping= + (positive) No clumping= -(negative)

Blood type	Antigens present	Genotypes possible	Reaction w/anti-A serum	Reaction w/anti-B serum
A				
B				
AB				
O				

Rh clumping = Rh + blood

ANALYSIS OF RESULTS

Do the experiments, and fill in the table below.
Blood agglutination (clumping) results:

(Hint: If the blood sticks together (agglutinates) after an anti-serum is added, then the suspect has that blood type).

Observations				
Source	**Anti-A serum**	**Anti-B serum**	**Rh serum**	**Blood Type**
Crime scene sample				
Weapon sample				
Victim - Mr Jeffrey B				
Suspect #1 (Oliver M)				
Suspect #2 (Agatha S)				
Suspect #3 (Sylvia Z)				

1 Which blood type will clump with the addition of Anti-A serum? Why?

ANALYSIS OF RESULTS

2 Why can't people with Type-O blood receive blood from any other type (A, B, or AB)?

3 Was the weapon found used to kill Mr. Jeffrey? How do you know?

ANALYSIS OF RESULTS

4 Based on the blood typing results, which of the suspects most likely committed the burglary? Why?

5 Why was it necessary to type the victim's blood?

ANALYSIS OF RESULTS

6 Can you think of some limitations to using blood typing in a criminal investigation?

7 Can you think of other biological evidence which can be taken from a crime scene by a detective that allow an individual to be linked to a crime?

PDF/Volume_01 ISBN 978-92-68-08600-1 DOI 10.2766/0545 NC-09-23-482-EN-N

Publications Office

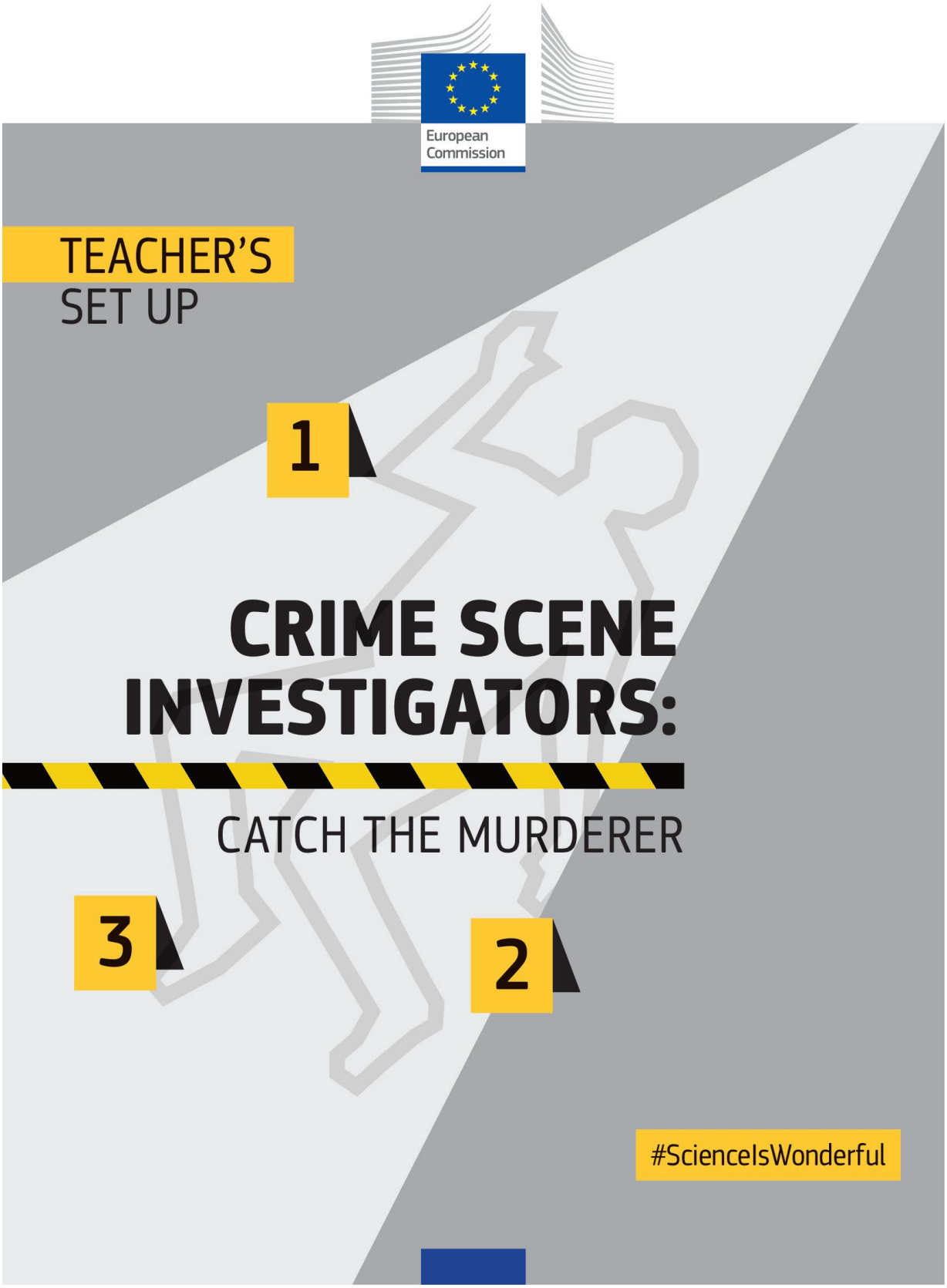
European Commission
TEACHER'S SET UP
1
CRIME SCENE INVESTIGATORS:
CATCH THE MURDERER
3
2
#ScienceIsWonderful

TEACHER'S CHECKLIST
FOR A SUCCESSFUL INVESTIGATION

You are running a crime scene investigation scenario and experiments with your students.
Here's what you need to do:

1. Read this package first.

2. Prepare the blood and set up testing labs, including a print-out of the crime scene.

3. Print the sections your students need, or have it set up digitally (e.g. on iPad) if you are able.

4. Ask your students to dress up as crime scene investigators – provide lab coats and equipment if you can.

5. Play the video – it will include instructions where to pause. Refer to this package when you pause the video.

6. Have fun! This should be an immersive, interactive learning experience, so make sure your students stay engaged throughout.

Good luck to you and your investigators!

#ScienceIsWonderful

BLOOD TEST KIT

1 MATERIALS FOR 6 KITS

2 cups milk

2 bottles of food colouring (red and green)

2 cups water (+ additional water for the serum bottles)

18 small cups (Dixie cup size)

6 permanent markers

6 boxes of toothpicks

white vinegar

18 small dropper bottles

6 small plastic storage containers

labels for bottles and containers

2 PREPARATION

1 - Mix 2 cups of milk with 2 cups of water. Add enough red food colouring to get a bright red colour and then add a few drops of green to make it a deeper red colour which looks more realistic.

2 - Label 6 dropper bottles to correspond with the three suspects, the victim, the weapon sample and the crime scene sample. Take time to label each of the 6 storage containers to correspond to the bottles of fake blood. Fill each bottle with the fake blood mixture.

3 - Label 6 dropper bottles with "Anti-A Serum", label 6 others with "Anti-B Serum", and label the final 6 "Anti-Rh". Use the information in the chart below to fill the bottles with either vinegar or water. (Note that the contents differ depending on the suspect or the sample!) You may want to code the bottles in a way that you can tell the contents easily, but it will not be obvious to the students.

4 - Create the testing kits by placing the correct bottle of fake blood in each kit along with the correct serums, a permanent marker, 3 small cups, and a box of toothpicks in a small plastic storage container.

DIRECTIONS

1. Discuss the Crime Summary and go over the directions for the lab.

Observations				
Source	**Anti-A serum**	**Anti-B serum**	**Rh serum**	**Blood Type**
Crime scene sample	vinegar	water	vinegar	A+
Weapon sample	water	water	vinegar	O+
Victim - Mr Jeffrey B	water	water	vinegar	O+
Suspect #1 (Oliver M)	vinegar	water	vinegar	A+
Suspect #2 (Agatha S)	water	vinegar	water	B-
Suspect #3 (Sylvia Z)	vinegar	vinegar	water	AB-

2. Provide one testing kit for each group of students and have then label the cups in the kit as directed.

3. Allow time for the groups to complete the testing of their blood sample as outlined in the directions.

CONCLUSION

Through this investigation, students should conclude that the crime scene sample matched suspect #1 Oliver M and the weapon sample matched the victim, Mr Jeffrey B.

PRE-LAB ANSWERS

1 What does a person's blood type tell you? Be specific.

A person's blood type reveals the presence or absence of antigens on the membrane of red blood cells; the ABO antigens ; antigen A; antigen B, and the RhD antigen. This creates the eight most common blood types: A+, A-, B+, B-, AB+, AB-, O+, and O-.

There is the A blood type if the blood has A antigens, B blood type if the blood has B antigens, AB type if your blood has the two antigens, and O blood type if no antigen is present.

In addition, a blood type is positive if the RhD antigen is present, and a blood type is negative if this antigen is absent

2 Complete the table below. Use your biology text for reference.
Hypothesize the reactions with anti-serums.
Clumping will indicate a (+) reaction.

Clumping= + (positive) No clumping= - (negative)

Blood type	Antigens present	Genotypes possible	Reaction w / anti-A serum	Reaction w / anti-B serum
A	**A**	**AA,AO**	**+**	**-**
B	**B**	**BB,BO**	**-**	**+**
AB	**A,B**	**AB**	**+**	**+**
O	**NONE**	**OO**	**-**	**-**

Rh clumping = Rh + blood

ANALYSIS OF RESULTS ANSWERS

Do the experiments, and fill in the table below.
Blood agglutination (clumping) results.

(Hint: If the blood sticks together (agglutinates) after an anti-serum is added, then the suspect has that blood type)

Observations				
Source	**Anti-A serum**	**Anti-B serum**	**Rh serum**	**Blood Type**
Crime scene sample	+	-	+	A+
Weapon sample	-	-	+	O+
Victim - Mr Jeffrey B	-	-	+	O+
Suspect #1 (Oliver M)	+	-	+	A+
Suspect #2 (Agatha S)	-	+	-	B-
Suspect #3 (Sylvia Z)	+	+	-	AB-

1 Which blood type will clump with the addition of Anti-A serum? Why?

Blood type A because red blood cells from this blood type have on their membranes Antigen A.

ANALYSIS OF RESULTS ANSWERS

2 Why can't people with Type-O blood receive blood from any other type (A, B, or AB)?

Because their blood contains anti-A and anti-B antibodies.
All the other blood types have antigens A and/or B.
This will trigger an agglutination reaction.

3 Was the weapon found used to kill Mr. Jeffrey?
How do you know?

Yes, the weapon found was used to kill Mr. Jeffrey because the blood of Mr. Jeffrey and the blood found on the weapon had the same blood type "O+".

ANALYSIS OF RESULTS ANSWERS

4 Based on the blood typing results, which of the suspects most likely committed the burglary? Why?

Suspect n°1 has most likely committed the burglary because its blood type matched the blood found in the crime scene "A+".

5 Why was it necessary to type the victim's blood?

It was necessary to type the victim's blood so it could be distinguished from other blood that may be found at the crime scene. It is a significant biological clue, necessary for the investigations to proceed.

ANALYSIS OF RESULTS ANSWERS

6 Can you think of some limitations to using blood typing in a criminal investigation?

Blood typing can be used to establish whether someone has A, B, AB, or O blood, but cannot point to a person. Indeed, if many suspects had the same blood type or shared the same blood type with the victim, we cannot discriminate which blood corresponds to which person, and this is confusing.

7 Can you think of other biological evidence which can be taken from a crime scene by a detective that allow an individual to be linked to a crime?

Fingerprints, hair, skin cells, saliva, sweat, semen, bones, tissues, urine, or any other biological sample source of DNA

PDF/Volume_01 ISBN 978-92-68-08621-6 DOI 110.2766/116431 NC-09-23-483-EN-N

Publications Office

Acknowledgments

First and foremost, I would like to express my heartfelt gratitude to my thesis director, Prof. Stéphane Egée, for his unwavering support and guidance over the past three years. *Your mentorship has been invaluable, and I am truly grateful for the opportunities you have given to me. Thanks to you, I have cherished every moment of this thesis; you have made it cooler, funnier, and fancier. I have learned so much from your wisdom. Thank you for being patient with me, and for teaching me how to become patient. I promise I will try! You are truly an amazing person and professor*. And now, I would like to thank Guillaume, my colleague and office neighbor. I can't remember a day during my Ph.D. when I didn't say "Merci Guillaume!", a phrase I think we can both hear. *Thank you, Guillaume, for everything. You have helped me so much during my Ph.D. Thank you for your kindness and good vibes, and for helping me during the experiments, analysis, etc… the list is long*. I would also like to thank Laurent, his presence brought happiness to my days. In addition, I would like to thank Elisabeth, for her presence, her care, and her kindness. *I hope you will be back in the office soon because you are missed.* Well, Red Blood Cell teams, you are the most wonderful team a person can hope to work with. Thank you for having me. I feel so lucky to have worked with you.

Secondly, I would like to thank all the staff of the "Station Biologique de Roscoff", especially the UMR8227. I am very grateful for every day at the station. I am especially grateful for the friends I have made, whether they are still here or have left: Roman, Emma, Charlotte, Gurvan, Jeremy, Sonia, Antonin, Etienne, Marine, Vittoria, Sylvie, Lisa, Louison, Yasmine, Gwendal, Samuel, Aurélien, Mariarita, Pélagie, Iris, Ahlem, Yacine, Erwan, Lucie, and all.

My sincere thanks go to Roscoff locals, who welcomed me into their homes and spoiled me all over my stay. In particular, I would like to thank the members of the Saint-Pol Aurélien parish: Jacqueline, Père Fidèle, Père Georges, Valérie et Laurent, Laurence et sa maman, Claire et Pascal, Soeur Miriam, Père Christophe, Frank, Maria, et Armelle. I would also like to thank my tango mates and the "Tango à la mer" association, especially Isabelle et Christian, Omid et Hajar, Cheryl et Bruno, Marie-Annick, and Romina.

Furthermore, I would like to thank each and every person I met in the ITN- EVIDENCE. What an enriching experience! Thank you for all the knowledge, expertise, meetings, and good moments. In particular, I would like to thank the host laboratories that welcomed me on secondments: Pr. Philippe Connes and Sofia, and Dr. Wassim El Nemer and Robert. I would also like to thank Pr. Lars Kaestner not only for coordinating this beautiful consortium but also for our collaboration on the TRPV2 paper. A big thank you to my friends and colleagues Min, Nicoletta, and Sofia for this concern. I enjoyed meeting all the PIs and ESRs during this experience: Amira, Carolina, Aishu, Pauline, Marcelle, Catarina, Yazdan, Mariam, Guilia, and Silvia. Thanks to this MSCA consortium, I had the chance to participate in Science is Wonderful, and make projects with the EU- DG EAC (Dora, Sybille, Aline), ICF Next (Cathy, Philip, Matthew), and 87s (Olivier, Maxime). I am deeply grateful for this bright part of my thesis.

Special thanks to the members of the Jury who accepted to make part of this journey despite their busy schedules: Pr. Marieke Von Lindern, Dr. Hélène Guizouarn, Pr. Lars Kaestner, Dr. Wassim El Nemer, and Dr. Olivier Silvie.

I am also grateful to the members of the thesis committee who guided me with their expertise: Dr. Bruno Constantin, Pr. Philippe Connes, and Dr. Olivier Silvie. Here, I would like to thank the doctoral school (ED515-Sorbonne Université) for continuously following up with us and for providing us with training courses.

Thanks to all our collaborators who provided us with blood samples from patients. And, of course, to the patients themselves, their families, and to the healthy donors.

Now, I would like to express my special and emotional gratitude to my boyfriend, Nathan. *You lit up my world with your constant support, you inspired me and gave me strength every day. You stood by me through thick and thin. Thank you for all your love and encouragement. As the song goes, "I am everything I am because you loved me". I love you too, so much.*

Finally, I would like to thank my parents: baba Elias, mama Aïda, and my brother Georges. *Thank you for shaping me into the person I am today. You have been my initial motivation and biggest support system throughout this thesis. I know how much you sacrificed to see me here, and here I am! I hope you are proud of me. I love you more than words can ever say. Bhebkon ktir!*

Abbreviations

$[X]_i$: The intracellular concentration of ion X

$[X]_o$: The extracellular concentration of ion X

2-APB: 2-aminoethoxydiphenyl borate

5HMF: aldehyde 5-hydroxymethyl-2-furfural

AD: Autosomal dominant

AE1: Anion Exchanger 1 (aka Band 3)

ALK: Anaplastic lymphoma kinase

ANT: Adenine nucleotide transporter

AQP: Aquaporin

AQP1-Aquaporin tetramer 1

AR: Autosomal recessive

ATP: Adenosine triphosphate

BFU-E: Burst-forming unit-erythroid

C: Coulombs

CA: Carbonic anhydrase

Ca^{2+}: Calcium

cAMP: cyclic adenosine monophosphate

CBD: cannabidiol

CCC: *cation-Cl^- cotransporters*

CD71: Transferrin receptor

CFTR: Cystic fibrosis transmembrane conductance regulator

CFU-E: Colony-forming unit-erythroid

ChTX: Charybdotoxin

Cl^-: Chloride anion

CO_2: Carbon dioxide

Covid19: Coronavirus disease appeared in 2019

Cs^{+}: Cesium ion

CTD: C-terminal domain

CVD: cardiovascular disease

dcs: dry cell solid

DHS: Dehydrated Hereditary Stomatocytosis

EC_{50}: half maximal effective concentration

ECD: Extracellular domain

EDTA: Ethylenediaminetetraacetic acid

E_m: the resting membrane potential, in millivolts

EMA: Eosine-5-maleimide

EMA: European Medicines Agency

e-NMDA-R: Erythroid N-methyl D-aspartate receptor

ERK: Extracellular signal-regulated kinases

ES: External solution

E_X: Potential membrane at the equilibrium of ion X

F: The Faraday constant

FDA: The US Food and Drugs Administration

Fe^{2+}: ferrous atom (iron)

G3PD: glyceraldehyde-3-phosphate dehydrogenase

G6PD: Gluose-6-phosphate dehydrogenase

GLUT1: Glucose transporter 1

GPA: Glycophorin A

GPB: Glycophorin B

GPC: Glycophorin C

GSH: Glutathione

GsMTx4: Grammastola spatulata mechanotoxin *#4*

G_x: Conductance for ion "X"

Hb: Hemoglobin

HbF: Fetal hemoglobin

HC: Hydroxycarbamide

Hct or HT: Hematocrit

HE: Hereditary Elliptocytosis

HPP: Hereditary Pyropoikilocytosis

HSC: Hematopoietic stem cell

HSPC: hematopoietic stem cell and progenitor cells

HX: Hereditary Xerocytosis

I_X: Currents generated due to the movement of ion X or due to the activity of a channel X.

IL-1: Interleukin 1

IL-3: Interleukin 3

lcw: litre of cell water

Li^+: Lithium ion

LIS: Low ionic strength condition

Ln: natural logarithm

m/s: meter per second

MBCD: methyl-β-cyclodextrin

MCH: Mean corpuscular hemoglobin

MCHC: mean corpuscular hemoglobin concentration

MCV: Mean corpuscular volume

MVB: Multi vesicular bodies

MPV: Mean platelet volume

NADPH: Nicotinamide adenine dinucleotide phosphate

NGS: Next generation sequencing

NMDA: N-methyl D-aspartate

NMDA-R: N-methyl D-aspartate receptor

NO: Nitric Oxide

NPP: New permeability pathway

NSC: Non-selective cation channel

NSCLC: Non-small cell lung cancer

NSVDC: Non-selective voltage-dependent cation channel

OMIM: Online mendelian inheritance in man

PAS: periodic acid Schiff reagent

PC: Phosphatidylcholine

PE: Phosphatidylethanolamine

PE: Primitive erythroblasts

PGE_2: Prostaglandin E_2

PI, PIP, PIP_2: phosphoinositide

PK: Pyruvate kinase

PKC: Protein Kinase C

PMCA: Plasma membrane calcium- ATPase

PS: Phosphatidylserine

pS: picosiemens

P_{Sickle}: Deoxygenation-sensitive cation channels activity

P_X: the permeability for ion X

Rb^+: Rubidium ion

RBC: Red Blood Cell

RDW: Red cell distribution width

Rh: Rhesus

RhAG: the Rh-associated glycoprotein

RT: Room temperature

SCA: Sickle Cell Anemia

SCD: Sickle Cell Disease

SCF: Stem cell factor

SDS-PAGE: sodium dodecyl sulphate polyacrylamide gel electrophoresis

SI: The international system of units

STAT5: Signal transducer and activator of transcription 5

STOML3: Stomatin-like protein 3

TM: transmembrane domain

TPO: Thrombopoietin

TRP: Transient receptor potential channel

TRPC: Transient receptor potential channel, canonical type

TRPV: Transient receptor potential channel, vanilloid type

TSPO: Translocator protein

V: Volts

V_M*: Potential Membrane*

VUS: Variant of uncertain significance

WBC: White blood cells

Δ^9*THC: delta9-tetrahydrocannabinol*

References

Abkarian, M., Faivre, M., Horton, R., Smistrup, K., Best-Popescu, C. A., and Stone, H. A. (2008). Cellular-scale hydrodynamics. *Biomed. Mater. Bristol Engl.* 3, 034011. doi: 10.1088/1748-6041/3/3/034011.

Abraham, E. H., Sterling Km, Kim Rj, Salikhova Ay, Huffman Hb, Crockett Ma, et al. (2001). Erythrocyte membrane ATP binding cassette (ABC) proteins: MRP1 and CFTR as well as CD39 (ecto-apyrase) involved in RBC ATP transport and elevated blood plasma ATP of cystic fibrosis. *Blood Cells. Mol. Dis.* 27. doi: 10.1006/bcmd.2000.0357.

Agarwal, J. J., Zhu, Y., Zhang, Q.-Y., Mongin, A. A., and Hough, L. B. (2013). TRAM-34, a Putatively Selective Blocker of Intermediate-Conductance, Calcium-Activated Potassium Channels, Inhibits Cytochrome P450 Activity. *PLoS ONE* 8, e63028. doi: 10.1371/journal.pone.0063028.

Aglialoro, F., Abay, A., Yagci, N., Rab, M. A. E., Kaestner, L., van Wijk, R., et al. (2021). Mechanical Stress Induces Ca2+-Dependent Signal Transduction in Erythroblasts and Modulates Erythropoiesis. *Int. J. Mol. Sci.* 22, 955. doi: 10.3390/ijms22020955.

Aglialoro, F., Hofsink, N., Hofman, M., Brandhorst, N., and van den Akker, E. (2020). Inside Out Integrin Activation Mediated by PIEZO1 Signaling in Erythroblasts. *Front. Physiol.* 11, 958. doi: 10.3389/fphys.2020.00958.

Agre, P., Preston, G. M., Smith, B. L., Jung, J. S., Raina, S., Moon, C., et al. (1993). Aquaporin CHIP: the archetypal molecular water channel. *Am. J. Physiol.* 265, F463-476. doi: 10.1152/ajprenal.1993.265.4.F463.

Agre, P., Saboori, A. M., Asimos, A., and Smith, B. L. (1987). Purification and partial characterization of the Mr 30,000 integral membrane protein associated with the erythrocyte Rh(D) antigen. *J. Biol. Chem.* 262, 17497–17503.

Akorsu, E. E., Adjabeng, L. B., Sulleymana, M. A., and Kwadzokpui, P. K. (2023). Variations in the full blood count parameters among apparently healthy humans in the Ho municipality using ethylenediamine tetraacetic acid (EDTA), sodium citrate and lithium heparin anticoagulants: A laboratory-based cross-sectional analytical study. *Heliyon* 9, e17311. doi: 10.1016/j.heliyon.2023.e17311.

Al Balushi, H., Dufu, K., Rees, D. C., Brewin, J. N., Hannemann, A., Oksenberg, D., et al. (2019). The effect of the antisickling compound GBT1118 on the permeability of red blood cells from patients with sickle cell anemia. *Physiol. Rep.* 7, e14027. doi: 10.14814/phy2.14027.

Alaarg, A., Schiffelers, R. M., van Solinge, W. W., and van Wijk, R. (2013). Red blood cell vesiculation in hereditary hemolytic anemia. *Front. Physiol.* 4, 365. doi: 10.3389/fphys.2013.00365.

Albuisson, J., Murthy, S. E., Bandell, M., Coste, B., Louis-Dit-Picard, H., Mathur, J., et al. (2013). Dehydrated hereditary stomatocytosis linked to gain-of-function mutations in mechanically activated PIEZO1 ion channels. *Nat. Commun.* 4, 1884. doi: 10.1038/ncomms2899.

Ali, M. (2020). Performance of complete blood count (CBC) upon use of different anticoagulants in rats. *Asian J. Med. Biol. Res.* Available at: https://www.ebupress.com/journal/ajmbr/2020/04/10/performance-of-complete-blood-count-cbc-upon-use-of-different-anticoagulants-in-rats [Accessed October 19, 2023].

Allegrini, B., Jedele, S., David Nguyen, L., Mignotet, M., Rapetti-Mauss, R., Etchebest, C., et al. (2022). New KCNN4 Variants Associated With Anemia: Stomatocytosis Without Erythrocyte Dehydration. *Front. Physiol.* 13, 918620. doi: 10.3389/fphys.2022.918620.

Allison, A. C. (1954). Protection afforded by sickle-cell trait against subtertian malareal infection. *Br. Med. J.* 1, 290–294. doi: 10.1136/bmj.1.4857.290.

Alper, S. L. (1991). The band 3-related anion exchanger (AE) gene family. *Annu. Rev. Physiol.* 53, 549–564. doi: 10.1146/annurev.ph.53.030191.003001.

Alper, S. L. (2017). Genetic Diseases of PIEZO1 and PIEZO2 Dysfunction. *Curr. Top. Membr.* 79, 97–134. doi: 10.1016/bs.ctm.2017.01.001.

An, X., Salomao, M., Guo, X., Gratzer, W., and Mohandas, N. (2007). Tropomyosin modulates erythrocyte membrane stability. *Blood* 109, 1284–1288. doi: 10.1182/blood-2006-07-036954.

An, X., Schulz, V. P., Li, J., Wu, K., Liu, J., Xue, F., et al. (2014). Global transcriptome analyses of human and murine terminal erythroid differentiation. *Blood* 123, 3466–3477. doi: 10.1182/blood-2014-01-548305.

Andersen, O. S., and Koeppe, R. E. (2007). Bilayer thickness and membrane protein function: an energetic perspective. *Annu. Rev. Biophys. Biomol. Struct.* 36, 107–130. doi: 10.1146/annurev.biophys.36.040306.132643.

Andolfo, I., Alper, S. L., De Franceschi, L., Auriemma, C., Russo, R., De Falco, L., et al. (2013a). Multiple clinical forms of dehydrated hereditary stomatocytosis arise from mutations in PIEZO1. *Blood* 121, 3925–3935, S1-12. doi: 10.1182/blood-2013-02-482489.

Andolfo, I., Alper, S. L., Delaunay, J., Auriemma, C., Russo, R., Asci, R., et al. (2013b). Missense mutations in the ABCB6 transporter cause dominant familial pseudohyperkalemia. *Am. J. Hematol.* 88, 66–72. doi: 10.1002/ajh.23357.

Andolfo, I., De Rosa, G., Errichiello, E., Manna, F., Rosato, B. E., Gambale, A., et al. (2019). PIEZO1 Hypomorphic Variants in Congenital Lymphatic Dysplasia Cause Shape and Hydration Alterations of Red Blood Cells. *Front. Physiol.* 10. Available at: https://www.frontiersin.org/articles/10.3389/fphys.2019.00258 [Accessed October 17, 2023].

Andolfo, I., Martone, S., Rosato, B. E., Marra, R., Gambale, A., Forni, G. L., et al. (2021). Complex Modes of Inheritance in Hereditary Red Blood Cell Disorders: A Case Series Study of 155 Patients. *Genes* 12, 958. doi: 10.3390/genes12070958.

Andolfo, I., Monaco, V., Cozzolino, F., Rosato, B. E., Marra, R., Cerbone, V., et al. (2023). Proteome alterations in erythrocytes with PIEZO1 gain-of-function mutations. *Blood Adv.* 7, 2681–2693. doi: 10.1182/bloodadvances.2022008673.

Andolfo, I., Russo, R., Gambale, A., and Iolascon, A. (2016). New insights on hereditary erythrocyte membrane defects. *Haematologica* 101, 1284–1294. doi: 10.3324/haematol.2016.142463.

Andolfo, I., Russo, R., Manna, F., Shmukler, B. E., Gambale, A., Vitiello, G., et al. (2015). Novel Gardos channel mutations linked to dehydrated hereditary stomatocytosis (xerocytosis). *Am. J. Hematol.* 90, 921–926. doi: 10.1002/ajh.24117.

Andolfo, I., Russo, R., Rosato, B. E., Manna, F., Gambale, A., Brugnara, C., et al. (2018). Genotype-phenotype correlation and risk stratification in a cohort of 123 hereditary stomatocytosis patients. *Am. J. Hematol.* 93, 1509–1517. doi: 10.1002/ajh.25276.

Andrews, D. A., Yang, L., and Low, P. S. (2002). Phorbol ester stimulates a protein kinase C-mediated agatoxin-TK-sensitive calcium permeability pathway in human red blood cells. *Blood* 100, 3392–3399. doi: 10.1182/blood.V100.9.3392.

Apovo, M., Beuzard, Y., Galacteros, F., Bachir, D., and Giraud, F. (1994). The involvement of the Ca-dependent K channel and of the KCl co-transport in sickle cell dehydration during cyclic deoxygenation. *Biochim. Biophys. Acta* 1225, 255–258. doi: 10.1016/0925-4439(94)90003-5.

Archer, N. M., Shmukler, B. E., Andolfo, I., Vandorpe, D. H., Gnanasambandam, R., Higgins, J. M., et al. (2014). Hereditary xerocytosis revisited. *Am. J. Hematol.* 89, 1142–1146. doi: 10.1002/ajh.23799.

Atlas genetics (2023). TRPV2 (transient receptor potential cation channel, subfamily V, member 2). Available at: https://atlasgeneticsoncology.org/gene/45817/trpv2-%28transient-receptor-potential-cation-channel-subfamily-v-member-2%29 [Accessed October 17, 2023].

Bae, C., Gnanasambandam, R., Nicolai, C., Sachs, F., and Gottlieb, P. A. (2013). Xerocytosis is caused by mutations that alter the kinetics of the mechanosensitive channel PIEZO1. *Proc. Natl. Acad. Sci. U. S. A.* 110, E1162-1168. doi: 10.1073/pnas.1219777110.

Bae, C., Sachs, F., and Gottlieb, P. A. (2011). The mechanosensitive ion channel Piezo1 is inhibited by the peptide GsMTx4. *Biochemistry* 50, 6295–6300. doi: 10.1021/bi200770q.

Balach, M. M., Casale, C. H., and Campetelli, A. N. (2019). Erythrocyte plasma membrane potential: past and current methods for its measurement. *Biophys. Rev.* 11, 995–1005. doi: 10.1007/s12551-019-00603-5.

Ballas, S. K., Clark, M. R., Mohandas, N., Colfer, H. F., Caswell, M. S., Bergren, M. O., et al. (1984). Red cell membrane and cation deficiency in Rh null syndrome. *Blood* 63, 1046–1055.

Bandaru, S. S., Killeen, R. B., and Gupta, V. (2023). "Poikilocytosis," in *StatPearls* (Treasure Island (FL): StatPearls Publishing). Available at: http://www.ncbi.nlm.nih.gov/books/NBK562141/ [Accessed September 15, 2023].

Barksmann, T. L., Kristensen, B. I., Christophersen, P., and Bennekou, P. (2004). Pharmacology of the human red cell voltage-dependent cation channel; Part I. Activation by clotrimazole and analogues. *Blood Cells. Mol. Dis.* 32, 384–388. doi: 10.1016/j.bcmd.2004.01.011.

Barneaud-Rocca, D., Etchebest, C., and Guizouarn, H. (2013). Structural Model of the Anion Exchanger 1 (SLC4A1) and Identification of Transmembrane Segments Forming the Transport Site. *J. Biol. Chem.* 288, 26372–26384. doi: 10.1074/jbc.M113.465989.

Barshtein, G., Pajic-Lijakovic, I., and Gural, A. (2021). Deformability of Stored Red Blood Cells. *Front. Physiol.* 12, 722896. doi: 10.3389/fphys.2021.722896.

Baunbaek, M., and Bennekou, P. (2008). Evidence for a random entry of Ca2+ into human red cells. *Bioelectrochemistry Amst. Neth.* 73, 145–150. doi: 10.1016/j.bioelechem.2008.04.006.

Bavi, N., Richardson, J., Heu, C., Martinac, B., and Poole, K. (2019). PIEZO1-Mediated Currents Are Modulated by Substrate Mechanics. *ACS Nano* 13, 13545–13559. doi: 10.1021/acsnano.9b07499.

Belkacemi, A., Fecher-Trost, C., Tinschert, R., Flormann, D., Malihpour, M., Wagner, C., et al. (2021). The TRPV2 channel mediates Ca2+ influx and the Δ9-THC-dependent decrease in osmotic fragility in red blood cells. *Haematologica* 106, 2246–2250. doi: 10.3324/haematol.2020.274951.

Beneteau, C., Thierry, G., Blesson, S., Le Vaillant, C., Picard, V., Béné, M. C., et al. (2014). Recurrent mutation in the PIEZO1 gene in two families of hereditary xerocytosis with fetal hydrops. *Clin. Genet.* 85, 293–295. doi: 10.1111/cge.12147.

Bennekou, P. (1993). The voltage-gated non-selective cation channel from human red cells is sensitive to acetylcholine. *Biochim. Biophys. Acta BBA - Biomembr.* 1147, 165–167. doi: 10.1016/0005-2736(93)90328-W.

Bennekou, P. (1999). The feasibility of pharmacological volume control of sickle cells is dependent on the quantization of the transport pathways. A model study. *J. Theor. Biol.* 196, 129–137. doi: 10.1006/jtbi.1998.0819.

Bennekou, P., Barksmann, T. L., Jensen, L. R., Kristensen, B. I., and Christophersen, P. (2004). Voltage activation and hysteresis of the non-selective voltage-dependent channel in the intact human red cell. *Bioelectrochemistry Amst. Neth.* 62, 181–185. doi: 10.1016/j.bioelechem.2003.08.006.

Bennekou, P., and Christophersen, P. (1986). Flux ratio of valinomycin-mediated K+ fluxes across the human red cell membrane in the presence of the protonophore CCCP. *J. Membr. Biol.* 93, 221–227. doi: 10.1007/BF01871176.

Bennekou, P., de Franceschi, L., Pedersen, O., Lian, L., Asakura, T., Evans, G., et al. (2001). Treatment with NS3623, a novel Cl-conductance blocker, ameliorates erythrocyte dehydration in transgenic SAD mice: a possible new therapeutic approach for sickle cell disease. *Blood* 97, 1451–1457. doi: 10.1182/blood.V97.5.1451.

Bennekou, P., Kristensen, B. I., and Christophersen, P. (2003). The human red cell voltage-regulated cation channel. The interplay with the chloride conductance, the Ca(2+)-activated K(+) channel and the Ca(2+) pump. *J. Membr. Biol.* 195, 1–8. doi: 10.1007/s00232-003-2036-6.

Bennett, V., and Stenbuck, P. J. (1979). Identification and partial purification of ankyrin, the high affinity membrane attachment site for human erythrocyte spectrin. *J. Biol. Chem.* 254, 2533–2541.

Bergfeld, G. R., and Forrester, T. (1992). Release of ATP from human erythrocytes in response to a brief period of hypoxia and hypercapnia. *Cardiovasc. Res.* 26, 40–47. doi: 10.1093/cvr/26.1.40.

Bernhardt, I., and Ellory, J. C. (2003). *Red Cell Membrane Transport in Health and Disease*. Berlin, Heidelberg: Springer Berlin Heidelberg Available at: http://public.ebookcentral.proquest.com/choice/publicfullrecord.aspx?p=3100185 [Accessed December 8, 2020].

Bernhardt, I., and Weiss, E. (2003). "Passive Membrane Permeability for Ions and the Membrane Potential," in *Red Cell Membrane Transport in Health and Disease*, eds. I. Bernhardt and J. C. Ellory (Berlin, Heidelberg: Springer), 83–109. doi: 10.1007/978-3-662-05181-8_4.

Bessis, M. (1972). Red cell shapes. An illustrated classification and its rationale. *Nouv. Rev. Fr. Hematol.* 12, 721–745.

Bessis, M. (1974). *Corpuscles- Atlas of Red Blood Cell Shapes*. First. Springer Berlin Heidelberg.

Bessis, M., and Delpech, G. (1981). Discovery of the red blood cell with notes on priorities and credits of discoveries, past, present and future. *Blood Cells* 7, 447–480.

Bevers, E. M., and Williamson, P. L. (2010). Phospholipid scramblase: an update. *FEBS Lett.* 584, 2724–2730. doi: 10.1016/j.febslet.2010.03.020.

Bianchi, P., Vercellati, C., and Fermo, E. (2020). How will next generation sequencing (NGS) improve the diagnosis of congenital hemolytic anemia? *Ann. Transl. Med.* 8, 268. doi: 10.21037/atm.2020.02.151.

Blank, M. E., and Ehmke, H. (2003). Aquaporin-1 and HCO3(-)-Cl- transporter-mediated transport of CO2 across the human erythrocyte membrane. *J. Physiol.* 550, 419–429. doi: 10.1113/jphysiol.2003.040113.

Bloj, B., Morero, R. D., Farías, R. N., and Trucco, R. E. (1973). Membrane lipid fatty acids and regulation of membrane-bound enzymes. Allosteric behaviour of erythrocyte Mg 2+ -ATPase, (Na + +K +)-ATPase and acetylcholinesterase from rats fed different fat-supplemented diets. *Biochim. Biophys. Acta* 311, 67–79. doi: 10.1016/0005-2736(73)90255-1.

Bogardus, H. H., Maksimova, Y. D., Forget, B. G., and Gallagher, P. G. (2012). A de novo band 3 mutation in hereditary spherocytosis. *Pediatr. Blood Cancer* 58, 1004. doi: 10.1002/pbc.23400.

Bogdanova, A., Makhro, A., Wang, J., Lipp, P., and Kaestner, L. (2013). Calcium in red blood cells-a perilous balance. *Int. J. Mol. Sci.* 14, 9848–9872. doi: 10.3390/ijms14059848.

Bohr, Hasselbalch, & Krogh (1904). Available at: https://www1.udel.edu/chem/white/C342/Bohr(1904).html [Accessed October 14, 2023].

Boisson, C., Rab, M. A. E., Nader, E., Renoux, C., van Oirschot, B. A., Joly, P., et al. (2021). Methodological aspects of oxygen gradient ektacytometry in sickle cell disease: Effects of sample storage on outcome parameters in distinct patient subgroups. *Clin. Hemorheol. Microcirc.* 77, 391–394. doi: 10.3233/CH-201037.

Bookchin, R. M., Etzion, Z., Sorette, M., Mohandas, N., Skepper, J. N., and Lew, V. L. (2000). Identification and characterization of a newly recognized population of high-Na+, low-K+, low-density sickle and normal red cells. *Proc. Natl. Acad. Sci. U. S. A.* 97, 8045–8050. doi: 10.1073/pnas.130198797.

Bookchin, R. M., and Lew, V. L. (1981). Effect of a "sickling pulse" on calcium and potassium transport in sickle cell trait red cells. *J. Physiol.* 312, 265–280. doi: 10.1113/jphysiol.1981.sp013628.

Bookchin, R. M., Ortiz, O. E., Shalev, O., Tsurel, S., Rachmilewitz, E. A., Hockaday, A., et al. (1988). Calcium transport and ultrastructure of red cells in beta-thalassemia intermedia. *Blood* 72, 1602–1607.

Borbiro, I., Badheka, D., and Rohacs, T. (2015). Activation of TRPV1 channels inhibits mechanosensitive Piezo channel activity by depleting membrane phosphoinositides. *Sci. Signal.* 8, ra15. doi: 10.1126/scisignal.2005667.

Botello-Smith, W. M., Jiang, W., Zhang, H., Ozkan, A. D., Lin, Y.-C., Pham, C. N., et al. (2019). A mechanism for the activation of the mechanosensitive Piezo1 channel by the small molecule Yoda1. *Nat. Commun.* 10, 4503. doi: 10.1038/s41467-019-12501-1.

Boulay, G., Zhu, X., Peyton, M., Jiang, M., Hurst, R., Stefani, E., et al. (1997). Cloning and expression of a novel mammalian homolog of Drosophila transient receptor potential (Trp) involved in calcium entry secondary to activation of receptors coupled by the Gq class of G protein. *J. Biol. Chem.* 272, 29672–29680. doi: 10.1074/jbc.272.47.29672.

Bouyer, G., Cueff, A., Egée, S., Kmiecik, J., Maksimova, Y., Glogowska, E., et al. (2011). Erythrocyte peripheral type benzodiazepine receptor/voltage-dependent anion channels are upregulated by Plasmodium falciparum. *Blood* 118, 2305–2312. doi: 10.1182/blood-2011-01-329300.

Bouyer, G., Egée, S., and Thomas, S. L. Y. (2007). Toward a unifying model of malaria-induced channel activity. *Proc. Natl. Acad. Sci. U. S. A.* 104, 11044–11049. doi: 10.1073/pnas.0704582104.

Božič, B., and Svetina, S. (2022). Membrane Localization of Piezo1 in the Context of Its Role in the Regulation of Red Blood Cell Volume. *Front. Physiol.* 13, 879038. doi: 10.3389/fphys.2022.879038.

Bretscher, M. S. (1971). A major protein which spans the human erythrocyte membrane. *J. Mol. Biol.* 59, 351–357. doi: 10.1016/0022-2836(71)90055-6.

Brown, A. M., and Lew, V. L. (1983). The effect of intracellular calcium on the sodium pump of human red cells. *J. Physiol.* 343, 455–493. doi: 10.1113/jphysiol.1983.sp014904.

Brown, M. F. (2017). Soft Matter in Lipid-Protein Interactions. *Annu. Rev. Biophys.* 46, 379–410. doi: 10.1146/annurev-biophys-070816-033843.

Browning, J. A., Staines, H. M., Robinson, H. C., Powell, T., Ellory, J. C., and Gibson, J. S. (2007). The effect of deoxygenation on whole-cell conductance of red blood cells from healthy individuals and patients with sickle cell disease. *Blood* 109, 2622–2629. doi: 10.1182/blood-2006-03-001404.

Bruce, L. J., and Gyorffy, G. (2019). Red cell membrane proteins. *HemaSphere* 3, 154–156. doi: 10.1097/HS9.0000000000000189.

Bruce, L. J., Robinson, H. C., Guizouarn, H., Borgese, F., Harrison, P., King, M.-J., et al. (2005). Monovalent cation leaks in human red cells caused by single amino-acid substitutions in the transport domain of the band 3 chloride-bicarbonate exchanger, AE1. *Nat. Genet.* 37, 1258–1263. doi: 10.1038/ng1656.

Brugnara, C. (2018). Sickle cell dehydration: Pathophysiology and therapeutic applications. *Clin. Hemorheol. Microcirc.* 68, 187–204. doi: 10.3233/CH-189007.

Brugnara, C., De Franceschi, L., and Alper, S. L. (1993a). Ca(2+)-activated K+ transport in erythrocytes. Comparison of binding and transport inhibition by scorpion toxins. *J. Biol. Chem.* 268, 8760–8768.

Brugnara, C., de Franceschi, L., and Alper, S. L. (1993b). Inhibition of Ca(2+)-dependent K+ transport and cell dehydration in sickle erythrocytes by clotrimazole and other imidazole derivatives. *J. Clin. Invest.* 92, 520–526. doi: 10.1172/JCI116597.

Brugnara, C., Gee, B., Armsby, C. C., Kurth, S., Sakamoto, M., Rifai, N., et al. (1996). Therapy with oral clotrimazole induces inhibition of the Gardos channel and reduction of erythrocyte dehydration in patients with sickle cell disease. *J. Clin. Invest.* 97, 1227–1234. doi: 10.1172/JCI118537.

Burton, N. M., and Bruce, L. J. (2011). Modelling the structure of the red cell membrane. *Biochem. Cell Biol. Biochim. Biol. Cell.* 89, 200–215. doi: 10.1139/o10-154.

Byers, T. J., and Branton, D. (1985). Visualization of the protein associations in the erythrocyte membrane skeleton. *Proc. Natl. Acad. Sci. U. S. A.* 82, 6153–6157. doi: 10.1073/pnas.82.18.6153.

Cabantchik, Z. I., and Rothstein, A. (1974). Membrane proteins related to anion permeability of human red blood cells. I. Localization of disulfonic stilbene binding sites in proteins involved in permeation. *J. Membr. Biol.* 15, 207–226. doi: 10.1007/BF01870088.

Cahalan, S. M., Lukacs, V., Ranade, S. S., Chien, S., Bandell, M., and Patapoutian, A. (2015). Piezo1 links mechanical forces to red blood cell volume. *eLife* 4, e07370. doi: 10.7554/eLife.07370.

Carquin, M., Conrard, L., Pollet, H., Van Der Smissen, P., Cominelli, A., Veiga-da-Cunha, M., et al. (2015). Cholesterol segregates into submicrometric domains at the living erythrocyte membrane: evidence and regulation. *Cell. Mol. Life Sci. CMLS* 72, 4633–4651. doi: 10.1007/s00018-015-1951-x.

Carquin, M., D'Auria, L., Pollet, H., Bongarzone, E. R., and Tyteca, D. (2016). Recent progress on lipid lateral heterogeneity in plasma membranes: From rafts to submicrometric domains. *Prog. Lipid Res.* 62, 1–24. doi: 10.1016/j.plipres.2015.12.004.

Carquin, M., Pollet, H., Veiga-da-Cunha, M., Cominelli, A., Van Der Smissen, P., N'kuli, F., et al. (2014). Endogenous sphingomyelin segregates into submicrometric domains in the living erythrocyte membrane. *J. Lipid Res.* 55, 1331–1342. doi: 10.1194/jlr.M048538.

Caulier, A., Jankovsky, N., Demont, Y., Ouled-Haddou, H., Demagny, J., Guitton, C., et al. (2020). PIEZO1 activation delays erythroid differentiation of normal and hereditary xerocytosis-derived human progenitor cells. *Haematologica* 105, 610–622. doi: 10.3324/haematol.2019.218503.

Caulier, A., Rapetti-Mauss, R., Guizouarn, H., Picard, V., Garçon, L., and Badens, C. (2018). Primary red cell hydration disorders: Pathogenesis and diagnosis. *Int. J. Lab. Hematol.* 40, 68–73. doi: 10.1111/ijlh.12820.

Chaney, S., Basirat, A., McDermott, R., Keenan, N., and Moloney, E. (2020). COVID-19 and hydroxychloroquine side-effects: glucose 6-phosphate dehydrogenase deficiency (G6PD) and acute haemolytic anaemia. *QJM Mon. J. Assoc. Physicians* 113, 890–891. doi: 10.1093/qjmed/hcaa267.

Chasis, J. A., Agre, P., and Mohandas, N. (1988). Decreased membrane mechanical stability and in vivo loss of surface area reflect spectrin deficiencies in hereditary spherocytosis. *J. Clin. Invest.* 82, 617–623. doi: 10.1172/JCI113640.

Chasis, J. A., and Mohandas, N. (2008). Erythroblastic islands: niches for erythropoiesis. *Blood* 112, 470–478. doi: 10.1182/blood-2008-03-077883.

Chen, M., and Boyle, F. J. (2017). An Enhanced Spring-Particle Model for Red Blood Cell Structural Mechanics: Application to the Stomatocyte-Discocyte-Echinocyte Transformation. *J. Biomech. Eng.* 139. doi: 10.1115/1.4037590.

Chen, Z., Jiang, J., Fu, N., and Chen, L. (2022). Targetting ferroptosis for blood cell-related diseases. *J. Drug Target.* 30, 244–258. doi: 10.1080/1061186X.2021.1971237.

Cheng, K., Haspel, H. C., Vallano, M. L., Osotimehin, B., and Sonenberg, M. (1980). Measurement of membrane potentials (psi) of erythrocytes and white adipocytes by the accumulation of triphenylmethylphosphonium cation. *J. Membr. Biol.* 56, 191–201. doi: 10.1007/BF01869476.

Christophersen, P. (1991). Ca2(+)-activated K+ channel from human erythrocyte membranes: single channel rectification and selectivity. *J. Membr. Biol.* 119, 75–83. doi: 10.1007/BF01868542.

Christophersen, P., and Bennekou, P. (1991). Evidence for a voltage-gated, non-selective cation channel in the human red cell membrane. *Biochim. Biophys. Acta BBA - Biomembr.* 1065, 103–106. doi: 10.1016/0005-2736(91)90017-3.

Chu, H., McKenna, M. M., Krump, N. A., Zheng, S., Mendelsohn, L., Thein, S. L., et al. (2016). Reversible binding of hemoglobin to band 3 constitutes the molecular switch that mediates O2 regulation of erythrocyte properties. *Blood* 128, 2708–2716. doi: 10.1182/blood-2016-01-692079.

Chuang, Y.-C., and Chen, C.-C. (2022). Force From Filaments: The Role of the Cytoskeleton and Extracellular Matrix in the Gating of Mechanosensitive Channels. *Front. Cell Dev. Biol.* 10. Available at: https://www.frontiersin.org/articles/10.3389/fcell.2022.886048 [Accessed November 14, 2023].

Cinar, E., Zhou, S., DeCourcey, J., Wang, Y., Waugh, R. E., and Wan, J. (2015). Piezo1 regulates mechanotransductive release of ATP from human RBCs. *Proc. Natl. Acad. Sci. U. S. A.* 112, 11783–11788. doi: 10.1073/pnas.1507309112.

Claret, M., Garay, R., and Giraud, F. (1978). The effect of membrane cholesterol on the sodium pump in red blood cells. *J. Physiol.* 274, 247–263. doi: 10.1113/jphysiol.1978.sp012145.

Cloos, A.-S., Ghodsi, M., Stommen, A., Vanderroost, J., Dauguet, N., Pollet, H., et al. (2020). Interplay Between Plasma Membrane Lipid Alteration, Oxidative Stress and Calcium-Based Mechanism for Extracellular Vesicle Biogenesis From Erythrocytes During Blood Storage. *Front. Physiol.* 11, 712. doi: 10.3389/fphys.2020.00712.

Conde, J., Pumroy, R. A., Baker, C., Rodrigues, T., Guerreiro, A., Sousa, B. B., et al. (2021). Allosteric Antagonist Modulation of TRPV2 by Piperlongumine Impairs Glioblastoma Progression. *ACS Cent. Sci.* 7, 868–881. doi: 10.1021/acscentsci.1c00070.

Conrard, L., Stommen, A., Cloos, A.-S., Steinkühler, J., Dimova, R., Pollet, H., et al. (2018). Spatial Relationship and Functional Relevance of Three Lipid Domain Populations at the Erythrocyte Surface. *Cell. Physiol. Biochem. Int. J. Exp. Cell. Physiol. Biochem. Pharmacol.* 51, 1544–1565. doi: 10.1159/000495645.

Conrard, L., and Tyteca, D. (2019). Regulation of Membrane Calcium Transport Proteins by the Surrounding Lipid Environment. *Biomolecules* 9, 513. doi: 10.3390/biom9100513.

Cooper, G. J., Zhou, Y., Bouyer, P., Grichtchenko, I. I., and Boron, W. F. (2002). Transport of volatile solutes through AQP1. *J. Physiol.* 542, 17–29. doi: 10.1113/jphysiol.2002.023218.

Corrons, J. L. V., Casafont, L. B., and Frasnedo, E. F. (2021). Concise review: how do red blood cells born, live, and die? *Ann. Hematol.* 100, 2425–2433. doi: 10.1007/s00277-021-04575-z.

Cossins, A. R., and Gibson, J. S. (1997). Volume-sensitive transport systems and volume homeostasis in vertebrate red blood cells. *J. Exp. Biol.* 200, 343–352. doi: 10.1242/jeb.200.2.343.

Coste, B., Mathur, J., Schmidt, M., Earley, T. J., Ranade, S., Petrus, M. J., et al. (2010). Piezo1 and Piezo2 Are Essential Components of Distinct Mechanically Activated Cation Channels. *Science* 330, 55–60. doi: 10.1126/science.1193270.

Coste, B., Murthy, S. E., Mathur, J., Schmidt, M., Mechioukhi, Y., Delmas, P., et al. (2015). Piezo1 ion channel pore properties are dictated by C-terminal region. *Nat. Commun.* 6, 7223. doi: 10.1038/ncomms8223.

Coste, B., Xiao, B., Santos, J. S., Syeda, R., Grandl, J., Spencer, K. S., et al. (2012). Piezo proteins are pore-forming subunits of mechanically activated channels. *Nature* 483, 176–181. doi: 10.1038/nature10812.

Cox, C. D., Bae, C., Ziegler, L., Hartley, S., Nikolova-Krstevski, V., Rohde, P. R., et al. (2016). Removal of the mechanoprotective influence of the cytoskeleton reveals PIEZO1 is gated by bilayer tension. *Nat. Commun.* 7, 10366. doi: 10.1038/ncomms10366.

Cox, C. D., Bavi, N., and Martinac, B. (2017). Origin of the Force: The Force-From-Lipids Principle Applied to Piezo Channels. *Curr. Top. Membr.* 79, 59–96. doi: 10.1016/bs.ctm.2016.09.001.

Cox, C. D., Bavi, N., and Martinac, B. (2019). Biophysical Principles of Ion-Channel-Mediated Mechanosensory Transduction. *Cell Rep.* 29, 1–12. doi: 10.1016/j.celrep.2019.08.075.

Crew, K. V., Tilley, L. A., Satchwell, T. J., AlSubhi, S. A., Jones, B., Spring, F. A., et al. (2023). Missense mutations in PIEZO1, which encodes the Piezo1 mechanosensor protein, define Er red blood cell antigens. *Blood* 141, 135–146. doi: 10.1182/blood.2022016504.

Da Costa, L., Galimand, J., Fenneteau, O., and Mohandas, N. (2013). Hereditary spherocytosis, elliptocytosis, and other red cell membrane disorders. *Blood Rev.* 27, 167–178. doi: 10.1016/j.blre.2013.04.003.

Da Costa, L., Suner, L., Galimand, J., Bonnel, A., Pascreau, T., Couque, N., et al. (2016). Diagnostic tool for red blood cell membrane disorders: Assessment of a new generation ektacytometer. *Blood Cells. Mol. Dis.* 56, 9–22. doi: 10.1016/j.bcmd.2015.09.001.

Danielczok, J. G., Terriac, E., Hertz, L., Petkova-Kirova, P., Lautenschläger, F., Laschke, M. W., et al. (2017). Red Blood Cell Passage of Small Capillaries Is Associated with Transient Ca2+-mediated Adaptations. *Front. Physiol.* 8, 979. doi: 10.3389/fphys.2017.00979.

D'auria, L., Van der Smissen, P., Bruyneel, F., Courtoy, P. J., and Tyteca, D. (2011). Segregation of fluorescent membrane lipids into distinct micrometric domains: evidence for phase compartmentation of natural lipids? *PloS One* 6, e17021. doi: 10.1371/journal.pone.0017021.

David-Dufilho, M., Montenay-Garestier, T., and Devynck, M. A. (1988). Fluorescence measurements of free Ca2+ concentration in human erythrocytes using the Ca2+-indicator fura-2. *Cell Calcium* 9, 167–179. doi: 10.1016/0143-4160(88)90021-8.

De Flora, A., Benatti, U., Guida, L., Forteleoni, G., and Meloni, T. (1985). Favism: disordered erythrocyte calcium homeostasis. *Blood* 66, 294–297.

De Franceschi, L., Franco, R. S., Bertoldi, M., Brugnara, C., Matté, A., Siciliano, A., et al. (2013). Pharmacological inhibition of calpain-1 prevents red cell dehydration and reduces Gardos channel activity in a mouse model of sickle cell disease. *FASEB J. Off. Publ. Fed. Am. Soc. Exp. Biol.* 27, 750–759. doi: 10.1096/fj.12-217836.

De Maria, R., Zeuner, A., Eramo, A., Domenichelli, C., Bonci, D., Grignani, F., et al. (1999). Negative regulation of erythropoiesis by caspase-mediated cleavage of GATA-1. *Nature* 401, 489–493. doi: 10.1038/46809.

Dean, L. (2005). "Blood and the cells it contains," in *Blood Groups and Red Cell Antigens [Internet]* (National Center for Biotechnology Information (US)). Available at: https://www.ncbi.nlm.nih.gov/books/NBK2263/ [Accessed September 4, 2023].

Delaunay, J. (2004). The hereditary stomatocytoses: genetic disorders of the red cell membrane permeability to monovalent cations. *Semin. Hematol.* 41, 165–172. doi: 10.1053/j.seminhematol.2004.02.005.

Delaunay, J. (2007). The molecular basis of hereditary red cell membrane disorders. *Blood Rev.* 21, 1–20. doi: 10.1016/j.blre.2006.03.005.

Delaunay, J., and Stewart, G. (2006). "Disorders of the Red Cell Membrane," in *Principles of Molecular Medicine*, 830–837. doi: 10.1007/978-1-59259-963-9_85.

Denker, B. M., Smith, B. L., Kuhajda, F. P., and Agre, P. (1988). Identification, purification, and partial characterization of a novel Mr 28,000 integral membrane protein from erythrocytes and renal tubules. *J. Biol. Chem.* 263, 15634–15642.

Deplaine, G., Safeukui, I., Jeddi, F., Lacoste, F., Brousse, V., Perrot, S., et al. (2011). The sensing of poorly deformable red blood cells by the human spleen can be mimicked in vitro. *Blood* 117, e88-95. doi: 10.1182/blood-2010-10-312801.

Desai, S. A., McCleskey, E. W., Schlesinger, P. H., and Krogstad, D. J. (1996). A novel pathway for Ca++ entry into Plasmodium falciparum-infected blood cells. *Am. J. Trop. Med. Hyg.* 54, 464–470. doi: 10.4269/ajtmh.1996.54.464.

Discher, D. E., and Carl, P. (2001). New insights into red cell network structure, elasticity, and spectrin unfolding--a current review. *Cell. Mol. Biol. Lett.* 6, 593–606.

Dodge, J. T., Mitchell, C., and Hanahan, D. J. (1963). The preparation and chemical characteristics of hemoglobin-free ghosts of human erythrocytes. *Arch. Biochem. Biophys.* 100, 119–130. doi: 10.1016/0003-9861(63)90042-0.

Dreher, K. L., Eaton, J. W., Breslawec, K. P., Berger, E., Blackshear, P. L., and White, J. G. (1980). Calcium-induced erythrocyte rigidity: the roles of cellular metabolism, hydration, and ionic balance. *Am. J. Pathol.* 101, 543–556.

Ducrocq, G., Puymirat, E., Steg, P. G., Henry, P., Martelet, M., Karam, C., et al. (2015). Blood transfusion, bleeding, anemia, and survival in patients with acute myocardial infarction: FAST-MI registry. *Am. Heart J.* 170, 726-734.e2. doi: 10.1016/j.ahj.2015.07.004.

Dumitru, A. C., Stommen, A., Koehler, M., Cloos, A.-S., Yang, J., Leclercqz, A., et al. (2021). Probing PIEZO1 Localization upon Activation Using High-Resolution Atomic Force and Confocal Microscopy. *Nano Lett.* 21, 4950–4958. doi: 10.1021/acs.nanolett.1c00599.

Dupire, J., Socol, M., and Viallat, A. (2012). Full dynamics of a red blood cell in shear flow. *Proc. Natl. Acad. Sci.* 109, 20808–20813. doi: 10.1073/pnas.1210236109.

Duranton, C., Huber, S. M., and Lang, F. (2002). Oxidation induces a Cl(-)-dependent cation conductance in human red blood cells. *J. Physiol.* 539, 847–855. doi: 10.1113/jphysiol.2001.013040.

Dyrda, A., Cytlak, U., Ciuraszkiewicz, A., Lipinska, A., Cueff, A., and Bouyer, G. (2010). Local Membrane Deformations Activate Ca2+-Dependent K+ and Anionic Currents in Intact Human Red Blood Cells. *PLoS ONE* 5, 14.

Dzierzak, E., and Philipsen, S. (2013). Erythropoiesis: development and differentiation. *Cold Spring Harb. Perspect. Med.* 3, a011601. doi: 10.1101/cshperspect.a011601.

Eaton, J. W., Skelton, T. D., Swofford, H. S., Kolpin, C. E., and Jacob, H. S. (1973). Elevated erythrocyte calcium in sickle cell disease. *Nature* 246, 105–106. doi: 10.1038/246105a0.

Eaton, W. A., and Bunn, H. F. (2017). Treating sickle cell disease by targeting HbS polymerization. *Blood* 129, 2719–2726. doi: 10.1182/blood-2017-02-765891.

Eaton, W. A., and Hofrichter, J. (1987). Hemoglobin S gelation and sickle cell disease. *Blood* 70, 1245–1266.

Eber, S., and Lux, S. E. (2004). Hereditary spherocytosis--defects in proteins that connect the membrane skeleton to the lipid bilayer. *Semin. Hematol.* 41, 118–141. doi: 10.1053/j.seminhematol.2004.01.002.

Eber, S. W., Armbrust, R., and Schröter, W. (1990). Variable clinical severity of hereditary spherocytosis: relation to erythrocytic spectrin concentration, osmotic fragility, and autohemolysis. *J. Pediatr.* 117, 409–416. doi: 10.1016/s0022-3476(05)81081-9.

Egée, S., and Kaestner, L. (2021). The Transient Receptor Potential Vanilloid Type 2 (TRPV2) Channel–A New Druggable Ca2+ Pathway in Red Cells, Implications for Red Cell Ion Homeostasis. *Front. Physiol.* 12, 677573. doi: 10.3389/fphys.2021.677573.

Egée, S., Lapaix, F., Decherf, G., Staines, H. M., Ellory, J. C., Doerig, C., et al. (2002). A stretch-activated anion channel is up-regulated by the malaria parasite Plasmodium falciparum. *J. Physiol.* 542, 795–801. doi: 10.1113/jphysiol.2002.022970.

Ellory, J. C., and Hall, A. C. (1988). Human red cell volume regulation in hypotonic media. *Comp. Biochem. Physiol. A* 90, 533–537. doi: 10.1016/0300-9629(88)90663-9.

Ellory, J. C., Kirk, K., Culliford, S. J., Nash, G. B., and Stuart, J. (1992). Nitrendipine is a potent inhibitor of the Ca(2+)-activated K+ channel of human erythrocytes. *FEBS Lett.* 296, 219–221. doi: 10.1016/0014-5793(92)80383-r.

Ellory, J. C., Robinson, H. C., Browning, J. A., Stewart, G. W., Gehl, K. A., and Gibson, J. S. (2007). Abnormal permeability pathways in human red blood cells. *Blood Cells. Mol. Dis.* 39, 1–6. doi: 10.1016/j.bcmd.2007.02.011.

Ellory, J. C., and Stewart, G. W. (1982). The human erythrocyte Cl-dependent Na-K cotransport system as a possible model for studying the action of loop diuretics. *Br. J. Pharmacol.* 75, 183–188. doi: 10.1111/j.1476-5381.1982.tb08771.x.

Ellsworth, M. L., Ellis, C. G., and Sprague, R. S. (2016). Role of erythrocyte-released ATP in the regulation of microvascular oxygen supply in skeletal muscle. *Acta Physiol. Oxf. Engl.* 216, 265–276. doi: 10.1111/apha.12596.

Ellsworth, M. L., Forrester, T., Ellis, C. G., and Dietrich, H. H. (1995). The erythrocyte as a regulator of vascular tone. *Am. J. Physiol.* 269, H2155-2161. doi: 10.1152/ajpheart.1995.269.6.H2155.

Endeward, V., Cartron, J.-P., Ripoche, P., and Gros, G. (2006). Red cell membrane CO2 permeability in normal human blood and in blood deficient in various blood groups, and effect of DIDS. *Transfus. Clin. Biol. J. Soc. Francaise Transfus. Sang.* 13, 123–127. doi: 10.1016/j.tracli.2006.02.007.

Evans, E. L., Cuthbertson, K., Endesh, N., Rode, B., Blythe, N. M., Hyman, A. J., et al. (2018). Yoda1 analogue (Dooku1) which antagonizes Yoda1-evoked activation of Piezo1 and aortic relaxation: Yoda1 antagonist. *Br. J. Pharmacol.* 175, 1744–1759. doi: 10.1111/bph.14188.

Evans, E. L., Povstyan, O. V., De Vecchis, D., Macrae, F., Lichtenstein, L., Futers, T. S., et al. (2020). RBCs prevent rapid PIEZO1 inactivation and expose slow deactivation as a mechanism of dehydrated hereditary stomatocytosis. *Blood* 136, 140–144. doi: 10.1182/blood.2019004174.

Fader, C. M., and Colombo, M. I. (2006). Multivesicular bodies and autophagy in erythrocyte maturation. *Autophagy* 2, 122–125. doi: 10.4161/auto.2.2.2350.

Fang, F., Hazegh, K., Sinchar, D., Guo, Y., Page, G. P., Mast, A. E., et al. (2019). Sex hormone intake in female blood donors: impact on haemolysis during cold storage and regulation of erythrocyte calcium influx by progesterone. *Blood Transfus. Trasfus. Sangue* 17, 263–273. doi: 10.2450/2019.0053-19.

Fang, Z., Jiang, C., Tang, J., He, M., Lin, X., Chen, X., et al. (2016). A comprehensive analysis of membrane and morphology of erythrocytes from patients with glucose-6-phosphate dehydrogenase deficiency. *J. Struct. Biol.* 194, 235–243. doi: 10.1016/j.jsb.2015.10.015.

Faucherre, A., Kissa, K., Nargeot, J., Mangoni, M. E., and Jopling, C. (2014). Piezo1 plays a role in erythrocyte volume homeostasis. *Haematologica* 99, 70–75. doi: 10.3324/haematol.2013.086090.

Fayer, S., Horton, C., Dines, J. N., Rubin, A. F., Richardson, M. E., McGoldrick, K., et al. (2021). Closing the gap: Systematic integration of multiplexed functional data resolves variants of uncertain significance in BRCA1, TP53, and PTEN. *Am. J. Hum. Genet.* 108, 2248–2258. doi: 10.1016/j.ajhg.2021.11.001.

Fedosov, D. A., Peltomäki, M., and Gompper, G. (2014). Deformation and dynamics of red blood cells in flow through cylindrical microchannels. *Soft Matter* 10, 4258–4267. doi: 10.1039/C4SM00248B.

Ferguson, B. S., Neidert, L. E., Rogatzki, M. J., Lohse, K. R., Gladden, L. B., and Kluess, H. A. (2021). Red blood cell ATP release correlates with red blood cell hemolysis. *Am. J. Physiol. Cell Physiol.* 321, C761–C769. doi: 10.1152/ajpcell.00510.2020.

Fermo, E., Bogdanova, A., Petkova-Kirova, P., Zaninoni, A., Marcello, A. P., Makhro, A., et al. (2017). 'Gardos Channelopathy': a variant of hereditary Stomatocytosis with complex molecular regulation. *Sci. Rep.* 7, 1744. doi: 10.1038/s41598-017-01591-w.

Fermo, E., Monedero-Alonso, D., Petkova-Kirova, P., Makhro, A., Pérès, L., Bouyer, G., et al. (2020). Gardos channelopathy: functional analysis of a novel *KCNN4* variant. *Blood Adv.* 4, 6336–6341. doi: 10.1182/bloodadvances.2020003285.

Filser, M., Giansily-Blaizot, M., Grenier, M., Monedero Alonso, D., Bouyer, G., Pérès, L., et al. (2021). Increased incidence of germline PIEZO1 mutations in individuals with idiopathic erythrocytosis. *Blood* 137, 1828–1832. doi: 10.1182/blood.2020008424.

FL Medical (2023). Fluoride Tubes, Blood Collection Tubes And Serum Separator Tubes - FL MEDICAL. Available at: https://www.flmedical.com/blood-collection-tubes-and-serum-separator-tubes/ [Accessed October 19, 2023].

Flatman, P. W. (2002). Regulation of Na–K–2Cl cotransport by phosphorylation and protein–protein interactions. *Biochim. Biophys. Acta BBA - Biomembr.* 1566, 140–151. doi: 10.1016/S0005-2736(02)00586-2.

Flatman, P. W. (2005). "Regulation of Na-K-2Cl Cotransport in Red Cells," in *Cell Volume and Signaling* Advances in Experimental Medicine and Biology., eds. P. K. Lauf and N. C. Adragna (Springer US), 77–88. doi: 10.1007/0-387-23752-6_7.

Flatt, J. F., and Bruce, L. J. (2018). The Molecular Basis for Altered Cation Permeability in Hereditary Stomatocytic Human Red Blood Cells. *Front. Physiol.* 9, 367. doi: 10.3389/fphys.2018.00367.

Flormann, D., Qiao, M., Murciano, N., Iacono, G., Darras, A., Hof, S., et al. (2022). Transient receptor potential channel vanilloid type 2 in red cells of cannabis consumer. *Am. J. Hematol.* 97, E180–E183. doi: 10.1002/ajh.26509.

Foller, M., Kasinathan, R. S., Koka, S., Lang, C., Shumilina, E., Birnbaumer, L., et al. (2008). TRPC6 contributes to the Ca(2+) leak of human erythrocytes. *Cell. Physiol. Biochem. Int. J. Exp. Cell. Physiol. Biochem. Pharmacol.* 21, 183–192. doi: 10.1159/000113760.

Forsyth, A. M., Braunmüller, S., Wan, J., Franke, T., and Stone, H. A. (2012). The effects of membrane cholesterol and simvastatin on red blood cell deformability and ATP release. *Microvasc. Res.* 83, 347–351. doi: 10.1016/j.mvr.2012.02.004.

Fowler, V. M. (2013). "Chapter Two - The Human Erythrocyte Plasma Membrane: A Rosetta Stone for Decoding Membrane–Cytoskeleton Structure," in *Current Topics in Membranes* Functional Organization of Vertebrate Plasma Membrane., ed. V. Bennett (Academic Press), 39–88. doi: 10.1016/B978-0-12-417027-8.00002-7.

Freedman, J. C., and Novak, T. S. (1997). Electrodiffusion, barrier, and gating analysis of DIDS-insensitive chloride conductance in human red blood cells treated with valinomycin or gramicidin. *J. Gen. Physiol.* 109, 201–216. doi: 10.1085/jgp.109.2.201.

Functions of blood: regulation (2021). *NHS Blood Donation*. Available at: https://www.blood.co.uk/news-and-campaigns/the-donor/latest-stories/functions-of-blood-regulation/ [Accessed October 13, 2023].

Galanello, R., and Origa, R. (2010). Beta-thalassemia. *Orphanet J. Rare Dis.* 5, 11. doi: 10.1186/1750-1172-5-11.

Gallagher, P. G. (2004). Hereditary elliptocytosis: spectrin and protein 4.1R. *Semin. Hematol.* 41, 142–164. doi: 10.1053/j.seminhematol.2004.01.003.

Gallagher, P. G. (2013). Abnormalities of the erythrocyte membrane. *Pediatr. Clin. North Am.* 60, 1349–1362. doi: 10.1016/j.pcl.2013.09.001.

Gallagher, P. G. (2017). Disorders of erythrocyte hydration. *Blood* 130, 2699–2708. doi: 10.1182/blood-2017-04-590810.

Gallagher, P. G., Weed, S. A., Tse, W. T., Benoit, L., Morrow, J. S., Marchesi, S. L., et al. (1995). Recurrent fatal hydrops fetalis associated with a nucleotide substitution in the erythrocyte beta-spectrin gene. *J. Clin. Invest.* 95, 1174–1182. doi: 10.1172/JCI117766.

Gardos, G. (1958). Effect of ethylenediaminetetraacetate on the permeability of human erythrocytes. *Acta Physiol. Acad. Sci. Hung.* 14, 1–5.

Garneau, A. P., Slimani, S., Tremblay, L. E., Fiola, M. J., Marcoux, A. A., and Isenring, P. (2019). K+-Cl− cotransporter 1 (KCC1): a housekeeping membrane protein that plays key supplemental roles in hematopoietic and cancer cells. *J. Hematol. Oncol.J Hematol Oncol* 12, 74. doi: 10.1186/s13045-019-0766-x.

Garneau, L., Klein, H., Banderali, U., Longprá-Lauzon, A., Parent, L., and Sauvá, R. (2009). Hydrophobic interactions as key determinants to the KCa3.1 channel closed configuration. An analysis of KCa3.1 mutants constitutively active in zero Ca2+. *J. Biol. Chem.* 284, 389–403. doi: 10.1074/jbc.M805700200.

Gatto, C., and Milanick, M. (2009). Red Blood Cell Na pump: Insights from Species Differences. *Blood Cells. Mol. Dis.* 42, 192–200. doi: 10.1016/j.bcmd.2009.01.011.

Gaub, B. M., and Müller, D. J. (2017). Mechanical Stimulation of Piezo1 Receptors Depends on Extracellular Matrix Proteins and Directionality of Force. *Nano Lett.* 17, 2064–2072. doi: 10.1021/acs.nanolett.7b00177.

Gautier, E.-F., Ducamp, S., Leduc, M., Salnot, V., Guillonneau, F., Dussiot, M., et al. (2016). Comprehensive Proteomic Analysis of Human Erythropoiesis. *Cell Rep.* 16, 1470–1484. doi: 10.1016/j.celrep.2016.06.085.

Gautier, E.-F., Leduc, M., Cochet, S., Bailly, K., Lacombe, C., Mohandas, N., et al. (2018). Absolute proteome quantification of highly purified populations of circulating reticulocytes and mature erythrocytes. *Blood Adv.* 2, 2646–2657. doi: 10.1182/bloodadvances.2018023515.

Gautier, E.-F., Leduc, M., Ladli, M., Schulz, V. P., Lefèvre, C., Boussaid, I., et al. (2020). Comprehensive proteomic analysis of murine terminal erythroid differentiation. *Blood Adv.* 4, 1464–1477. doi: 10.1182/bloodadvances.2020001652.

Ge, J., Li, W., Zhao, Q., Li, N., Chen, M., Zhi, P., et al. (2015). Architecture of the mammalian mechanosensitive Piezo1 channel. *Nature* 527, 64–69. doi: 10.1038/nature15247.

Gedde, M. M., and Huestis, W. H. (1997). Membrane potential and human erythrocyte shape. *Biophys. J.* 72, 1220–1233. doi: 10.1016/S0006-3495(97)78769-1.

Geekiyanage, N. M., Balanant, M. A., Sauret, E., Saha, S., Flower, R., Lim, C. T., et al. (2019). A coarse-grained red blood cell membrane model to study stomatocyte-discocyte-echinocyte morphologies. *PLOS ONE* 14, e0215447. doi: 10.1371/journal.pone.0215447.

Genetet, S., Ripoche, P., Picot, J., Bigot, S., Delaunay, J., Armari-Alla, C., et al. (2012). Human RhAG ammonia channel is impaired by the Phe65Ser mutation in overhydrated stomatocytic red cells. *Am. J. Physiol. Cell Physiol.* 302, C419-428. doi: 10.1152/ajpcell.00092.2011.

Geng, J., Liu, W., Zhou, H., Zhang, T., Wang, L., Zhang, M., et al. (2020). A Plug-and-Latch Mechanism for Gating the Mechanosensitive Piezo Channel. *Neuron* 106, 438-451.e6. doi: 10.1016/j.neuron.2020.02.010.

George, A., Pushkaran, S., Konstantinidis, D. G., Koochaki, S., Malik, P., Mohandas, N., et al. (2013). Erythrocyte NADPH oxidase activity modulated by Rac GTPases, PKC, and plasma cytokines contributes to oxidative stress in sickle cell disease. *Blood* 121, 2099–2107. doi: 10.1182/blood-2012-07-441188.

George, A., Pushkaran, S., Li, L., An, X., Zheng, Y., Mohandas, N., et al. (2010). Altered Phosphorylation of Cytoskeleton Proteins in Sickle Red Blood Cells: The Role of Protein Kinase C, Rac GTPases, and Reactive Oxygen Species. *Blood Cells. Mol. Dis.* 45, 41–45. doi: 10.1016/j.bcmd.2010.02.006.

Ghanshani, S., Coleman, M., Gustavsson, P., Wu, A. C., Gargus, J. J., Gutman, G. A., et al. (1998). Human calcium-activated potassium channel gene KCNN4 maps to chromosome 19q13.2 in the region deleted in diamond-blackfan anemia. *Genomics* 51, 160–161. doi: 10.1006/geno.1998.5333.

Gibson, J. S., and Ellory, J. C. (2002). Membrane Transport in Sickle Cell Disease. *Blood Cells. Mol. Dis.* 28, 303–314. doi: 10.1006/bcmd.2002.0515.

Gibson, J. S., Speake, P. F., and Ellory, J. C. (1998). Differential oxygen sensitivity of the K+-Cl- cotransporter in normal and sickle human red blood cells. *J. Physiol.* 511 (Pt 1), 225–234. doi: 10.1111/j.1469-7793.1998.225bi.x.

Gibson, J. S., and Stewart, G. W. (2023). A critical role for altered red cell cation permeability in pathogenesis of sickle cell disease and other haemolytic anaemias. *Br. J. Haematol.*, bjh.18832. doi: 10.1111/bjh.18832.

Gillen, C. M., Brill, S., Payne, J. A., and Forbush, B. (1996). Molecular Cloning and Functional Expression of the K-Cl Cotransporter from Rabbit, Rat, and Human: A NEW MEMBER OF THE CATION-CHLORIDE COTRANSPORTER FAMILY*. *J. Biol. Chem.* 271, 16237–16244. doi: 10.1074/jbc.271.27.16237.

Girodon, F., Garçon, L., Bergoin, E., Largier, M., Delaunay, J., Fénéant-Thibault, M., et al. (2008). Usefulness of the eosin-5'-maleimide cytometric method as a first-line screening test for the diagnosis of hereditary spherocytosis: comparison with ektacytometry and protein electrophoresis. *Br. J. Haematol.* 140, 468–470. doi: 10.1111/j.1365-2141.2007.06944.x.

Glodek, A. M., Mirchev, R., Golan, D. E., Khoory, J. A., Burns, J. M., Shevkoplyas, S. S., et al. (2010). Ligation of complement receptor 1 increases erythrocyte membrane deformability. *Blood* 116, 6063–6071. doi: 10.1182/blood-2010-04-273904.

Glogowska, E., and Gallagher, P. G. (2015). Disorders of erythrocyte volume homeostasis. *Int. J. Lab. Hematol.* 37, 85–91. doi: 10.1111/ijlh.12357.

Glogowska, E., Lezon-Geyda, K., Maksimova, Y., Schulz, V. P., and Gallagher, P. G. (2015). Mutations in the Gardos channel (KCNN4) are associated with hereditary xerocytosis. *Blood* 126, 1281–1284. doi: 10.1182/blood-2015-07-657957.

Glogowska, E., Schneider, E. R., Maksimova, Y., Schulz, V. P., Lezon-Geyda, K., Wu, J., et al. (2017). Novel mechanisms of PIEZO1 dysfunction in hereditary xerocytosis. *Blood* 130, 1845–1856. doi: 10.1182/blood-2017-05-786004.

Gnanasambandam, R., Bae, C., Gottlieb, P. A., and Sachs, F. (2015). Ionic Selectivity and Permeation Properties of Human PIEZO1 Channels. *PLOS ONE* 10, e0125503. doi: 10.1371/journal.pone.0125503.

Gnanasambandam, R., Ghatak, C., Yasmann, A., Nishizawa, K., Sachs, F., Ladokhin, A. S., et al. (2017). GsMTx4: Mechanism of Inhibiting Mechanosensitive Ion Channels. *Biophys. J.* 112, 31–45. doi: 10.1016/j.bpj.2016.11.013.

Goldman, D. E. (1943). POTENTIAL, IMPEDANCE, AND RECTIFICATION IN MEMBRANES. *J. Gen. Physiol.* 27, 37–60. doi: 10.1085/jgp.27.1.37.

Gonzalez, L. J., Gibbons, E., Bailey, R. W., Fairbourn, J., Nguyen, T., Smith, S. K., et al. (2009). The influence of membrane physical properties on microvesicle release in human erythrocytes. *PMC Biophys.* 2, 7. doi: 10.1186/1757-5036-2-7.

Gopinath, R. M., and Vincenzi, F. F. (1979). (Ca2++Mg2+)-ATPase activity of sickle cell membranes: decreased activation by red blood cell cytoplasmic activator. *Am. J. Hematol.* 7, 303–312. doi: 10.1002/ajh.2830070402.

Gottlieb, P. A., Bae, C., and Sachs, F. (2012). Gating the mechanical channel Piezo1: a comparison between whole-cell and patch recording. *Channels Austin Tex* 6, 282–289. doi: 10.4161/chan.21064.

Groenland, S. L., Geel, D. R., Janssen, J. M., de Vries, N., Rosing, H., Beijnen, J. H., et al. (2021). Exposure–Response Analyses of Anaplastic Lymphoma Kinase Inhibitors Crizotinib and Alectinib in Non-Small Cell Lung Cancer Patients. *Clin. Pharmacol. Ther.* 109, 394–402. doi: 10.1002/cpt.1989.

Gründer, S., Thiemann, A., Pusch, M., and Jentsch, T. J. (1992). Regions involved in the opening of CIC-2 chloride channel by voltage and cell volume. *Nature* 360, 759–762. doi: 10.1038/360759a0.

Grunze, M., Forst, B., and Deuticke, B. (1980). Dual effect of membrane cholesterol on simple and mediated transport processes in human erythrocytes. *Biochim. Biophys. Acta* 600, 860–869. doi: 10.1016/0005-2736(80)90489-7.

Grygorczyk, R., and Schwarz, W. (1983). Properties of the CA2+-activated K+ conductance of human red cells as revealed by the patch-clamp technique. *Cell Calcium* 4, 499–510. doi: 10.1016/0143-4160(83)90025-8.

Grygorczyk, R., and Schwarz, W. (1985). Ca2+-activated K+ permeability in human erythrocytes: modulation of single-channel events. *Eur. Biophys. J. EBJ* 12, 57–65. doi: 10.1007/BF00260428.

Grygorczyk, R., Schwarz, W., and Passow, H. (1984). Ca2+-activated K+ channels in human red cells. Comparison of single-channel currents with ion fluxes. *Biophys. J.* 45, 693–698. doi: 10.1016/S0006-3495(84)84211-3.

Guo, J., Gu, D., Zhao, T., Zhao, Z., Xiong, Y., Sun, M., et al. (2021). Trends in Piezo Channel Research Over the Past Decade: A Bibliometric Analysis. *Front. Pharmacol.* 12, 668714. doi: 10.3389/fphar.2021.668714.

Guo, Y. R., and MacKinnon, R. (2017). Structure-based membrane dome mechanism for Piezo mechanosensitivity. *eLife* 6, e33660. doi: 10.7554/eLife.33660.

Guzman, D. S.-M., Mitchell, M. A., Gaunt, S. D., Beaufrère, H., and Tully, T. N. (2008). Comparison of hematologic values in blood samples with lithium heparin or dipotassium ethylenediaminetetraacetic acid anticoagulants in Hispaniolan Amazon parrots (Amazona ventralis). *J. Avian Med. Surg.* 22, 108–113. doi: 10.1647/2007-011.1.

Haas, M. (1989). Properties and diversity of (Na-K-Cl) cotransporters. *Annu. Rev. Physiol.* 51, 443–457. doi: 10.1146/annurev.ph.51.030189.002303.

Hall, J. E. (2015). *Guyton and Hall Textbook of Medical Physiology*. Elsevier Health Sciences.

Halperin, J. A., Brugnara, C., and Nicholson-Weller, A. (1989). Ca2+-activated K+ efflux limits complement-mediated lysis of human erythrocytes. *J. Clin. Invest.* 83, 1466–1471. doi: 10.1172/JCI114039.

Hamasaki, N. (1999). The role of band 3 protein in oxygen delivery by red blood cells. *Indian J. Clin. Biochem.* 14, 49–58. doi: 10.1007/BF02869151.

Hamill, O. P. (1983). "Potassium and Chloride Channels in Red Blood Cells," in *Single-Channel Recording*, eds. B. Sakmann and E. Neher (Boston, MA: Springer US), 451–471. doi: 10.1007/978-1-4615-7858-1_24.

Handelsman, D. J. (2000). “Performance Enhancing Hormone Doping in Sport,” in *Endotext*, eds. K. R. Feingold, B. Anawalt, M. R. Blackman, A. Boyce, G. Chrousos, E. Corpas, et al. (South Dartmouth (MA): MDText.com, Inc.). Available at: http://www.ncbi.nlm.nih.gov/books/NBK305894/ [Accessed September 21, 2023].

Hänggi, P., Makhro, A., Gassmann, M., Schmugge, M., Goede, J. S., Speer, O., et al. (2014). Red blood cells of sickle cell disease patients exhibit abnormally high abundance of N-methyl D-aspartate receptors mediating excessive calcium uptake. *Br. J. Haematol.* 167, 252–264. doi: 10.1111/bjh.13028.

Hannemann, A., Cytlak, U. M. C., Gbotosho, O. T., Rees, D. C., Tewari, S., and Gibson, J. S. (2014a). Effects of o-vanillin on K^+ transport of red blood cells from patients with sickle cell disease. *Blood Cells. Mol. Dis.* 53, 21–26. doi: 10.1016/j.bcmd.2014.02.004.

Hannemann, A., Cytlak, U. M., Rees, D. C., Tewari, S., and Gibson, J. S. (2014b). Effects of 5-hydroxymethyl-2-furfural on the volume and membrane permeability of red blood cells from patients with sickle cell disease. *J. Physiol.* 592, 4039–4049. doi: 10.1113/jphysiol.2014.277681.

Harayama, T., and Riezman, H. (2018). Understanding the diversity of membrane lipid composition. *Nat. Rev. Mol. Cell Biol.* 19, 281–296. doi: 10.1038/nrm.2017.138.

Harrison, D. G., and Long, C. (1968). The calcium content of human erythrocytes. *J. Physiol.* 199, 367–381. doi: 10.1113/jphysiol.1968.sp008658.

Hatem, A., Esperti, S., Murciano, N., Qiao, M., Giustina Rotordam, M., Becker, N., et al. (2023). Adverse effects of delta-9-tetrahydrocannabinol on sickle red blood cells. *Am. J. Hematol.* doi: 10.1002/ajh.27109.

Hegemann, I., Sasselli, C., Valeri, F., Makhro, A., Müller, R., Bogdanova, A., et al. (2020). MEMSID: Results From a Phase 2 Pilot Study on Memantine Treatment for Sickle Cell Disease. *HemaSphere* 4, e452. doi: 10.1097/HS9.0000000000000452.

Hematology Glossary (2021). Available at: https://www.hematology.org/education/patients/blood-basics [Accessed September 4, 2023].

Henry, E. R., Cellmer, T., Dunkelberger, E. B., Metaferia, B., Hofrichter, J., Li, Q., et al. (2020). Allosteric control of hemoglobin S fiber formation by oxygen and its relation to the pathophysiology of sickle cell disease. *Proc. Natl. Acad. Sci. U. S. A.* 117, 15018–15027. doi: 10.1073/pnas.1922004117.

Hertz, L., Flormann, D., Birnbaumer, L., Wagner, C., Laschke, M. W., and Kaestner, L. (2023). Evidence of in vivo exogen protein uptake by red blood cells: a putative therapeutic concept. *Blood Adv.* 7, 1033–1039. doi: 10.1182/bloodadvances.2022008404.

Hertz, L., Huisjes, R., Llaudet-Planas, E., Petkova-Kirova, P., Makhro, A., Danielczok, J. G., et al. (2017). Is Increased Intracellular Calcium in Red Blood Cells a Common Component in the Molecular Mechanism Causing Anemia? *Front. Physiol.* 8, 673. doi: 10.3389/fphys.2017.00673.

Higgs, D. R., Engel, J. D., and Stamatoyannopoulos, G. (2012). Thalassaemia. *The Lancet* 379, 373–383. doi: 10.1016/S0140-6736(11)60283-3.

Hillery, C. A., Kerstein, P. C., Vilceanu, D., Barabas, M. E., Retherford, D., Brandow, A. M., et al. (2011). Transient receptor potential vanilloid 1 mediates pain in mice with severe sickle cell disease. *Blood* 118, 3376–3383. doi: 10.1182/blood-2010-12-327429.

Hoffman, J. F. (1987). “Chapter 5 Functional Roles of lntracellular Potassium in Red Blood Cells,” in *Current Topics in Membranes and Transport* Potassium Transport: Physiology and Pathophysiology., ed. G. Giebisch (Academic Press), 87–96. doi: 10.1016/S0070-2161(08)60409-8.

Hoffman, J. F. (2016). Biconcave shape of human red-blood-cell ghosts relies on density differences between the rim and dimple of the ghost’s plasma membrane. *Proc. Natl. Acad. Sci.* 113, 14847–14851. doi: 10.1073/pnas.1615452113.

Hoffman, J. F., Dodson A, Wickrema A, and Dib-Hajj Sd (2004). Tetrodotoxin-sensitive Na+ channels and muscarinic and purinergic receptors identified in human erythroid progenitor cells and red blood cell ghosts. *Proc. Natl. Acad. Sci. U. S. A.* 101. doi: 10.1073/pnas.0404228101.

Hoffman, J. F., and Geibel, J. P. (2005). Fluorescent imaging of Cl- in Amphiuma red blood cells: how the nuclear exclusion of Cl- affects the plasma membrane potential. *Proc. Natl. Acad. Sci. U. S. A.* 102, 921–926. doi: 10.1073/pnas.0408597102.

Hoffman, J. F., Joiner, W., Nehrke, K., Potapova, O., Foye, K., and Wickrema, A. (2003). The hSK4 (KCNN4) isoform is the Ca2+-activated K+ channel (Gardos channel) in human red blood cells. *Proc. Natl. Acad. Sci.* 100, 7366–7371. doi: 10.1073/pnas.1232342100.

Huber, S. M., Duranton, C., Henke, G., Van De Sand, C., Heussler, V., Shumilina, E., et al. (2004). Plasmodium induces swelling-activated ClC-2 anion channels in the host erythrocyte. *J. Biol. Chem.* 279, 41444–41452. doi: 10.1074/jbc.M407618200.

Huber, S. M., Gamper, N., and Lang, F. (2001). Chloride conductance and volume-regulatory nonselective cation conductance in human red blood cell ghosts. *Pflugers Arch.* 441, 551–558. doi: 10.1007/s004240000456.

Huber, S. M., Uhlemann, A.-C., Gamper, N. L., Duranton, C., Kremsner, P. G., and Lang, F. (2002). Plasmodium falciparum activates endogenous Cl(-) channels of human erythrocytes by membrane oxidation. *EMBO J.* 21, 22–30. doi: 10.1093/emboj/21.1.22.

Huestis, M. A. (2007). Human cannabinoid pharmacokinetics. *Chem. Biodivers.* 4, 1770–1804. doi: 10.1002/cbdv.200790152.

Huisjes, R., Bogdanova, A., van Solinge, W. W., Schiffelers, R. M., Kaestner, L., and van Wijk, R. (2018). Squeezing for Life – Properties of Red Blood Cell Deformability. *Front. Physiol.* 9, 656. doi: 10.3389/fphys.2018.00656.

Iglic, A., Kralj-Iglic, V., and Hägerstrand, H. (1998). Amphiphile induced echinocyte-spheroechinocyte transformation of red blood cell shape. *Eur. Biophys. J. EBJ* 27, 335–339. doi: 10.1007/s002490050140.

Ingram, V. M. (1957). Gene mutations in human haemoglobin: the chemical difference between normal and sickle cell haemoglobin. *Nature* 180, 326–328. doi: 10.1038/180326a0.

Inusa, B. P. D., Hsu, L. L., Kohli, N., Patel, A., Ominu-Evbota, K., Anie, K. A., et al. (2019). Sickle Cell Disease—Genetics, Pathophysiology, Clinical Presentation and Treatment. *Int. J. Neonatal Screen.* 5. doi: 10.3390/ijns5020020.

Iolascon, A., De Falco, L., Borgese, F., Esposito, M. R., Avvisati, R. A., Izzo, P., et al. (2009). A novel erythroid anion exchange variant (Gly796Arg) of hereditary stomatocytosis associated with dyserythropoiesis. *Haematologica* 94, 1049–1059. doi: 10.3324/haematol.2008.002873.

Iolascon, A., Perrotta, S., and Stewart, G. W. (2003). Red blood cell membrane defects. *Rev. Clin. Exp. Hematol.* 7, 22–56.

Isenring, P., and Forbush, B. (2001). Ion transport and ligand binding by the Na-K-Cl cotransporter, structure-function studies. *Comp. Biochem. Physiol. A. Mol. Integr. Physiol.* 130, 487–497. doi: 10.1016/s1095-6433(01)00420-2.

Jacobs, M. H., and Stewart, D. R. (1942). THE ROLE OF CARBONIC ANHYDRASE IN CERTAIN IONIC EXCHANGES INVOLVING THE ERYTHROCYTE. *J. Gen. Physiol.* 25, 539–552. doi: 10.1085/jgp.25.4.539.

Jaferzadeh, K., and Moon, I. (2015). Quantitative investigation of red blood cell three-dimensional geometric and chemical changes in the storage lesion using digital holographic microscopy. *J. Biomed. Opt.* 20, 111218. doi: 10.1117/1.JBO.20.11.111218.

Jamerson, B. D., Haryadi, T. H., and Bohannon, A. (2020). Glucose-6-Phosphate Dehydrogenase Deficiency: An Actionable Risk Factor for Patients with COVID-19? *Arch. Med. Res.* 51, 743–744. doi: 10.1016/j.arcmed.2020.06.006.

Jankovsky, N., Caulier, A., Demagny, J., Guitton, C., Djordjevic, S., Lebon, D., et al. (2021). Recent advances in the pathophysiology of PIEZO1-related hereditary xerocytosis. *Am. J. Hematol.* 96, 1017–1026. doi: 10.1002/ajh.26192.

Jansen, J., Qiao, M., Hertz, L., Wang, X., Fermo, E., Zaninoni, A., et al. (2021). Mechanistic ion channel interactions in red cells of patients with Gárdos channelopathy. *Blood Adv.* 5, 3303–3308. doi: 10.1182/bloodadvances.2020003823.

Jentsch, T. J., Stein, V., Weinreich, F., and Zdebik, A. A. (2002). Molecular structure and physiological function of chloride channels. *Physiol. Rev.* 82, 503–568. doi: 10.1152/physrev.00029.2001.

Jiang, M., Zhang, Y.-X., Bu, W.-J., Li, P., Chen, J.-H., Cao, M., et al. (2023). Piezo1 channel activation stimulates ATP production through enhancing mitochondrial respiration and glycolysis in vascular endothelial cells. *Br. J. Pharmacol.* 180, 1862–1877. doi: 10.1111/bph.16050.

Jiang, W., Del Rosario, J. S., Botello-Smith, W., Zhao, S., Lin, Y.-C., Zhang, H., et al. (2021). Crowding-induced opening of the mechanosensitive Piezo1 channel in silico. *Commun. Biol.* 4, 84. doi: 10.1038/s42003-020-01600-1.

Jiang, W., Ding, Y., Su, Y., Jiang, M., Hu, X., and Zhang, Z. (2006a). Interaction of glucose transporter 1 with anion exchanger 1 in vitro. *Biochem. Biophys. Res. Commun.* 339, 1255–1261. doi: 10.1016/j.bbrc.2005.11.138.

Jiang, W., Yu, G., Liu, P., Geng, Q., Chen, L., Lin, Q., et al. (2006b). Structure and function of glucose-6-phosphate dehydrogenase-deficient variants in Chinese population. *Hum. Genet.* 119, 463–478. doi: 10.1007/s00439-005-0126-5.

John Scott Haldane | Respiratory Physiology, Gases & Hypoxia | Britannica (2019). Available at: https://www.britannica.com/biography/John-Scott-Haldane [Accessed October 14, 2023].

Johnson, R. M. (1994). Membrane stress increases cation permeability in red cells. *Biophys. J.* 67, 1876–1881. doi: 10.1016/S0006-3495(94)80669-1.

Joiner, C. H. (1993). Cation transport and volume regulation in sickle red blood cells. *Am. J. Physiol.* 264, C251-270. doi: 10.1152/ajpcell.1993.264.2.C251.

Joiner, C. H., Dew, A., and Ge, D. L. (1988). Deoxygenation-induced cation fluxes in sickle cells: relationship between net potassium efflux and net sodium influx. *Blood Cells* 13, 339–358.

Joiner, C. H., Franco, R. S., Jiang, M., Franco, M. S., Barker, J. E., and Lux, S. E. (1995). Increased cation permeability in mutant mouse red blood cells with defective membrane skeletons. *Blood* 86, 4307–4314.

Joiner, C. H., Morris, C. L., and Cooper, E. S. (1993). Deoxygenation-induced cation fluxes in sickle cells. III. Cation selectivity and response to pH and membrane potential. *Am. J. Physiol.* 264, C734-744. doi: 10.1152/ajpcell.1993.264.3.C734.

Kaestner, L. (2015). Channelizing the red blood cell: molecular biology competes with patch-clamp. *Front. Mol. Biosci.* 2, 46. doi: 10.3389/fmolb.2015.00046.

Kaestner, L., and Bernhardt, I. (2002). Ion channels in the human red blood cell membrane: their further investigation and physiological relevance. *Bioelectrochemistry Amst. Neth.* 55, 71–74. doi: 10.1016/s1567-5394(01)00164-5.

Kaestner, L., and Bianchi, P. (2020). Trends in the Development of Diagnostic Tools for Red Blood Cell-Related Diseases and Anemias. *Front. Physiol.* 11, 387. doi: 10.3389/fphys.2020.00387.

Kaestner, L., Bogdanova, A., and Egee, S. (2020). Calcium Channels and Calcium-Regulated Channels in Human Red Blood Cells. *Adv. Exp. Med. Biol.* 1131, 625–648. doi: 10.1007/978-3-030-12457-1_25.

Kaestner, L., Bollensdorff, C., and Bernhardt, I. (1999). Non-selective voltage-activated cation channel in the human red blood cell membrane. *Biochim. Biophys. Acta* 1417, 9–15. doi: 10.1016/s0005-2736(98)00240-5.

Kaestner, L., Christophersen, P., Bernhardt, I., and Bennekou, P. (2000). The non-selective voltage-activated cation channel in the human red blood cell membrane: reconciliation between two conflicting reports and further characterisation. *Bioelectrochemistry Amst. Neth.* 52, 117–125. doi: 10.1016/s0302-4598(00)00110-0.

Kaestner, L., and Minetti, G. (2017). The potential of erythrocytes as cellular aging models. *Cell Death Differ.* 24, 1475–1477. doi: 10.1038/cdd.2017.100.

Kaestner, L., Tabellion W, Lipp P, and Bernhardt I (2004). Prostaglandin E2 activates channel-mediated calcium entry in human erythrocytes: an indication for a blood clot formation supporting process. *Thromb. Haemost.* 92. doi: 10.1160/TH04-06-0338.

Kaplan, J. H., Pring, M., and Passow H (1983). Band-3 protein-mediated anion conductance of the red cell membrane. Slippage vs ionic diffusion. *FEBS Lett.* 156. doi: 10.1016/0014-5793(83)80272-5.

Karayel, Ö., Xu, P, Bludau, I, Velan Bhoopalan, S, Yao, Y, Fc, A. R., et al. (2020). Integrative proteomics reveals principles of dynamic phosphosignaling networks in human erythropoiesis. *Mol. Syst. Biol.* 16. doi: 10.15252/msb.20209813.

Karsten, E., and Herbert, B. R. (2020). The emerging role of red blood cells in cytokine signalling and modulating immune cells. *Blood Rev.* 41, 100644. doi: 10.1016/j.blre.2019.100644.

Kato, G. J., Gladwin, M. T., and Steinberg, M. H. (2007). Deconstructing sickle cell disease: reappraisal of the role of hemolysis in the development of clinical subphenotypes. *Blood Rev.* 21, 37–47. doi: 10.1016/j.blre.2006.07.001.

Kaufman, H. W., Niles, J. K., Gallagher, D. R., Rivera, A., Alper, S. L., Brugnara, C., et al. (2018). Revised prevalence estimate of possible Hereditary Xerocytosis as derived from a large U.S. Laboratory database. *Am. J. Hematol.* 93, E9–E12. doi: 10.1002/ajh.24923.

Kedar, P. S., Colah, R. B., Kulkarni, S., Ghosh, K., and Mohanty, D. (2003). Experience with eosin-5'-maleimide as a diagnostic tool for red cell membrane cytoskeleton disorders. *Clin. Lab. Haematol.* 25, 373–376. doi: 10.1046/j.0141-9854.2003.00557.x.

Kim, K. M., Lui, L.-Y., Browner, W. S., Cauley, J. A., Ensrud, K. E., Kado, D. M., et al. (2020). Association Between Variation in Red Cell Size and Multiple Aging-Related Outcomes. *J. Gerontol. A. Biol. Sci. Med. Sci.* 76, 1288–1294. doi: 10.1093/gerona/glaa217.

Kirk, K. (2000). Malaria. Channelling nutrients. *Nature* 406, 949, 951. doi: 10.1038/35023209.

Kirk, K. (2015). Ion Regulation in the Malaria Parasite. 22.

Kirk, K., Horner, H. A., Elford, B. C., Ellory, J. C., and Newbold, C. I. (1994). Transport of diverse substrates into malaria-infected erythrocytes via a pathway showing functional characteristics of a chloride channel. *J. Biol. Chem.* 269, 3339–3347.

Kirkpatrick, F. H., Muhs, A. G., Kostuk, R. K., and Gabel, C. W. (1979). Dense (aged) circulating red cells contain normal concentrations of adenosine triphosphate (ATP). *Blood* 54, 946–950.

Klei, T. R. L., Dalimot, J. J., Beuger, B. M., Veldthuis, M., Ichou, F. A., Verkuijlen, P. J. J. H., et al. (2020). The Gardos effect drives erythrocyte senescence and leads to Lu/BCAM and CD44 adhesion molecule activation. *Blood Adv.* 4, 6218–6229. doi: 10.1182/bloodadvances.2020003077.

Koulnis, M., Porpiglia, E., Hidalgo, D., and Socolovsky, M. (2014). Erythropoiesis: from molecular pathways to system properties. *Adv. Exp. Med. Biol.* 844, 37–58. doi: 10.1007/978-1-4939-2095-2_3.

Kramer, R., and Ginsburg, H. (1991). Calcium transport and compartment analysis of free and exchangeable calcium in Plasmodium falciparum-infected red blood cells. *J. Protozool.* 38, 594–601.

Krebs, J. (2017). The Plasma Membrane Calcium Pump (PMCA): Regulation of Cytosolic Ca2+, Genetic Diversities and Its Role in Sub-plasma Membrane Microdomains. *Adv. Exp. Med. Biol.* 981, 3–21. doi: 10.1007/978-3-319-55858-5_1.

Kubitscheck, U., Pratsch, L., Passow, H., and Peters, R. (1995). Calcium pump kinetics determined in single erythrocyte ghosts by microphotolysis and confocal imaging. *Biophys. J.* 69, 30–41. doi: 10.1016/S0006-3495(95)79875-7.

Kuchel, P. W., and Shishmarev, D. (2017). Accelerating metabolism and transmembrane cation flux by distorting red blood cells. *Sci. Adv.* 3, eaao1016. doi: 10.1126/sciadv.aao1016.

Kuesap, J., Chaijaroenkul, W., Rungsihirunrat, K., Pongjantharasatien, K., and Na-Bangchang, K. (2015). Coexistence of Malaria and Thalassemia in Malaria Endemic Areas of Thailand. *Korean J. Parasitol.* 53, 265–270. doi: 10.3347/kjp.2015.53.3.265.

Kuhn, V., Diederich, L., Keller, T. C. S., Kramer, C. M., Lückstädt, W., Panknin, C., et al. (2017). Red Blood Cell Function and Dysfunction: Redox Regulation, Nitric Oxide Metabolism, Anemia. *Antioxid. Redox Signal.* 26, 718–742. doi: 10.1089/ars.2016.6954.

Kunz, J., Wiedemann, C., Grosch, H., Kriegsmann, K., Gryzik, S., Felden, J., et al. (2022). Early Development of Ubiquitous Acanthocytosis and Extravascular Hemolysis in Lung Cancer Patients Receiving Alectinib. *Cancers* 14, 2720. doi: 10.3390/cancers14112720.

Kuo, M.-S., Chuang, C.-H., Cheng, H.-C., Lin, H.-R., Wang, J.-S., and Hsu, K. (2021). Different Involvement of Band 3 in Red Cell Deformability and Osmotic Fragility—A Comparative GP.Mur Erythrocyte Study. *Cells* 10, 3369. doi: 10.3390/cells10123369.

Kuypers, F. A. (2007). Membrane lipid alterations in hemoglobinopathies. *Hematol. Am. Soc. Hematol. Educ. Program*, 68–73. doi: 10.1182/asheducation-2007.1.68.

Kuzich, J. A., Heynemann, S., Geoghegan, N., Evelyn, C., O'Mahoney, S., Wilson, S., et al. (2021). Alectinib induces marked red cell spheroacanthocytosis in a near-ubiquitous fashion and is associated with reduced eosin-5-maleimide binding. *Pathology (Phila.)* 53, 608–612. doi: 10.1016/j.pathol.2020.10.023.

Lacroix, J. J., Botello-Smith, W. M., and Luo, Y. (2018). Probing the gating mechanism of the mechanosensitive channel Piezo1 with the small molecule Yoda1. *Nat. Commun.* 9, 2029. doi: 10.1038/s41467-018-04405-3.

Lai, A., Cox, C. D., Chandra Sekar, N., Thurgood, P., Jaworowski, A., Peter, K., et al. (2022). Mechanosensing by Piezo1 and its implications for physiology and various pathologies. *Biol. Rev.* 97, 604–614. doi: 10.1111/brv.12814.

Lakna (2018). What is the Difference Between Bohr and Haldane Effect. *Pediaa.Com*. Available at: https://pediaa.com/what-is-the-difference-between-bohr-and-haldane-effect/ [Accessed September 5, 2023].

Lang, E., Qadri, S. M., and Lang, F. (2012). Killing me softly - suicidal erythrocyte death. *Int. J. Biochem. Cell Biol.* 44, 1236–1243. doi: 10.1016/j.biocel.2012.04.019.

Lang, K. S., Duranton, C., Poehlmann, H., Myssina, S., Bauer, C., Lang, F., et al. (2003a). Cation channels trigger apoptotic death of erythrocytes. *Cell Death Differ.* 10, 249–256. doi: 10.1038/sj.cdd.4401144.

Lang, K. S., Myssina, S., Lang, P. A., Tanneur, V., Kempe, D. S., Mack, A. F., et al. (2004). Inhibition of erythrocyte phosphatidylserine exposure by urea and Cl-. *Am. J. Physiol. Renal Physiol.* 286, F1046-1053. doi: 10.1152/ajprenal.00263.2003.

Lang, P. A., Kaiser, S., Myssina, S., Wieder, T., Lang, F., and Huber, S. M. (2003b). Role of Ca2+-activated K+ channels in human erythrocyte apoptosis. *Am. J. Physiol. Cell Physiol.* 285, C1553-1560. doi: 10.1152/ajpcell.00186.2003.

Lang, P. A., Kempe, D. S., Myssina, S., Tanneur, V., Birka, C., Laufer, S., et al. (2005). PGE(2) in the regulation of programmed erythrocyte death. *Cell Death Differ.* 12, 415–428. doi: 10.1038/sj.cdd.4401561.

Lange, T., Jungmann, P., Haberle, J., Falk, S., Duebbers, A., Bruns, R., et al. (2006). Reduced number of CFTR molecules in erythrocyte plasma membrane of cystic fibrosis patients. *Mol. Membr. Biol.* 23, 317–323. doi: 10.1080/09687860600738304.

Lange, Y., and Slayton, J. M. (1982). Interaction of cholesterol and lysophosphatidylcholine in determining red cell shape. *J. Lipid Res.* 23, 1121–1127.

Larsen, F. L., Katz, S., Roufogalis, B. D., and Brooks, D. E. (1981). Physiological shear stresses enhance the Ca2+ permeability of human erythrocytes. *Nature* 294, 667–668. doi: 10.1038/294667a0.

Leal Denis, M. F., Alvarez, H. A., Lauri, N., Alvarez, C. L., Chara, O., and Schwarzbaum, P. J. (2016). Dynamic Regulation of Cell Volume and Extracellular ATP of Human Erythrocytes. *PloS One* 11, e0158305. doi: 10.1371/journal.pone.0158305.

Lee, A. G. (2004). How lipids affect the activities of integral membrane proteins. *Biochim. Biophys. Acta* 1666, 62–87. doi: 10.1016/j.bbamem.2004.05.012.

Lee, C.-H., and MacKinnon, R. (2018). Activation mechanism of a human SK-calmodulin channel complex elucidated by cryo-EM structures. *Science* 360, 508–513. doi: 10.1126/science.aas9466.

Lee, J. C., and Discher, D. E. (2001). Deformation-enhanced fluctuations in the red cell skeleton with theoretical relations to elasticity, connectivity, and spectrin unfolding. *Biophys. J.* 81, 3178–3192. doi: 10.1016/S0006-3495(01)75954-1.

Lee, P., Ye, Z., Van Dyke, K., and Kirk, R. G. (1988). X-ray microanalysis of Plasmodium falciparum and infected red blood cells: effects of qinghaosu and chloroquine on potassium, sodium, and phosphorus composition. *Am. J. Trop. Med. Hyg.* 39, 157–165. doi: 10.4269/ajtmh.1988.39.157.

Legland Ép Dejean, A.-M., Plantamura, J., Arnoux, I., Paleiron, N., Loosveld, M., and Buono Ép Foucher, B. (2022). Acanthocytosis in an alectinib-treated patient. *Br. J. Haematol.* 197, 131. doi: 10.1111/bjh.18020.

Leonard, C., Conrard, L., Guthmann, M., Pollet, H., Carquin, M., Vermylen, C., et al. (2017). Contribution of plasma membrane lipid domains to red blood cell (re)shaping. *Sci. Rep.* 7, 4264. doi: 10.1038/s41598-017-04388-z.

Leonzino, M., Reinisch, K. M., and De Camilli, P. (2021). Insights into VPS13 properties and function reveal a new mechanism of eukaryotic lipid transport. *Biochim. Biophys. Acta Mol. Cell Biol. Lipids* 1866, 159003. doi: 10.1016/j.bbalip.2021.159003.

Lew, V. L. (2023). The circulatory dynamics of human red blood cell homeostasis: Oxy-deoxy and PIEZO1-triggered changes. *Biophys. J.* 122, 484–495. doi: 10.1016/j.bpj.2022.12.038.

Lew, V. L., and Bookchin, R. M. (2005). Ion Transport Pathology in the Mechanism of Sickle Cell Dehydration. *Physiol. Rev.* 85, 179–200. doi: 10.1152/physrev.00052.2003.

Lew, V. L., Daw, N., Perdomo, D., Etzion, Z., Bookchin, R. M., and Tiffert, T. (2003). Distribution of plasma membrane Ca2+ pump activity in normal human red blood cells. *Blood* 102, 4206–4213. doi: 10.1182/blood-2003-06-1787.

Lew, V. L., Etzion, Z., and Bookchin, R. M. (2002). Dehydration response of sickle cells to sickling-induced Ca(++) permeabilization. *Blood* 99, 2578–2585. doi: 10.1182/blood.v99.7.2578.

Lew, V. L., Raftos, J. E., Sorette, M., Bookchin, R. M., and Mohandas, N. (1995). Generation of normal human red cell volume, hemoglobin content, and membrane area distributions by "birth" or regulation? *Blood* 86, 334–341.

Lew, V. L., and Tiffert, T. (2017). On the Mechanism of Human Red Blood Cell Longevity: Roles of Calcium, the Sodium Pump, PIEZO1, and Gardos Channels. *Front. Physiol.* 8, 7.

Lew, V. L., Tsien, R. Y., Miner, C., and Bookchin, R. M. (1982). Physiological [Ca2+]i level and pump-leak turnover in intact red cells measured using an incorporated Ca chelator. *Nature* 298, 478–481. doi: 10.1038/298478a0.

Lewis, A. H., and Grandl, J. (2015). Mechanical sensitivity of Piezo1 ion channels can be tuned by cellular membrane tension. *eLife* 4, e12088. doi: 10.7554/eLife.12088.

Li, H., and Lykotrafitis, G. (2014). Erythrocyte Membrane Model with Explicit Description of the Lipid Bilayer and the Spectrin Network. *Biophys. J.* 107, 642–653. doi: 10.1016/j.bpj.2014.06.031.

Li, N., Chen, S., Xu, K., He, M.-T., Dong, M.-Q., Zhang, Q. C., et al. (2023). Structural basis of membrane skeleton organization in red blood cells. *Cell* 186, 1912-1929.e18. doi: 10.1016/j.cell.2023.03.017.

Li, X., Dao, M., Lykotrafitis, G., and Karniadakis, G. E. (2017a). Biomechanics and biorheology of red blood cells in sickle cell anemia. *J. Biomech.* 50, 34–41. doi: 10.1016/j.jbiomech.2016.11.022.

Li, X., Li, H., Chang, H.-Y., Lykotrafitis, G., and Em Karniadakis, G. (2017b). Computational Biomechanics of Human Red Blood Cells in Hematological Disorders. *J. Biomech. Eng.* 139, 0210081–02100813. doi: 10.1115/1.4035120.

Liang, G., Stephenson, A. H., Lonigro, A. J., and Sprague, R. S. (2005). Erythrocytes of humans with cystic fibrosis fail to stimulate nitric oxide synthesis in isolated rabbit lungs. *Am. J. Physiol. Heart Circ. Physiol.* 288, H1580-1585. doi: 10.1152/ajpheart.00807.2004.

Liang, X., and Howard, J. (2018). Structural Biology: Piezo Senses Tension through Curvature. *Curr. Biol. CB* 28, R357–R359. doi: 10.1016/j.cub.2018.02.078.

Lin, Y.-C., Guo, Y. R., Miyagi, A., Levring, J., MacKinnon, R., and Scheuring, S. (2019). Force-induced conformational changes in PIEZO1. *Nature* 573, 230–234. doi: 10.1038/s41586-019-1499-2.

Locovei, S., Bao, L., and Dahl, G. (2006). Pannexin 1 in erythrocytes: function without a gap. *Proc. Natl. Acad. Sci. U. S. A.* 103, 7655–7659. doi: 10.1073/pnas.0601037103.

Lohia, R., Allegrini, B., Berry, L., Guizouarn, H., Cerdan, R., Abkarian, M., et al. (2023). Pharmacological activation of PIEZO1 in human red blood cells prevents Plasmodium falciparum invasion. *Cell. Mol. Life Sci. CMLS* 80, 124. doi: 10.1007/s00018-023-04773-0.

Lopes, M. G. M., Recktenwald, S. M., Simionato, G., Eichler, H., Wagner, C., Quint, S., et al. (2023). Big Data in Transfusion Medicine and Artificial Intelligence Analysis for Red Blood Cell Quality Control. *Transfus. Med. Hemotherapy* 50, 163–173. doi: 10.1159/000530458.

Lu, D. C.-Y., Wadud, R., Hannemann, A., Rees, D. C., Brewin, J. N., and Gibson, J. S. (2021). Pathophysiological Relevance of Renal Medullary Conditions on the Behaviour of Red Cells From Patients With Sickle Cell Anaemia. *Front. Physiol.* 12, 653545. doi: 10.3389/fphys.2021.653545.

Lupski, J. R. (2012). Digenic inheritance and Mendelian disease. *Nat. Genet.* 44, 1291–1292. doi: 10.1038/ng.2479.

Lux, S. E. (2015). "Red cell membrane," in *Hematology and oncology of infancy and childhood* (Philadelphia: Elsevier Saunders), 455–514.

Lux, S. E. (2016). Anatomy of the red cell membrane skeleton: unanswered questions. *Blood* 127, 187–199. doi: 10.1182/blood-2014-12-512772.

Luzzatto, L. (1967). Regulation of the activity of glucose-6-phosphate dehydrogenase by NADP+ and NADPH. *Biochim. Biophys. Acta* 146, 18–25. doi: 10.1016/0005-2744(67)90069-1.

Luzzatto, L., Ally, M., and Notaro, R. (2020). Glucose-6-phosphate dehydrogenase deficiency. *Blood* 136, 1225–1240. doi: 10.1182/blood.2019000944.

Lybaek, H., Øyen, N., Fauske, L., and Houge, G. (2008). A 2.1 Mb deletion adjacent but distal to a 14q21q23 paracentric inversion in a family with spherocytosis and severe learning difficulties. *Clin. Genet.* 74, 553–559. doi: 10.1111/j.1399-0004.2008.01072.x.

Ma, S., Cahalan, S., LaMonte, G., Grubaugh, N. D., Zeng, W., Murthy, S. E., et al. (2018). Common PIEZO1 Allele in African Populations Causes RBC Dehydration and Attenuates Plasmodium Infection. *Cell* 173, 443-455.e12. doi: 10.1016/j.cell.2018.02.047.

Ma, Y.-L., Rees, D. C., Gibson, J. S., and Ellory, J. C. (2012). The conductance of red blood cells from sickle cell patients: ion selectivity and inhibitors. *J. Physiol.* 590, 2095–2105. doi: 10.1113/jphysiol.2012.229609.

Macey, R. I. (1984). Transport of water and urea in red blood cells. *Am. J. Physiol.* 246, C195-203. doi: 10.1152/ajpcell.1984.246.3.C195.

Macey, R. I., Adorante, J. S., and Orme, F. W. (1978). Erythrocyte membrane potentials determined by hydrogen ion distribution. *Biochim. Biophys. Acta BBA - Biomembr.* 512, 284–295. doi: 10.1016/0005-2736(78)90253-5.

Maher, A. D., and Kuchel, P. W. (2003). The Gárdos channel: a review of the Ca2+-activated K+ channel in human erythrocytes. *Int. J. Biochem. Cell Biol.* 35, 1182–1197. doi: 10.1016/S1357-2725(02)00310-2.

Makhro, A., Haider, T., Wang, J., Bogdanov, N., Steffen, P., Wagner, C., et al. (2016a). Comparing the impact of an acute exercise bout on plasma amino acid composition, intraerythrocytic Ca(2+) handling, and red cell function in athletes and untrained subjects. *Cell Calcium* 60, 235–244. doi: 10.1016/j.ceca.2016.05.005.

Makhro, A., Hänggi, P., Goede, J. S., Wang, J., Brüggemann, A., Gassmann, M., et al. (2013). N-methyl-D-aspartate receptors in human erythroid precursor cells and in circulating red blood cells contribute to the intracellular calcium regulation. *Am. J. Physiol. Cell Physiol.* 305, C1123-1138. doi: 10.1152/ajpcell.00031.2013.

Makhro, A., Huisjes, R., Verhagen, L. P., Mañú-Pereira, M. D. M., Llaudet-Planas, E., Petkova-Kirova, P., et al. (2016b). Red Cell Properties after Different Modes of Blood Transportation. *Front. Physiol.* 7, 288. doi: 10.3389/fphys.2016.00288.

Malaria and Thalassemia in the Mediterranean Basin (2021). Available at: https://ashpublications.org/ashclinicalnews/news/4268/Malaria-and-Thalassemia-in-the-Mediterranean-Basin [Accessed October 5, 2023].

Malaria Genomic Epidemiology Network and Malaria Genomic Epidemiology Network (2014). Reappraisal of known malaria resistance loci in a large multicenter study. *Nat. Genet.* 46, 1197–1204. doi: 10.1038/ng.3107.

Mankelow, T. J., Satchwell, T. J., and Burton, N. M. (2012). Refined views of multi-protein complexes in the erythrocyte membrane. *Blood Cells. Mol. Dis.* 49, 1–10. doi: 10.1016/j.bcmd.2012.03.001.

Mansour-Hendili, L., Aissat, A., Badaoui, B., Sakka, M., Gameiro, C., Ortonne, V., et al. (2020). Exome sequencing for diagnosis of congenital hemolytic anemia. *Orphanet J. Rare Dis.* 15, 180. doi: 10.1186/s13023-020-01425-5.

Mansour-Hendili, L., Egée, S., Monedero-Alonso, D., Bouyer, G., Godeau, B., Badaoui, B., et al. (2021). Multiple thrombosis in a patient with Gardos channelopathy and a new KCNN4 mutation. *Am. J. Hematol.* 96, E318–E321. doi: 10.1002/ajh.26245.

Marchesi, S. L., Letsinger, J. T., Speicher, D. W., Marchesi, V. T., Agre, P., Hyun, B., et al. (1987). Mutant forms of spectrin alpha-subunits in hereditary elliptocytosis. *J. Clin. Invest.* 80, 191–198. doi: 10.1172/JCI113047.

Marchesi, V. T., and Steers, E. (1968). Selective solubilization of a protein component of the red cell membrane. *Science* 159, 203–204. doi: 10.1126/science.159.3811.203.

Marginedas-Freixa, I., Alvarez, C. L., Moras, M., Leal Denis, M. F., Hattab, C., Halle, F., et al. (2018). Human erythrocytes release ATP by a novel pathway involving VDAC oligomerization independent of pannexin-1. *Sci. Rep.* 8, 11384. doi: 10.1038/s41598-018-29885-7.

Masana, M., Rodriguez, M. J., and Alberch, J. (2021). Proceedings of the Tenth International Meeting on Neuroacanthocytosis Syndromes. *Tremor Hyperkinetic Mov. N. Y. N* 11, 19. doi: 10.5334/tohm.622.

Maurer, F., John, T., Makhro, A., Bogdanova, A., Minetti, G., Wagner, C., et al. (2022). Continuous Percoll Gradient Centrifugation of Erythrocytes—Explanation of Cellular Bands and Compromised Age Separation. *Cells* 11, 1296. doi: 10.3390/cells11081296.

McMahon, T. J., Darrow, C. C., Hoehn, B. A., and Zhu, H. (2021). Generation and Export of Red Blood Cell ATP in Health and Disease. *Front. Physiol.* 12, 754638. doi: 10.3389/fphys.2021.754638.

McNamara, M. K., and Wiley, J. S. (1986). Passive permeability of human red blood cells to calcium. *Am. J. Physiol.* 250, C26-31. doi: 10.1152/ajpcell.1986.250.1.C26.

Melia, T. J., and Reinisch, K. M. (2022). A possible role for VPS13-family proteins in bulk lipid transfer, membrane expansion and organelle biogenesis. *J. Cell Sci.* 135, jcs259357. doi: 10.1242/jcs.259357.

Merrikh, A. A., and Lage, J. L. (2008). Plasma microcirculation in alveolar capillaries: Effect of parachute-shaped red cells on gas exchange. *Int. J. Heat Mass Transf.* 51, 5712–5720. doi: 10.1016/j.ijheatmasstransfer.2008.04.016.

Mesarec, L., Góźdź, W., Iglič, A., Kralj-Iglič, V., Virga, E. G., and Kralj, S. (2019). Normal red blood cells' shape stabilized by membrane's in-plane ordering. *Sci. Rep.* 9, 19742. doi: 10.1038/s41598-019-56128-0.

Migliaccio, A. R., Campisi, S., and Migliaccio, G. (2001). Standardization of progenitor cell assay for cord blood banking. *Ann. Ist. Super. Sanita* 37, 595–600.

Minetti, G., Ciana, A., Profumo, A., Zappa, M., Vercellati, C., Zanella, A., et al. (2001). Cell age-related monovalent cations content and density changes in stored human erythrocytes. *Biochim. Biophys. Acta* 1527, 149–155. doi: 10.1016/s0304-4165(01)00159-3.

Minetti, G., Egée, S., Mörsdorf, D., Steffen, P., Makhro, A., Achilli, C., et al. (2013). Red cell investigations: art and artefacts. *Blood Rev.* 27, 91–101. doi: 10.1016/j.blre.2013.02.002.

Minetti, G., Kaestner, L., and Dorn, I. (2023). Terminal maturation of human reticulocytes to red blood cells by extensive remodelling and progressive liquid ordering of membrane lipids. 2023.06.02.543386. doi: 10.1101/2023.06.02.543386.

Misawa, K., Nakamichi, S., Iida, H., Nagano, A., Mikami, E., Tozuka, T., et al. (2023). Alectinib-Induced Severe Hemolytic Anemia in a Patient with ALK-Positive Non-Small Cell Lung Cancer: A Case Report. *OncoTargets Ther.* 16, 65–69. doi: 10.2147/OTT.S398375.

Misiti, J., and Spivak, J. L. (1979). Erythropoiesis in vitro. Role of calcium. *J. Clin. Invest.* 64, 1573–1579. doi: 10.1172/JCI109618.

Miya, K., Shimojima, K., Sugawara, M., Shimada, S., Tsuri, H., Harai-Tanaka, T., et al. (2012). A de novo interstitial deletion of 8p11.2 including ANK1 identified in a patient with spherocytosis, psychomotor developmental delay, and distinctive facial features. *Gene* 506, 146–149. doi: 10.1016/j.gene.2012.06.086.

Modell, B., and Darlison, M. (2008). Global epidemiology of haemoglobin disorders and derived service indicators. *Bull. World Health Organ.* 86, 480–487. doi: 10.2471/blt.06.036673.

Moersdorf, D., Egee, S., Hahn, C., Hanf, B., Ellory, C., Thomas, S., et al. (2013). Transmembrane potential of red blood cells under low ionic strength conditions. *Cell. Physiol. Biochem. Int. J. Exp. Cell. Physiol. Biochem. Pharmacol.* 31, 875–882. doi: 10.1159/000350105.

Mohandas, N., and Chasis, J. A. (1993). Red blood cell deformability, membrane material properties and shape: regulation by transmembrane, skeletal and cytosolic proteins and lipids. *Semin. Hematol.* 30, 171–192.

Mohandas, N., and Evans, E. (1985). Sickle erythrocyte adherence to vascular endothelium. Morphologic correlates and the requirement for divalent cations and collagen-binding plasma proteins. *J. Clin. Invest.* 76, 1605–1612. doi: 10.1172/JCI112144.

Mohandas, N., and Evans, E. (1994). Mechanical Properties of the Red Cell Membrane in Relation to Molecular Structure and Genetic Defects. *Annu. Rev. Biophys. Biomol. Struct.* 23, 787–818. doi: 10.1146/annurev.bb.23.060194.004035.

Mohandas, N., and Gallagher, P. G. (2008). Red cell membrane: past, present, and future. *Blood* 112, 3939–3948. doi: 10.1182/blood-2008-07-161166.

Mohandas, N., Rossi, M. E., and Clark, M. R. (1986). Association between morphologic distortion of sickle cells and deoxygenation-induced cation permeability increase. *Blood* 68, 450–454.

Monedero Alonso, D. (2019). Characterization of cationic conductances of human erythrocytes and their involvement in health and disease. Available at: http://www.theses.fr/2019SORUS554 [Accessed June 24, 2021].

Monedero Alonso, D., Pérès, L., Hatem, A., Bouyer, G., and Egée, S. (2021). The Chloride Conductance Inhibitor NS3623 Enhances the Activity of a Non-selective Cation Channel in Hyperpolarizing Conditions. *Front. Physiol.* 12, 743094. doi: 10.3389/fphys.2021.743094.

Moore, C., and Liedtke, W. B. (2017). “Osmomechanical-Sensitive TRPV Channels in Mammals,” in *Neurobiology of TRP Channels* Frontiers in Neuroscience., ed. T. L. R. Emir (Boca Raton (FL): CRC Press/Taylor & Francis). Available at: http://www.ncbi.nlm.nih.gov/books/NBK476118/ [Accessed September 14, 2023].

More, T. A., Dongerdiye, R., Devendra, R., Warang, P. P., and Kedar, P. S. (2020). Mechanosensitive Piezo1 ion channel protein (PIEZO1 gene): update and extended mutation analysis of hereditary xerocytosis in India. *Ann. Hematol.* 99, 715–727. doi: 10.1007/s00277-020-03955-1.

Mortensen, S. P., González-Alonso, J., Bune, L. T., Saltin, B., Pilegaard, H., and Hellsten, Y. (2009). ATP-induced vasodilation and purinergic receptors in the human leg: roles of nitric oxide, prostaglandins, and adenosine. *Am. J. Physiol. Regul. Integr. Comp. Physiol.* 296, R1140-1148. doi: 10.1152/ajpregu.90822.2008.

Morth, J. P., Pedersen, B. P., Toustrup-Jensen, M. S., Sørensen, T. L.-M., Petersen, J., Andersen, J. P., et al. (2007). Crystal structure of the sodium–potassium pump. *Nature* 450, 1043–1049. doi: 10.1038/nature06419.

Moura, P. L., Hawley, B. R., Dobbe, J. G. G., Streekstra, G. J., Rab, M. A. E., Bianchi, P., et al. (2020). PIEZO1 gain-of-function mutations delay reticulocyte maturation in hereditary xerocytosis. *Haematologica* 105, e268–e271. doi: 10.3324/haematol.2019.231159.

Mukhopadhyay, R., Lim H W, G., and Wortis, M. (2002). Echinocyte shapes: bending, stretching, and shear determine spicule shape and spacing. *Biophys. J.* 82, 1756–1772. doi: 10.1016/s0006-3495(02)75527-6.

Muller, C., Morales, P., and Reggio, P. H. (2018). Cannabinoid Ligands Targeting TRP Channels. *Front. Mol. Neurosci.* 11, 487. doi: 10.3389/fnmol.2018.00487.

Murate, M., and Kobayashi, T. (2016). Revisiting transbilayer distribution of lipids in the plasma membrane. *Chem. Phys. Lipids* 194, 58–71. doi: 10.1016/j.chemphyslip.2015.08.009.

Muravyov, A., and Tikhomirova, I. (2012). Role Ca(2+) in mechanisms of the red blood cells microrheological changes. *Adv. Exp. Med. Biol.* 740, 1017–1038. doi: 10.1007/978-94-007-2888-2_47.

Murciano, N., and Kaestner, L. (2023). The Putative Role of the Transient Receptor Potential Ion Channel of Vanilloid Type 2 in Red Blood Cell Storage Lesion. *Transfus Med Hemother*. doi: 10.1159/000531282.

Murthy, S. E., Dubin, A. E., and Patapoutian, A. (2017). Piezos thrive under pressure: mechanically activated ion channels in health and disease. *Nat. Rev. Mol. Cell Biol.* 18, 771–783. doi: 10.1038/nrm.2017.92.

Myssina, S., Lang, P. A., Kempe, D. S., Kaiser, S., Huber, S. M., Wieder, T., et al. (2004). Cl- channel blockers NPPB and niflumic acid blunt Ca(2+)-induced erythrocyte “apoptosis.” *Cell. Physiol. Biochem. Int. J. Exp. Cell. Physiol. Biochem. Pharmacol.* 14, 241–248. doi: 10.1159/000080333.

Nader, E., Conran, N., Leonardo, F. C., Hatem, A., Boisson, C., Carin, R., et al. (2023). Piezo1 activation augments sickling propensity and the adhesive properties of sickle red blood cells in a calcium-dependent manner. *Br. J. Haematol.* n/a. doi: 10.1111/bjh.18799.

Nakahara, E., Yamamoto, K. S., Ogura, H., Aoki, T., Utsugisawa, T., Azuma, K., et al. (2023). Variant spectrum of PIEZO1 and KCNN4 in Japanese patients with dehydrated hereditary stomatocytosis. *Hum. Genome Var.* 10, 8. doi: 10.1038/s41439-023-00235-y.

Narla, A., and Mohandas, N. (2020). Staying hydrated is important also for erythroblasts. *Haematologica* 105, 528–529. doi: 10.3324/haematol.2019.233999.

Narla, J., and Mohandas, N. (2017). Red cell membrane disorders. *Int. J. Lab. Hematol.* 39, 47–52. doi: 10.1111/ijlh.12657.

Nayani, K., Evans, A. A., Spagnolie, S. E., and Abbott, N. L. (2020). Dynamic and reversible shape response of red blood cells in synthetic liquid crystals. *Proc. Natl. Acad. Sci. U. S. A.* 117, 26083–26090. doi: 10.1073/pnas.2007753117.

Nelson, R. A. (1953). The immune-adherence phenomenon; an immunologically specific reaction between microorganisms and erythrocytes leading to enhanced phagocytosis. *Science* 118, 733–737. doi: 10.1126/science.118.3077.733.

Nguetse, C. N., Purington, N., Ebel, E. R., Shakya, B., Tetard, M., Kremsner, P. G., et al. (2020). A common polymorphism in the mechanosensitive ion channel PIEZO1 is associated with protection from severe malaria in humans. *Proc. Natl. Acad. Sci. U. S. A.* 117, 9074–9081. doi: 10.1073/pnas.1919843117.

Nguyen, D. B., Wagner-Britz, L., Maia, S., Steffen, P., Wagner, C., Kaestner, L., et al. (2011). Regulation of phosphatidylserine exposure in red blood cells. *Cell. Physiol. Biochem. Int. J. Exp. Cell. Physiol. Biochem. Pharmacol.* 28, 847–856. doi: 10.1159/000335798.

Niggli, V., Adunyah, E. S., Cameron, B. F., Bababunmi, E. A., and Carafoli, E. (1982). The Ca2+-pump of sickle cell plasma membranes. Purification and reconstitution of the ATPase enzyme. *Cell Calcium* 3, 131–151. doi: 10.1016/0143-4160(82)90010-0.

Noguchi, H., and Gompper, G. (2005). Shape transitions of fluid vesicles and red blood cells in capillary flows. *Proc. Natl. Acad. Sci. U. S. A.* 102, 14159–14164. doi: 10.1073/pnas.0504243102.

Nosyreva, E. D., Thompson, D., and Syeda, R. (2021). Identification and functional characterization of the Piezo1 channel pore domain. *J. Biol. Chem.* 296, 100225. doi: 10.1074/jbc.RA120.015905.

Nykamp, K., Anderson, M., Powers, M., Garcia, J., Herrera, B., Ho, Y.-Y., et al. (2017). Sherloc: a comprehensive refinement of the ACMG-AMP variant classification criteria. *Genet. Med. Off. J. Am. Coll. Med. Genet.* 19, 1105–1117. doi: 10.1038/gim.2017.37.

Ohkawa, R., Low, H., Mukhamedova, N., Fu, Y., Lai, S.-J., Sasaoka, M., et al. (2020). Cholesterol transport between red blood cells and lipoproteins contributes to cholesterol metabolism in blood. *J. Lipid Res.* 61, 1577–1588. doi: 10.1194/jlr.RA120000635.

Oikonomidou, P. R., and Rivella, S. (2018). What can we learn from ineffective erythropoiesis in thalassemia? *Blood Rev.* 32, 130–143. doi: 10.1016/j.blre.2017.10.001.

Orlov, S. N., Koltsova, S. V., Kapilevich, L. V., Gusakova, S. V., and Dulin, N. O. (2015). NKCC1 and NKCC2: The pathogenetic role of cation-chloride cotransporters in hypertension. *Genes Dis.* 2, 186–196. doi: 10.1016/j.gendis.2015.02.007.

Overman, R. R. (1948). Reversible cellular permeability alterations in disease; in vivo studies on sodium, potassium and chloride concentrations in erythrocytes of the malarious monkey. *Am. J. Physiol.* 152, 113–121. doi: 10.1152/ajplegacy.1947.152.1.113.

Oxygenscan – Lorrca – Functional RBC Analysis (2020). Available at: https://lorrca.com/wikilorrca/oxygenscan-test/ [Accessed November 13, 2023].

Paessler, M., and Hartung, H. (2015). Dehydrated hereditary stomatocytosis masquerading as MDS. *Blood* 125, 1841. doi: 10.1182/blood-2014-11-612184.

Palfrey, H. C., and Rao, M. C. (1983). Na/K/Cl co-transport and its regulation. *J. Exp. Biol.* 106, 43–54.

Pandolfi, P. P., Sonati, F., Rivi, R., Mason, P., Grosveld, F., and Luzzatto, L. (1995). Targeted disruption of the housekeeping gene encoding glucose 6-phosphate dehydrogenase (G6PD): G6PD is dispensable for pentose synthesis but essential for defense against oxidative stress. *EMBO J.* 14, 5209–5215. doi: 10.1002/j.1460-2075.1995.tb00205.x.

Park, J., Jang, W., Han, E., Chae, H., Yoo, J., Kim, Y., et al. (2018). Hereditary dehydrated stomatocytosis with splicing site mutation of PIEZO1 mimicking myelodysplastic syndrome diagnosed by targeted next-generation sequencing. *Pediatr. Blood Cancer* 65, e27053. doi: 10.1002/pbc.27053.

Park, J.-S., and Neiman, A. M. (2020). XK is a partner for VPS13A: a molecular link between Chorea-Acanthocytosis and McLeod Syndrome. *Mol. Biol. Cell* 31, 2425–2436. doi: 10.1091/mbc.E19-08-0439-T.

Peikert, K., and Danek, A. (2023). VPS13 Forum Proceedings: XK, XK-Related and VPS13 Proteins in Membrane Lipid Dynamics. *Contact Thousand Oaks Ventura Cty. Calif* 6, 25152564231156990. doi: 10.1177/25152564231156994.

Peng, Z., Asaro, R. J., and Zhu, Q. (2010). Multiscale simulation of erythrocyte membranes. *Phys. Rev. E Stat. Nonlin. Soft Matter Phys.* 81, 031904. doi: 10.1103/PhysRevE.81.031904.

Perálvarez-Marín, A., Doñate-Macian, P., and Gaudet, R. (2013). What do we know about the transient receptor potential vanilloid 2 (TRPV2) ion channel? *FEBS J.* 280, 5471–5487. doi: 10.1111/febs.12302.

Pérès, L., Monedero Alonso, D., Nudel, M., Figeac, M., Bruge, J., Sebda, S., et al. (2021). Characterisation of Asp669Tyr Piezo1 cation channel activity in red blood cells: an unexpected phenotype. *Br. J. Haematol.* 194. doi: 10.1111/bjh.17467.

Perrotta, S., Gallagher, P. G., and Mohandas, N. (2008). Hereditary spherocytosis. *Lancet Lond. Engl.* 372, 1411–1426. doi: 10.1016/S0140-6736(08)61588-3.

Peter Klinken, S. (2002). Red blood cells. *Int. J. Biochem. Cell Biol.* 34, 1513–1518. doi: 10.1016/s1357-2725(02)00087-0.

Peters, L. L., Jindel, H. K., Gwynn, B., Korsgren, C., John, K. M., Lux, S. E., et al. (1999). Mild spherocytosis and altered red cell ion transport in protein 4. 2-null mice. *J. Clin. Invest.* 103, 1527–1537. doi: 10.1172/JCI5766.

Peyronnet, R., Martins, J. R., Duprat, F., Demolombe, S., Arhatte, M., Jodar, M., et al. (2013). Piezo1-dependent stretch-activated channels are inhibited by Polycystin-2 in renal tubular epithelial cells. *EMBO Rep.* 14, 1143–1148. doi: 10.1038/embor.2013.170.

Picard, V., Guitton, C., Thuret, I., Rose, C., Bendelac, L., Ghazal, K., et al. (2019). Clinical and biological features in PIEZO1-hereditary xerocytosis and Gardos channelopathy: a retrospective series of 126 patients. *Haematologica* 104, 1554–1564. doi: 10.3324/haematol.2018.205328.

Piccinini, G., Minetti, G., Balduini, C., and Brovelli, A. (1995). Oxidation state of glutathione and membrane proteins in human red cells of different age. *Mech. Ageing Dev.* 78, 15–26. doi: 10.1016/0047-6374(94)01511-j.

Piel, F. B., Hay, S. I., Gupta, S., Weatherall, D. J., and Williams, T. N. (2013). Global burden of sickle cell anaemia in children under five, 2010-2050: modelling based on demographics, excess mortality, and interventions. *PLoS Med.* 10, e1001484. doi: 10.1371/journal.pmed.1001484.

Piel, F. B., and Weatherall, D. J. (2014). The α-thalassemias. *N. Engl. J. Med.* 371, 1908–1916. doi: 10.1056/NEJMra1404415.

Pietrobon, D. (2010). CaV2.1 channelopathies. *Pflugers Arch.* 460, 375–393. doi: 10.1007/s00424-010-0802-8.

Pirahanchi, Y., Jessu, R., and Aeddula, N. R. (2023). "Physiology, Sodium Potassium Pump," in *StatPearls* (Treasure Island (FL): StatPearls Publishing). Available at: http://www.ncbi.nlm.nih.gov/books/NBK537088/ [Accessed October 4, 2023].

Pivkin, I. V., and Karniadakis, G. E. (2008). Accurate coarse-grained modeling of red blood cells. *Phys. Rev. Lett.* 101, 118105. doi: 10.1103/PhysRevLett.101.118105.

Poole, K., Herget, R., Lapatsina, L., Ngo, H.-D., and Lewin, G. R. (2014). Tuning Piezo ion channels to detect molecular-scale movements relevant for fine touch. *Nat. Commun.* 5, 3520. doi: 10.1038/ncomms4520.

Potts, K. S., Sargeant, T. J., Markham, J. F., Shi, W., Biben, C., Josefsson, E. C., et al. (2014). A lineage of diploid platelet-forming cells precedes polyploid megakaryocyte formation in the mouse embryo. *Blood* 124, 2725–2729. doi: 10.1182/blood-2014-02-559468.

Pumroy, R. A., Protopopova, A. D., Fricke, T. C., Lange, I. U., Haug, F. M., Nguyen, P. T., et al. (2022). Structural insights into TRPV2 activation by small molecules. *Nat. Commun.* 13, 2334. doi: 10.1038/s41467-022-30083-3.

Pumroy, R. A., Samanta, A., Liu, Y., Hughes, T. E., Zhao, S., Yudin, Y., et al. (2019). Molecular mechanism of TRPV2 channel modulation by cannabidiol. *eLife* 8, e48792. doi: 10.7554/eLife.48792.

Pusch, M., Jordt, S. E., Stein, V., and Jentsch, T. J. (1999). Chloride dependence of hyperpolarization-activated chloride channel gates. *J. Physiol.* 515 (Pt 2), 341–353. doi: 10.1111/j.1469-7793.1999.341ac.x.

Ranade, S. S., Syeda, R., and Patapoutian, A. (2015). Mechanically Activated Ion Channels. *Neuron* 87, 1162–1179. doi: 10.1016/j.neuron.2015.08.032.

Rapetti-Mauss, R., Lacoste, C., Picard, V., Guitton, C., Lombard, E., Loosveld, M., et al. (2015). A mutation in the Gardos channel is associated with hereditary xerocytosis. *Blood* 126, 1273–1280. doi: 10.1182/blood-2015-04-642496.

Rapetti-Mauss, R., Picard, V., Guitton, C., Ghazal, K., Proulle, V., Badens, C., et al. (2017). Red blood cell Gardos channel (KCNN4): the essential determinant of erythrocyte dehydration in hereditary xerocytosis. *Haematologica* 102, e415–e418. doi: 10.3324/haematol.2017.171389.

Rapetti-Mauss, R., Soriani, O., Vinti, H., Badens, C., and Guizouarn, H. (2016). Senicapoc: a potent candidate for the treatment of a subset of hereditary xerocytosis caused by mutations in the Gardos channel. *Haematologica* 101, e431–e435. doi: 10.3324/haematol.2016.149104.

Recktenwald, S. M., Lopes, M. G. M., Peter, S., Hof, S., Simionato, G., Peikert, K., et al. (2022). Erysense, a Lab-on-a-Chip-Based Point-of-Care Device to Evaluate Red Blood Cell Flow Properties With Multiple Clinical Applications. *Front. Physiol.* 13, 884690. doi: 10.3389/fphys.2022.884690.

Reinhart, W. H., Geissmann-Ott, C., and Bogdanova, A. (2011). Activation of N-methyl D-aspartate (NMDA) receptors has no influence on rheological properties of erythrocytes. *Clin. Hemorheol. Microcirc.* 49, 307–313. doi: 10.3233/CH-2011-1481.

Ren, Y., Yan, C., and Yang, H. (2023). Erythrocytes: Member of the immune system that should not be ignored. *Crit. Rev. Oncol. Hematol.* 187, 104039. doi: 10.1016/j.critrevonc.2023.104039.

Research gate (2015). What is the difference between EDTA and Heparin during plasma separation? *ResearchGate*. Available at: https://www.researchgate.net/post/What-is-the-difference-between-EDTA-and-Heparin-during-plasma-separation [Accessed October 19, 2023].

Reyes-Pardo, H., and Sánchez-Herrera, D. P. (2019). Mechanosensitive ion channel inhibitors promote the stiffening of the plasma membrane of mouse sensory neurons. *Soft Matter* 15, 8320–8328. doi: 10.1039/c9sm01230c.

Rhoda, M. D., Apovo, M., Beuzard, Y., and Giraud, F. (1990). Ca2+ permeability in deoxygenated sickle cells. *Blood* 75, 2453–2458.

Ribeiro, M. L., Alloisio, N., Almeida, H., Gomes, C., Texier, P., Lemos, C., et al. (2000). Severe hereditary spherocytosis and distal renal tubular acidosis associated with the total absence of band 3. *Blood* 96, 1602–1604.

Richards, S., Aziz, N., Bale, S., Bick, D., Das, S., Gastier-Foster, J., et al. (2015). Standards and guidelines for the interpretation of sequence variants: a joint consensus recommendation of the American College of Medical Genetics and Genomics and the Association for Molecular Pathology. *Genet. Med. Off. J. Am. Coll. Med. Genet.* 17, 405–424. doi: 10.1038/gim.2015.30.

Ridone, P., Pandzic, E., Vassalli, M., Cox, C. D., Macmillan, A., Gottlieb, P. A., et al. (2020). Disruption of membrane cholesterol organization impairs the activity of PIEZO1 channel clusters. *J. Gen. Physiol.* 152, e201912515. doi: 10.1085/jgp.201912515.

Riordan, J. R., Rommens, J. M., Kerem, B., Alon, N., Rozmahel, R., Grzelczak, Z., et al. (1989). Identification of the cystic fibrosis gene: cloning and characterization of complementary DNA. *Science* 245, 1066–1073. doi: 10.1126/science.2475911.

Risinger, M., and Kalfa, T. A. (2020). Red cell membrane disorders: structure meets function. *Blood* 136, 1250–1261. doi: 10.1182/blood.2019000946.

Rivella, S. (2015). β-thalassemias: paradigmatic diseases for scientific discoveries and development of innovative therapies. *Haematologica* 100, 418–430. doi: 10.3324/haematol.2014.114827.

Rivera, A., Nasburg, J. A., Shim, H., Shmukler, B. E., Kitten, J., Wohlgemuth, J. G., et al. (2022). The erythroid K-Cl cotransport inhibitor [(dihydroindenyl)oxy]acetic acid blocks erythroid Ca2+-activated K+ channel KCNN4. *Am. J. Physiol. Cell Physiol.* 323, C694–C705. doi: 10.1152/ajpcell.00240.2022.

Rivera, A., Vandorpe, D. H., Shmukler, B. E., Andolfo, I., Iolascon, A., Archer, N. M., et al. (2019). Erythrocyte ion content and dehydration modulate maximal Gardos channel activity in KCNN4 V282M/+ hereditary xerocytosis red cells. *Am. J. Physiol. Cell Physiol.* 317, C287–C302. doi: 10.1152/ajpcell.00074.2019.

Rivera, A., Vandorpe, D. H., Shmukler, B. E., Gallagher, D. R., Fikry, C. C., Kuypers, F. A., et al. (2017). Erythrocytes from hereditary xerocytosis patients heterozygous for KCNN4 V282M exhibit increased spontaneous Gardos channel-like activity inhibited by senicapoc: RIVERA ET AL. *Am. J. Hematol.* 92, E108–E110. doi: 10.1002/ajh.24716.

Rodighiero, S., De Simoni, A., and Formenti, A. (2004). The voltage-dependent nonselective cation current in human red blood cells studied by means of whole-cell and nystatin-perforated patch-clamp techniques. *Biochim. Biophys. Acta BBA - Biomembr.* 1660, 164–170. doi: 10.1016/j.bbamem.2003.11.011.

Rogers, S., and Lew, V. L. (2021a). PIEZO1 and the mechanism of the long circulatory longevity of human red blood cells. *PLoS Comput. Biol.* 17, e1008496. doi: 10.1371/journal.pcbi.1008496.

Rogers, S., and Lew, V. L. (2021b). Up-down biphasic volume response of human red blood cells to PIEZO1 activation during capillary transits. *PLoS Comput. Biol.* 17, e1008706. doi: 10.1371/journal.pcbi.1008706.

Rooks, H., Brewin, J., Gardner, K., Chakravorty, S., Menzel, S., Hannemann, A., et al. (2019). A gain of function variant in PIEZO1 (E756del) and sickle cell disease. *Haematologica* 104, e91–e93. doi: 10.3324/haematol.2018.202697.

Rotordam, M. G., Fermo, E., Becker, N., Barcellini, W., Brüggemann, A., Fertig, N., et al. (2019). A novel gain-of-function mutation of Piezo1 is functionally affirmed in red blood cells by high-throughput patch clamp. *Haematologica* 104, e179–e183. doi: 10.3324/haematol.2018.201160.

Rudenko, S. V. (2010). Erythrocyte morphological states, phases, transitions and trajectories. *Biochim. Biophys. Acta* 1798, 1767–1778. doi: 10.1016/j.bbamem.2010.05.010.

Rungaldier, S., Oberwagner, W., Salzer, U., Csaszar, E., and Prohaska, R. (2013). Stomatin interacts with GLUT1/SLC2A1, band 3/SLC4A1, and aquaporin-1 in human erythrocyte membrane domains. *Biochim. Biophys. Acta* 1828, 956–966. doi: 10.1016/j.bbamem.2012.11.030.

Russo, R., Andolfo, I., Manna, F., Gambale, A., Marra, R., Rosato, B. E., et al. (2018). Multi-gene panel testing improves diagnosis and management of patients with hereditary anemias. *Am. J. Hematol.* 93, 672–682. doi: 10.1002/ajh.25058.

Russo, R., Marra, R., Rosato, B. E., Iolascon, A., and Andolfo, I. (2020). Genetics and Genomics Approaches for Diagnosis and Research Into Hereditary Anemias. *Front. Physiol.* 11, 613559. doi: 10.3389/fphys.2020.613559.

Sabban, E., Marchesi, V., Adesnik, M., and Sabatini, D. D. (1981). Erythrocyte membrane protein band 3: its biosynthesis and incorporation into membranes. *J. Cell Biol.* 91, 637–646. doi: 10.1083/jcb.91.3.637.

Sabirov, R. Z., and Merzlyak, P. G. (2012). Plasmalemmal VDAC controversies and maxi-anion channel puzzle. *Biochim. Biophys. Acta* 1818, 1570–1580. doi: 10.1016/j.bbamem.2011.09.024.

Salvemini, F., Franzé, A., Iervolino, A., Filosa, S., Salzano, S., and Ursini, M. V. (1999). Enhanced glutathione levels and oxidoresistance mediated by increased glucose-6-phosphate dehydrogenase expression. *J. Biol. Chem.* 274, 2750–2757. doi: 10.1074/jbc.274.5.2750.

Samanta, A., Hughes, T. E. T., and Moiseenkova-Bell, V. Y. (2018). "Transient Receptor Potential (TRP) Channels," in *Membrane Protein Complexes: Structure and Function* Subcellular Biochemistry., eds. J. R. Harris and E. J. Boekema (Singapore: Springer Singapore), 141–165. doi: 10.1007/978-981-10-7757-9_6.

Saotome, K., Murthy, S. E., Kefauver, J. M., Whitwam, T., Patapoutian, A., and Ward, A. B. (2018). Structure of the mechanically activated ion channel Piezo1. *Nature* 554, 481–486. doi: 10.1038/nature25453.

Sarafian, T. A., Habib, N., Oldham, M., Seeram, N., Lee, R.-P., Lin, L., et al. (2006). Inhaled marijuana smoke disrupts mitochondrial energetics in pulmonary epithelial cells in vivo. *Am. J. Physiol.-Lung Cell. Mol. Physiol.* 290, L1202–L1209. doi: 10.1152/ajplung.00371.2005.

Satchwell, T. J., and Toye, A. M. (2021). Band 3, an essential red blood cell hub of activity. *Haematologica* 106, 2792–2793. doi: 10.3324/haematol.2021.278643.

Scanlon, S. M., Williams, D. C., and Schloss, P. (2001). Membrane cholesterol modulates serotonin transporter activity. *Biochemistry* 40, 10507–10513. doi: 10.1021/bi010730z.

Scharff, O., and Foder, B. (1982). Rate constants for calmodulin binding to Ca2+-ATPase in erythrocyte membranes. *Biochim. Biophys. Acta* 691, 133–143. doi: 10.1016/0005-2736(82)90222-x.

Schatzmann, H. J. (1966). ATP-dependent Ca++-extrusion from human red cells. *Experientia* 22, 364–365. doi: 10.1007/BF01901136.

Schatzmann, H. J. (1983). The red cell calcium pump. *Annu. Rev. Physiol.* 45, 303–312. doi: 10.1146/annurev.ph.45.030183.001511.

Schillers, H. (2008). Imaging CFTR in its native environment. *Pflüg. Arch. Eur. J. Physiol.* 456, 163–77. doi: 10.1007/s00424-007-0399-8.

Schindelin, J., Arganda-Carreras, I., Frise, E., Kaynig, V., Longair, M., Pietzsch, T., et al. (2012). Fiji: an open-source platform for biological-image analysis. *Nat. Methods* 9, 676–682. doi: 10.1038/nmeth.2019.

Scott, M. D., Zuo, L., Lubin, B. H., and Chiu, D. T. (1991). NADPH, not glutathione, status modulates oxidant sensitivity in normal and glucose-6-phosphate dehydrogenase-deficient erythrocytes. *Blood* 77, 2059–2064.

Seki, M., Arashiki, N., Takakuwa, Y., Nitta, K., and Nakamura, F. (2020). Reduction in flippase activity contributes to surface presentation of phosphatidylserine in human senescent erythrocytes. *J. Cell. Mol. Med.* 24, 13991–14000. doi: 10.1111/jcmm.16010.

Semplicini, A., Mozzato, M. G., Sama', B., Nosadini, R., Fioretto, P., Trevisan, R., et al. (1989). Na/H and Li/Na exchange in red blood cells of normotensive and hypertensive patients with insulin dependent diabetes mellitus (IDDM). *Am. J. Hypertens.* 2, 174–177. doi: 10.1093/ajh/2.3.174.

Shiokawa, N., Nakamura, M., Sameshima, M., Deguchi, A., Hayashi, T., Sasaki, N., et al. (2013). Chorein, the protein responsible for chorea-acanthocytosis, interacts with β-adducin and β-actin. *Biochem. Biophys. Res. Commun.* 441, 96–101. doi: 10.1016/j.bbrc.2013.10.011.

Shmukler, B. E., Vandorpe, D. H., Rivera, A., Auerbach, M., Brugnara, C., and Alper, S. L. (2014). Dehydrated stomatocytic anemia due to the heterozygous mutation R2456H in the mechanosensitive cation channel PIEZO1: a case report. *Blood Cells. Mol. Dis.* 52, 53–54. doi: 10.1016/j.bcmd.2013.07.015.

Short, B. (2020). Cholesterol helps PIEZO1 use the force. *J. Gen. Physiol.* 152, e202012693. doi: 10.1085/jgp.202012693.

Sikora, J., Orlov, S. N., Furuya, K., and Grygorczyk, R. (2014). Hemolysis is a primary ATP-release mechanism in human erythrocytes. *Blood* 124, 2150–2157. doi: 10.1182/blood-2014-05-572024.

Simionato, G., Hinkelmann, K., Chachanidze, R., Bianchi, P., Fermo, E., van Wijk, R., et al. (2021). Red blood cell phenotyping from 3D confocal images using artificial neural networks. *PLoS Comput. Biol.* 17, e1008934. doi: 10.1371/journal.pcbi.1008934.

Simmonds, M. J., Detterich, J. A., and Connes, P. (2014). Nitric oxide, vasodilation and the red blood cell. *Biorheology* 51, 121–134. doi: 10.3233/BIR-140653.

Simmonds, M. J., Meiselman, H. J., and Baskurt, O. K. (2013). Blood rheology and aging. *J. Geriatr. Cardiol. JGC* 10, 291–301. doi: 10.3969/j.issn.1671-5411.2013.03.010.

Skou, J. C. (1957). The influence of some cations on an adenosine triphosphatase from peripheral nerves. *Biochim. Biophys. Acta* 23, 394–401. doi: 10.1016/0006-3002(57)90343-8.

Soderblom, E. J., Thompson, J. W., Schwartz, E. A., Chiou, E., Dubois, L. G., Moseley, M. A., et al. (2013). Proteomic analysis of ERK1/2-mediated human sickle red blood cell membrane protein phosphorylation. *Clin. Proteomics* 10, 1. doi: 10.1186/1559-0275-10-1.

Soldati, L., Adamo, D., Zerbi, S., Caumo, A., Spaventa, R., Bianchi, G., et al. (1999). Erythrocyte voltage-dependent calcium influx is reduced in hemodialyzed patients. *Kidney Int.* 56, 190–197. doi: 10.1046/j.1523-1755.1999.00535.x.

Sprague, R. S., and Ellsworth, M. L. (2012). Erythrocyte-derived ATP and perfusion distribution: role of intracellular and intercellular communication. *Microcirc. N. Y. N 1994* 19, 430–439. doi: 10.1111/j.1549-8719.2011.00158.x.

Sprague, R. S., Ellsworth, M. L., Stephenson, A. H., Kleinhenz, M. E., and Lonigro, A. J. (1998). Deformation-induced ATP release from red blood cells requires CFTR activity. *Am. J. Physiol.* 275, H1726-1732. doi: 10.1152/ajpheart.1998.275.5.H1726.

Sprague, R. S., Olearczyk, J. J., Spence, D. M., Stephenson, A. H., Sprung, R. W., and Lonigro, A. J. (2003). Extracellular ATP signaling in the rabbit lung: erythrocytes as determinants of vascular resistance. *Am. J. Physiol. Heart Circ. Physiol.* 285, H693-700. doi: 10.1152/ajpheart.01026.2002.

Sprague, R. S., Stephenson, A. H., and Ellsworth, M. L. (2007). Red not dead: signaling in and from erythrocytes. *Trends Endocrinol. Metab. TEM* 18, 350–355. doi: 10.1016/j.tem.2007.08.008.

Srivastava, S., Li, Z., Ko, K., Choudhury, P., Albaqumi, M., Johnson, A. K., et al. (2006). Histidine phosphorylation of the potassium channel KCa3.1 by nucleoside diphosphate kinase B is required for activation of KCa3.1 and CD4 T cells. *Mol. Cell* 24, 665–675. doi: 10.1016/j.molcel.2006.11.012.

Stefanovic, M., Puchulu-Campanella, E., Kodippili, G., and Low, P. S. (2013). Oxygen regulates the band 3-ankyrin bridge in the human erythrocyte membrane. *Biochem. J.* 449, 143–150. doi: 10.1042/BJ20120869.

Steffen, P., Jung, A., Nguyen, D. B., Müller, T., Bernhardt, I., Kaestner, L., et al. (2011). Stimulation of human red blood cells leads to Ca2+-mediated intercellular adhesion. *Cell Calcium* 50, 54–61. doi: 10.1016/j.ceca.2011.05.002.

Sterling, K. M., Shah, S., Kim, R. J., Johnston, N. I. F., Salikhova, A. Y., and Abraham, E. H. (2004). Cystic fibrosis transmembrane conductance regulator in human and mouse red blood cell membranes and its interaction with ecto-apyrase. *J. Cell. Biochem.* 91, 1174–1182. doi: 10.1002/jcb.20017.

Stieger, B., Steiger, J., and Locher, K. P. (2021). Membrane lipids and transporter function. *Biochim. Biophys. Acta BBA - Mol. Basis Dis.* 1867, 166079. doi: 10.1016/j.bbadis.2021.166079.

Stocker, J. W., De Franceschi, L., McNaughton-Smith, G. A., Corrocher, R., Beuzard, Y., and Brugnara, C. (2003). ICA-17043, a novel Gardos channel blocker, prevents sickled red blood cell dehydration in vitro and in vivo in SAD mice. *Blood* 101, 2412–2418. doi: 10.1182/blood-2002-05-1433.

Su, Y., Ding, Y., Jiang, M., Jiang, W., Hu, X., and Zhang, Z. (2006). Associations of protein 4.2 with band 3 and ankyrin. *Mol. Cell. Biochem.* 289, 159–166. doi: 10.1007/s11010-006-9159-x.

Subczynski, W. K., Pasenkiewicz-Gierula, M., Widomska, J., Mainali, L., and Raguz, M. (2017). High Cholesterol/Low Cholesterol: Effects in Biological Membranes: A Review. *Cell Biochem. Biophys.* 75, 369–385. doi: 10.1007/s12013-017-0792-7.

Subczynski, W. K., Wisniewska, A., Yin, J. J., Hyde, J. S., and Kusumi, A. (1994). Hydrophobic barriers of lipid bilayer membranes formed by reduction of water penetration by alkyl chain unsaturation and cholesterol. *Biochemistry* 33, 7670–7681. doi: 10.1021/bi00190a022.

Sugie, J., Intaglietta, M., and Sung, L. A. (2018). Water transport and homeostasis as a major function of erythrocytes. *Am. J. Physiol.-Heart Circ. Physiol.* 314, H1098–H1107. doi: 10.1152/ajpheart.00263.2017.

Sullivan, I., and Planchard, D. (2016). ALK inhibitors in non-small cell lung cancer: the latest evidence and developments. *Ther. Adv. Med. Oncol.* 8, 32–47. doi: 10.1177/1758834015617355.

Svetina, S., Švelc Kebe, T., and Božič, B. (2019). A Model of Piezo1-Based Regulation of Red Blood Cell Volume. *Biophys. J.* 116, 151–164. doi: 10.1016/j.bpj.2018.11.3130.

Syeda, R., Florendo, M. N., Cox, C. D., Kefauver, J. M., Santos, J. S., Martinac, B., et al. (2016). Piezo1 Channels Are Inherently Mechanosensitive. *Cell Rep.* 17, 1739–1746. doi: 10.1016/j.celrep.2016.10.033.

Syeda, R., Xu, J., Dubin, A. E., Coste, B., Mathur, J., Huynh, T., et al. (2015). Chemical activation of the mechanotransduction channel Piezo1. *eLife* 4, e07369. doi: 10.7554/eLife.07369.

Tachev, K. D., Danov, K. D., and Kralchevsky, P. A. (2004). On the mechanism of stomatocyte-echinocyte transformations of red blood cells: experiment and theoretical model. *Colloids Surf. B Biointerfaces* 34, 123–140. doi: 10.1016/j.colsurfb.2003.12.011.

Tahiri, N., Biben, T., Ez-Zahraouy, H., Benyoussef, A., and Misbah, C. (2013). On the problem of slipper shapes of red blood cells in the microvasculature. *Microvasc. Res.* 85, 40–45. doi: 10.1016/j.mvr.2012.10.001.

Tanner, M. J. (1997). The structure and function of band 3 (AE1): recent developments (review). *Mol. Membr. Biol.* 14, 155–165. doi: 10.3109/09687689709048178.

Teissie, J., and Yow Tsong, T. (1981). Voltage modulation of Na+/K+ transport in human erythrocytes. *J. Physiol. (Paris)* 77, 1043–1053.

Teng, J., Loukin, S., Anishkin, A., and Kung, C. (2015). The force-from-lipid (FFL) principle of mechanosensitivity, at large and in elements. *Pflugers Arch.* 467, 27–37. doi: 10.1007/s00424-014-1530-2.

Tepper, T., Sluiter, W. J., Huisman, R. M., and de Zeeuw, D. (1998). Erythrocyte Na+/Li+ countertransport and Na+/K+–2Cl− co-transport measurement in essential hypertension: useful diagnostic tools or failure? A meta-analysis of 17 years of literature. *Clin. Sci.* 95, 649–657. doi: 10.1042/cs0950649.

Teramoto, T., Kuwada, M., Niidome, T., Sawada, K., Nishizawa, Y., and Katayama, K. (1993). A novel peptide from funnel web spider venom, omega-Aga-TK, selectively blocks, P-type calcium channels. *Biochem. Biophys. Res. Commun.* 196, 134–140. doi: 10.1006/bbrc.1993.2225.

Therien, A. G., and Blostein, R. (2000). Mechanisms of sodium pump regulation. *Am. J. Physiol.-Cell Physiol.* 279, C541–C566. doi: 10.1152/ajpcell.2000.279.3.C541.

Thiagarajan, P., Parker, C. J., and Prchal, J. T. (2021). How Do Red Blood Cells Die? *Front. Physiol.* 12, 655393. doi: 10.3389/fphys.2021.655393.

Thiemann, A., Gründer, S., Pusch, M., and Jentsch, T. J. (1992). A chloride channel widely expressed in epithelial and non-epithelial cells. *Nature* 356, 57–60. doi: 10.1038/356057a0.

Tian, W. N., Braunstein, L. D., Pang, J., Stuhlmeier, K. M., Xi, Q. C., Tian, X., et al. (1998). Importance of glucose-6-phosphate dehydrogenase activity for cell growth. *J. Biol. Chem.* 273, 10609–10617. doi: 10.1074/jbc.273.17.10609.

Tiffert, T., and Lew, V. L. (1997). Cytoplasmic calcium buffers in intact human red cells. *J. Physiol.* 500 (Pt 1), 139–154. doi: 10.1113/jphysiol.1997.sp022005.

Tiffert, T., and Lew, V. L. (2011). Elevated intracellular Ca2+ reveals a functional membrane nucleotide pool in intact human red blood cells. *J. Gen. Physiol.* 138, 381–391. doi: 10.1085/jgp.201110660.

Tiffert, T., Lew, V. L., Ginsburg, H., Krugliak, M., Croisille, L., and Mohandas, N. (2005). The hydration state of human red blood cells and their susceptibility to invasion by Plasmodium falciparum. *Blood* 105, 4853–4860. doi: 10.1182/blood-2004-12-4948.

Tong, Q., Hirschler-Laszkiewicz, I., Zhang, W., Conrad, K., Neagley, D. W., Barber, D. L., et al. (2008). TRPC3 is the erythropoietin-regulated calcium channel in human erythroid cells. *J. Biol. Chem.* 283, 10385–10395. doi: 10.1074/jbc.M710231200.

Tosteson, D. C., and Hoffman, J. F. (1960). Regulation of cell volume by active cation transport in high and low potassium sheep red cells. *J. Gen. Physiol.* 44, 169–194. doi: 10.1085/jgp.44.1.169.

Tóth, A., Czikora, Á., Pásztor, E. T., Dienes, B., Bai, P., Csernoch, L., et al. (2014). Vanilloid Receptor-1 (TRPV1) Expression and Function in the Vasculature of the Rat. *J. Histochem. Cytochem.* 62, 129–144. doi: 10.1369/0022155413513589.

Tsiftsoglou, A. S. (2021). Erythropoietin (EPO) as a Key Regulator of Erythropoiesis, Bone Remodeling and Endothelial Transdifferentiation of Multipotent Mesenchymal Stem Cells (MSCs): Implications in Regenerative Medicine. *Cells* 10, 2140. doi: 10.3390/cells10082140.

Tyteca, D., D'Auria, L., Der Smissen, P. V., Medts, T., Carpentier, S., Monbaliu, J. C., et al. (2010). Three unrelated sphingomyelin analogs spontaneously cluster into plasma membrane micrometric domains. *Biochim. Biophys. Acta* 1798, 909–927. doi: 10.1016/j.bbamem.2010.01.021.

Uhlén, M., Fagerberg, L., Hallström, B. M., Lindskog, C., Oksvold, P., Mardinoglu, A., et al. (2015). Proteomics. Tissue-based map of the human proteome. *Science* 347, 1260419. doi: 10.1126/science.1260419.

Ulirsch, J. C., Lareau, C. A., Bao, E. L., Ludwig, L. S., Guo, M. H., Benner, C., et al. (2019). Interrogation of human hematopoiesis at single-cell and single-variant resolution. *Nat. Genet.* 51, 683–693. doi: 10.1038/s41588-019-0362-6.

Utsugisawa, K., Nagane, Y., Akaishi, T., Suzuki, Y., Imai, T., Tsuda, E., et al. (2017). Early fast-acting treatment strategy against generalized myasthenia gravis. *Muscle Nerve* 55, 794–801. doi: 10.1002/mus.25397.

Vaisey, G., Banerjee, P., North, A. J., Haselwandter, C. A., and MacKinnon, R. (2022). Piezo1 as a force-through-membrane sensor in red blood cells. *eLife* 11, e82621. doi: 10.7554/eLife.82621.

Vallese, F., Kim, K., Yen, L. Y., Johnston, J. D., Noble, A. J., Calì, T., et al. (2022). Architecture of the human erythrocyte ankyrin-1 complex. *Nat. Struct. Mol. Biol.* 29, 706–718. doi: 10.1038/s41594-022-00792-w.

Van Beek, G. G., and De Bruin, S. H. (1980). Identification of the residues involved in the oxygen-linked chloride-ion binding sites in human deoxyhemoglobin and oxyhemoglobin. *Eur. J. Biochem.* 105, 353–360. doi: 10.1111/j.1432-1033.1980.tb04508.x.

van der Harst, P., Zhang, W., Mateo Leach, I., Rendon, A., Verweij, N., Sehmi, J., et al. (2012). Seventy-five genetic loci influencing the human red blood cell. *Nature* 492, 369–375. doi: 10.1038/nature11677.

Vandorpe, D. H., Be, S., Y, I., S, B., B, T., A, R., et al. (2021a). A Grammastola spatulata mechanotoxin-4 (GsMTx4)-sensitive cation channel mediates increased cation permeability in human hereditary spherocytosis of multiple genetic etiologies. *Haematologica* 106. doi: 10.3324/haematol.2021.278770.

Vandorpe, D. H., Rivera, A., Shmukler, B. E., Wohlgemuth, J. G., Dlott, J. S., Snyder, L. M., et al. (2021b). Trpv1 and Trpa1 are not essential for Psickle-like activity in red cells of the SAD mouse model of sickle cell disease. *Blood Cells. Mol. Dis.* 92, 102619. doi: 10.1016/j.bcmd.2021.102619.

Vandorpe, D. H., Shmukler, B. E., Jiang, L., Lim, B., Maylie, J., Adelman, J. P., et al. (1998). cDNA cloning and functional characterization of the mouse Ca2+-gated K+ channel, mIK1. Roles in regulatory volume decrease and erythroid differentiation. *J. Biol. Chem.* 273, 21542–21553. doi: 10.1074/jbc.273.34.21542.

Vandorpe, D. H., Xu, C., Shmukler, B. E., Otterbein, L. E., Trudel, M., Sachs, F., et al. (2010). Hypoxia Activates a Ca2+-Permeable Cation Conductance Sensitive to Carbon Monoxide and to GsMTx-4 in Human and Mouse Sickle Erythrocytes. *PLoS ONE* 5, e8732. doi: 10.1371/journal.pone.0008732.

Verloo, P., Kocken, C. H. M., Van der Wel, A., Tilly, B. C., Hogema, B. M., Sinaasappel, M., et al. (2004). Plasmodium falciparum-activated chloride channels are defective in erythrocytes from cystic fibrosis patients. *J. Biol. Chem.* 279, 10316–10322. doi: 10.1074/jbc.M311540200.

Vincenzi, F. F., Hinds, T. R., and Raess, B. U. (1980). Calmodulin and the plasma membrane calcium pump. *Ann. N. Y. Acad. Sci.* 356, 232–244. doi: 10.1111/j.1749-6632.1980.tb29614.x.

von Lindern, M., Egée, S., Bianchi, P., and Kaestner, L. (2022). The Function of Ion Channels and Membrane Potential in Red Blood Cells: Toward a Systematic Analysis of the Erythroid Channelome. *Front. Physiol.* 13, 824478. doi: 10.3389/fphys.2022.824478.

Vuckovic, D., Bao, E. L., Akbari, P., Lareau, C. A., Mousas, A., Jiang, T., et al. (2020). The Polygenic and Monogenic Basis of Blood Traits and Diseases. *Cell* 182, 1214-1231.e11. doi: 10.1016/j.cell.2020.08.008.

Wadud, R., Hannemann, A., Rees, D. C., Brewin, J. N., and Gibson, J. S. (2020). Yoda1 and phosphatidylserine exposure in red cells from patients with sickle cell anaemia. *Sci. Rep.* 10, 20110. doi: 10.1038/s41598-020-76979-2.

Wagner-Britz, L., Wang, J., Kaestner, L., and Bernhardt, I. (2013). Protein kinase Cα and P-type Ca channel CaV2.1 in red blood cell calcium signalling. *Cell. Physiol. Biochem. Int. J. Exp. Cell. Physiol. Biochem. Pharmacol.* 31, 883–891. doi: 10.1159/000350106.

Walencik, J., and Witeska, M. (2007). The effects of anticoagulants on hematological indices and blood cell morphology of common carp (Cyprinus carpio L.). *Comp. Biochem. Physiol. Toxicol. Pharmacol. CBP* 146, 331–335. doi: 10.1016/j.cbpc.2007.04.004.

Wang, Y., Chi, S., Guo, H., Li, G., Wang, L., Zhao, Q., et al. (2018). A lever-like transduction pathway for long-distance chemical- and mechano-gating of the mechanosensitive Piezo1 channel. *Nat. Commun.* 9, 1300. doi: 10.1038/s41467-018-03570-9.

Wang, Y., and Xiao, B. (2018). The mechanosensitive Piezo1 channel: structural features and molecular bases underlying its ion permeation and mechanotransduction. *J. Physiol.* 596, 969–978. doi: 10.1113/JP274404.

Waugh, R. E., Narla, M., Jackson, C. W., Mueller, T. J., Suzuki, T., and Dale, G. L. (1992). Rheologic properties of senescent erythrocytes: loss of surface area and volume with red blood cell age. *Blood* 79, 1351–1358.

Weber, D., and Nakashima, M. O. (2021). Platelet count in sodium citrate-anticoagulated whole blood: Comparison to EDTA-anticoagulated results and stability over time. *Int. J. Lab. Hematol.* 43, e35–e37. doi: 10.1111/ijlh.13350.

Wells, M., and Steiner, L. (2022). Epigenetic and Transcriptional Control of Erythropoiesis. *Front. Genet.* 13. Available at: https://www.frontiersin.org/articles/10.3389/fgene.2022.805265 [Accessed September 25, 2023].

Whitfield, C. F., Follweiler, J. B., Lopresti-Morrow, L., and Miller, B. A. (1991). Deficiency of alpha-spectrin synthesis in burst-forming units-erythroid in lethal hereditary spherocytosis. *Blood* 78, 3043–3051.

Wölwer, C. B., Pase, L. B., Russell, S. M., and Humbert, P. O. (2016). Calcium Signaling Is Required for Erythroid Enucleation. *PloS One* 11, e0146201. doi: 10.1371/journal.pone.0146201.

Woon, L. A., Holland, J. W., Kable, E. P., and Roufogalis, B. D. (1999). Ca2+ sensitivity of phospholipid scrambling in human red cell ghosts. *Cell Calcium* 25, 313–320. doi: 10.1054/ceca.1999.0029.

World Health Organization (2011). Haemoglobin concentrations for the diagnosis of anaemia and assessment of severity. World Health Organization Available at: https://apps.who.int/iris/handle/10665/85839 [Accessed September 4, 2023].

Wu, J., Lewis, A. H., and Grandl, J. (2017). Touch, Tension, and Transduction - The Function and Regulation of Piezo Ion Channels. *Trends Biochem. Sci.* 42, 57–71. doi: 10.1016/j.tibs.2016.09.004.

Xia, X., Liu, S., and Zhou, Z. H. (2022). Structure, dynamics and assembly of the ankyrin complex on human red blood cell membrane. *Nat. Struct. Mol. Biol.* 29, 698–705. doi: 10.1038/s41594-022-00779-7.

Yamaguchi, Y., Allegrini, B., Rapetti-Mauss, R., Picard, V., Garçon, L., Kohl, P., et al. (2021). Hereditary Xerocytosis: Differential Behavior of PIEZO1 Mutations in the N-Terminal Extracellular Domain Between Red Blood Cells and HEK Cells. *Front. Physiol.* 12, 736585. doi: 10.3389/fphys.2021.736585.

Yang, H.-C., Ma, T.-H., Tjong, W.-Y., Stern, A., and Chiu, D. T.-Y. (2021). G6PD deficiency, redox homeostasis, and viral infections: implications for SARS-CoV-2 (COVID-19). *Free Radic. Res.* 55, 364–374. doi: 10.1080/10715762.2020.1866757.

Yuan, Y., Mapp, S., and Xu, W. (2020). Two cases of marked red cell anisopoikilocytosis and haemolysis with alectinib, an anaplastic lymphoma kinase inhibitor. *Br. J. Haematol.* 190, 642. doi: 10.1111/bjh.16813.

Zamora, E. A., and Schaefer, C. A. (2023). "Hereditary Spherocytosis," in *StatPearls* (Treasure Island (FL): StatPearls Publishing). Available at: http://www.ncbi.nlm.nih.gov/books/NBK539797/ [Accessed October 16, 2023].

Zarkowsky, H. S., Mohandas, N., Speaker, C. B., and Shohet, S. B. (1975). A congenital haemolytic anaemia with thermal sensitivity of the erythrocyte membrane. *Br. J. Haematol.* 29, 537–543. doi: 10.1111/j.1365-2141.1975.tb02740.x.

Zarychanski, R., Schulz, V. P., Houston, B. L., Maksimova, Y., Houston, D. S., Smith, B., et al. (2012). Mutations in the mechanotransduction protein PIEZO1 are associated with hereditary xerocytosis. *Blood* 120, 1908–1915. doi: 10.1182/blood-2012-04-422253.

Zhang, F., Hanson, S. M., Jara-Oseguera, A., Krepkiy, D., Bae, C., Pearce, L. V., et al. (2016). Engineering vanilloid-sensitivity into the rat TRPV2 channel. *eLife* 5, e16409. doi: 10.7554/eLife.16409.

Zhang, R., Zhang, C., Zhao, Q., and Li, D. (2013). Spectrin: structure, function and disease. *Sci. China Life Sci.* 56, 1076–1085. doi: 10.1007/s11427-013-4575-0.

Zhang, W., Cheng, L. E., Kittelmann, M., Li, J., Petkovic, M., Cheng, T., et al. (2015). Ankyrin Repeats Convey Force to Gate the NOMPC Mechanotransduction Channel. *Cell* 162, 1391–1403. doi: 10.1016/j.cell.2015.08.024.

Zhao, Q., Wu, K., Geng, J., Chi, S., Wang, Y., Zhi, P., et al. (2016). Ion Permeation and Mechanotransduction Mechanisms of Mechanosensitive Piezo Channels. *Neuron* 89, 1248–1263. doi: 10.1016/j.neuron.2016.01.046.

Zhao, Q., Zhou, H., Chi, S., Wang, Y., Wang, J., Geng, J., et al. (2018). Structure and mechanogating mechanism of the Piezo1 channel. *Nature* 554, 487–492. doi: 10.1038/nature25743.

Zheng, S., Krump, N. A., McKenna, M. M., Li, Y.-H., Hannemann, A., Garrett, L. J., et al. (2019). Regulation of erythrocyte Na+/K+/2Cl- cotransport by an oxygen-switched kinase cascade. *J. Biol. Chem.* 294, 2519–2528. doi: 10.1074/jbc.RA118.006393.

Zwaal, R. F. A., Comfurius, P., and Bevers, E. M. (2005). Surface exposure of phosphatidylserine in pathological cells. *Cell. Mol. Life Sci. CMLS* 62, 971–988. doi: 10.1007/s00018-005-4527-3.